

BACTERIA, MICROBIAL COMMUNITIES AND ENGINEERING: STUDIES ON THE
MICROBIAL ECOLOGY OF SELECTED ENGINEERED SYSTEMS

By

Fan Yang

A DISSERTATION

Submitted to
Michigan State University
in partial fulfillment of the requirements
for the degree of

Environmental Engineering – Doctor of Philosophy

2013

ABSTRACT

BACTERIA, MICROBIAL COMMUNITIES AND ENGINEERING: STUDIES ON THE MICROBIAL ECOLOGY OF SELECTED ENGINEERED SYSTEMS

By

Fan Yang

Environmental contaminants, such as soluble metal ions and agricultural wastes pose great risks for both human health and ecosystems. To reduce these risks, environmental engineers have developed remediation approaches that take the advantage of microbial communities and populations. Understanding these microbial resources is instrumental to manage and apply them in various engineered systems. In this dissertation, I study microbial communities and populations from three different approaches and demonstrate how basic microbial information can assist us in optimizing engineered systems.

The first part of my dissertation focuses on understanding the genomic advantages of *Ralstonia pickettii* strains, which allows them to adapt to high copper environments. We have previously shown that these two strains were able to sequester a large amount of copper. Hence, these two bacterial strains have a great potential in for application to industrial wastewater treatment. Understanding the genomic evolution and adaptation behind the copper binding phenomenon could unveil the industrial potential of these bacterial strains.

The second part of this dissertation focuses on understanding the role of anaerobic bacterial populations and communities in uranium immobilization. A large amount of research has been conducted on identifying the bacterial communities involved in *in situ* uranium immobilization. However, the extant of soil microbial diversity made it difficult to identify the most important specific populations. We employed enrichment culture methods to in-

crease the abundance of potential important bacterial populations and to link the community functions.

Finally, I present a study on microbial communities in methane producing agricultural waste co-bioreactors. Methane production has been reported as a highly cooperative reaction between bacteria and archaea. Linking bacterial populations to specific functions would help optimize agricultural waste degradation as well as alternative energy production.

I chose these three topics to emphasize the importance of microbial populations in engineered systems. By understanding the roles of individual bacteria populations as well as their interactions with each other in a community, I hope to manage and utilize these microbial resources to improve our living environment.

Copyright by
FAN YANG
2013

This thesis is dedicated to my parents, Hanying Yang and Ning Shen.

ACKNOWLEDGEMENTS

This dissertation marks the end of my journey as a Ph.D. student. Throughout the past five years, there was excitement, frustration, as well as a tremendous amount of support from people around me. I would like to begin the acknowledgement by thanking Dr. Terence L. Marsh, who graciously took me in as an undergraduate research assistant, from where I grew into loving microbial ecology. From 2004 to 2012, I have learned the importance of bacteria and their applicabilities in sustainably managing our environments. I thank Dr. Thomas C. Voice, who took the responsibility of being my major advisor in the department of Civil and Environmental Engineering. It was a drastic change switching from microbiology to engineering. I am grateful for Dr. Voice's guidance on how to think and solve problems like an engineer, which sets me up for applied science. I would like to thank my research committee members, Dr. Alison Cupples and Dr. David T. Long, who have always been supportive and taught me many valuable lessons through the past five years.

My thank goes to countless supportive friends. I'm especially thankful for Dr. Adina Howe and Mike Howe's hospitality, great advice and the tremendous amount of support for the past one year and a half, which was definitely special and eventful. I would like to thank Dr. Juliana Bordowitz and Dr. Zarraz May-ping Lee for their great friendship, without whom, the transition to the Ph.D. program would not be easy. My thank goes to the entire Ribosomal Database Project members, who have been extremely helpful in preparing me for the big bioinformatic world. I truly appreciate the great relationships I have with the past and current Tiedje group members. My special thank goes to the entire

ROME lab, especially, Chirstina Harzman, Natasha Issacs-Cosgrove, Joe Duris, and Lisa Reynolds Fogarty, without whom, I would not think graduate school is fun. I also would like to acknowledge all of the hard work Katherine Ivens, Rachael Rossi, and Brian Lovett have done as undergraduate research assistants. My thank also goes to all of the secretaries in both the Department of Microbiology and Molecular Genetics and the Department of Civil and Environmental Engineering, especially Lori Larner, without whom, I would not be able to make it through the first year.

Finally, I would like to thank my parents, Hanying Yang and Ning Shen, for the wonderful opportunity they gave me to study abroad at Michigan State University. It has been a long journey and I am thankful that I was not doing this alone.

TABLE OF CONTENTS

LIST OF TABLES	xii
LIST OF FIGURES	xiii
CHAPTER 1 INTRODUCTION	1
1.1 Bioremediation of Metals	1
1.1.1 Biosequestration of Metals	3
1.1.1.1 Metal Contamination at Torch Lake	6
1.1.1.2 Adaptation of <i>Raltonisa pickettii</i> in High Copper	6
1.1.2 Bioimmobilization of Metals	11
1.1.2.1 Metal Contamination at Oak Ridge Reservation	12
1.1.2.2 Bacterial Community Profiling	14
1.1.2.3 Reconstruct Uranium Immobilizing Bacterial Communities	14
1.2 Bioremediation of Agriculture Wastes	16
1.2.1 The Role of Class Clostridia in Methane Producing Anaerobic Co-bioreactors	19
1.3 Managing Complex Microbial Communities for Sustainable Environment	20
CHAPTER 2 CO-EVOLUTION OF <i>RALSTONIA PICKETTII</i> STRAIN 12D AND 12J: GENOME REARRANGEMENTS AND THEIR INFLUENCES ON THE EVOLUTION OF METAL RESISTANCE	24
2.1 Abstract	24
2.2 Introduction	25
2.3 Materials and Methods	26
2.3.1 Genome Retrieval and Gene Annotations	26
2.3.2 Genome Comparisons	26
2.3.3 Identification of the Metal Resistant Genes	27
2.4 Results	28
2.4.1 Genome Overview	28
2.4.2 Co-evolution of <i>R. pickettii</i> 12D and 12J	39
2.4.2.1 16S rRNA Gene Sequence Variations	39
2.4.2.2 <i>dif</i> Site Sequence Variations	40
2.4.2.3 Filamentous Phage Elements in <i>R. pickettii</i> 12D and 12J	42
2.4.3 Genome Syntenies of <i>R. pickettii</i> 12D and 12J	43
2.4.4 The Acquisition and Duplication of Resistance Determinants in <i>R. pickettii</i> 12D and 12J	49
2.4.4.1 Metal Resistant Genes in <i>R. pickettii</i> 12D and 12J	49
2.4.4.2 The Phylogenetic Lineage of <i>czcA</i> Copies in <i>R. pickettii</i> 12D and 12J	53

2.4.4.3	The Phylogenetic Lineage of <i>copA</i> Copies in <i>R. pickettii</i> 12D and 12J	58
2.5	Discussion	60
2.6	Conclusion	65

CHAPTER 3 RESOURCE-INDUCED BACTERIAL STRUCTURE SHIFTS AND THEIR INFLUENCE ON COMMUNITY FUNCTIONS 67

3.1	Abstract	67
3.2	Introduction	68
3.3	Materials and Methods	71
3.3.1	Anaerobic Media and Stocks	71
3.3.2	Bacterial Community Enrichments	71
3.3.3	Quantitative Analyses	72
3.3.4	DNA Extraction and Community Profiling	73
3.3.5	Community Analysis	74
3.4	Results	75
3.4.1	Monitoring the Enrichment Cultures	75
3.4.2	Overview of the Community Dynamics	76
3.4.3	Shifts in the Enrichment Bacterial Community Structures	77
3.4.4	Shared Genera	81
3.4.5	Functional Gene Profiles	83
3.4.6	Non-metric multidimensional scaling (NMDS) analysis	86
3.5	Discussion	92
3.6	Conclusion	94

CHAPTER 4 THE ROLE OF FIRMICUTES IN URANIUM IMMOBILIZATION 96

4.1	Abstract	96
4.2	Introduction	97
4.3	Materials and Methods	98
4.3.1	Uranium Immobilization by FW107 and FW102-2 Enrichment Cultures	98
4.3.2	Quantitative Analyses	98
4.3.3	DNA Extraction and Sequencing Preparation	99
4.3.4	Community Analysis	100
4.3.5	Isolation of Potential Uranium Immobilizing Bacteria	101
4.3.6	Growth Curves of Isolates	101
4.3.7	Isolate Identifications	102
4.3.8	Cell Suspension Assay	103
4.4	Results	103
4.4.1	Soluble U ⁶⁺ Immobilization by FW107 and FW102-2 Enrichments	103
4.4.2	Bacterial Community Compositions of FW107 and FW102-2 Enrichments	104
4.4.3	Potential U ⁶⁺ Immobilizers	111
4.4.4	U ⁶⁺ Immobilization By Isolates	117

4.5	Discussion	119
4.6	Conclusion	121
CHAPTER 5 PHYLOGENETIC COMPOSITION OF BACTERIA IN ANAEROBIC CO-DIGESTION OF DAIRY MANURE AND CORN STOVER 122		
5.1	Abstract	122
5.2	Introduction	123
5.3	Materials and Methods	124
5.3.1	Anaerobic Bioreactors	124
5.3.2	DNA Extraction and Targeted Gene Amplifications	125
5.3.3	Preparation for Pyrosequencing and Construction of Clone Libraries	126
5.3.4	Sequence and Community Analyses	127
5.4	Results	128
5.4.1	The Influence of HRT and Corn Stover on System Performance	128
5.4.2	Phylogenetic Comparisons of Anaerobic Bioreactor Bacterial Communities	130
5.4.3	Bacteroidetes	140
5.4.4	Hydrogen Producing Population Profiles	143
5.4.5	Non-metric multidimensional scaling (NMDS) analysis	148
5.5	Discussion	150
5.6	Conclusion	159
APPENDICES 161		
APPENDIX A COMPARATIVE GENOMICS OF <i>RALSTONIA PICKETTII</i> 12D AND 12J 162		
A.1	Metabolic Pathways of <i>R. pickettii</i> 12D and 12J	162
A.2	Clustering of <i>R. pickettii</i> 12D and 12J and other 23 Proteobacteria	163
A.3	Genetic Elements in <i>R. pickettii</i> 12D and 12J	164
A.4	Variation of <i>R. pickettii</i> 12D and 12J <i>dif</i> Sites	165
A.5	Genome Synteny of <i>R. pickettii</i> 12D and 12J	167
APPENDIX B ANAEROBIC ENRICHMENTS 169		
B.1	Media Preparation	169
B.2	Functional Gene Profiles	171
APPENDIX C URANIUM IMMOBILIZATION BY FIRMICUTES 172		
C.1	Uranium-azide Assay	172
C.2	5X Gitschier Buffer	173
C.3	Growth Curves of Isolates in Minimal Media	173
APPENDIX D BACTERIAL COMMUNITIES IN ANAEROBIC CO-BIOREACTORS 176		
D.1	Deep Sequencing of Bacterial Communities in Anaerobic Co-bioreactors	176
D.2	Anaerobic Co-bioreactor Bacterial Community Compositions at Phylum Level	178

BIBLIOGRAPHY 182

LIST OF TABLES

Table 2.1	Gene summaries of <i>R. solanacearum</i> GMI1000, <i>C. metallidurans</i> CH34, <i>R. pickettii</i> 12D and 12J.	30
Table 2.2	The abundance of Co-Zn-Cd, Cu, and Hg resistant genes in <i>R. pickettii</i> 12D and 12J, <i>R. solanacearum</i> GMI1000, and <i>C. metallidurans</i> CH34. . .	51
Table 3.1	Ecological indices of iFRC enrichment bacterial communities. O represents original soil sediment samples. Fe, NO ₃ , and U supplemented enrichment cultures.	78
Table A.1	Side-by-side genome comparison of <i>R. pickettii</i> 12D and 12J genetic elements by genomic scaffolds.	164
Table B.1	The composition of the modified FWM.	169
Table B.2	The composition of the mineral mix (100X).	169
Table B.3	The composition of the vitamin mix (1000X).	170
Table C.1	Ingredients for 200 ml of 5X Gitschier Buffer.	173
Table D.1	Measurements of sampling size and estimation of ecological indices of bacterial community in six anaerobic bioreactors. Calculations were based on the complete linkage clustering of chimera removed and trimmed bacterial 16S rRNA gene sequence alignments at 97% similarity. N represents the total number of non-chimera sequences that passed quality trimming. Shannon index (H') and Simpson's index (D) were expressed in $e^{H'}$ and 1-D, respectively to emphasize the differences. C represents the sampling coverage via gene targeted pyrosequencing.	176

LIST OF FIGURES

Figure 2.1	<i>R. pickettii</i> 12D genome scaffolds. The distribution of putative horizontally transferred genes (HGT genes) identified by JGI-IMG are marked as black dashes in rings 4-10. The scaffold sizes are in units of Mb. For interpretation of the references to color in this and all other figures, the reader is referred to the electronic version of this dissertation.	31
Figure 2.2	<i>R. pickettii</i> 12J genome scaffolds. The distribution of putative horizontally transferred genes (HGT genes) identified by JGI-IMG are marked as black dashes in rings 4-9. The scaffold sizes are in units of Mb.	35
Figure 2.3	Minimal evolution phylogenetic tree of β -Proteobacteria <i>dif</i> sequences. The numbers on branches are bootstrap values. The scale at the left hand lower corner represents the distance.	41
Figure 2.4	Filamentous phage p12J gene compositions and their homologs on <i>R. pickettii</i> 12D and 12J chromosomes. Fragments of the same fragments represent homologous genes. Genes colored yellow with a red border represent genes that share no homology to p12J Orf7 but are orthologs to each other. Grey colored fragments represent other phage related genes (not p12J related). White colored blocks are other non-phage related genes.	42
Figure 2.5	Genome synteny between <i>R. pickettii</i> 12D and 12J scaffolds. Panel A, 12D_C1, 12J_C1 and 12D_P2; Panel B, 12D_C2 and 12J_C2; Panel C, 12D_P3 and 12J_P1. Arrows indicate location of <i>oriC</i> on the chromosomes. Blocks with the same color represent the regions that are similar (connected by lines). The amount of color indicates the percentage of identity. White areas within the blocks indicate absence of a homologous sequence.	44
Figure 2.6	BLAST results mapped onto the 1.72 Mb-1.94 Mb region of <i>R. pickettii</i> 12J_C1. The top scale indicates the length of the query region. Similar genes are shown underneath the query sequence. The short thin black bars indicate that the next stretch of sequence is on the opposite strand of DNA.	47
Figure 2.7	Phylogenetic position of <i>R. pickettii</i> 12D and 12J <i>czcA</i> genes. The numbers on the branches represent bootstrap values.	54
Figure 2.8	Phylogenetic position of <i>R. pickettii</i> 12D and 12J <i>copA</i> genes. The numbers on the branches represent bootstrap values.	59

Figure 3.1	The concentration of Fe^{2+} (panels A and B), lactate and acetate (panels C and D) in each ferric citrate enrichment cultures. The first generation enrichments are presented in panel A and C and the second generation enrichments are presented in panel B and D. Error bars represent the differences between two replicates.	79
Figure 3.2	The top ten (summed across all samples) most abundant genera identified via RDP multiclassifier. Sample replicates were labeled as "_1" and "_2". Original soil sediment samples were denoted with "_O."	80
Figure 3.3	The shared genera among FW107 samples. The color of sample font is the same as the cognate ellipse.	81
Figure 3.4	The shared genera among FW102-2 samples. The color of sample font is the same as the cognate ellipse.	82
Figure 3.5	The shared genera among FW102-3 samples. The color of sample font is the same as the cognate ellipse.	83
Figure 3.6	The functional gene profiles of the original soil sediment and enrichment samples. The functional gene signals of all samples (columns) were standardized to the same amount. Each functional gene (row) was then scaled among all 21 samples to show the differences in abundance. Green indicates high abundance and red indicates low abundance.	85
Figure 3.7	NMDS analysis of NO_3^- enrichments (grey), Fe^{3+} enrichments (pink), U^{6+} enrichments (yellow), and original samples (green). Each ellipse was drawn around each group centroid based on a group distance standard error at 95% confidence level. The changes in genera abundances that drive comparative community differences are indicated with red arrows. The arrows point to the areas of high abundance. The red arrows indicate the abundance of genera that changed significantly ($P \leq 0.001$). The specific genera are shown in red according to the group labeling.	88
Figure 3.8	NMDS analysis of NO_3^- enrichments (grey), Fe^{3+} enrichments (pink), U^{6+} enrichments (yellow), and original samples (green). Each ellipse was drawn around each group centroid based on group distance standard error at 95% confidence level. The changes in functional gene (with the specific microorganism from which the probes were designed) abundance were correlated to the shifts observed in community structures. The red arrows indicate the abundance of functional genes that changed significantly ($P \leq 0.001$). The specific genera are shown in red according to the group labeling. The arrows point to the areas of high abundance.	89

Figure 3.9	NMDS analysis of NO_3^- enrichments (grey), Fe^{3+} enrichments (pink), and U^{6+} enrichments (yellow). Each ellipse was drawn around each group centroid based on group distance standard error at 95% confidence level. The changes in genera abundance were correlated to the shifts observed in community structures. The colored arrows indicate the abundance of genera that changed significantly (red: $P \leq 0.001$, blue: $P \leq 0.05$, and green: $P \leq 0.01$). The genera names are shown in the same color according to the group labeling. The arrows point to the areas of high abundance.	90
Figure 3.10	NMDS analysis of NO_3^- enrichments (grey), Fe^{3+} enrichments (pink), and U^{6+} enrichments (yellow). Each ellipse was drawn around each group centroid based on group distance standard error at 95% confidence level. The changes in functional gene abundance were correlated to the shifts observed in community structures. The red arrows indicate the abundance of functional genes that changed significantly ($P \leq 0.001$). The functional genes and the specific microorganisms from which the probes were designed are shown in the red according to the group labeling on the side. The arrows point to the areas of high abundance.	91
Figure 4.1	The removal of soluble U^{6+} in FW107 and FW102-2 enrichments. The high soluble U(VI) concentration in the control culture (No Cells) was due to the excess amount of uranyl acetate carried over from the syringe needle during inoculation.	106
Figure 4.2	Bacterial community shifts with the increasing of incubation time in FW107 U-PBAGW microcosm.	107
Figure 4.3	Bacterial community shifts with the increase of incubation time in FW102-2 U-PBAGW microcosm.	108
Figure 4.4	Distribution of [FeFe]-hydrogenase containing bacteria in FW107 and FW102-2 grown in 1/2X R2B media (U 0 days) and in uranyl acetate enrichments (U 64 days). The bacterial populations represented by the small fractions of each pie chart are listed on the right hand side with color blocks corresponding to the colors found in each pie chart. The distribution of genera <i>Clostridium</i> (cyan color) and <i>Desulfotomaculum</i> (purple color) are shown as the outer ring of each pie chart.	109
Figure 4.5	The phylogenetic distribution of the anaerobic isolates based on their 16S rRNA gene sequences. The numbers on the branches represent the bootstrap values (1000 permutations).	112
Figure 4.6	The growth curves of FRC isolates in 1/2X R2B under anaerobic condition ($\text{H}_2:\text{CO}_2:\text{N}_2$ 3:10:87). See next page for legends.	114

Figure 4.7	REP-BOX-(GTG) ₅ -PCR profiles of potential uranium immobilizing bacteria. Branches labeled Dhaf represent control samples. The rest represents enrichment isolates.	116
Figure 4.8	Soluble U ⁶⁺ removal by Firmicutes isolates (from FW107) and FW107 uranium enriched community after 70 hours (T70) of incubation at room temperature in an anaerobic chamber (H ₂ :CO ₂ :N ₂ 3:10:87). Sample "neg" represents a control culture without the addition of any bacterial cells. The error bars represent measurements of two replicates.	118
Figure 5.1	The total solids (TS) reduction efficiency (diagonal and grid lined columns) and the production rate of biogas (grey and white columns) in the DM and DM+CS bioreactors at four HRTs: a HRT of 30 days (HRT30d), a HRT of 40 days (HRT40d) and a HRT of 50 days (HRT50d). Solid diamonds and solid triangles represent the amount of methane produced in the DM and DM+CS bioreactors, respectively.	129
Figure 5.2	The abundance and diversity (OTU at 97% sequence similarity) of phyla Bacteroidetes (panel A1), class Clostridia (panel B1), and <i>Escherichia</i> / <i>Shigella</i> (panel C1) in each bioreactor bacterial community. The distribution of OTUs among samples are presented as Venn diagrams in panel A2 (Bacteroidetes), B2 (Clostridia) and C2 (<i>Escherichia/Shigella</i>). The colors of the bioreactor/HRT font corresponds to an area bounded by the same color. Labels HRT30d, HRT40d and HRT50d represent bioreactors with a HRT of 30, 40, and 50 days, respectively.	131
Figure 5.3	The abundance of phyla Bacteroidetes (vertical stripes) in each bioreactor bacterial communities. The distribution of classified and unclassified Bacteroidetes within phylum Bacteroidetes were calculated and displayed in left panel (white and diagonal striped bars) and right panel (black and gridded bars) respectively. Labels HRT30d, HRT40d and HRT50d represent bioreactors with a HRT of 30, 40, and 50 days, respectively.	142
Figure 5.4	The comparisons of Bacteroidetes clusters (97% sequence similarity) between the DM+CS bioreactor with a HRT of 40 days and other bioreactor samples. Labels HRT30d, HRT40d and HRT50d represent bioreactors with a HRT of 30, 40, and 50 days, respectively. Symbol * denote peaks that are clusters of unclassified Bacteroidetes that are highly abundant in all DM+CS bioreactors (#11 and #14), in DM+CS bioreactors at long HRTs (#43), and in the DM+CS bioreactor with a HRT of 40 days (#69).	144

Figure 5.5	The shifts of abundance of the three most abundant [FeFe]-hydrogenases containing bacterial groups in anaerobic bioreactors fed with DM and DM+CS. Labels HRT30d, HRT40d and HRT50d represent bioreactors with a HRT of 30, 40, and 50 days, respectively.	146
Figure 5.6	The abundance of [FeFe]-hydrogenase containing bacteria in anaerobic bioreactor samples compared to the abundance pattern of unclassified Bacteroidetes (background) determined by 16S rRNA gene sequencing. The distribution of clusters #11, #14, #43 and #69 were also plotted as part of unclassified Bacteroidetes within each sample. Labels HRT30d, HRT40d and HRT50d represent bioreactors with a HRT of 30, 40, and 50 days, respectively.	147
Figure 5.7	NMDS analysis of the bacterial community in anaerobic bioreactors (based on 16S rRNA gene sequences at 97% similarity cutoff). The green arrows indicate the increase of biogas production (Biogas), HRT (HRT) and dairy manure degradation rate (Degradation). The red and blue arrows indicate bacterial genera that shifted significantly, where $P \leq 0.001$ and $P \leq 0.01$, respectively. The black, yellow and purple arrows represent the [FeFe]-hydrogenase phylogenetic affiliations that shifted significantly ($P \leq 0.001$, $P \leq 0.05$, and $P \leq 0.01$, respectively). All arrows point towards the abundant range of the gradients. Labels HRT30d, HRT40d and HRT50d represent bioreactors with a HRT of 30, 40, and 50 days, respectively.	149
Figure 5.8	Diagram (adapted from Schink et al. [140]) of microbial corporation during methane generation in DM and DM+CS bioreactors operated at HRT 40 days. The thickness of the arrow represent the relative abundance of microbial populations possibly associated with the methanogenesis step.	151
Figure A.1	Distance tree of <i>R. pickettii</i> 12D and 12J in relationship to 23 other Proteobacteria based on their 16S rRNA gene sequences. The bar in the bottom left corner represents the distance scale.	163
Figure A.2	The sequence variations of <i>dif</i> sites of <i>R. pickettii</i> 12D and 12J. The consensus reveals the conserved the regions.	165
Figure A.3	Genome synteny of <i>R. pickettii</i> 12D and 12J revealed by a DNA sequence dotplot. Blue dots represent matching genes on the same direction strands. Red dots represent matching genes on the opposite direction strands. The scaffold nucleotide coordinates are ranked from left to right on the x-axis and bottom to top on the y-axis.	168

Figure B.1	Functional gene profiles of original soil communities and the enriched communities (replicate 1). Symbol "O" indicates original communities and "Fe", "NO ₃ " and "U" indicate supplemented electron acceptors in enrichments.	171
Figure C.1	Standard curve of the uranium-azide assay. The error bars represent data from two replicates.	172
Figure C.2	The growth curves of FRC isolates (first replicate) in minimal media supplemented with sodium pyruvate alone (blue) and minimal media supplemented with sodium pyruvate and uranyl acetate (red) under anaerobic condition.	174
Figure C.3	The growth curves of FRC isolates (second replicate) in minimal media supplemented with sodium pyruvate alone (blue) and minimal media supplemented with sodium pyruvate and uranyl acetate (red) under anaerobic condition.	175
Figure D.1	Estimation of community coverage by rarefaction analysis. Rarefaction curves of anaerobic bioreactor 16S rRNA gene sequences were constructed based on the estimation of OTUs and ChaoI indices at 97% similarity.	177
Figure D.2	The distribution of the top three most abundant phyla (wide columns) in bioreactor samples. The narrow columns represent the abundance of genera <i>Escherichia/Shigella</i> (checker box), group unclassified Bacteroidetes (diagonal stripes) and class Clostridia (blacks) in each community.	180

CHAPTER 1

INTRODUCTION

Environmental engineering technologies frequently take advantage of microbial communities and populations. My dissertation is focused on the investigations of microbial communities involved with bioremediation of metal contaminated sites and the anaerobic digestion of farm waste. In both cases, increasing our knowledge base regarding the microbial communities that are instrumental in each of these activities is critical to efficient remediation and long-term management. In this background section I will first discuss bioremediation of metals followed by anaerobic digestion of farm wastes.

1.1 Bioremediation of Metals

Metals are naturally occurring elements that are important components of the earth's crust and have played significant roles in the development of human civilizations. The discovery and utilization of metals signify the development of different culture eras associated with the history of human civilizations, the Bronze Age, the Iron Age, the Steel Age, and finally the Nuclear Age. Each era is represented by the mining and smelting of a particular metal ore, e.g., Cu, Fe, iron alloys, and U. As the primary method to expose and collect metals in the earth crust, mining became one of the most important industries in human history [55].

Although the development of mining was instrumental in the evolution of human civilizations, mining does massive damage to the environment. Commonly known issues such as land erosion and formation of sinkholes may accompany mining processes. The toxic

chemicals (e.g., sulfuric acid, cyanide, alkyl xanthate salt) used during mining to enrich specific metals (e.g., Cu, Au) can contaminate surrounding soil, surface and subsurface water bodies. The metal-containing tailing solutions along with naturally occurring oxidation on exposed metals, can mobilize metals from the earth's crust and cause further contamination of the surrounding environment via river and aquifers. Although the toxicity of metals varies, ingestion of soluble metals, especially heavy metals, can be life threatening. Hence, the immense impact of mining on biodiversity and ecosystems cannot be ignored.

The mobility and toxicity of metals in the environment are controlled by local acid-base and redox reactions. Shifts in pH can largely influence metal mobilities. Take the most abundant transition metal, iron, as an example. Oxidized iron (Fe^{3+}) precipitates as $\text{Fe}(\text{OH})_3$ or other Fe^{3+} minerals at near-neutral pH but it becomes more soluble when pH decreases. Therefore, Fe^{3+} is mobile in acidic environments. Environmental redox reactions control the formation and dissolution of minerals. For example, iron can be oxidized to Fe^{3+} by exposure to oxygen. In the presence of sulfide or reduced humics, Fe^{3+} can be readily reduced to Fe^{2+} . At neutral pH, Fe^{2+} is much more soluble than Fe^{3+} . Hence, in the form of Fe^{2+} , iron can be readily absorbed by living organisms. For this reason, Fe^{2+} is more toxic than Fe^{3+} at near-neutral pH [8].

Bacteria contribute substantially to metal mobility and toxicity. The growth of bacteria can change local pH. Through metabolic processes, such as denitrification, bacteria can increase the pH of local environments. When this pH shift occurs in an acidic habitat, the precipitation of metal ions would occur due to the increase of pH [187]. Also through metabolic processes, such as oxidation of pyrite by *Acidithiobacillus* species, bacteria can decrease the pH of the local environment. This decline of pH may result in metal leaching from

rocks increasing the mobility and toxicity of heavy metals [54]. Bacteria can also physically reduce the concentration of mobile metal ions via biosequestration. Due to their large surface to volume ratios and the composition of the cell envelopes, bacteria (alive or dead) can naturally absorb mobile metal ions [178]. Studies have also shown that some bacteria can sequester a large amount of metals in the outer envelope of the cell and thus remove metal ions from aqueous solution [90, 136, 191]. Finally, bacteria play an essential role in environmental redox processes. Some bacteria can derive energy by transferring electrons from organic carbon or inorganic compounds to electron acceptors, including transition metals, metalloids and actinides. Studies have demonstrated that anaerobic bacteria, such as *Geobacter metallireducens*, *Shewanella oneidensis*, and *Desulfuromonas acetoxidans*, can dissimilatorily reduce metal ions (e.g., from Fe^{3+} to Fe^{2+}) under anoxic conditions [65]. These indirect and direct interactions between bacteria and metals have been observed across a wide spectrum of heavy metals, including Mn, Cu, Cr, Co, Hg, and U. The unique attributes of bacterial metal sequestration and immobilization have been cultivated by environmental engineers for remediation of metal contamination.

1.1.1 Biosequestration of Metals

Biosequestration of metals herein refers to metal adsorption and accumulation by either live or treated bacteria. Biosorption usually refers to the passive binding of metals to biological materials. The sorptivity of metals by the cell envelope is independent of active metabolism but directly related to sorbent surface area. The composition of the bacterial cell envelope also contributes greatly to metal specificity and binding affinity [139]. Due to their small sizes, bacteria naturally have high surface to volume ratios. *Escherichia coli* cells achieve

a surface area of over 21 m²/g dry cell weight [108, 158]. With appropriate treatments, including physical crushing, treating and caustic treatment, bacterial biomass can be an efficient adsorbent [177]. Indeed, treated bacterial cells are preferred over live bacterial cells because of convenience (e.g., little maintenance cost and easy to transport). The term bioaccumulation refers specifically to metabolism-dependent metal uptake. While some metals at trace levels are required to maintain life (e.g., Se, Cu, Fe), toxic effects can be observed in bacteria when large amounts of metals are present. Research has shown that 500 μ M of Cu²⁺ (0.125 g/L) is toxic to *E. coli*. The ability to grow at elevated levels of copper are largely due to resistance mechanisms including bioaccumulation, membrane bound e-flux pumps and metal transporters [147]. The active metal accumulation process is primarily driven by efflux pumps that relocate metals from the interior to the exterior of cells. Active bioaccumulation is likely to be slower than biosorption and subject to growth condition, such as narrow ranges of pH, temperature and salt content. However, bioaccumulation has a great potential in metal remediation because living metal sequestering bacteria have high specificity in metal binding and can regenerate biomass via growth [95].

Biosequestration can be practically applied in metal removal/recovery from industrial waste streams [177]. Wastewater produced from various industries, including mining, leather working, energy production, and electroplating, contain different heavy metals. Discharging this waste into the environment poses serious risk (e.g., toxic metals like Hg and radioactive metals like U) as well as being a waste of resources (e.g., precious metals like Au). Conventional methods like chemical precipitation and coagulation are able to reduce metal concentrations in waste streams only down to the mg/L level. Ion-exchange techniques can remove and recover metals from wastewater to μ g/L levels, however, the cost of exchange

resins is high and the resins are prone to poisoning by organics and solids in the wastewater. Membrane-based processes (e.g., reverse osmosis) are effective at obtaining pure effluents but are extremely expensive for at large flow rates and they are prone to failure as a results of membrane fouling [81, 177]. Compared to conventional metal removal/recovery methods, biosequestration offers several potential advantages and may offer the potential of a cost-effective alternative method. Bacterial biomass can be relatively inexpensive and can serve as a sink to all metals except the alkali cations (e.g., Na^+ and K^+). Biosorbents developed from bacteria biomass have a broad range of metal binding affinities that could be exploited in selective metal removal/recovery. For example, Ogi et al. showed that *Shewanella algae* can be used in rare metal indium recovery from solutions at low concentrations. This study revealed that at pH 3.8, *S. algae* cells were able to remove 100% of the soluble indium in solution at concentrations up to 0.2 mol/m^3 (229 mg/l). Indium concentrates could be prepared from indium bound to cells by burning at approximately at 800°C [115]. Several species of the genus *Bacillus* have shown to be effective at removing Cu and Pb from aqueous solutions [122, 165, 133]. As reported by Tsuruta, *Arthrobacter* sp., *Bacillus* sp. and *Lactobacillus* sp. isolated from uranium deposits removed 10.9-98.3% of U in solution. Some of the *Lactobacillus* isolates were able to remove uranium from seawater as well. A selective accumulation study conducted using one of the *Arthrobacter* isolates revealed that UO_2^{2+} is preferentially accumulated over six other metal ions including Cu^{2+} , Mn^{2+} , Co^{2+} , Zn^{2+} , Cd^{2+} and Ni^{2+} [164]. Although biosequestration is still under development and has not yet been applied to real wastewater treatment problems, these initial studies suggest that biosequestration could be a viable process.

1.1.1.1 Metal Contamination at Torch Lake

Torch Lake, located in Houghton county, MI, has been on the National Priorities List since 1986. The area formerly known as the Copper Country, was well-known for its metallic copper ore that was extensively mined from 1890's to 1969. During the mining period, the 2,700 acre Torch Lake served as a waste disposal site for milling, smelting and leaching chemicals and by-products. The U.S. Environmental Protection Agency estimated that approximately 20% of the lake volume was made up of copper mill stamp sands (~200 million tons). It was also estimated that the contaminated sediments are up to 70 ft deep and contain up to 5,500 ppm of copper. The ecosystem around the lake was further damaged by a cupric ammonium carbonate (a common herbicide) spillage (~27,000 gallons) in 1972 and the disposal of industrial processing water, which contained copper and ammonium that are 2,400 times and 100 times of the local sewage allowable limits, respectively, in the early 1980's. With the discovery of extensive ecological degradation and three impairments of beneficial use (fish tumors, degraded benthos and fish consumption advisories), Torch Lake was also enlisted as a Great Lakes Areas of Concern in 1987. The area has been under remediation construction since 2003. While tumorous fish were no longer captured, the recovery of the area is minimal [169].

1.1.1.2 Adaptation of *Ralstonia pickettii* in High Copper

Eleven *Ralstonia pickettii* strains were previously isolated from the highly contaminated Torch Lake sediments, where copper concentration ranged from 1,000 to 2,500 ppm. Previous studies revealed that all eleven *R. pickettii* isolates were Cu resistant, while seven of

them were also resistant to Zn and Cd and the rest were resistant to Ni and to low levels of Cd. Konstantinidis et al. [80] observed that the colonies of these *R. pickettii* isolates obtained a greenish blue color when growing on copper supplemented agar plates. It was hypothesized that these isolates could uptake copper from the medium and deposit it in the outer cell envelope [80]. Scanning electron microscopy (SEM) and transmission electron microscopy (TEM) supported this hypothesis and revealed drastic changes to the cells when the isolates were grown in the presence of copper, including a substantial increase of the amount of extracellular material and the deposition of high-density materials in the outer envelope. Electron diffraction scanning of the copper-grown cells revealed the presence of a large amount of copper, which was not observed in the cells grown in the absence of copper. X-ray absorption near edge structure (XANES) and Extended X-ray absorption fine edge structure (EXAFS) analyses suggest that the cell associated copper is likely to be an organic bound tetrahedral cupric complex and the copper sequestration process is not via (hydr)oxide mineral precipitation [191]. A systematic copper sequestration study revealed that the isolate representatives *R. pickettii* strain 12D (Cu-Ni-Cd resistant) and strain 12J (Cu-Zn-Cd resistant) are well adapted to the high copper environment and the binding mechanisms were different between the viable and heat-killed cells. The live cells can actively sequester copper up to 27.44 (12D) and 38.19 (12J) mg Cu/g dry weight of cells, which is 1.5 to over 2 times more than what heat-killed 12D and 12J cells adsorb. The study also suggests that distinct binding/transporting mechanisms are involved in copper sequestration by live *R. pickettii* 12D and 12J cells and that live 12J cells bind significantly more copper than live 12D cells [191]. These attributes suggest that *R. pickettii* strain 12D and 12J may be exploitable in the remediation of copper.

From the copper sequestering studies performed on *R. pickettii* strain 12D and 12J, we concluded that the active uptake of copper by living *R. pickettii* cells is likely a display of a detoxification process associated with metal resistance systems. In a 2005 review, Silver et al. noted that bacteria developed metal resistance systems to overcome the toxicity of various toxic metal ions, including Zn^{2+} , Ni^{2+} , Cu^{2+} , Cd^{2+} , Co^{2+} , and Hg^{2+} . The majority of these systems function as energy-dependent (e.g., ATPase and chemiosmotic ion/proton exchange) efflux pumps and some also involve metal-binding proteins. For example, a classic Cd^{2+} , Zn^{2+} , and Co^{2+} resistance system (Czc) is a polypeptide chemiosmotic system. It is comprised of membrane polypeptide chemiosmotic efflux pumps, inner and outer membrane proteins, and periplasmic coupling proteins to form channels between the cytoplasm and outside of cells. To reduce metal toxicity, this system utilizes a proton gradient to transfer excess amounts of Cd^{2+} , Zn^{2+} , and Co^{2+} from inside to outside of the cell [147]. Exploiting the mechanisms of metal resistance will increase our understanding of how bacteria adapt and thrive in high metal environments. This information is also important in evaluating the potential and optimizing the ability of live bacterial cells in removing/recovering metals from industrial wastewater.

One can envision a number of mechanisms for the acquisition of metal resistance, including the gradual selection of point mutations to develop a new functionality, the duplication/amplification of existing metal resistance genes to increase resistance level, and the acquisition of additional resistance determinants via horizontal gene transfer. Point mutations occur randomly and take a long period of time to evolve a new function from an old one. Starting from small genetic modifications, point mutations alter a single base at a time. Many point mutations are synonymous and therefore will not change the amino acids, which

determine genetic functions. Slowly, point mutations may accumulate and eventually change the amino acids and modify the old function. This process may accelerate under selective pressure in that suitable mutants adapt to the new environmental factors better [92]. In conclusion, point mutation is a prolonged process for evolving a completely new function. Unlike point mutations, gene duplication and amplification (GDA) allows bacteria to gain resistance rapidly [135]. GDA, described by its name, allows a bacterium to evolve by duplicating its own existing resistance determinants. This mechanism confers increased levels of resistance by increasing the number of metal resistance gene copies, thereby increasing the levels of metal resistance gene expression [135]. Bacteria can also obtain new functions from other bacteria (sometimes across species, genus, even domain boundaries), referred to as horizontal gene transfer (HGT), through transformation (foreign gene direct uptake), transduction (foreign gene insertion by bacterial phages), and conjugation (plasmid transfer via cell-cell contact). Both GDA and HGT provide a road to rapid acquisition of resistant genes. Because they both depend on existing resistance determinants, GDA and HGT are distinguishable on a sequenced genome. The presence of plasmids or phage indicates that HGT may have occurred via conjugation or transduction. A stretch of genes on a bacterial genome with different guanosine/cytosine (GC) content compared to the rest of the genome also can be used to detect putative foreign genes inserted. Similarly, the possible occurrence of GDA could be identified by finding multiple copies of the same gene, frequently repeated in tandem, in a genome. It is also possible that HGT of the same gene occurred several times, which would result in multiple copies of the same gene on chromosome. To confirm GDA and differentiate from HGT, one has to rely on phylogenetic analyses of gene copies to reveal the evolutionary lineages of each copy [92, 114, 135].

We have demonstrated that *R. pickettii* strain 12D and 12J have a great potential in copper removal/recovery from wastewater streams. It has also been shown that these two strains shared similar attributes (e.g., same species, ability to thrive in high copper environments, and active sequestration of copper) but have important differences (e.g., different genome sizes, 12J is resistant to Zn but not Ni, 12D is resistant to Ni but not Zn, 12J grows better in the presence of copper and sequesters more copper than 12D). Hence, these two strains are great model organisms for studying how genetic element variations influence the manifestation of biosequestration by living bacteria. Konstantinidis et al. previously observed that *R. pickettii* 12D and 12J are resistant to multiple metals [80]. Therefore, it is likely that these two bacterial strains obtained multiple metal resistance systems. From both metal resistance and copper sequestration studies, we observed that *R. pickettii* 12D and 12J are different both genetically and physiologically. It was observed that these two strains belonged to different genomovar groups and strain 12J appeared to adapt to high copper environment better than strain 12D [80, 191]. Hence, we suspect that *R. pickettii* 12D and 12J either acquired different metal resistant determinants or developed different regulation mechanisms during evolution. In their 2009 review, Sandegren et al. suggested that GDA is a common adaptive mechanism of bacteria to various antibiotics [135]. Chan et al. observed that GDA and HGT contributed greatly to the development of virulence, antibiotic and metal resistance among *Staphylococcus* isolates [21]. Thus, as an adaptation mechanism, we expect that GDA and HGT played a substantial role in *R. picket* 12D and 12J.

1.1.2 Bioimmobilization of Metals

Besides biosequestration, metals also can be removed from aqueous solution via bioimmobilization. Bioimmobilization of metals herein refers to 1) co-precipitation of metals and metabolic by-products and 2) precipitation of metals via dissimilatory reduction. Co-precipitation of metals and bacterial metabolic by-products describes a chemical process where soluble metal cations combine with sulfides [82, 183] or phosphate compounds to form insoluble metal complexes [130]. Large amounts of sulfide in the subsurface result from the reduction of anthropogenically deposited sulfate (e.g., mining). Anaerobic sulfate-reducing-bacteria (SRB) obtain metabolic energy ($\delta G = -190$ kcal/mol) by reducing sulfate to sulfide. Sulfide is subsequently complexed with soluble heavy metal ions to form precipitates [121]. Besides sulfide, biogenic phosphate has been observed to be effective in bacterial cell associated metal precipitations. Phosphate is liberated from bacterial storage polyphosphate (e.g., *Acinetobacter* spp., *Citrobacter* sp.) via phosphatase activities when the growth condition changes, such as changing from aerobic to anaerobic metabolism [9, 91, 97]. Research has revealed that with the presence of soluble heavy metals, the secreted phosphate forms cell-bound metal-phosphate precipitates [9, 91, 97]. Co-precipitation of heavy metals occurs in accord with the chemistry solubility rules and it does not change the oxidation state of metal ions. Compared to co-precipitation of metals and metabolic by-products, metal precipitation via dissimilatory reduction changes the oxidation state of metal ions directly via redox reactions. Similar to the conversion of sulfate to sulfide, anaerobic bacteria conserve energy by enzymatically transferring electrons to metals ions. While the reduced form of iron (Fe^{2+}) and manganese (Mn^{2+}) are more bioavailable than their oxidized forms (i.e., Fe^{3+}

and Mn^{4+}), other heavy metals are more insoluble in the reduced state (e.g., Se^{6+} VS. Se^0 , Cr^{6+} VS. Cr^{3+} , U^{6+} VS. U^{4+}). The dissimilatory reduction and precipitation of heavy metals immobilizes metals *in situ* without additional growth requirements, such as the presence of sulfate and the need of changing growth conditions. However, the disadvantage of this dissimilatory metal reduction is that the reduced metals can readily be reoxidized to their oxidized state by the exposure to oxygen. In contrast, the co-precipitates of heavy metal and sulfide or phosphate are relatively stable in the presence of oxygen. These metabolism dependent characteristics of bioimmobilization are particularly attractive to *in situ* subsurface metal remediations for it is sustainable and relatively inexpensive for a large area.

1.1.2.1 Metal Contamination at Oak Ridge Reservation

Historical weapons development and improper disposal of inorganic, organic and radioactive wastes have caused extensive areas of subsurface contamination at the Oak Ridge Reservation site (Oak Ridge National Laboratory, TN). For 31 years, the unlined S-3 pond was used to store these toxic wastes. It was later discovered that much of the original contaminants are now associated with soil and subsurface sediments and became secondary contaminant sources encompassing an expanding area. The challenge of remediation at Oak Ridge Integrated Field Research Challenge (iFRC) site is the combination of mixed contaminants, large subsurface area and low pH environment. The wide-spread contamination of both soil and groundwater makes traditional remediation methods, including *in situ* containment and solidification, mechanical separation, and pyrometallurgical processes, unfeasible [106]. While the low pH environment is not favorable for either chemical remediation or bioimmobilization, increasing pH *in situ* would cause the precipitation of aluminum and calcium

and result in clogging of subsurface pores. In addition, denitrification is likely to occur if growth conditions are optimized because of the high concentration of nitrate (133 mM) in the groundwater. *in situ* denitrification should be avoided because bacteria will preferably use nitrate rather than U^{6+} and hence inhibit uranium reduction [187].

Wu et al. [187] explored the approach of combining *ex situ* denitrification and *in situ* bioimmobilization by installing a nested recirculation system at the Oak Ridge iFRC S-3 site. The system creates a pH neutral zone by pump and treat, where groundwater is extracted for above-ground pH adjustment, removal of clogging agents and bulk denitrification. To maintain required flow rates, treated water was mixed with tap water prior to reinjection. The biostimulation zone is located in the center of the pH neutral zone, where ethanol was injected as a carbon source and electron donor for bioimmobilization of uranium [187]. The system was able to maintain a stable near-neutral pH for over 500 days. In addition to removing bulk Al^{3+} , Ca^{2+} , and nitrate, flushing also reduced soluble uranium from over 100 μM to $\sim 2-7 \mu M$ in 69 days. Soluble uranium concentration in the biostimulation zone persisted at around 5 μM until day 177 due to the presence of residue nitrate but decreased to less than 1 μM by day 268 and to levels below EPA drinking water standard (0.126 μM) after 2 year of stimulation. Meanwhile, the uranium content in the biostimulation zone soil increased accordingly and mixed U^{6+} and U^{4+} were detected via x-ray absorption near-edge structure spectroscopy (XANES) [188]. Bacterial community studies of the biostimulated soil revealed iron reducing bacteria (FeRB), sulfate reducing bacteria (SRB) and denitrifiers were grown in the treatment area. Bacteria belonging to groups that were previously identified as uranium reducers (e.g., *Geobacter*, *Clostridium*) were abundant in the stimulation zone. Cardenas et al. also observed that the abundance of the SRB group (e.g., *Desulfovibrio*,

Desulfosporosinus) followed the U^{6+} reduction pattern and suggested that SRB played a prominent role in uranium immobilization at Oak Ridge iFRC site [16, 17].

1.1.2.2 Bacterial Community Profiling

Field studies conducted at Oak Ridge iFRC site proved that *in situ* bioimmobilization of uranium is a suitable strategy. However, complex field conditions complicate the identification of uranium immobilizing bacteria due to the presence of other metals and minerals. It was also extremely difficult to study the interactions between different bacterial strains in response to the presence of uranium. Hence, we took the approach of enriching uranium immobilizing bacterial consortia from the iFRC and anaerobically isolating potential uranium immobilizers in the laboratory.

1.1.2.3 Reconstruct Uranium Immobilizing Bacterial Communities

In general, microbes exist as communities in the environment, where the diversity of species reflects the diversity of nutrients and the abiotic conditions. In such a diverse community, interactions between species is complex and includes mutualism, commensalism, competition and parasitism. One of the most studied relationships is the syntrophism between bacteria and archaea in methanogenesis. The *Methanobacillus omelianskii* culture Barker et al.[140] isolated was identified later as a co-culture of S strain and M.o.H strain. The two strains could not be separated because each strain depended on the other under the isolation conditions. Strain S ferments ethanol and strain M.o.H scavenges H_2 produced by strain S. The collaborative process generates methane as well as 112 kJ of energy per mole of methane produced [140]. Besides methanogenesis, Kato et al. [74] reported a mixed-culture composed

of cellulolytic *Clostridium* and non-cellulolytic bacteria that can degrade lignocellulose more effectively than isolates. The study showed that it is critical to have non-cellulolytic bacteria scavenge cellulose derivatives and metabolites, maintain the anaerobic condition, and neutralize the pH of the system. It was also revealed that not all non-cellulolytic isolates contributed to cellulose degradation [74]. A further study by the same group showed that the four strains in the assembled cellulolytic community formed a complex network [75]. Besides the collaborative effort on consuming metabolites, a recent study demonstrated that electrons can also be transferred between two different bacterial species. Kato et al. co-cultured *Geobacter sulfurreducens* and *Thiobacillus denitrificans*. The study showed that *G. sulfurreducens* transferred electrons from acetate to *T. denitrificans*, where the electron was further passed onto nitrate to produce ammonia [76]. These studies suggest that microbial interactions and cooperations are important and cannot be ignored in engineered microbial systems.

Uranium immobilizing bacterial communities have been studied using two approaches: bottom-up and top-down. A bottom-up approach refers to the strategy of studying the system from individual components, where individual bacterial species are isolated and studied separately. Under strictly controlled conditions, one can determine the uranium immobilization ability of individual bacterial isolates. This approach is effective in understanding cell physiologies of each microorganism. However, the bottom-up approach suffers from a focus on strains that are easily cultivated while neglecting the often more numerous and difficult to cultivate strains. A top-down approach is also used in studying uranium immobilizing communities in order to correlate the total diversity of the community using cultivation-independent techniques with the abiotic conditions (e.g., pH, uranium concentration, etc.).

This community information is used to tentatively identify the important bacterial species responsible for uranium immobilization. This approach is extremely powerful because the cultivation-independent approach reveals nearly all populations. However, top-down approaches cannot be used to precisely evaluate population functions due to the large number of variables and in addition, physiology does not always follow phylogeny. Zengler et al. made the point that both top-down and bottom-up approaches should not be treated separately but, rather, should be integrated [193]. It was suggested that bacterial community analyses should be used as a guide for cultivation and in-depth understanding of individual populations. In return, the comprehensive understanding at the cellular level would assist in prediction of complex biological systems.

Integrating the two approaches, reconstruction of uranium immobilizing bacterial communities would give insights on population interactions in uranium bioremediation systems. As part of my dissertation, I investigated the uranium immobilizing bacterial communities with a top-down approach. I also cultivated individual bacterial isolates and studied their abilities in uranium immobilization.

1.2 Bioremediation of Agriculture Wastes

Agriculture is a significant part of the US economy. The Food and Agriculture Organization of the United Nations (FAO) estimates that approximately \$0.2 trillion worth of production (0.67 billion tons) was contributed by agriculture in the US alone in 2010. The top three produced commodities based on value were indigenous cattle meat, dairy products and maize. Maize was also the most abundantly produced based on quantity (at least three times more

than other commodities) in the US in 2010. The large level of agricultural production resulted a contaminant amount of waste production. Approximated 6.7 million tons of agriculture wastes were produced in 2010 in the US (estimated based on 1993 facts) [44]. The consequence of improper treatment and disposal of agricultural wastes can be serious. Manures produced by diary and swine farms often contain human pathogens and can be life threatening if the wastes come into contact with water sources. The direct disposal of wastes that are rich in nutrients into the environment can alter the local ecosystems, causing for example, algal blooms. Crop wastes, such as corn stalks are much harder to degrade due to their lignin and cellulose content. Under strict regulations, wastes may be recycled by applying them to fields as fertilizer or they can be used to generate biofuels (e.g., bioethanol). Currently, the most common treatments for agricultural waste are composting and lagoons [166]. Although the typical farm waste management strategy includes waste storage and decomposing, it does lead to concerns regarding air and water quality and greenhouse gas emissions [46].

Methane is a potent greenhouse gas and has a unique role in global climate change and carbon cycling. Petit et al. [125] revealed the high correlation between temperature variation and atmospheric green house gas concentration from the Vostock ice-core record. The past 420 kyr of record also suggested that the present day atmospheric CH_4 concentrations are unprecedentedly elevated [125]. As the main component of natural gas, methane is naturally produced by syntrophic microorganisms (i.e., hydrogen producing bacteria and methane generating archaea) during degradation of organic matter via anaerobic methanogenesis [6, 140]. Methanogenesis generates the least amount of energy ($\sim 15\%$ of aerobic degradation of the same organic molecule) and occurs as the last step in microbial anaerobic respiration.

Methane production is common in organic-rich sediments [140]. Bastviken et al. [6] estimated that the global freshwater methane emission rate corresponds to at least 0.65 Pg of C (CO₂ equivalent, assuming 1 kg of CH₄ equals to 25 kg of CO₂ over a 100 year period). Besides the naturally emitted methane, anthropogenic methane emission rose substantially along with the development of industry. Stern and Kaufmann [153] estimated that the total amount of global methane emitted from anthropogenic activities increased from 79.3 Tg in 1860 to 371 Tg in 1994 (0.5 Pg and 2.3 Pg CO₂ equivalent C, respectively). Over 50% of this was emitted from agricultural activities including livestock production and rice farming [153]. While the terrestrial land surface has been considered an important carbon sink (2.6 ± 1.7 Pg of C), the amount of natural and anthropogenic methane emissions offsets the continental green house gas balance. Thus the impact of global methane emission rate on global climate change should not be overlooked [6].

Besides being a major contributor to global climate change, methane is also an alternative energy source for heat and electricity [46, 78]. With decreasing of fossil fuel discovery rates, the need for renewable energy source increases [15, 66]. Anaerobic digestion of farm wastes not only eliminates some of the environmental concerns of traditional farm waste management methods, such as odor and water contamination, it also can be used to generate and capture methane rich biogas. However, system optimization is critical for anaerobic digestion. Operational parameters, including temperature, HRT, and the carbon to nitrogen ratio of the substrate have been studied extensively [42, 46, 110, 120]. While these studies provide insights on maintaining an efficient anaerobic bioreactor, the microbial communities and species interactions responsible for methane production are not well understood. In this section, I will focus on studying the microbial community aspects of methane producing

anaerobic co-bioreactors.

1.2.1 The Role of Class Clostridia in Methane Producing Anaerobic Co-bioreactors

Anaerobic methanogenesis is a group effort between bacteria and archaea. Methanogens, a group of archaea, are primary responsible for methane production. However, the process cannot be carried out without the help of bacteria [6, 140]. Schink et al. [140] noted in a recent review that methanogenic degradation of complex organic matter involves a mutual dependency of five groups of microorganisms, primary fermentative bacteria, secondary fermentative bacteria, homoacetogenic bacteria, hydrogen oxidizing methanogens, and acetate-cleaving methanogens. The concentration of hydrogen in the system plays a critical role in determining how methane is produced. When the hydrogen partial pressure is less than 10^{-4} bar, majority of the methane is generated exclusively via the cooperation of primary fermenters and either H_2 oxidizing methanogens or acetate cleaving methanogens. Under conditions where hydrogen accumulates in the system (e.g., excess substrate), the secondary fermenters and homo-acetogenic bacteria contribute to methane production by converting hydrogen to acetate. This alternative process shifts the methane producers from hydrogen oxidizing methanogens to acetate-cleaving methanogens [140].

Bacteria class Clostridia categorizes a group of anaerobic bacteria with versatile metabolic pathways. Species belonging to this class are noted for their ability to ferment various substrates, including saccharides, amino acids, and cellulose. Cellulose degradation is particularly relevant as it is a major component of plants. Thus, it is widely abundant, rich in carbon and yet difficult to decompose. Studies have shown that several *Clostridium* species can decompose and partially hydrolyzed cellulose [36, 74]. Interestingly, many

members of Clostridia are also homo-acetogens, such as *C. methoxybenzovorans*, *C. thermoautotrophicum* and *C. thermoaceticum*. These attributes of class Clostridia suggest that this group of bacteria may play a substantial role in anaerobic degradation of agricultural wastes and methane generation. In fact, research studies have repeatedly reported that Clostridia populations were abundant in hydrogen and methane producing anaerobic bioreactors [23, 116, 119, 126, 179]. Bacterial hydrogen production from protons and electrons is catalyzed by hydrogenases. There are two major groups of hydrogenase, [FeFe]-hydrogenase and [NiFe]-hydrogenase, which is composed of two iron atoms and one iron and one nickel atom, respectively. The two groups of hydrogenases are phylogenetically different. While [NiFe]-hydrogenases widely occur in bacteria and archaea, [FeFe]-hydrogenases are found only in anaerobic bacteria and eukaryotes [11, 103]. It is known that [NiFe]-hydrogenases are more abundant in bacteria than [FeFe]-hydrogenase. However, it was suggested that most of [NiFe]-hydrogenases are involved in hydrogen uptake. This is consistent with the observation that [NiFe]-hydrogenases are often found in hydrogen consuming bacteria [10, 176]. In contrast, [FeFe]-hydrogenase is 10-100 times more active than [NiFe]-hydrogenase and energetically prefers to catalyze the reduction of protons to produce hydrogen [47, 189]. Therefore, I hypothesize that class Clostridia is a substantial player in anaerobic co-bioreactors and is the dominant bacterial group in methane producing anaerobic co-bioreactors.

1.3 Managing Complex Microbial Communities for Sustainable Environment

Microorganisms reside in various environments, such as soil, water, air, and the intestines of living organisms. Among all microorganisms, bacteria and archaea are highly abundant

on earth. Whitman et al. estimated that there are $4\text{-}6\times 10^{30}$ bacteria and archaea cells in terrestrial and marine environment [184]. It was estimated that there are at least 4.5×10^6 different bacterial species globally and 2×10^4 platonic marine archaea taxa [31]. These bacteria and archaea are the important components of primary global productivity (e.g. photosynthesis) and geochemical cycling. To date, approximately 2.9×10^5 bacterial and archaeal strains have been isolated and approximately 1.3×10^4 bacterial and archaeal taxa have been identified [40]. The bacterial and archaeal diversity we have discovered is less than 0.3% of the total diversity based on conservative estimates. Although our knowledge is still limited, studies have shown that microbial communities are valuable resources and effectively managing these resources are the essential to a sustainable environment [175].

Human beings has taken advantage of microbial systems for millennia, dating back to early wine and cheese making. More recently we have used bacterial communities and populations to remediate organic wastes, produce commodity chemicals and contain subsurface contamination. Understanding the interactions among microbial populations is a vital step in managing microbial resources. Microbial populations react to system changes and undesirable shifts in a microbial community can result in system failures. As an example, sludge bulking in wastewater treatment plants is caused by the excessive growth of filamentous microorganisms in activated sludge. While the presence of filamentous microorganisms helps in the degradation of organic matter, when abundant, filamentous microorganisms prevent activated sludge from settling, resulting in failure of the wastewater treatment system [61, 131]. Recent advances in our understanding of the human microbiome also suggest that the changes in composition of bacterial communities, which reside in different parts of human body, can alter human health [4, 127, 150, 173]. Microbial ecology studies the micro-

bial population interactions, community structures and interactions with the environment including changes due to external factors. Knowing more about these interactions will help us to better utilize microbial resources and control engineered systems.

Each topic of my dissertation involves a different microbial community with a unique energetic strategy. The lake sediment community of Torch Lake has been under extreme pressure from unnaturally high contamination of metals and the *R. pickettii* strains isolated from these sediments are uniquely adapted to high copper concentrations. Thus, these strains can provide insight into how microbial populations adapt to high metal concentrations. The sediment communities of Oak Ridge National Laboratory iFRC sites have responded to metal, acid and hydrocarbon contamination and many strains isolated from these communities can immobilize uranium. We have extended the community analyses of these sediments, as well as identified new strains capable of uranium immobilization. This work contributes to our understanding of the interactions between uranium and microbial populations and provide insights to *in situ* bioremediation of uranium. Finally, The microbial community of an anaerobic bioreactor managing farm waste has a complex community of bacteria and archaea that removes organic matter and generates methane. We have identified a community structure that correlates with production of a large amount of methane. In each instance, knowing the conditions under which the community operates optimally is advantageous to the engineer. By "optimally" we refer to an outcome that is successful for long-term bioremediation and sustainability. In most cases knowing first, who is there (i.e. what species are present and their growth preferences) and second, what is the metabolic strategy of the community, can assist engineers in designing and controlling an environment that imposes sufficient constraints on the community such that it becomes predictable. Successful

management requires predictable outcomes.

CHAPTER 2

CO-EVOLUTION OF *RALSTONIA PICKETTII* STRAIN 12D AND 12J: GENOME REARRANGEMENTS AND THEIR INFLUENCES ON THE EVOLUTION OF METAL RESISTANCE

2.1 Abstract

The analysis of natural divergence of phylogenetically closely related bacteria residing in the same habitat can reveal fine-scale evolution events. We have previously reported on *Ralstonia pickettii* strains (12J and 12D) isolated from the same cubic centimeter of copper-contaminated lake sediment that bioaccumulate copper. While these strains have nearly identical 16S rRNA gene sequences (99% similar), they have distinct genomic structures on which we report here. Strain 12J has two chromosomes, a single plasmid, and a filamentous phage, while strain 12D has two chromosomes, three plasmids, and a larger genome by 359,629 bases. Both strains have adapted to the high concentrations of metals using gene duplication and horizontal transfer of metal resistance genes. Plasmids and phage have played a role in the genetic divergence of the strains. Plasmid 2 of strain 12D contains 31 copper and cobalt-zinc-cadmium resistance genes. This plasmid was inserted into the primary chromosome and initiated, we postulate, a cascade of genetic events that have continued the divergence of the two strains. Subsequent events included differences in horizontally transferred genes, acquisition of a filamentous phage, and differences of transposase carriage, with ISXo4 and IS4 unique to strain 12J and the mutator type of transposase unique to strain 12D. Five transposase types are found in both strains. The genomic evolution of strains 12D and 12J provide a view into a collection of dynamic events shaping and reshaping the

Ralstonia genome.

2.2 Introduction

Microdiversity describes a group of bacterial populations found in the same environmental niche that are phylogenetically closely related (ie. same species) but physiologically distinct [1, 124, 141]. Studying genomic variations within a bacterial population can give us insights into: 1) the impacts of the environmental factors on the bacteria populations; 2) the incidences of horizontal gene transfer (HGT) and gene duplication and amplification (GDA), that led to the divergence; 3) the extent and location of plasticity within the genome; 4) and the functional potential of the microdiversity [21, 98, 124, 135, 146].

We have a collection of bacteria strains from a *Ralstonia pickettii* microdiversity. Two representative strains, *R. pickettii* 12D and 12J were isolated from within the same 1 cm³ of heavy metal (especially copper) contaminated lake sediment (16 cm below the sediment surface at a lake depth of 37 m from Torch Lake, MI). Konstantinidis et al. [80] showed that these two strains are 99% identical according to their 16S rRNA gene sequences. Previous research showed that both strains thrived in copper supplemented media with minor differences in growth rates and copper sequestration abilities [191]. Metal resistance tests revealed that *R. pickettii* 12D is Cu-Ni-Cd resistant and 12J is Cu-Zn-Cd resistant [80]. We also found that *R. pickettii* 12J contains filamentous phage (p12J) particles and strain 12D is p12J resistant [191]. These physiological differences indicate that *R. pickettii* 12D and 12J have distinct genome structures.

By studying the genomic variations of these two *R. pickettii* strains we will better un-

derstand the evolutionary consequences of a high copper environment, produce a detailed description of the genomic changes that have occurred between strains and improve our understanding of strain divergence and speciation. Herein, we report our findings on the genomic differences, evidence of HGT and GDA, identification of metal resistance determinants and the evolutionary events that led to the differentiation of *R. pickettii* 12D and 12J.

2.3 Materials and Methods

2.3.1 Genome Retrieval and Gene Annotations

The genomic DNA of *R. pickettii* 12D and 12J were isolated in our laboratory and sequenced by Joint Genome Institute (JGI) as reported previously [191]. The genome sequences of *R. pickettii* 12D and 12J were retrieved from GeneBank database by using the following IDs, NC_012849, NC_012851, NC_012855–57, NC_010678, NC_010682-83, and NC_005131. The basic gene annotations were obtained from Joint Genome Institute Integrated Microbial Genomes (JGI-IMG) database. Basic Local Alignment Search Tool (BLAST) and JGI-IMG genome BLAST was used to identify and confirm gene annotations (E-value $\leq 10^{-2}$, protein identity $\geq 30\%$, unless specified).

2.3.2 Genome Comparisons

Functional groups identified as clusters of orthologous groups (COG) were used to find shared and unique genes present in *R. pickettii* 12D and 12J. Metabolic pathway information was retrieved from MetaCyc [19] and Kyoto Encyclopedia of Genes and Genomes

(KEGG) database [73]. Genome replication origins (*oriC*) of *R. pickettii* 12D and 12J were retrieved from the DoriC database [48]. The replication resolution sites (*dif*) of 12D and 12J were located by searching for sequences comparable to the *R. solanacearum* GMI1000 *dif* sequence by BLAST (BLASTN). The phylogenetic positions of strain 12D and 12J were analyzed, along with a collection of β -Proteobacteria *dif* sequences [18], by using Molecular Evolutionary Genetics Analysis (MEGA) [161]. Briefly, the *dif* sequences were aligned by ClustalW and a minimal evolution (ME) phylogenetic tree was constructed with the following parameters: the Jukes-Cantor substitution model assuming uniform rate among sites, gaps/missing data treated as pairwise deletions, and finally clustering with the ME heuristic method by allowing close-neighbor-interchange. Bootstrapping (1000 replications) was used to test the confidence level of branching.

Genome statistics (e.g., copies of rRNA coding genes, protein coding genes, horizontally transferred genes, etc.) of *R. pickettii* 12D and 12J and phylogenetically related bacteria (*R. solanacearum* GM1000 and *Cupriavidus metallidurans* CH34) were retrieved from JGI-IMG and compared based on their annotation. Transposases encoding sequences were identified by JGI-IMG. The genomic synteny of *R. pickettii* 12D and 12J were assessed by using Mauve [33], a multiple genome alignment tool.

2.3.3 Identification of the Metal Resistant Genes

Metal (Co-Zn-Cd, Cu, and Hg) resistant genes in *R. pickettii* 12D and 12J were extrapolated from JGI-IMG based on the metal resistant genes identified in *C. metallidurans* CH34. The abundances of these gene copies in *R. pickettii* strains were compared to those found in *C. metallidurans* CH34 and *R. solanacearum* GMI1000. The evolution lineage of the

main subunit of these resistance determinant coding genes in *R. pickettii* 12D and 12J was determined by comparing to similar coding sequences found in 23 other Proteobacteria species retrieved from JGI-IMG (Figure A.1). The phylogenetic analysis of these genes was conducted by using MEGA. Briefly, the DNA sequences were aligned via ClustalW and the bootstrapped (1000 replications) ME trees were constructed with the following parameters: the Jukes-Cantor substitution model assuming uniform rate among sites, gaps/missing data treated as pairwise deletion, and close-neighbor-interchange for ME heuristic method.

2.4 Results

2.4.1 Genome Overview

JGI-IMG annotations identified 1936 and 1945 COG groups in 12D and 12J, respectively. Between the two strains, 1876 COG groups are shared. KEGG data revealed that the metabolic pathway maps of both strains are highly similar with minor differences (Appendix A). MetaCyc revealed that both strain 12D and 12J contain several detoxification pathways involved in arsenate reduction, cytoplasm Hg^{2+} reduction, methylglyoxal detoxification, cyanate degradation and superoxide radical degradation (Appendix A). *R. pickettii* 12D and 12J clustered closely to *R. solanacearum* GMI1000 and *Cupriavidus metallidurans* CH34 based on their 16S rRNA gene sequences (Figure A.1). Basic comparisons among these four strains showed that *R. pickettii* 12D and 12J are smaller in genome size compared to *R. solanacearum* GMI1000 and *C. metallidurans* CH34. *R. pickettii* 12J has the least number of bases and protein coding genes (Table 2.1). Multiple copies of rRNA genes are found in all four bacterial strains. Both *R. pickettii* strains contain three copies of the 16S

rRNA genes. IMG annotations indicate that all four strains contain comparable numbers of orthologs and paralogs and *R. pickettii* 12D and 12J contain the least number of horizontally transferred genes. All four strains contain many signal peptide and transmembrane protein encoding genes (Table 2.1).

The complete genome sequences revealed that the *R. pickettii* 12D genome is composed of a primary chromosome (12D_C1) of 3.6 Mb, a secondary chromosome (12D_C2) of 1.3 Mb, and three plasmids of 0.39 Mb (12D_P1), 0.27 Mb (12D_P2), and 0.051 Mb (12D_P3) (Figure 2.1). *R. pickettii* 12J contains a primary chromosome (12J_C1) of 3.9 Mb, a secondary chromosome (12J_C2) of 1.3 Mb, and a plasmid (12J_P1) of 0.08 Mb (Figure 2.2). *R. pickettii* 12J_C1 is approximately 0.3 Mb larger than 12D_C1. The secondary chromosomes of both strains are approximately the same size and substantially smaller than the primary chromosomes. *R. pickettii* 12D_P3 and 12J_P1 are comparable in size. Two large plasmids (P1 and P2) in 12D are absent in 12J. We also found that strain 12J contains filamentous phage particles (p12J), which is absent in strain 12D.

Horizontally transferred foreign genes (JGI-IMG prediction) are scattered across all genome scaffolds and are twice as abundant in 12D than 12J (Table A.1). A total of 123 genes were predicted as being horizontally transferred genes in *R. pickettii* 12J and the majority of them are in 12J_C1 (Table A.1). Out of the 287 horizontally transferred genes in strain 12D, 115 are in 12D_C1 and 157 are in 12D_P1 (Table A.1). The JGI-IMG gene profiler revealed that strain 12D and 12J share only one gene among all 410 predicted horizontally transferred genes (JGI-IMG gene profiler with E-value $\leq 1E-5$ and protein identity $\geq 80\%$). This gene is annotated as an IS30 family integrase catalytic region (locus Rpic12D_1028 and Rpic_2522).

Table 2.1: Gene summaries of *R. solanacearum* GMI1000, *C. metallidurans* CH34, *R. pickettii* 12D and 12J.

Genome Features	<i>R. solanacearum</i> GMI1000	<i>C. metallidurans</i> CH34	<i>R. pickettii</i> 12D	<i>R. pickettii</i> 12J
Bases	5810922	6913352	5685358	5325729
GC (%)	66.98	63.53	63.3	63.65
Total Number of Genes	5204	6430	5518	5092
Protein Coding Genes	5120	6340	5452	5027
rRNA (5S, 16S, 23S)	4,4,4	2,4,4	3,3,3	3,3,3
tRNA	57	62	54	55
Orthologs	4774 (91.74%)	5951 (92.55%)	4951 (89.72%)	4774 (93.75%)
Paralogs	1106 (21.25%)	1753 (27.26%)	1089 (19.74%)	1106 (21.72%)
Signal Peptides	1232 (23.67%)	1568 (24.39%)	1349 (24.45%)	1286 (25.26%)
Transmembrane Proteins	1188 (22.83%)	1514 (23.55%)	1339 (24.27%)	1291 (25.35%)
Horizontally transferred	271 (5.21%)	510 (7.93%)	287 (5.20%)	123 (2.42%)

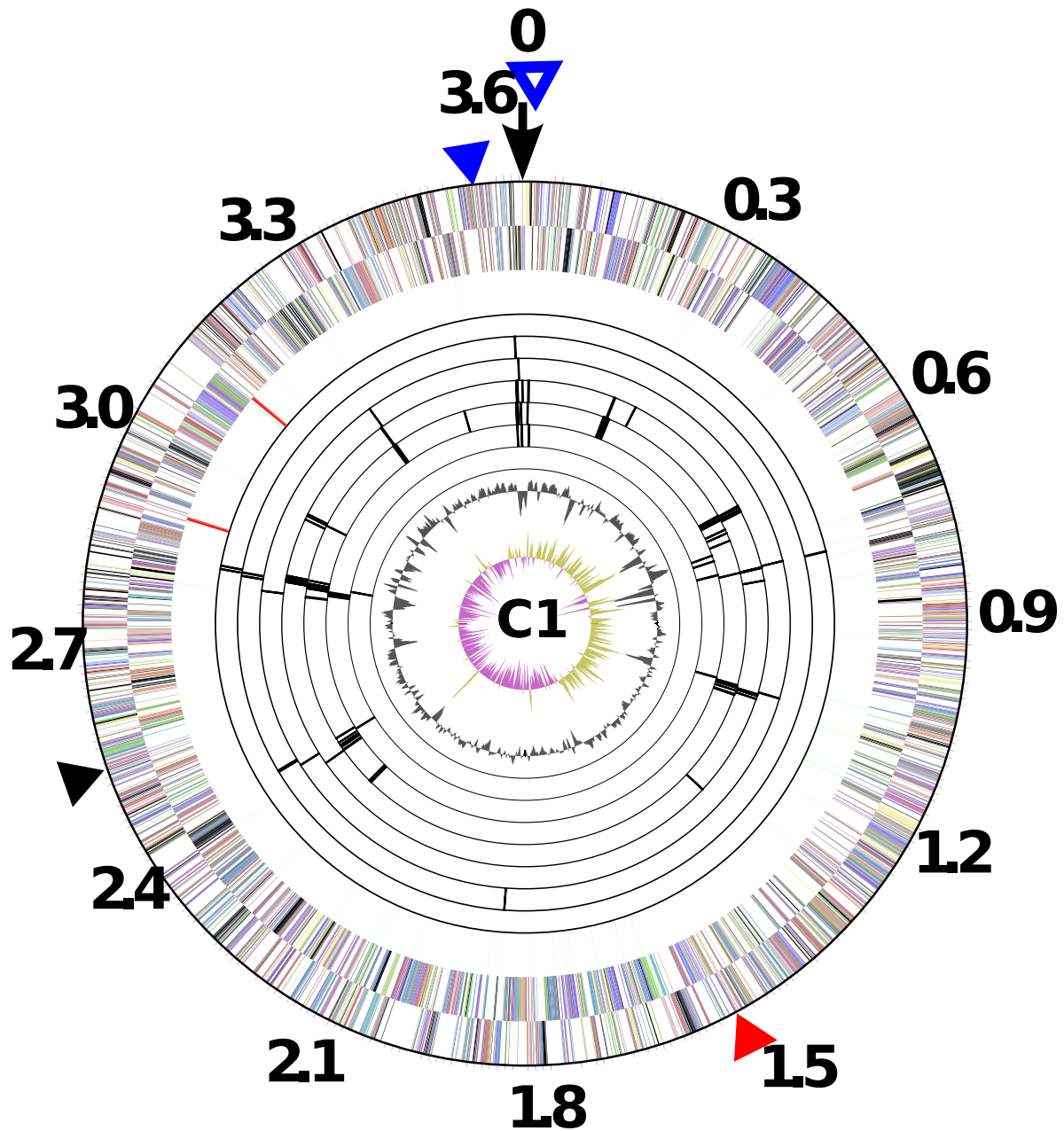


Figure 2.1: *R. pickettii* 12D genome scaffolds. The distribution of putative horizontally transferred genes (HGT genes) identified by JGI-IMG are marked as black dashes in rings 4-10. The scaffold sizes are in units of Mb. For interpretation of the references to color in this and all other figures, the reader is referred to the electronic version of this dissertation.

Figure 2.1 (cont'd)

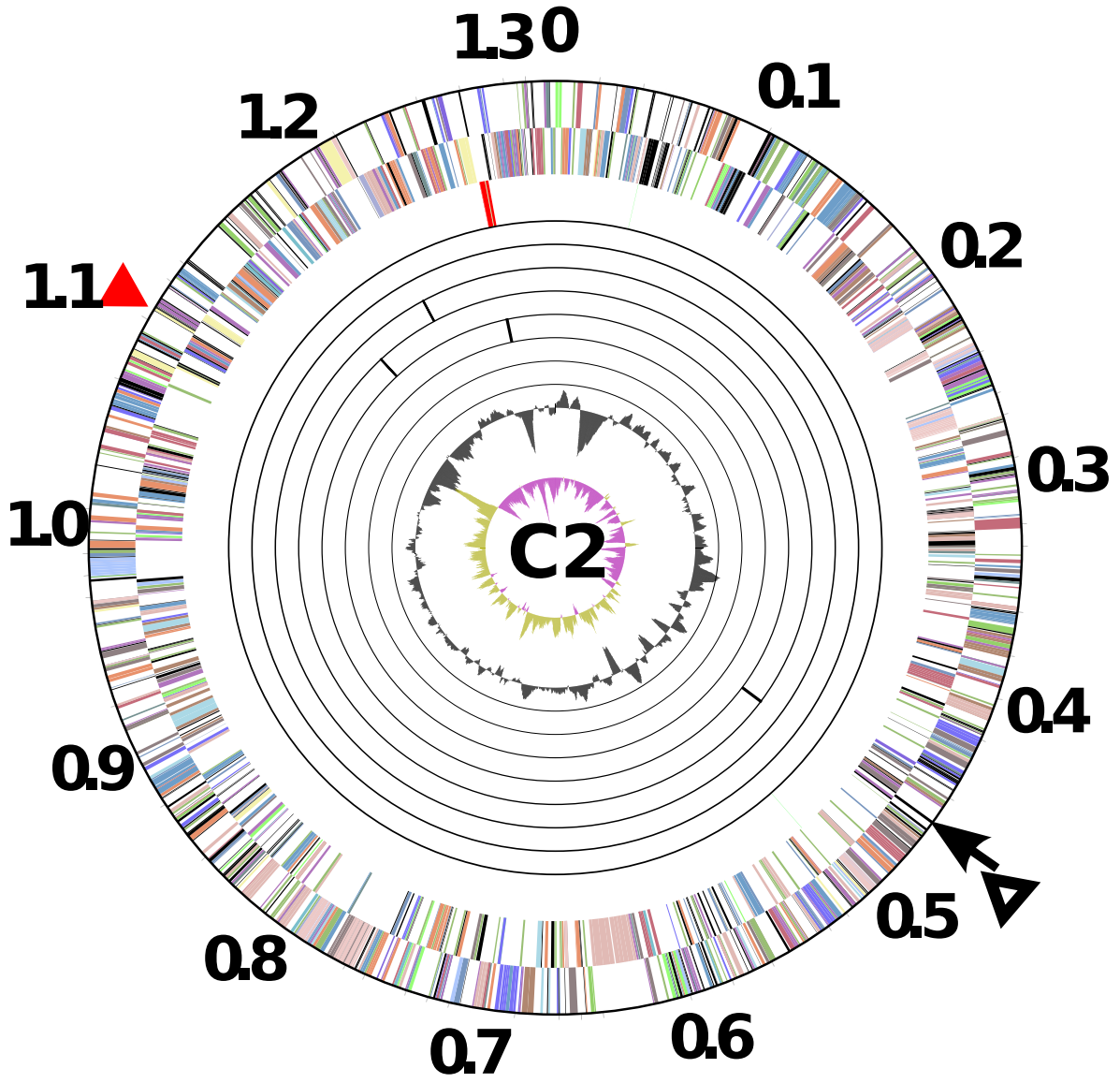


Figure 2.1 (cont'd)

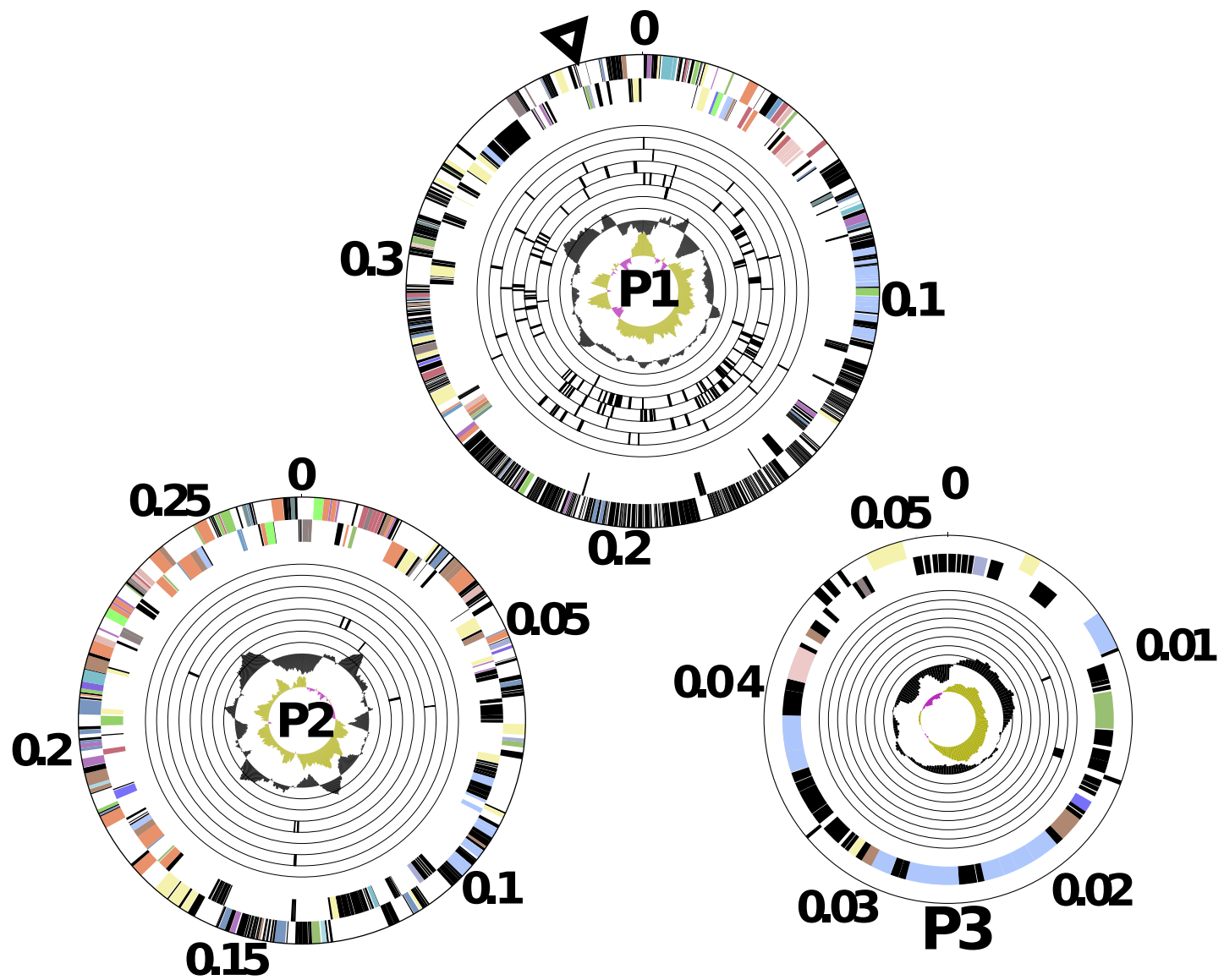
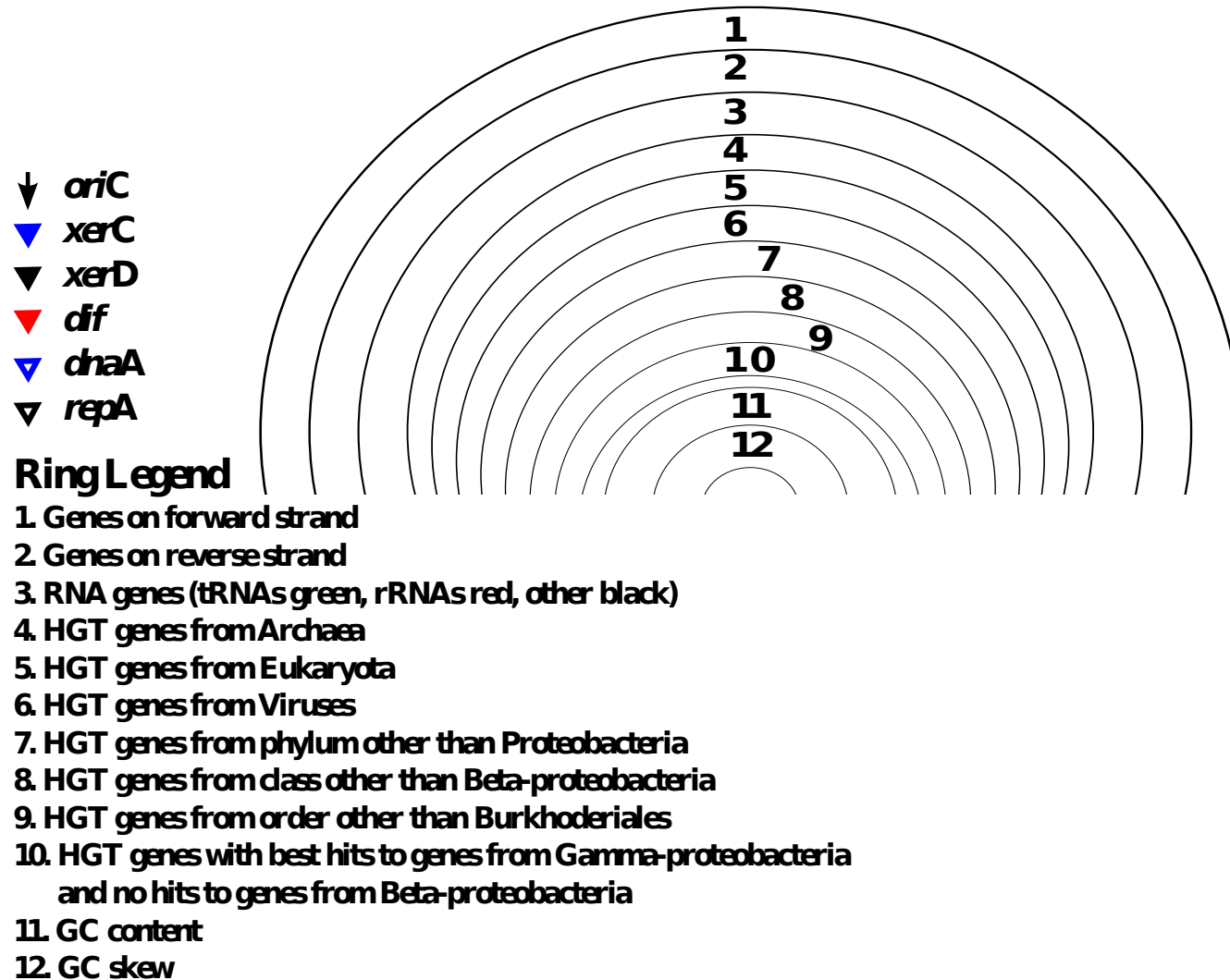


Figure 2.1 (cont'd)



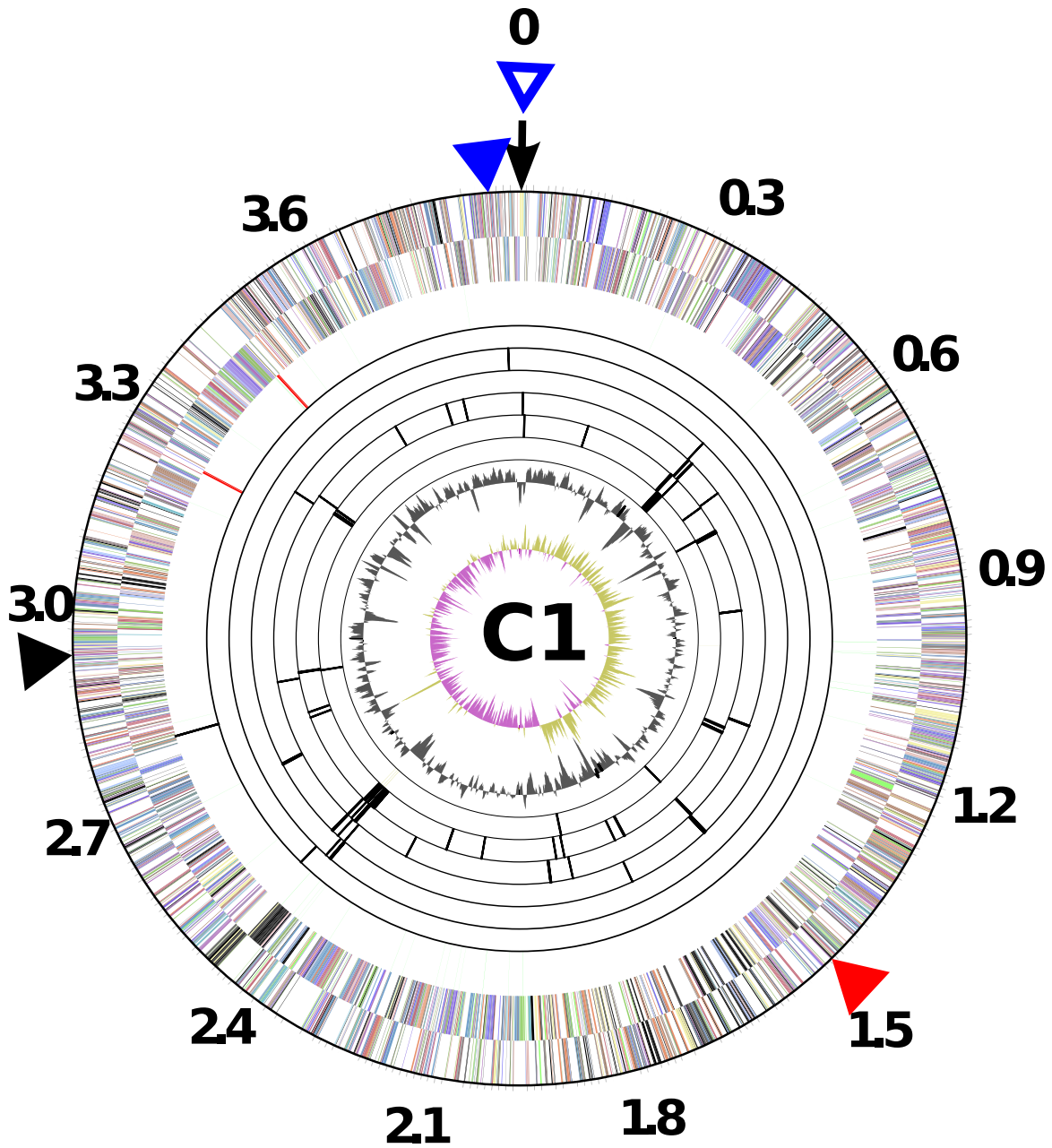


Figure 2.2: *R. pickettii* 12J genome scaffolds. The distribution of putative horizontally transferred genes (HGT genes) identified by JGI-IMG are marked as black dashes in rings 4-9. The scaffold sizes are in units of Mb.

Figure 2.2 (cont'd)

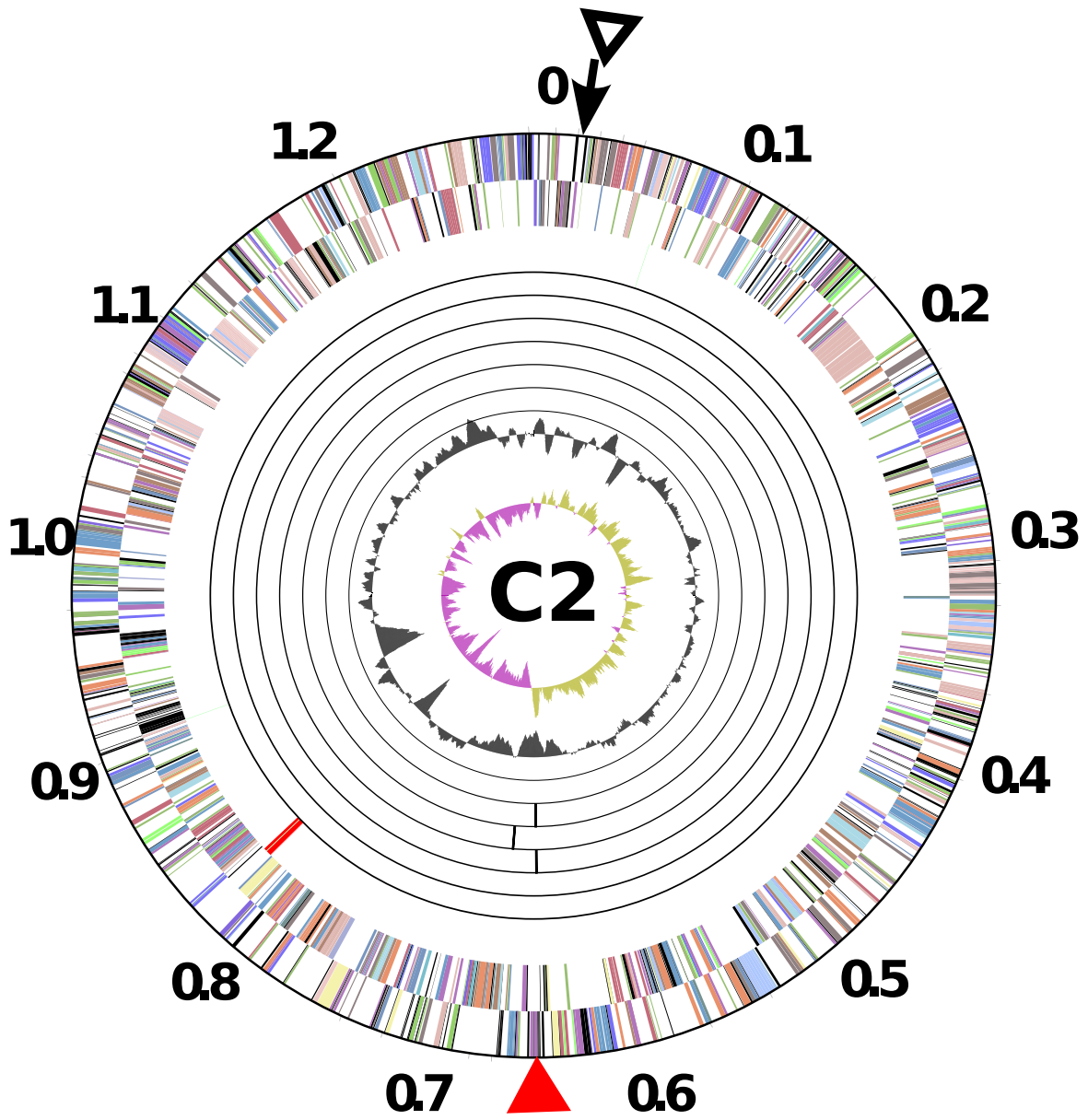


Figure 2.2 (cont'd)

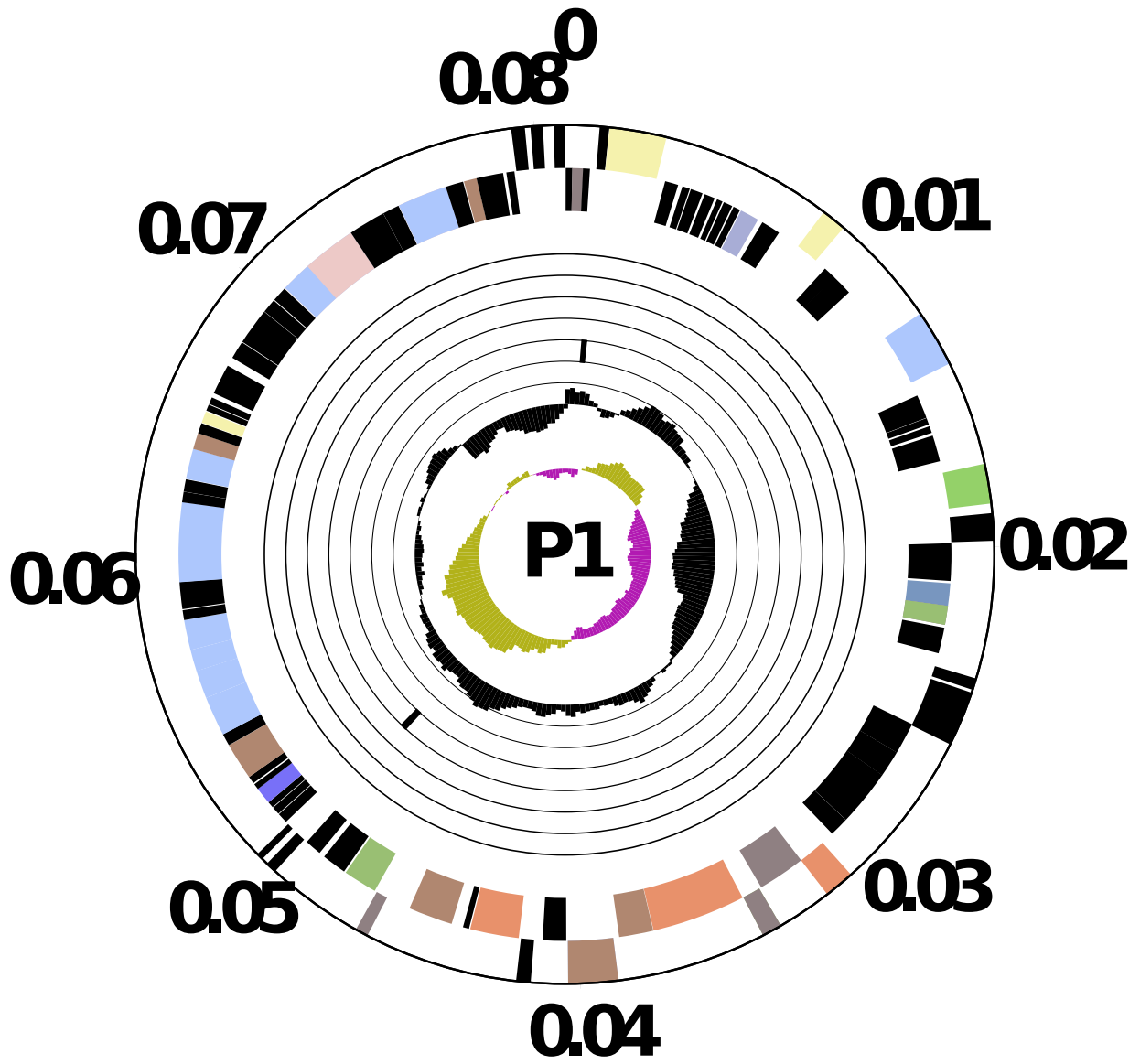
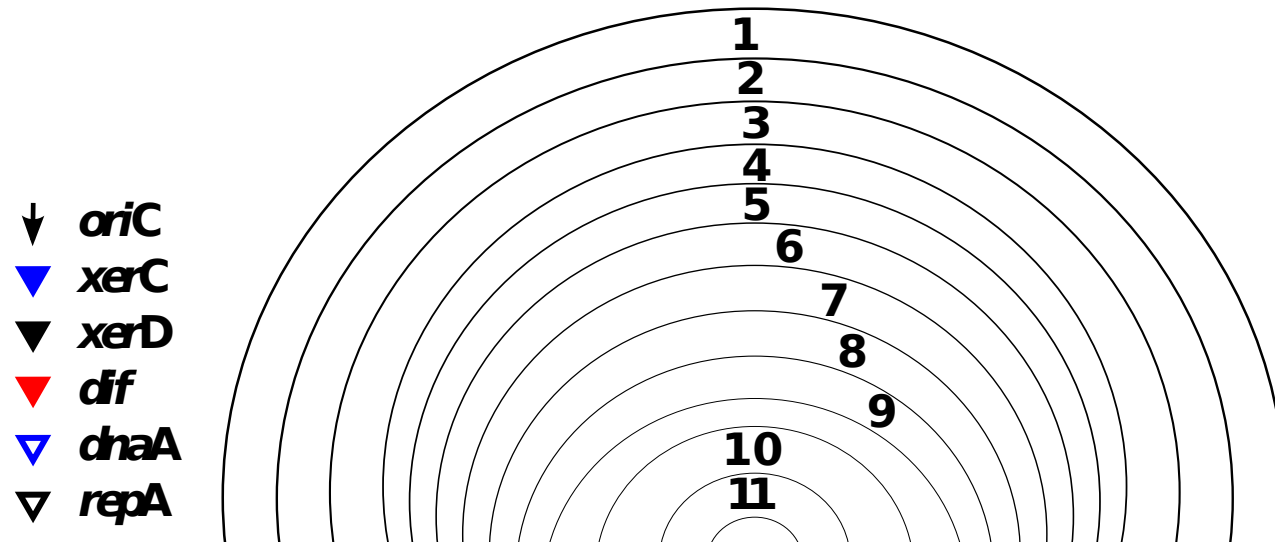


Figure 2.2 (cont'd)



Ring Legend

1. Genes on forward strand
2. Genes on reverse strand
3. RNA genes (tRNAs green, rRNAs red, other RNAs black)
4. HGT genes from Archaea
5. HGT genes from Eukaryota
6. HGT genes from Viruses
7. HGT genes from phylum other than Proteobacteria
8. HGT genes from class other than Beta-proteobacteria
9. HGT genes from order other than Burkholderiales
10. GC content
11. GC skew

Both *R. pickettii* strains are abundant in transposases (Table A.1). Strain 12J has 32 transposase genes which belong to seven transposase families and 12D has 33 transposase genes that belong to eight transposase families. Five of these transposase types are found in both strains. Among the abundant transposases, type ISXo4 and IS4 are unique to strain 12J and the mutator type of transposase unique to strain 12D.

The genome replication initiation positions (*oriC*) are labeled as black arrows in Figure 2.1 and Figure 2.2. The estimated *oriC* positions are just upstream of *dnaA* (C1) or *repA* (C2) genes. *R. pickettii* 12D_P1 also has a *repA* gene (Figure 2.1 P1 black hollow arrow), which was not observed in the other plasmids of 12D and 12J. The identification of *dif/xerCD* system in both strains suggest that this is used to resolve dimers created during replication [56]. Each strain has a pair of *xerCD* located on the primary chromosomes (Figure 2.1 and Figure 2.2 black and blue solid triangles). Each strain also contains two *dif* sites, one is located on C1 and the other one is on C2 (Figure 2.1 and Figure 2.2 red solid triangles). There are four copies of *kfrA* gene in each strain that presumably contribute to plasmid stability. Two of the four *kfrA* copies are located on the secondary chromosomes, and the other two were found on 12J_C1 and 12D_P1, respectively.

2.4.2 Co-evolution of *R. pickettii* 12D and 12J

2.4.2.1 16S rRNA Gene Sequence Variations

For the three copies of 16S rRNA genes in each *R. pickettii* strain, we observed that two copies are located on the primary chromosome and the third copy is found on the secondary chromosome. The three copies in strain 12J are all identical. The 16S rRNA gene copy on

the 12D secondary chromosome (12D_C2) is identical to the copies in 12J. The two copies of 16S rRNA on the primary chromosome of 12D (12D_C1) are identical to each other but different to the copy on 12D_C2, with a distance of 0.001.

2.4.2.2 *dif* Site Sequence Variations

Many bacteria employ the *dif/xerCD* system to resolve dimers formed during chromosome replication [18, 25, 34, 68, 109, 144]. This system is comprised of a set of recombinase encoding genes, *xerC* and *xerD*, and a 28 bp binding site (*dif* site) near the replication terminus [18]. Genome sequences revealed that *R. pickettii* 12D and 12J also utilizes *dif/xerCD* system. We found each strain contains one set of *xerCD* genes and two *dif* sites (one on each chromosome). The *dif* site sequences from the primary and secondary chromosomes of *R. pickettii* vary substantially, although they presumably interact with the same sets of XerCD protein. *R. pickettii* 12J_C1 *dif* appears to be the most different. The *dif* sequences on the secondary chromosomes are highly similar (Figure A.2). The ME phylogenetic tree revealed that the *R. pickettii dif* sequences clustered together, away from other β -Proteobacteria *dif* sequences (Figure 2.3). The *dif* sequence of 12J_C1 appears to be the most ancestral among all four *R. pickettii*. We observed that 12D_C1 and both secondary chromosomes branched out from 12J_C1 and the secondary chromosome *dif* sequences appeared to more distant to 12D_C1 than 12D_C1 (Figure 2.3).

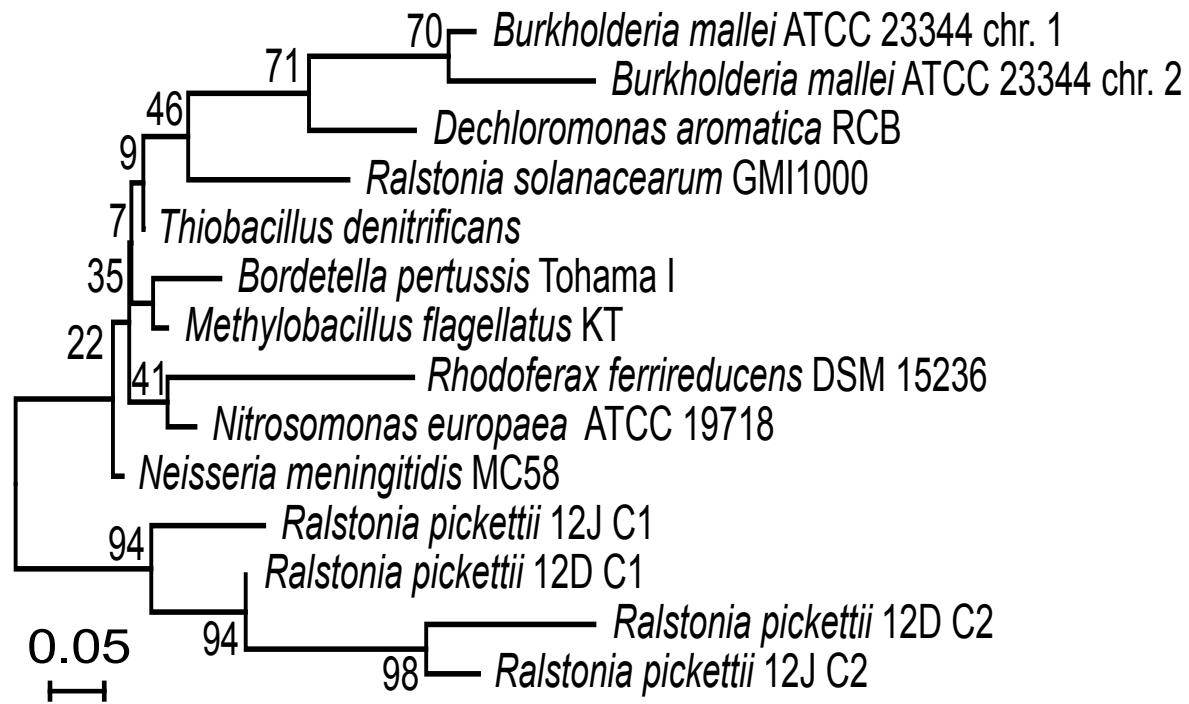


Figure 2.3: Minimal evolution phylogenetic tree of β -Proteobacteria *dif* sequences. The numbers on branches are bootstrap values. The scale at the left hand lower corner represents the distance.

2.4.2.3 Filamentous Phage Elements in *R. pickettii* 12D and 12J

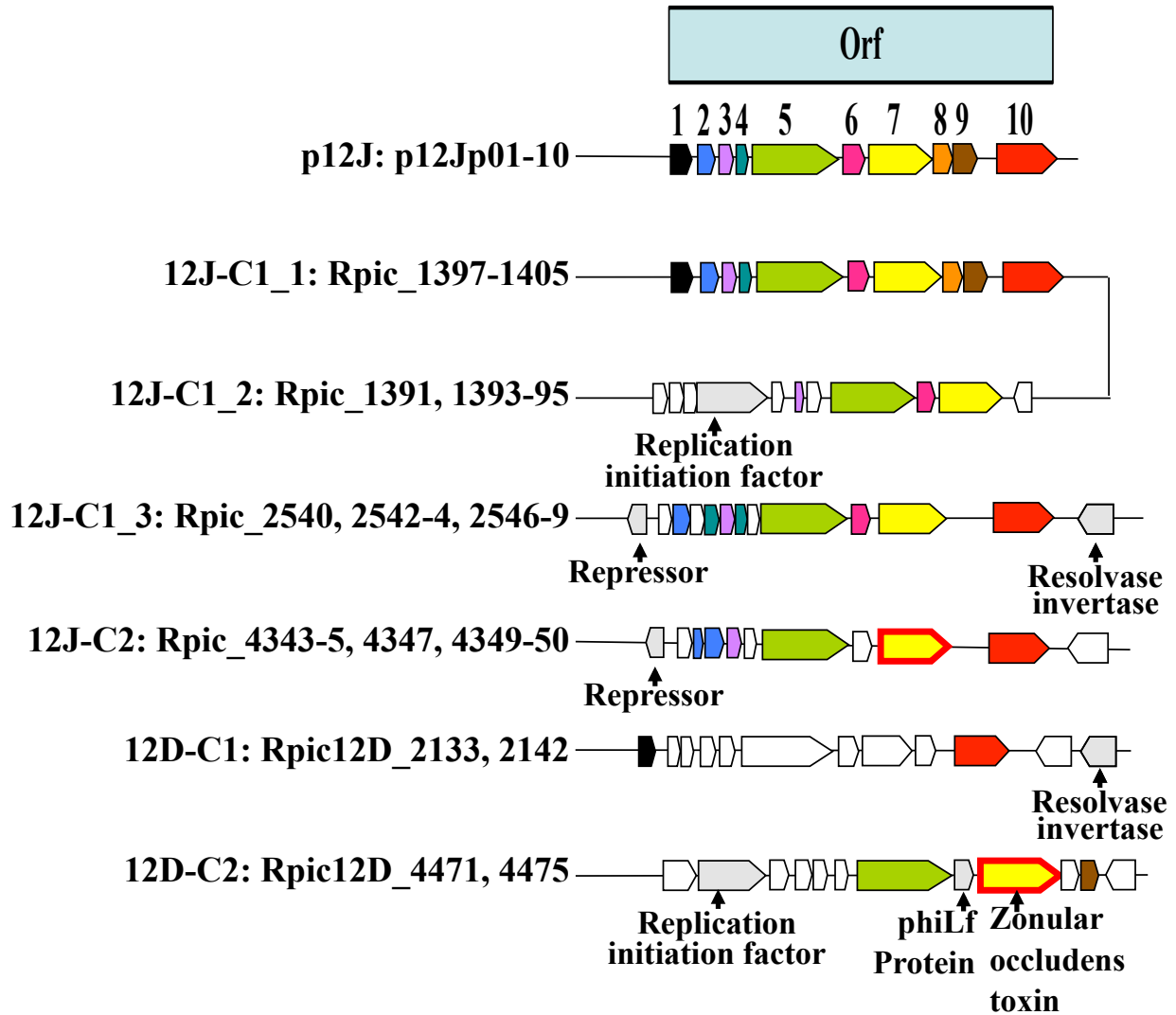


Figure 2.4: Filamentous phage p12J gene compositions and their homologs on *R. pickettii* 12D and 12J chromosomes. Fragments of the same fragments represent homologous genes. Genes colored yellow with a red border represent genes that share no homology to p12J Orf7 but are orthologs to each other. Grey colored fragments represent other phage related genes (not p12J related). White colored blocks are other non-phage related genes.

Filamentous phage p12J (NC_005131) is comprised of ten open reading frames (orf), locus p12Jp01-10 (Figure 2.4 p12J). Three (orf8 - orf10) out of ten of the p12J orf's were annotated as phage proteins but with little information. Orf5, orf7 and orf10 are the main

phage assembly proteins and orf7 was identified as a zonular occludens toxin coding gene. We located four incidents of p12J insertion in *R. pickettii* 12J (Table A.1). It was observed that the complete phage genome is located on 12J_C1, 464 bp upstream from the 12J_C1 *dif* site (Figure 2.4 12J-C1_1). Upstream adjacent to this complete phage genome is a partial p12J copy with a non-p12J related phage replication initiation factor encoding gene (Figure 2.4 12J-C1_2). The third insertion is also located on on 12J_C1 (Figure 2.4 12J-C1_3). We found the fourth partial copy on 12J_C2 (Figure 2.4 12J-C2), which is located 931 bp downstream of 12J_C2 *dif* site. All three insertions in 12J contain at least four p12J gene homologs, two out of which are primary phage components (orfs 5 & 7). In contrast, only two p12J partial copies were found on 12D_C1 (Figure 2.4 12D-C1) and 12D_C2 (Figure 2.4 12D-C2). Both insertions are distal from *R. pickettii* 12D *dif* sites and appear to be highly truncated by either non-phage related genes or other phage (non-p12J) related genes. These 12D partial copies contain only two p12J homologs. Annotation showed that one of the genes encodes zonular occludens toxin. However, it shares no synteny with p12J orf7 (Figure 2.4 12D-C2).

2.4.3 Genome Synteny of *R. pickettii* 12D and 12J

Genomic DNA sequence dotplot revealed that *R. pickettii* 12D and 12J share high synteny (Figure A.3). Detailed genomic sequence alignments showed that *R. pickettii* 12J_C1 could be viewed as homologs of *R. pickettii* 12D_C1 and 12D_P2. The 12D_P2 homolog was located between 1.56 Mb and 1.95 Mb on 12J_C1, approximately 0.07 Mb downstream of the *dif* site (Figure 2.5 A). Figure 2.5 panel B indicated where the genomes were rearranged. The replication initiation region of 12D_C2 appears to be drastically different from

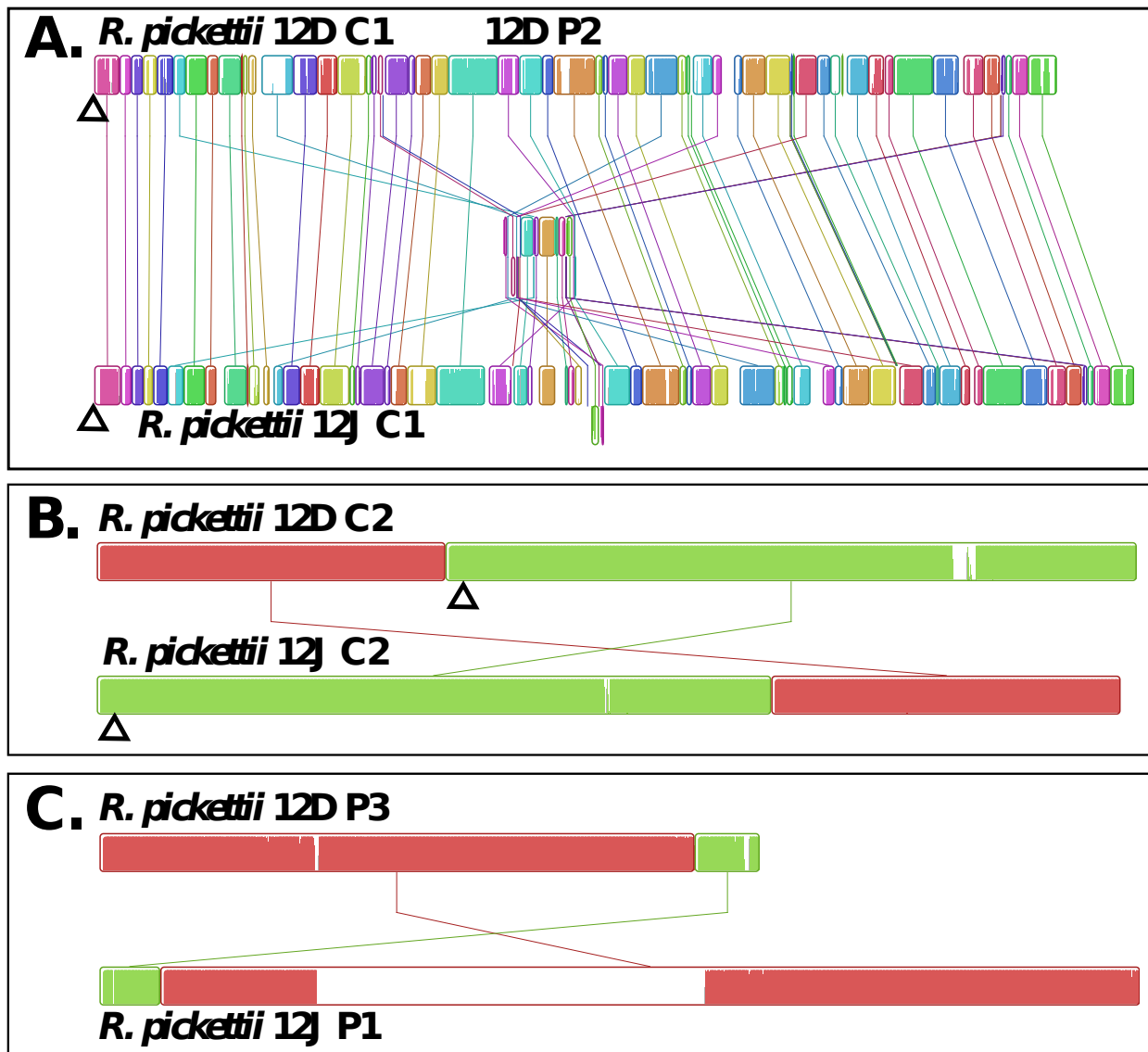


Figure 2.5: Genome synteny between *R. pickettii* 12D and 12J scaffolds. Panel A, 12D_C1, 12J_C1 and 12D_P2; Panel B, 12D_C2 and 12J_C2; Panel C, 12D_P3 and 12J_P1. Arrows indicate location of *oriC* on the chromosomes. Blocks with the same color represent the regions that are similar (connected by lines). The amount of color indicates the percentage of identity. White areas within the blocks indicate absence of a homologous sequence.

annotated 0 position. If repositioned, both secondary chromosomes would start with *repA* (12D_C2 is almost identical with 12J_C2, Figure refmauve B). The 12J_P1 and 12D_P3 alignment revealed a similar genome rearrangement pattern (Figure 2.5 C). We could not locate the origins of replication in this study. The large plasmid of strain 12D (12D_P1) showed little synteny with the other scaffolds and appears unique to itself.

The 0.39 Mb 12D_P2 homolog inserted into 12J_C1 is comprised of two distinct portions. The region from 1.56 Mb to 1.72 Mb appears to be abundant with low GC content genes that encode secretion systems and cytoskeleton. Within this region, we observed two copies of plasmid partition protein coding gene *parB* (locus Rpic_1509 and Rpic_1596) [123]. The section from 1.72 to 1.95 Mb codes for multiple metal resistance genes [191]. This region was extracted and annotated by hand using BLAST targeting the non-redundant protein database of GenBank. We obtained 408 hits with alignment scores over 200 with diverse taxonomy indicating that the region is a phylogenetic mosaic of horizontally transferred genes (Figure 2.6). The query sequence revealed itself as a "mosaic", where multiple genes from different bacteria were assembled to reconstruct the 0.23 Mb region of *R. pickettii* 12J_C1 (Figure 2.6). As we expected, 12D_P2 shares the most similarities. A fragment of 12J_C1 sequence (between 134000 and 150000) was highly similar (99% identity) to 25 genes on plasmid pMOL30 of *C. metallidurans* CH34 (0.71 Mb to 0.87 Mb). Finally, the KfrA protein coding gene is also found in the query sequence, which is 100% identical to those *kfrA* genes observed in *R. pickettii* 12J_C2, 12D_C2, and 12D_P1 (Figure 2.6). Within this region of *R. pickettii* 12J_C1, we observed four copies of genes related to cobalt-zinc-cadmium resistance (*czcA*), one mercury resistance operon and three copper resistance operons. Besides these specific metal resistances, this region also contains multiple copies of genes encoding

for heavy metal translocating P-type ATPase, ABC transporter, iron permease, cation diffusion transporter, and heavy metal transport/detoxification protein. Scattered among these resistance genes, were transposes, tyrosine-based site-specific recombinase, and hypothetical protein encoding genes (Figure 2.6).

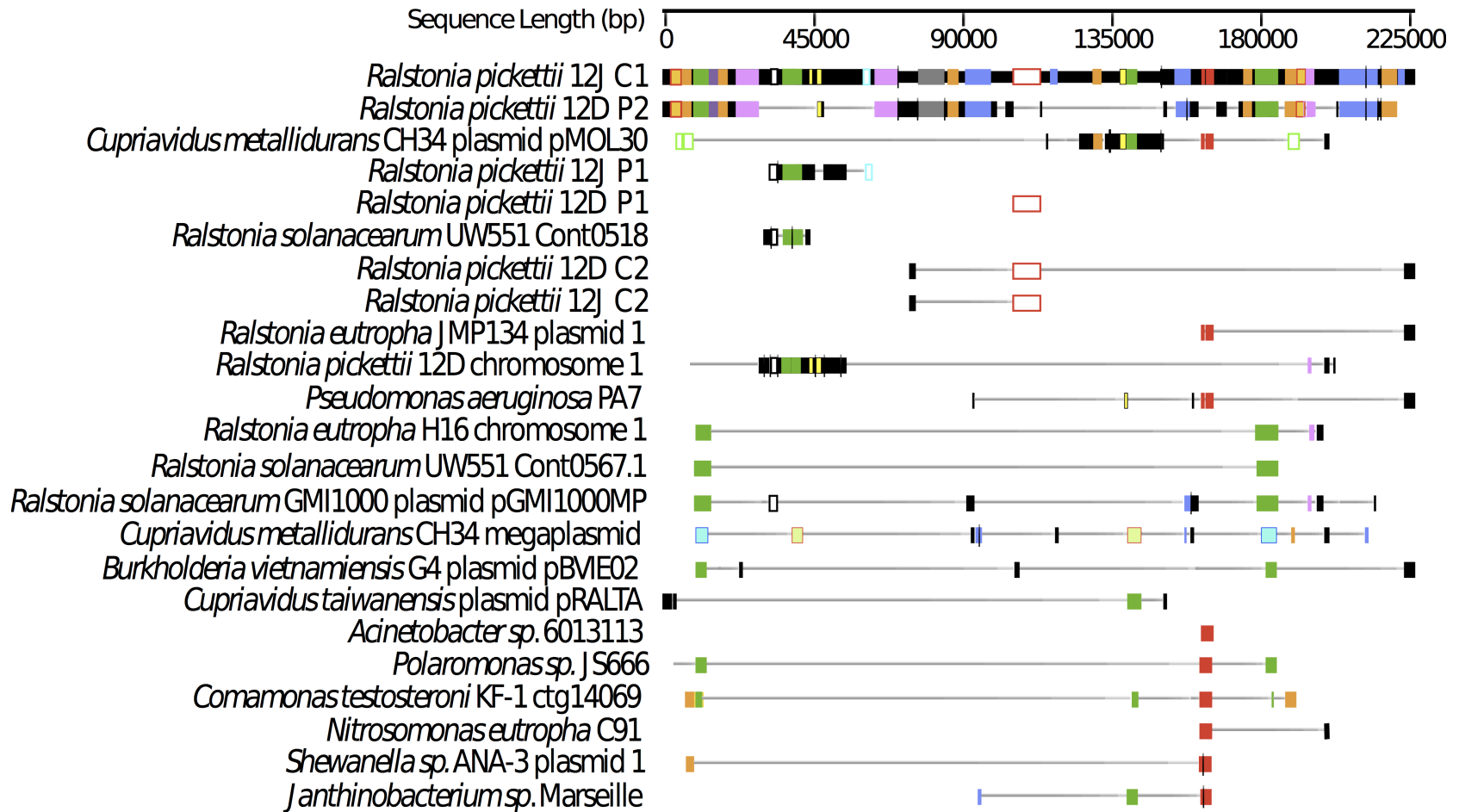


Figure 2.6: BLAST results mapped onto the 1.72 Mb-1.94 Mb region of *R. pickettii* 12J_C1. The top scale indicates the length of the query region. Similar genes are shown underneath the query sequence. The short thin black bars indicate that the next stretch of sequence is on the opposite strand of DNA.

Figure 2.6 (cont'd)

-  Cobalt-zinc-cadmium resistance
-  Mercury resistance
-  Heavy metal translocating P-type ATPase
-  Copper Resistance
-  ABC transporter
-  Cation diffusion facilitator family transporter
-  Copper and silver tricomponent efflux
-  Heavy metal cation tricomponent efflux
-  Heavy metal transport/detoxification protein
-  Iron permease
-  Natural resistance-associated macrophage proteins
-  KfrA protein
-  Metallophosphoesterase
-  Pb(II) resistance
-  Transposase/tyrosine-based site-specific recombinases/hypothetic proteins

2.4.4 The Acquisition and Duplication of Resistance Determinants in *R. pickettii* 12D and 12J

2.4.4.1 Metal Resistant Genes in *R. pickettii* 12D and 12J

Annotations from the *R. pickettii* 12D_P2 and the inserted region of 12J_C1 revealed a high abundance of ABC transporters, P-type ATPase, and metal (Cu, Co-Zn-Cd, and Hg) resistance determinant encoding genes (Figure 2.6). To determine the number of metal resistant gene copies that reside in *R. pickettii* 12D and 12J, we employed IMG genome BLAST to extrapolated possible metal resistant genes specifically related to Co-Zn-Cd, Cu and Hg resistance. Co-Zn-Cd (*czc* operon), Cu (*cop* operon) and Hg (*mer* operons) resistant genes found in *C. metallidurans* CH34 were used as reference genes. Two *cop* operon genes, *copR* and *copS*, were not detected in *C. metallidurans* CH34. Thus, *copRS* found in *Pseudomonas aeruginosa* LESB58 were used as references for identifying *copR* and *copS*. The abundance and distribution of these genes are reported in Table 2.2. We observed multiple occurrence of *czc* operon in all four bacterial strains. The major Co-Zn-Cd pump encoding gene, *czcA* is the most abundant, which was found 13 times in CH34, 9 times in 12J, 8 times in 12D, and 4 times in GMI1000. Two different sets of *czcBCD* were located on all four strains. *R. pickettii* 12J contains the most copies of *czcD* (13) and the least amount of *czcC* (2). *R. pickettii* 12J contains the most amount of *czcE*, a copper binding protein coding gene [195], and *czcP*, which is a transition metal efflux coding gene [138]. Of the four strains, only *C. metallidurans* CH34 and *R. pickettii* 12J carry *czcN* while *czcI* was found only in CH34. Copper resistant determinants were found in all four strains but were most abundant in *R. pickettii* 12D and 12J. *C. metallidurans* contains two copies of each *cop* operon gene and

only one copy of each *cop* gene was found in *R. solanacearum* GMI1000. The major *cop* operon component, *copA*, a Cu(I)-translocating P-type ATPase was observed 5 and 3 times in 12J and 12D, respectively. The regulatory and signaling protein encoding genes of *czc* and *cop* operon appear to be highly similar and were reported together. A mercury resistant determinant is found in *R. pickettii* 12J and *C. metallidurans* CH34 only. Although the regulatory gene, *merR*, was observed in both *R. pickettii* 12D and *R. solanacearum* GMI1000, the gene encoding for mercury reductase (*merA*) was absent from both. We identified two copies of *merP*, a mercuric transporter protein encoding gene, and one copy of *merA* in *R. pickettii* 12J. In contrast, three copies of *merA* and four copies of *merP* were found in *C. metallidurans* CH34. The distribution of metal resistant genes on *R. pickettii* 12D and 12J genome revealed that majority of the metal resistant genes are located on 12D_P2 and 12J_C1. The secondary chromosomes of both strains carry the same number of the metal resistant genes. No Co-Zn-Cd, Cu, or Hg resistant genes were found on *R. pickettii* 12D_P1 and 12D_P3. The total copy number of each metal resistant gene revealed that strain 12J contains an equal or great number of copies than 12D, with the exception of *czcC* (Table 2.2).

Table 2.2: The abundance of Co-Zn-Cd, Cu, and Hg resistant genes in *R. pickettii* 12D and 12J, *R. solanacearum* GMI1000, and *C. metallidurans* CH34.

Metal Resistance Genes		C1		P2	C2		P3	P1	P1
		12D	12J	12D	12D	12J	12D	12J	12D
<i>czc</i> Operon	<i>czcA</i>	1	5	4	3	3	0	1	0
	<i>czcB</i>	0	1	3	0	0	0	0	0
	<i>czcC</i>	0	4	2	1	1	0	0	0
	<i>czcD</i>	0	0	0	1	1	0	0	0
	<i>czcD</i>	0	0	1	1	1	0	0	0
	<i>czcD</i>	1	7	1	0	0	0	0	0
	<i>czcD</i>	2	5 ^a	0	0	0	0	1	0
	<i>czcE</i>	0	4	1	0	0	0	0	0
	<i>czcP</i>	0	3	2	0	0	0	0	0
<i>czcI</i>	0	0	0	0	0	0	0	0	
<i>czcN</i>	0	1	0	0	0	0	0	0	
<i>cop</i> Operon	<i>copA</i>	0	5	3	0	0	0	0	0
	<i>copB</i>	0	4	4	0	0	0	0	0
	<i>copC</i>	0	4	4	1	1	0	0	0
	<i>copD</i>	0	3	2	1	1	0	0	0
<i>czc/cop</i>	<i>czcR/copR</i>	0	5	2	0	0	0	0	0
	<i>czcS/copS</i>	1	6	2	1	1	0	0	0
<i>mer</i> Operon	<i>merA</i>	0	1	0	0	0	0	0	0
	<i>merE</i>	0	0	0	0	0	0	0	0
	<i>merP</i>	0	2	0	0	0	0	0	0
	<i>merR</i>	3	5	0	2	2	0	0	0
	<i>merT</i>	0	1	0	0	0	0	0	0

a. Two out of five matches are shared by Rmet_5979 matches.

b. IMG genome BLAST with e-value of 1E-2 and at least 40% identity.

Table 2.2 (cont'd)

Metal Resistance Genes		<i>R. pickettii</i> 12D	<i>R. pickettii</i> 12J	<i>R. solanacearum</i> GMI1000	<i>C. metallidurans</i> CH34	Reference Locus
<i>czc</i> Operon	<i>czcA</i>	8	9	4	13	Rmet_5980
	<i>czcB</i>	3	1	1	4	Rmet_5981
		3	5	4	4	Rmet_4121
	<i>czcC</i>	1	1	1	2	Rmet_5982
		2	1	2	1	Rmet_4120
	<i>czcD</i>	2	7	1	1	Rmet_5979
		2	6	1	1	Rmet_3406
	<i>czcE</i>	1	4	0	3	Rmet_5976
	<i>czcP</i>	2	3	0	2	Rmet_5970 ^b
<i>czcI</i>	0	0	0	1	Rmet_4595	
<i>czcN</i>	0	1	0	1	Rmet_5984	
<i>cop</i> Operon	<i>copA</i>	3	5	1	2	Rmet_6112 ^c
	<i>copB</i>	4	4	1	2	Rmet_6113
	<i>copC</i>	5	5	1	2	Rmet_6114
	<i>copD</i>	3	4	1	2	Rmet_6115
<i>czc/cop</i>	<i>czcR/copR</i>	2	5	2	5	Rmet_5978/PLES_22631 ^d
	<i>czcS/copS</i>	4	7	2	12	Rmet_5977/PLES_22621 ^e
<i>mer</i> Operon	<i>merA</i>	0	1	0	3	Rmet_6174
	<i>merE</i>	0	0	0	1	Rmet_6176
	<i>merP</i>	0	2	0	4	Rmet_6173 ^b
	<i>merR</i>	5	7	5	12	Rmet_6171
	<i>merT</i>	0	1	0	3	Rmet_6172

c. IMG genome BLAST with e-value of 1E-5 and at least 50% identity. Matches contain all 3 Pfam domains.

d. IMG genome BLAST with e-value of 1E-5 and at least 60% identity. Both reference loci return the same results.

e. IMG genome BLAST with e-value of 1E-2 and at least 40% identity for PLES_22621.

2.4.4.2 The Phylogenetic Lineage of *czcA* Copies in *R. pickettii* 12D and 12J

Table 2.2 shows that copies of *czcA* are distributed on 12D_C1 (1), 12D_C2 (3), and 12D_P2 (4) in *R. pickettii* 12D and 12J_C1 (5), 12J_C2 (3), and 12J_P1 (1) in *R. pickettii* 12J. To determine their phylogenetic lineage, a collection of 85 *czcA* sequences from 25 Proteobacteria (Figure A.1) was used to construct a minimal evolution phylogenetic tree (Figure 2.7). We observed that both *R. pickettii* 12D and 12J contain *czcA* genes that share evolutionary lineages to copies found in *C. metallidurans* CH34, *R. eutropha* JMP134, *R. solanacearum* Po82 and GMI1000. We observed that of eight copies of *czcA* genes in 12D, six copies clustered with those from 12J (Figure 2.7 Group I-VI). The phylogenetic tree showed that some copies of *czcA* from the same strain clustered together, such as 12D P2 copy 1 and copy2, and 12J C1 copy 4 and copy 5. One of the *R. pickettii* 12J *czcA* copy (12J C1 copy 1) appeared to be unique and did not cluster with the rest of the *R. pickettii* copies (Figure 2.7).

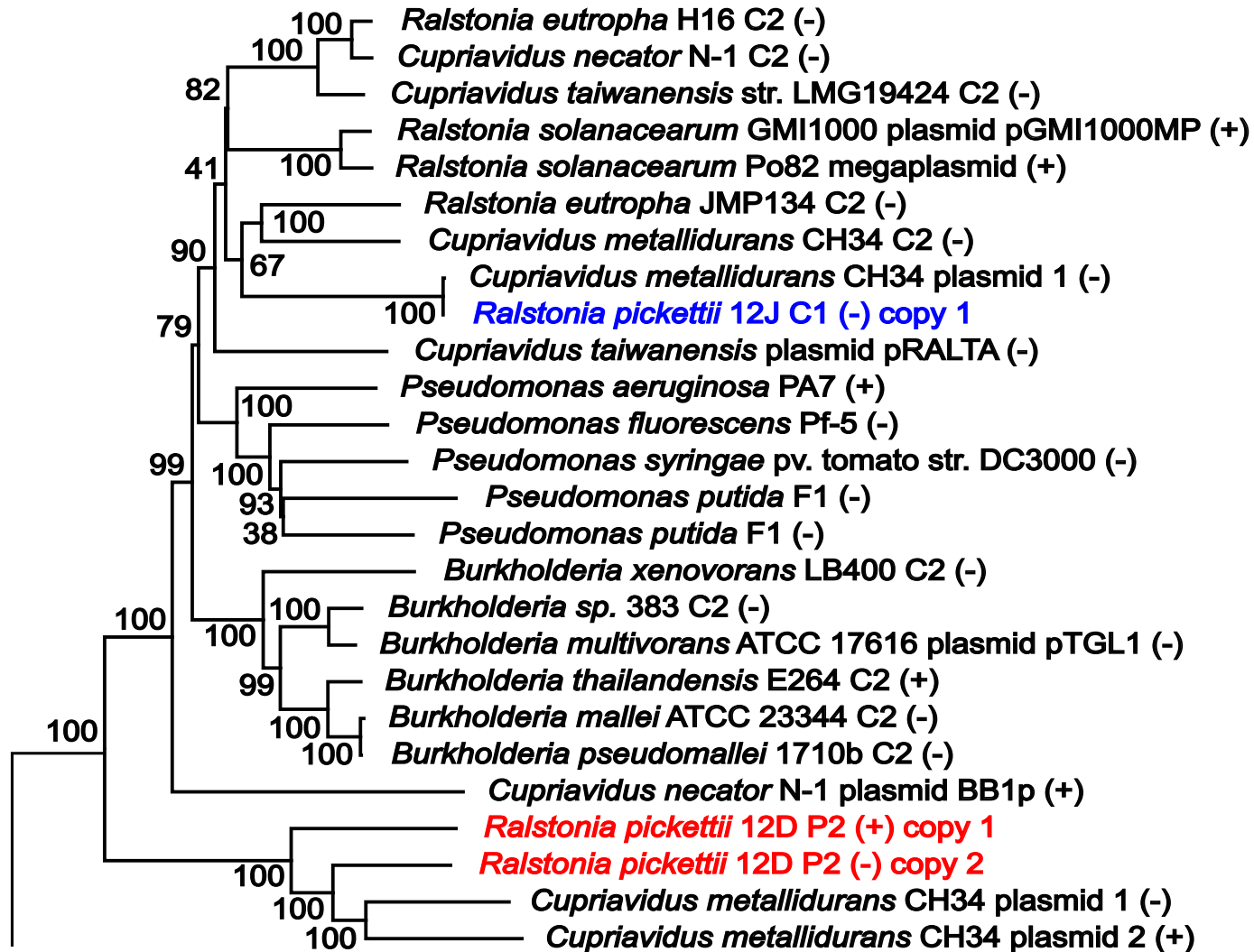


Figure 2.7: Phylogenetic position of *R. pickettii* 12D and 12J *czcA* genes. The numbers on the branches represent bootstrap values.

Figure 2.7 (cont'd)

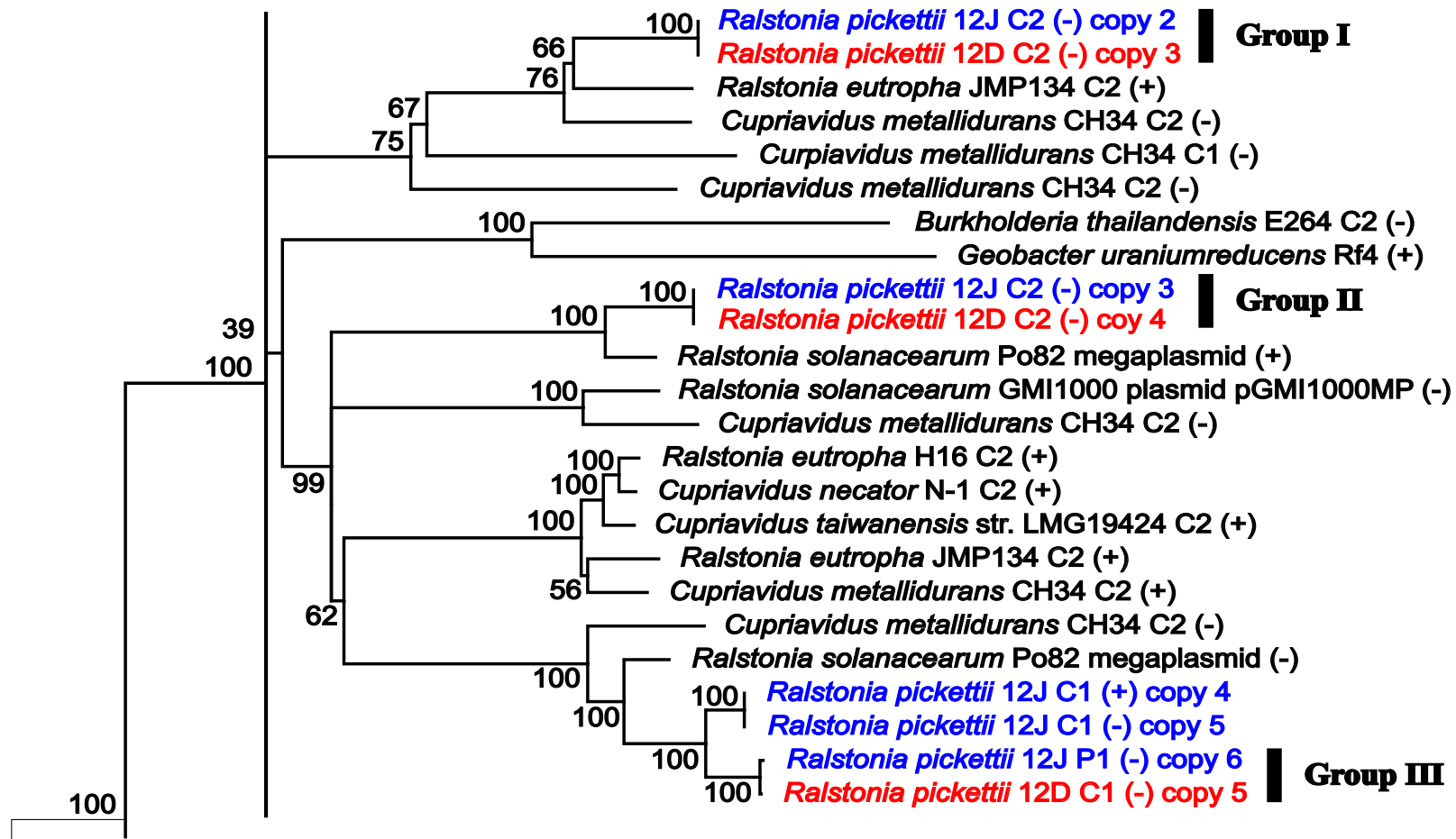


Figure 2.7 (cont'd)

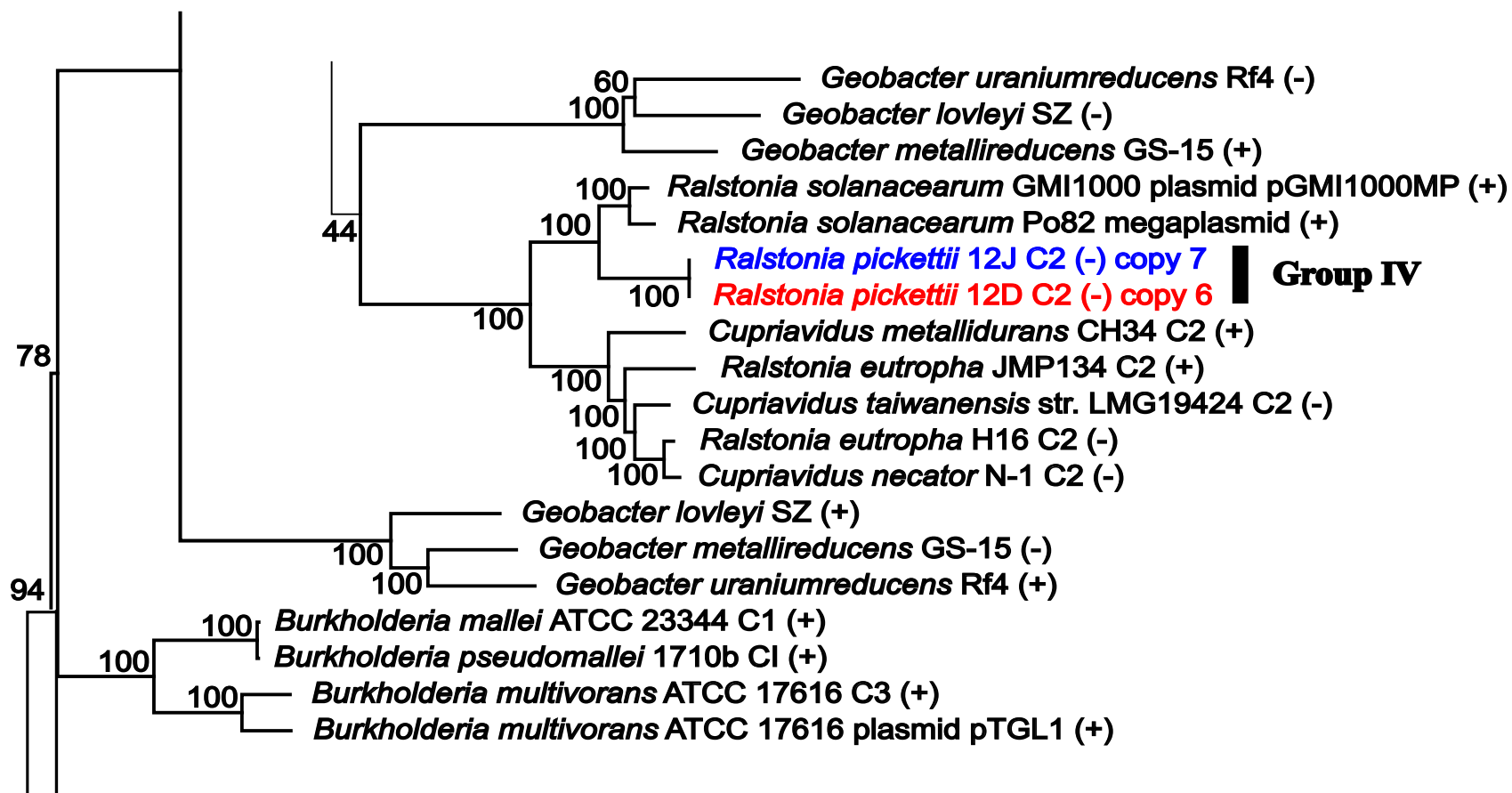
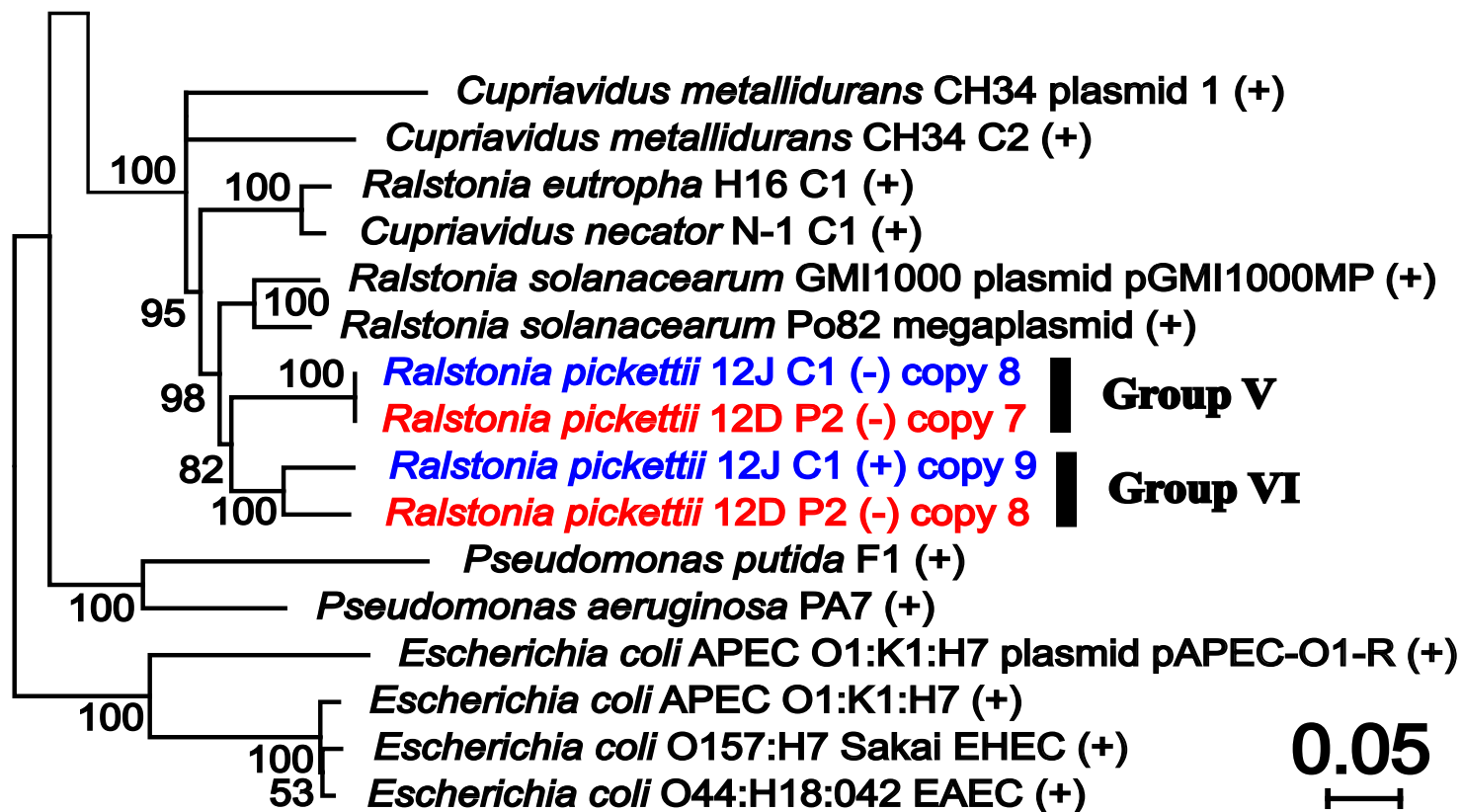


Figure 2.7 (cont'd)



2.4.4.3 The Phylogenetic Lineage of *copA* Copies in *R. pickettii* 12D and 12J

We obtained 24 *copA* sequences from 25 genomes reported in Figure A.1 and constructed a minimal evolution tree (Figure 2.8). Fewer *copA* copies were found and they appeared to be highly similar to those found in *R. solanacearum* Po82, *C. metallidurans* CH34, and γ -*proteobacteria* (*Pseudomonas* and *Escherichia* groups). We observed three incidences where *copA* copies from 12J and 12D clustered together (Figure 2.8 Group I-III). *R. pickettii* 12J C1 copy 2 clustered close to Group I and 12J C1 copy 5 appeared to be distant from all of the other copies (Figure 2.8). *R. pickettii* 12D_P2 carries three *copA* copies which were clustered into two distinct groups (Figure 2.8 12D P2 copy 1/2 and 12D P2 copy 3), suggesting the occurrence of multiple horizontal transfer events.

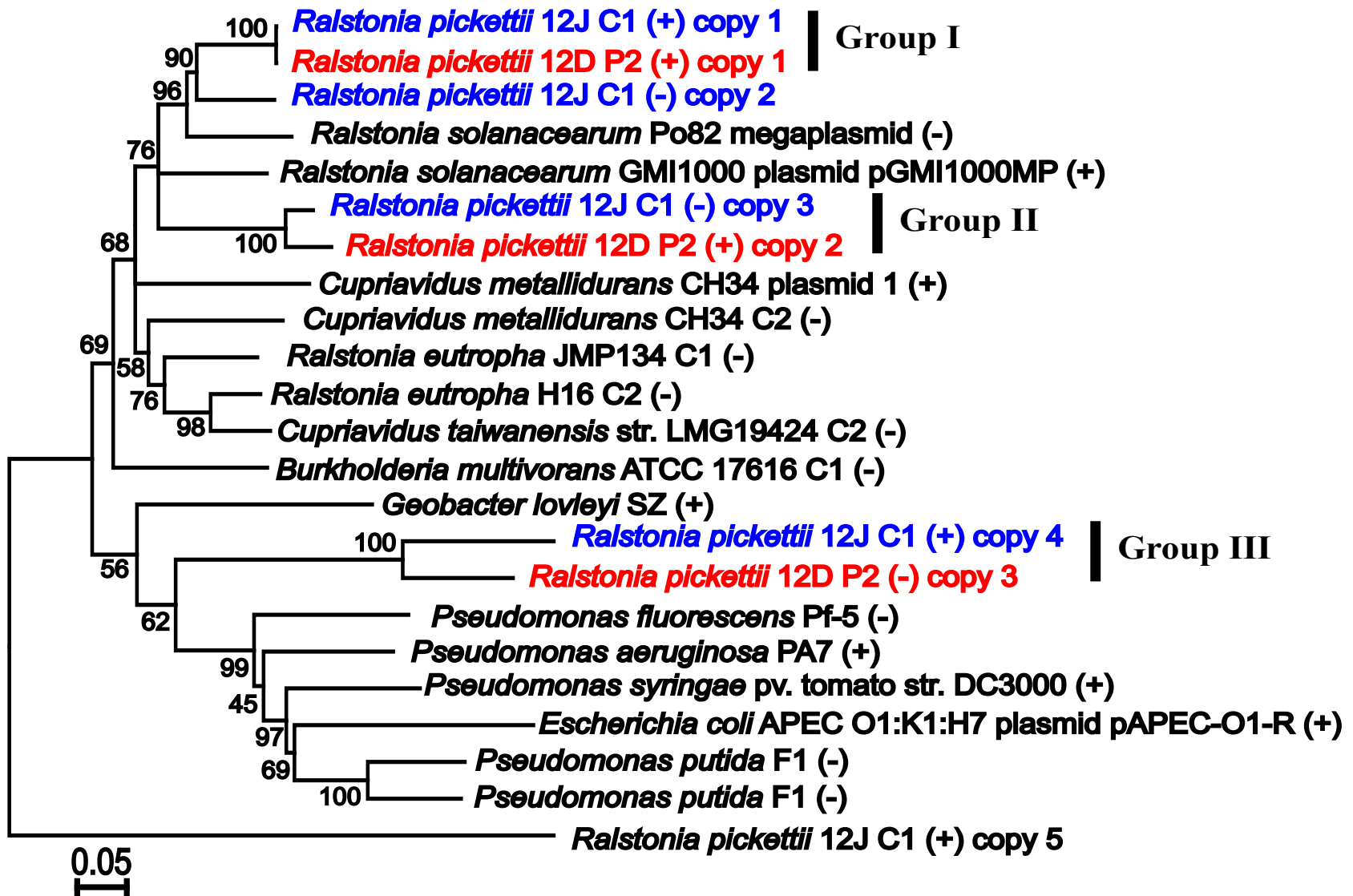


Figure 2.8: Phylogenetic position of *R. pickettii* 12D and 12J *copA* genes. The numbers on the branches represent bootstrap values.

2.5 Discussion

Studying the development of microdiversities gives insights on how environmental factors influence the evolutionary events and how the specific adaptation strategies evolved. In this study, we investigated the genomic differences of *R. pickettii* 12D and 12J and identified possible evolutionary events that occurred as a result of the selective pressure of metal contamination. Under the same amount of heavy metal stress, *R. pickettii* diverged and evolved into two distinct genomovars. Herein, we report the genomic differences between the two strains and the possible evolutionary events behind the divergence.

Interestingly, in what would appear to be a relatively constant environment, the genome structures of *R. pickettii* 12D and 12J are drastically different (5 scaffolds in 12D and 3 scaffolds in 12J). However, both strains share large amounts of genetic information (Figure 2.5 and Figure A.3). Figure 2.5 revealed that 12J_C1 is composed of 12D_C1 and 12D_P2, the secondary chromosomes of both strains are nearly identical, and 12J_P1 could be viewed as 12D_P3 with the addition (or insertion) of 0.028 Mb of 12D_C1. The largest plasmid 12D_P1 is unique to strain 12D. Thus *R. pickettii* 12D and 12J in fact share genetic information across four genome scaffolds.

We observed substantial variations in the *R. pickettii dif* site sequences. Both *R. pickettii* 12D and 12J utilize the same set of *xerCD* genes, located on the primary chromosomes, to resolve dimers created during replications on both the primary and secondary chromosomes. Carnoy et al. [18] have reported that this is a common phenomenon observed in bacteria with multiple chromosomes. It has also been shown that a single set of *xerCD* can bind to distinct *dif* sequences [18, 170]. The ME tree of β -Proteobacteria *dif* sequences suggested

that the 12D_C1 *dif* copy is the closest to the ancestral *R. pickettii* copy and the other three copies from 12D and 12J were derived from the *dif* sequence that is similar to 12J_C1 *dif* (Figure 2.3).

We have previously reported that live filamentous phage particles were isolated from strain 12J and the intracellular replicative form of the virus [191]. This is consistent with our genome analysis, where an intact copy of the filamentous phage genome was found on *R. pickettii* 12J_C1. Besides the integrated p12J, there are three copies of p12J like sequences in *R. pickettii* 12J (two on 12J_C1, and one on 12J_C2). These three copies contain at least four genes that share synteny with p12J genes (Figure 2.4). Two out of three vestigial copies were integrated near 12J *dif* sites. Huber et al. [63] has shown that filamentous phage can be integrated into bacterial chromosomes near *dif* sites only with the assistance of *dif/xerCD* systems. This is consistent with our observation of the integrated filamentous phage. Copy 12J-C1_3, which locates distant to the *dif* site, might be originally integrated into ancestral *R. pickettii* and degraded through evolutionary events. Similarly, we located two vestigial p12J copies in 12D_C1 and 12J_C2. These two copies resemble p12J in structure but contain only two genes that share homology with p12J and their insertion positions are distal to 12D *dif* sites. This observation suggests that copies 12D-C1 and 12D-C2 were integrated into ancestral *R. pickettii* and later mutated (Figure 2.4). Unpublished work in our lab demonstrated that *R. pickettii* 12D could not be infected by p12J. One could speculate that the two vestigial p12J copies in 12D_C1 and 12J_C2 that resemble p12J in structure might be contributing to the phage resistance.

The analyses of 16S rRNA gene sequences, *dif* sites variations, and p12J insertions suggest that the secondary chromosome was present in the common ancestor to 12J and 12D.

It has been frequently proposed that bacterial secondary chromosomes evolved from plasmids with insertions of house keeping genes [123, 149]. Supporting this hypothesis, we have found that both secondary chromosomes of *R. pickettii* 12D and 12J contain the plasmid stabilization protein encoding gene, *kfrA*. Cooper et al. [28] also demonstrated that secondary chromosomes evolve faster than primary chromosomes. Surprisingly, the secondary chromosomes of *R. pickettii* 12D and 12J appeared to undergo many fewer changes than the primary chromosomes (Figure 2.5). We do not know the reasons for this apparent discrepancy in *Ralstonia*.

One obviously major evolutionary event in *R. pickettii* 12D and 12J was the integration of 12D_P2 into the ancestral *R. pickettii* primary chromosome. This inserted region is 0.07 Mb downstream of 12J_C1 *dif* site. The "mosaic" pattern of the inserted region in 12J_C1 indicates that the ancestral primary chromosome acquired more genes from other bacteria after the insertion (Figure 2.6). With this in mind, it is logical to assume that plasmid 12D_P2 transferred into the common ancestor and eventually became inserted into chromosome 1 of what was to become 12J. This common ancestor also contained 12J_P1 (12D_P3) that has been preserved in the two lineages along with C1 and C2. A 0.03 Mb portion of 12D_C1, which was missing in 12J_C1, was also found in 12J_P1 (Figure 2.5 C). This suggests that the insertion in 12J_P1 was due to the integration of 12D_P2 into the ancestral primary chromosome. Hence, the ancestral *R. pickettii* likely contained two chromosomes and two plasmids and lacked a virulent copy of the filamentous phage p12J.

Both *R. pickettii* 12D and 12J have multiple copies of Cu and Co-Zn-Cd resistant genes (Table 2.2). The majority of these copies are located either on a plasmid (12D_P2) or the insertion region that share high synteny to the plasmid (12J_C1). The phylogenetic trees of

czcA and *copA* genes showed that ancestral *R. pickettii* contained a large number of *czcA* and *copA* genes. Both Figure 2.7 and Figure 2.8 revealed that several groups of *czcA* (Group I, II, and VI) and *copA* (Group I-III) genes grouped together on the same branch of lineage. These co-existing groups suggest that these gene copies existed in the ancestral *R. pickettii* genome. Thus, the divergence of *R. pickettii* 12D and 12J appeared to be a recent event.

Horizontal gene transfer (HGT) and gene duplication/amplification (GDA) played a substantial role in the *R. pickettii* 12D and 12J adaptation to the high copper environment. We observed a large number of horizontally transferred foreign genes in both strains (Figure 2.1 and Figure 2.2). *R. pickettii* 12D P1 is especially abundant with foreign genes from Eukaryotes (Figure 2.1 and Table A.1). Previous studies suggested that HGT and GDA have been frequently used by other bacterial strains (e.g. *C. metallidurans* and *Staphylococcus sp.*) to acquire or amplify metal and antibiotic resistance genes [21, 98, 104, 135, 146]. Figure 2.5 showed that strain 12J obtained metal resistant genes, such as *mer* operon and *czc* operon, from other β -Proteobacteria. The phylogenetic trees of *czcA* and *copA* genes revealed that many copies of *czcA* and *copA* genes share lineages with *R. metallidurans* CH34, *R. eutropha* JMP134, *R. solanocentrum* Po82 and GMI1000 and γ -Proteobacteria (*copA* only). These close lineages to other bacteria further confirmed that many of these genes were obtained via HGT. We also observed copies of *czcA* genes (12D P2 copy 2, 12J C1 copy 4 and 5, and Group V) and *copA* genes (12J C1 copy 2) grouped together with other *R. pickettii* 12D and 12J *czcA* and *copA* genes (Figure 2.7 and Figure 2.8). This suggests that these copies of genes were duplicated to confer the metal stress.

We observed that *R. pickettii* 12D and 12J contain fewer copies of Co-Zn-Cd resistant genes and more copies of Cu resistant genes compared to *C. metallidurans* CH34, the model

organism to study the metal resistant determinants (Table 2.2) [67, 71, 105, 111, 160]. This is interesting because *C. metallidurans* CH34 was isolated from a Zn rich environment and *R. pickettii* 12D and 12J were isolated from a Cu rich environment [80, 171]. It is clearly shown here that *C. metallidurans* contains more Co-Zn-Cd resistant genes because it was isolated from a high Zn environment and *R. pickettii* 12D and 12J contains more Cu resistant genes because it was isolated from a high copper environment. This is consistent with the environmental conditions from which the strains were isolated and presumably reflecting the selection pressures they were subjected to.

We observed that *R. pickettii* 12D and 12J contain a large number of *cop* gene copies and they are more abundant in 12J than 12D (Table 2.2). We found four copies of *czcE*, a copper binding protein encoding gene described by Zoropogui et al. in 12J and only three in 12D [195]. Together, these high copy numbered copper resistant and binding genes could elucidate the larger amount of copper sequestered by *R. pickettii* 12D and 12J [191]. The larger copy numbers of *czcE* genes in 12J also correlates with the larger amount of copper sequestered by 12J cells which was previously reported [191].

Passot et al. previously suggested that we are witnessing the emergence of the third chromosome in 12J [123]. However, our results indicate that 12J actively integrates genes rather than splitting chromosomes. Interestingly, we noticed that *R. pickettii* 12D_P1 is large in size and contains a large amount of horizontally transferred genes and IS elements. This plasmid is substantially different from the other plasmids in 12D and 12J. It contains *kfrA* and replication *repA* gene like the secondary chromosomes. Thus, it resembles a possible early stage tertiary chromosome. All of this adaptation and evolution evidence suggests that we are witnessing the co-evolution of two strains and the rising of diversity within the species.

The different evolutionary strategies *R. pickettii* 12D and 12J took for adaptation in a heavy metal environment might be the beginning of speciation.

2.6 Conclusion

In this study, we compare the genomic variations between two *R. pickettii* strains to reveal the development of *R. pickettii* microdiversity in Torch Lake, Houghton, MI. Our results indicated that *R. pickettii* 12D and 12J acquired metal (eg. copper, cobalt-zinc-cadmium, mercury) resistant genes from other bacteria, such as *R. solanocerum* and *C. metallodurans*, via horizontal gene transfer. Under the pressure of high copper in the environment, both strains also increased the number of metal resistant gene copies via gene duplication/amplification. We found that a larger number of copper resistant gene copies (12J > 12D) corresponds to a greater amount of actively sequestered copper (12J > 12D). The comparative genomic analysis suggests that both strains co-evolved under the pressure of high copper. Gaining the resistance to filamentous phage in *R. pickettii* 12D might be the beginning of the divergence. We predict that the ancestral *R. pickettii* had one primary chromosome (similar to 12J_C1 minus the insertion from 12D_P2), a secondary chromosome (similar to 12J_C2 or 12D_C2), two plasmids (similar to 12D_P2 and 12D_P3) and a filamentous phage particle. After the divergence, strain 12J actively integrated mobile elements containing metal resistant genes and strain 12D maintained original plasmids and acquired another large plasmid (12D_P1), which was largely composed of horizontally transferred foreign genes. We suspect that 12D_P1 is undergoing the process of being transformed to a third chromosome. The differences in metal-resistant gene copies and genome scaffolds suggested the development

of *R. pickettii* microdiversity might be the first step in speciation. Our results also showed that secondary chromosomes of *R. pickettii* 12D and 12J appeared to be much more stable than the primary chromosomes during the evolution. This finding was to our surprise because it is the opposite of the observations of Cooper et al., which suggested that secondary chromosomes mutate and evolve faster than primary chromosomes [28]. We suspect that secondary chromosomes are preferably preserved in microdiversity but preferably modified across species.

CHAPTER 3

RESOURCE-INDUCED BACTERIAL STRUCTURE SHIFTS AND THEIR INFLUENCE ON COMMUNITY FUNCTIONS

3.1 Abstract

Subsurface uranium contamination poses serious health risks and is costly to remove by traditional physical-chemical methods. A more cost-effective method has proven to be *in situ* immobilization of subsurface uranium via the microbially mediated process. The full potential of this approach would be facilitated by the identification of all microbial species, including previously uncultured strains, that play a substantial role in uranium immobilization. However, *in situ* studies are influenced by uncontrolled environmental factors and soil bacterial communities are complex. Thus, we used standard enrichment protocols on bacterial communities from uranium contaminated sediments to select for strains capable of immobilizing uranium. Previous studies have indicated that many uranium reducing bacteria are also able to reduce nitrate and iron. Therefore, minimal media supplemented with lactate in combination with nitrate, ferric citrate, or uranyl acetate were used as the conditions of enrichment. Culture independent bacterial community analyses showed that bacterial communities shifted drastically upon enrichment and Firmicutes were observed in all enrichments. Genera *Psychrosinus* and *Clostridium* were particularly abundant in uranyl acetate enrichments and were commonly detected in both uranium and iron enriched communities. Despite the drastic structural shifts, we observed a stable functional gene profile in all enrichment communities. Our findings indicated that phylum Firmicutes might play a substantial

role in uranium immobilization. The stable functional gene profiles targeting over 44,000 genes of the enriched bacterial communities suggested that the net function of the bacterial communities that resided in the uranium contaminated environments remained unchanged.

3.2 Introduction

Uranium is a naturally occurring radioactive metal that can be detected in rocks, soil and streams. Due to weathering, oxidized uranium (U^{6+}) is commonly found in the environment. Human beings are exposed to this background uranium at low levels via food and water (~ 0.7 - $1.1 \mu\text{g}/\text{day}$) without potential health threats. However, human activities such as mining and weapon development released elevated amounts of uranium in the environment. Among 1,517 former and current United States Environmental Protection Agency (USEPA) National Priority List (NPL) sites, at least 54 sites were identified as uranium contaminated [167, 168]. The uranium contaminants can permeate into ground water and become a health threat to human beings. The Oak Ridge National Laboratory (ORNL) integrated Field Research Center (iFRC) is an example of a site with extensive underground uranium contamination. The uranium containing wastes penetrated an unlined waste pond (S-3 area), contaminated the groundwater, and formed secondary contaminant sources with the soil sediments in subsurface. This large area subsurface contamination site poses a great challenge the development of cost-effective remediation methods.

Lovley et al. [89, 88] discovered that some microorganisms were able to utilize oxidized metals (e.g., Fe^{3+} , Mn^{4+}) as electron acceptors to generate energy under anaerobic conditions. It was also shown and proven by Gorby et al. that U^{6+} could also be used as the

electron acceptor during bacterial anaerobic respiration [52]. The reduced uranium, U^{4+} is less stable (can be readily oxidized to U^{6+}) but insoluble in water [14, 43]. Thus, by decreasing the solubility of uranium (e.g., forming uraninite), uranium could be removed from ground water. Several studies have also shown that iron and sulfate reducing bacteria have the potential to immobilize uranium via enzymatic activities [97, 102, 148, 186]. Encouraged by these laboratory results, researches on *in situ* bioremediation have been performed at several Department of Energy (DOE) uranium contaminated research sites [16, 17, 64, 77, 187, 188, 190].

Wu et al. conducted *in situ* uranium immobilization studies at Oak Ridge National Laboratory (ORNL) integrated Field Research Challenge (iFRC) site S-3 area [187, 188]. Uranium reduction in this area is particularly challenging because of the inhibition caused by pore water with low pH and high concentrations of nitrate and aluminum [187]. To overcome the inhibition of uranium reduction, Wu et al. [187] designed a nested circulation system, where a pH neutral zone (the outer loop) was created and a biostimulation zone (the inner loop) was established within the pH neutral zone. Within the biostimulation zone, Wu et al. successfully demonstrated that U^{6+} was immobilized in its reduced form (U^{4+}) [188]. Cardenas et al. investigated the bacterial community shifts accompanied the reduction of uranium in the biostimulation zone and suggested that sulfate reducing bacteria might play a substantial role in uranium reduction [16, 17].

In situ bacterial community shifts reflecting uranium reduction are particularly informative in the identification of novel uranium immobilizers. However, these populations are usually difficult to isolate and their activities cannot be directly confirmed. In addition, the *in situ* community dynamics are strongly influenced by the field environmental factors

[35]. For these reasons, a controlled system that leads to cultivation of potential uranium immobilizers is desirable.

Herein, we report our studies on identifying the potential uranium immobilizing populations by enriching uranium exposed soil sediments in the laboratory. Soil sediments were collected from ORNL iFRC site, specifically within the biostimulation zone (FW102-2 and FW102-3) and pH neutral zone (FW107) of the nested circulation system. Sample FW102-2 and FW102-3 were collected from the same monitoring well but at two depths (13.7 m bgs and 12.2 bgs, respectively). Cardenas et al. [16] previously reported that soluble uranium concentrations decreased in monitoring well FW102. No bacterial community studies have been conducted in the pH neutral zone. All three samples contained a large amount of uranium (700 ppm in FW107, 1600 ppm in FW102-2, 300 ppm in FW102-3). Thus, we hypothesized that all three samples contain strains capable of immobilizing uranium. Besides uranium, the ORNL iFRC S-3 area where these samples were collected are also abundant in nitrate and iron [187]. It is known thermodynamically that anaerobic energy yield ranks as $\text{NO}_3^- > \text{Fe}^{3+} > \text{U}^{6+}$. Research studies have also shown that uranium reducers are capable of nitrate and iron reduction [2, 163]. Therefore, we enriched soil sediments in minimal media supplemented with NO_3^- , or Fe^{3+} , or U^{6+} . By doing this we expected to identify specific bacterial community shifts associated with uranium enriching processes.

3.3 Materials and Methods

3.3.1 Anaerobic Media and Stocks

Minimal growth media (FWM and FWM-Fe) were modified based on previously reported freshwater-medium and ferric-citrate media [87]. The detailed composition of FWM is listed in Table B.1, Table B.2 and Table B.3. FWM-Fe medium is the same as FWM but supplemented with 56 mM of ferric citrate. Supplement stocks, sodium lactate (2 M) and sodium nitrate (1 M) solutions were prepared by dissolving chemicals in deionized water to desired concentrations. Stocks solutions were filter (0.22 μm) sterilized. Uranyl acetate stock (100 mM) was prepared by dissolving uranyl acetate powder in 30 mM pH7 sodium bicarbonate solution. Filter sterilization was also applied. All media and stock solutions were bubbled under $\text{N}_2:\text{CO}_2$ (80:20) to eliminate oxygen.

3.3.2 Bacterial Community Enrichments

Three uranium contaminated soil samples (FW102-2, FW102-3, and FW107) were collected anaerobically from the nested recirculation experimental site at Oak Ridge iFRC S-3 area (denoted as "O" in sample labels). Bacterial consortia from these soil sediments (10%, v/v) were enriched in FWM [86] supplemented with sodium lactate (20 mM) combined with either sodium nitrate (10 mM, denoted as "NO3" in sample labels), or ferric citrate (56 mM, denoted as "Fe" in sample labels) or uranyl acetate (0.25 mM, denoted as "U" in sample labels) in duplicates at 15 °C. One control culture without the addition of inocula was also set up for each enrichment condition. The soil sediments were enriched for a total of 35 days and another 20mM lactate was injected on the 17th day after sampling to provide additional

nutrients (after sampling). Two-ml samples were taken from ferric citrate enrichments and passed through 0.22 μm HPLC certified syringe filters (Sun SRI Titan2 17mm Syringe Filters, Thermo Fisher Scientific) on the 1st, 17th and 35th day of incubation. Samples were mixed with HCl to obtain a final concentration of 0.5 M HCl and stored at -20°C until being processed. Half of the sample was used to monitor the depletion of lactate and half for the reduction of Fe^{3+} . The enrichments were then used as inocula (1% v/v) for secondary enrichments under the same conditions. Additional sodium lactate was added on the 13th day. The ferric citrate enrichments were again monitored for 35 days. Bacterial consortia samples were collected at the end of second enriching period (70th day) for 16S rRNA gene and community functional gene profiling. From each enrichment, two 1 ml samples were withdrawn and centrifuged at 10,000 RPM for 20 minutes in a Sorvall SS-34 rotor and the pellet was stored at -20°C until extraction of community DNA. The remaining material was processed using GeoChip [57].

3.3.3 Quantitative Analyses

The concentration of sodium lactate was determined using high-performance liquid chromatography (HPLC) with an Aminex HPX-87H column (polystyrene-divinylbenzene ion exchange resins, Bio-Rad, Hercules, CA). Sodium lactate and acetate mixtures were used as standards (0.04 μM - 0.4 μM) and freshly prepared in triplicate prior to sample analyses. A mixture of acetonitrile and sulfuric acid (5%) was used as the eluent.

Iron reduction was determined by the previously published ferrozine assay [154]. Briefly, 0.1 ml of filtered acidified ferric citrate sample was added to 0.9 ml 1 M HCl. This mixture (0.1 ml) was then added to 1 ml ferrozine buffer (a mixture of 50 mM HEPES and 0.1%

ferrozine with a final pH of 7) and incubated for 10 minutes at room temperature. After incubation, 200 μ l was added to a clear flat-bottom Corning 96-well microtiter plate (Corning Scientific, Tewksbury, MA) and absorbance was measured at 520 nm.

3.3.4 DNA Extraction and Community Profiling

Community DNA was extracted by using Powersoil DNA Extraction Kit (Mo Bio Laboratory, Carlsbad, CA). Two pyrosequencing chemistries (454 FLX and 454 Titanium) were used to evaluate the bacterial 16S community structure. For samples in replicate 1, bacterial 16S rRNA gene V4-V5 regions (Forward 5'AYTGGGYDTAAAGNG3' and Reverse 5'TACN-VGGGTATCTAATCC3') were amplified as previously described [157]. Samples from replicate 2 were amplified with primer sets developed by Human Microbiome Project (HMP) targeting the V3-V5 region (357F 5'CCTACGGGAGGCAGCAG3' and 926R: 5'CCGT-CAATTCMTTTRAGT3') of 16S rRNA genes. Both polymerase Chain Reactions (PCR) were carried out by mixing 1X Taq reaction buffer, 2 mM MgSO₄, 0.1 mg/ml BSA, 0.2 mM of each dNTP, 0.33 μ M of each primer, 0.125 U/ μ l of Platinum High Fidelity Taq Polymerase (Invitrogen, Carlsbad, CA), 10 ng DNA template and DNase and RNase free water. The amplification conditions include an initial denaturing step at 95°C for 5 minutes, followed by 30 cycles of 3 temperature step consisted of denaturing at 95°C for 45 seconds, annealing at 50°C for 45 seconds, and elongation at 72°C for 90 seconds, and a final extension at 72°C for 5 minutes. All amplified 16S rRNA gene PCR products were visualized on 2% Tris-Borate-EDTA (TBE) agarose gel. DNA fragments at \sim 450 bp (V4-V5) and \sim 569 bp (V3-V5) were excised and extracted from the gels by using Qiagen Gel Extraction Kit and further purified with QiaQuick PCR Product Purification Kit (Qiagen, Valencia, CA). All

purified DNA products were quantitated with Qubit HS Double-stranded DNA Kit (Invitrogen, Carlsbad, CA) then composited at equal mass for a final DNA concentration of 0.5 ng/ μ l. Pyrosequencing was performed at Michigan State University RTSF by using a Roche 454 GSFLX and 454 GSFLX Titanium Sequencers.

Functional gene profiling of the enriched consortia was performed at Oklahoma University. Community DNA were extracted as previously described [172]. GeoChip 3.0 was used to access the functional gene profiles of U^{6+} and NO_3^- enriched samples in replicate 2. GeoChip 5.0 was used to access the functional gene profiles of the original soil sediment communities and the Fe^{3+} , U^{6+} and NO_3^- enriched communities in replicate 1 and Fe^{3+} and NO_3^- enriched communities in replicate 2. GeoChip 3.0 and GeoChip 5.0 data were combined and GeoChip 3.0 replicate 2 NO_3^- enrichment data were omitted for analysis purpose.

3.3.5 Community Analysis

Bacterial 16S rRNA gene sequences obtained from pyrosequencing were processed and analyzed using the Ribosomal Database Project (RDP) Pyrosequencing pipeline [180]. Sequences that were shorter than 250 bp, containing any N's in the sequencing region, or with an average quality score less than 20 were discarded. Chimeras were removed from RDP processed sequences by using USEARCH (UCHIME reference mode with Silva gold alignment database as reference). RDP complete linkage clustering was used to determine bacterial operational taxonomic units (OTUs) based on 97% sequence similarity. To eliminate the clustering artifacts, sequences were trimmed to the same length (144 bp model position) based on RDP alignment profiles prior to clustering. RDP Multi-classifier was used to identify each sequence to bacterial genus level (threshold 80). Any identified genus that has a

total count of 1 across all samples (21 samples) was omitted from analyses. RDP SeqMatch was used for further identification of bacterial clusters of interest.

OTU- and phylotype-based community analyses were performed by using statistical software R [128]. Ecological indices were estimated for each bioreactor sample based on clustered sequences by using R package Vegan [117]. Specifically, community richness (ChaoI), diversity indices (Shannon H') and community evenness (E) were calculated based on equations previously described [94]. Diversity index Shannon H' was expressed as magnified H' ($e^{H'}$) to emphasize the differences among samples [94]. The sampling coverage (C) of each sample was calculated based on Good's method, $C=1-n_1/N$, where n_1 represents number of OTUs that was observed once and N is the total number of sequences in the sample [39]. R package Vegan was also used to perform non-metric multidimensional scaling analysis (NMDS) to correlate the dissimilarities among bioreactor samples and the shifts in phylotype abundance [117]. To identify the shared genera among different enrichments, genera found in both duplicated enrichments were extrapolated first. Venn diagrams of these dereplicated genera were then constructed by using the R package Vennerable [159].

3.4 Results

3.4.1 Monitoring the Enrichment Cultures

Three soil sediments were collected from locations containing 700 ppm (FW107), 1600 ppm (FW102-2) and 300 ppm (FW102-3) uranium. Among three electron acceptor supplemented enrichments, we observed growth in nitrate supplemented enrichments as early as the 5th day. All enrichments grew equally well. Between the 15th and 30th day, we observed Fe^{3+}

reduction in ferric citrate enrichments, where the culture turned dark brown. The change of colors were first observed in FW102-2 and FW102-3 enrichments. FW107 enrichments changed color by day 30. A large amount of precipitates were formed upon the addition of uranyl acetate. Hence, it was difficult to differentiate the growth of the uranium enrichment cultures from the turbidity due to precipitation. However, we did observe abundant live cells under the microscope throughout the enrichment process.

The monitored ferric citrate enrichments revealed that iron was actively reduced to Fe^{2+} while sodium lactate was used as the electron donor and carbon source (Figure 3.1). No growth was observed in the control microcosms and we did not detect Fe^{2+} (above background level) in these control cultures. Under the same enrichment condition, we observed that the FW-107 culture reduced the least amount of Fe^{3+} (Figure 3.1 A and B) and accumulated the most amount of acetate (Figure 3.1 C and D). Some acetate accumulated in FW102-2 and FW102-3 ferric citrate enrichments by the 13th day of incubation. However, this acetate was consumed by the end of the incubation period (Figure 3.1 C and D). Second generation enrichments were more efficient at iron reduction and lactate utilization than the first generation.

3.4.2 Overview of the Community Dynamics

Bacterial communities of the original iFRC soil sediments and the enrichment cultures were investigated based on bacterial 16S rRNA sequences. We obtained 703 to 8213 sequences per sample. Although two different sequencing chemistry were used, the ecological indices indicated that the data obtain between two replicates are comparable (Table 3.1). Pyrosequencing was able to cover at least 97% of the sample community, except for FW1022_O,

the original soil sediment sample from well FW102-2, which also had the least number of sequences (Table 3.1 column C). All of the original soil sediments appeared to be more even and diverse than the enriched samples, as we expected. We also found that the original community in FW107 contained only 75 OTUs, considerably fewer than were found in FW102-2 and FW102-3. ChaoI, Magnified Simpson ($e^{H'}$) and evenness (E) indices also showed that the original community of FW107 was much less diverse and more skewed than the other two. Uranyl acetate and ferric citrate enrichments were the most skewed and least diverse samples in both FW102 groups and FW107 group, respectively (Table 3.1).

3.4.3 Shifts in the Enrichment Bacterial Community Structures

A detailed comparison of the bacterial community structures showed substantial shifts among enrichments (Figure 3.2). The ten most abundant genera summed from all 21 samples and their distributions in each community were compared side-by-side. Consistent with the ecological indices, we observed that community structures between replicates were similar, however substantial differences were observed among enrichments. FW107 group appeared to be different from the others. FW107 original sample and enrichment samples were highly dominated by one or two genera. The original soil sediment sample collected from FW107 was abundant with *Sulfuricurvum*, which was not found in other samples. Over 80% of sequences from the FW107 ferric citrate enrichments were unclassified *Veillonellaceae*. *Psychrosinus* were found dominant in FW107 uranyl acetate enrichment cultures. FW102-2 and FW102-3 bacterial consortia enriched under the same condition appeared to be similar. While all ten genera constituted less than 10% of the populations in FW102-2 and FW102-3 soil sediment samples, *Sulfuricurvum* comprised of over 70% of the FW107 original community

Table 3.1: Ecological indices of iFRC enrichment bacterial communities. O represents original soil sediment samples. Fe, NO₃, and U supplemented enrichment cultures.

		Total					
	Replicate	Sequences	OTU	ChaoI	$e^{H'}$	E	C (%)
FW1022_O	0	703	146	286.05	53.33	0.80	88.76%
FW1022_Fe	1	6623	57	91.20	13.48	0.64	99.71
	2	5891	72	107.00	14.86	0.63	99.64
FW1022_NO3	1	2293	67	92.00	6.49	0.44	98.91
	2	8213	65	89.00	9.14	0.53	99.81
FW1022_U	1	1125	16	19.75	1.95	0.24	99.47
	2	5152	44	49.14	3.81	0.35	99.83
FW1023_O	0	6078	203	309.24	26.87	0.62	98.70
FW1023_Fe	1	3700	60	77.10	7.68	0.50	99.49
	2	4315	50	71.38	7.08	0.50	99.56
FW1023_NO3	1	878	31	37.43	5.76	0.51	98.86
	2	5488	70	101.63	9.31	0.53	99.58
FW1023_U	1	6008	53	78.67	4.09	0.35	99.63
	2	6055	49	62.00	5.38	0.43	99.79
FW107_O	0	1410	75	117.00	4.04	0.32	97.45
FW107_Fe	1	1664	17	22.60	2.17	0.27	99.52
	2	2956	15	29.00	1.21	0.07	99.73
FW107_NO3	2	3596	56	123.67	5.05	0.40	99.19
	1	4102	62	76.25	7.64	0.49	99.54
FW107_U	1	771	32	36.67	3.87	0.39	98.96
	2	4679	46	50.20	3.40	0.32	99.85

sequences. A large amount of *Geobacter* were detected in the ferric citrate and uranyl acetate enrichments. The proportion of these ten genera increased as the enrichment stress went from nitrate to iron to uranium (Figure 3.2). We also observed that *Psychrosinus* was found in all samples (except FW107 ferric citrate enrichments) and its abundance increased as the enrichment stress increased (Figure 3.2).

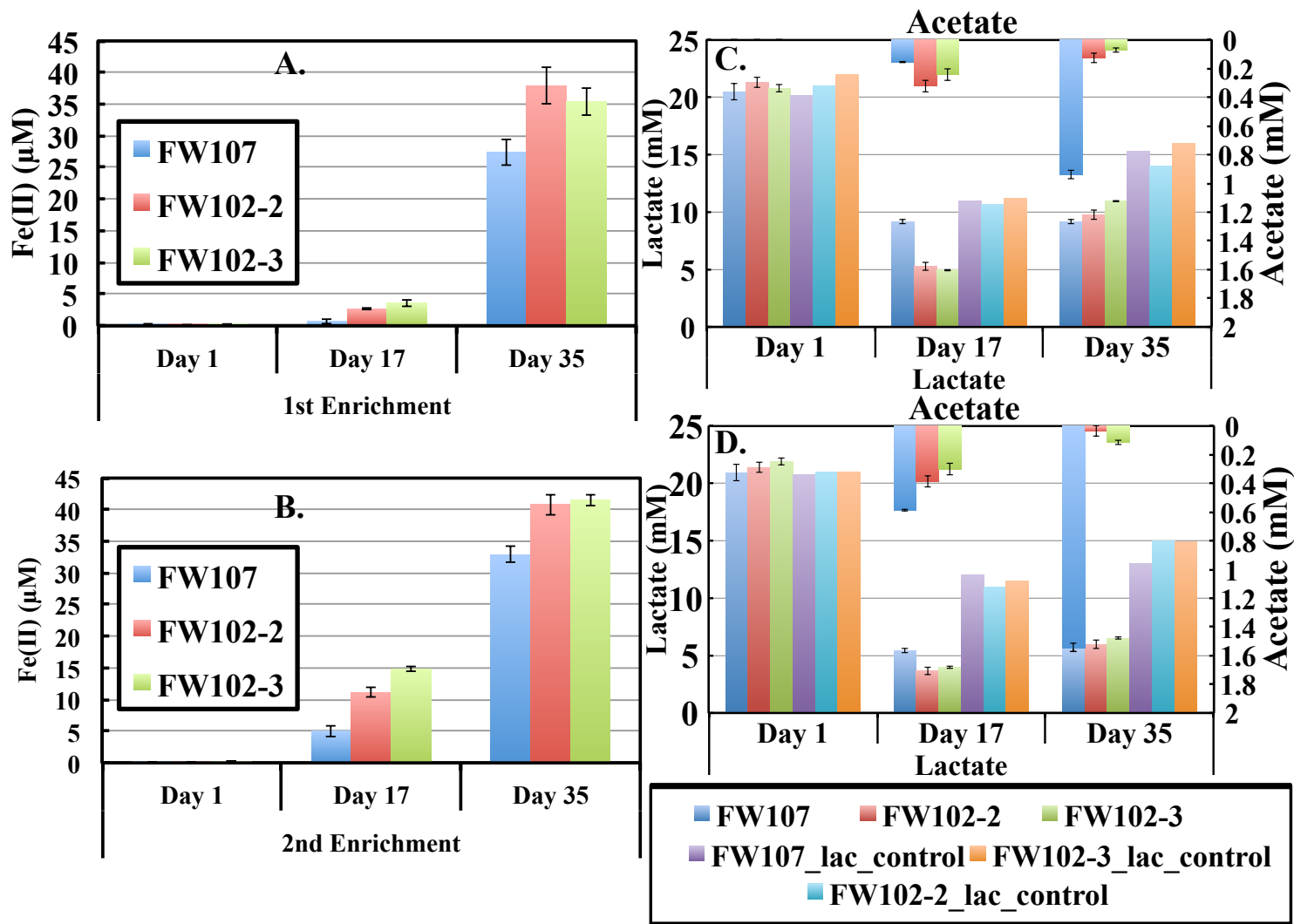


Figure 3.1: The concentration of Fe^{2+} (panels A and B), lactate and acetate (panels C and D) in each ferric citrate enrichment cultures. The first generation enrichments are presented in panel A and C and the second generation enrichments are presented in panel B and D. Error bars represent the differences between two replicates.

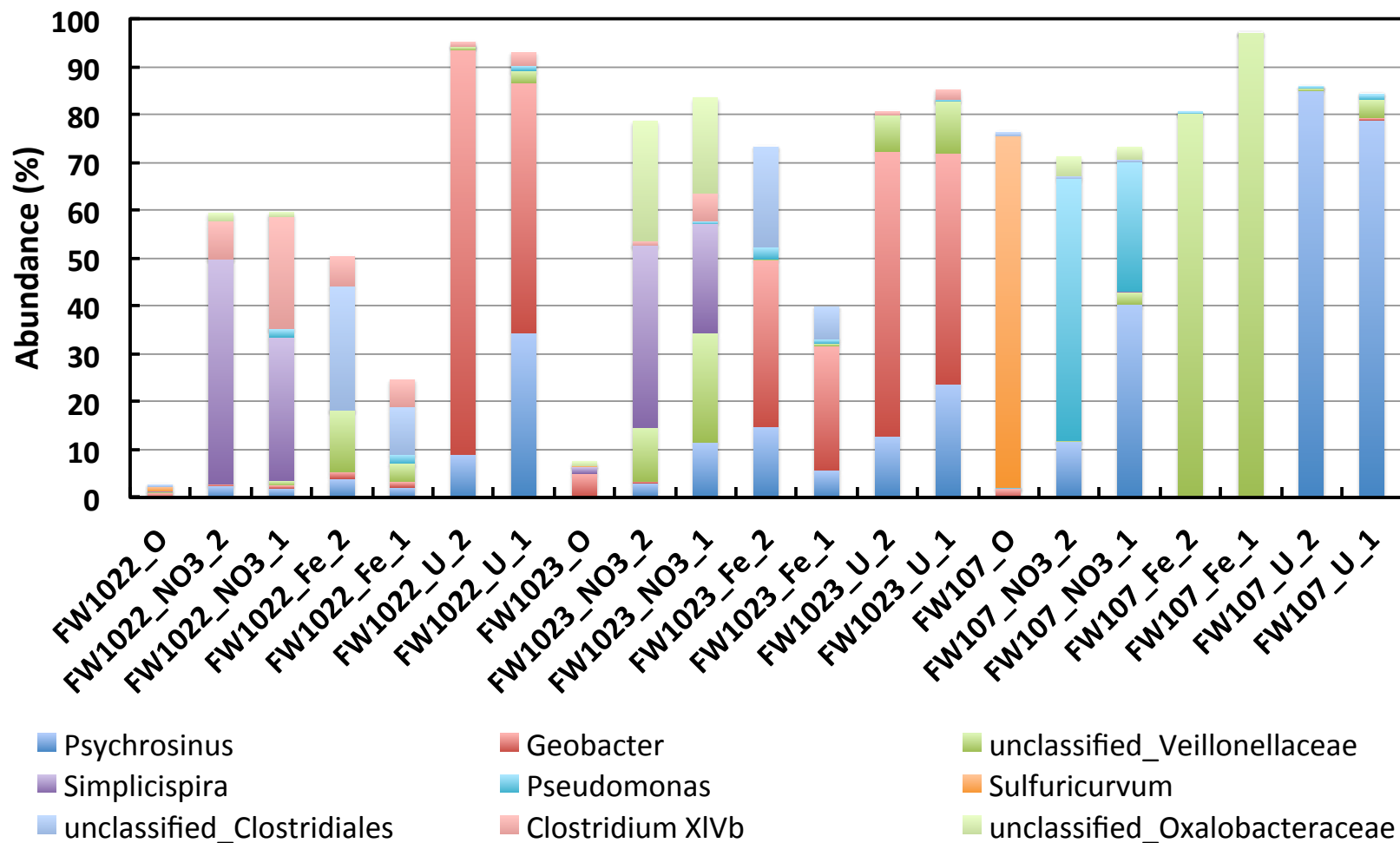


Figure 3.2: The top ten (summed across all samples) most abundant genera identified via RDP multiclassifier. Sample replicates were labeled as "_1" and "_2". Original soil sediment samples were denoted with "_O."

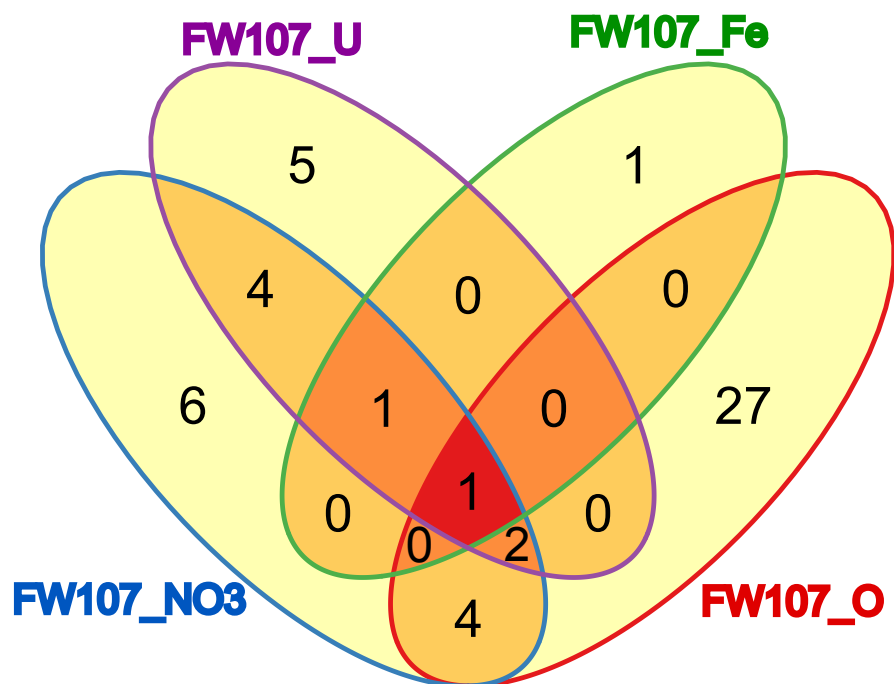


Figure 3.3: The shared genera among FW107 samples. The color of sample font is the same as the cognate ellipse.

3.4.4 Shared Genera

We identify the bacterial genera that were shared among enrichments. Venn diagrams were constructed on essential genera that were shared between the replicated cultures of FW107, FW102-2 and FW102-3 samples. Among 51 genera identified in the original FW107 sediment and enriched consortia, over 50% were unique to FW107 and only one (*Sulfurospirillum*) was shared by all four samples (Figure 3.3). The unique genus in FW107 iron enrichment was *Trichococcus*. FW107 uranium and nitrate enrichment cultures shared 5 genera, out of which, one was also detected in iron enrichment consortia and the other four were *Psychrosinus*, *Pseudomonas* and two groups of *Clostridium*. Five genera, unclassified *Ruminococcaceae*, *Oscillibacter*, *Clostridium sensu stricto*, *Clostridium IV*, and *Acidovorax* were found only in uranium enriched FW107 cultures. Unclassified *Veillonellaceae* was found in uranium, iron

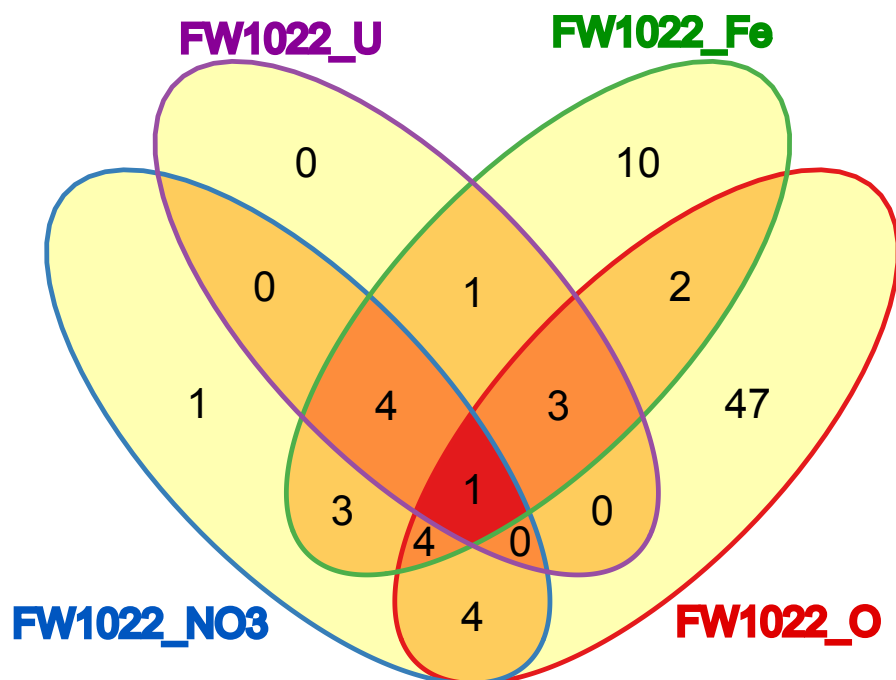


Figure 3.4: The shared genera among FW102-2 samples. The color of sample font is the same as the cognate ellipse.

and nitrate enriched consortia.

A large number of unique genera (47) were found in FW102-2 original soil sediment sample (Figure 3.4). Uranyl acetate enrichment of FW102-2 appeared to be a subset of FW102-2 ferric citrate enrichment. The four genera shared by ferric citrate, nitrate and uranium enrichments were *Sulfurospirillum*, *Sporomusa*, *Psychrosinus*, and *Geobacter*.

FW102-3 samples contained a total number of 107 bacterial genera, 70 of which were unique in the FW102-3 original soil sediment (Figure 3.5). *Psychrosinus* was found common in iron, nitrate and uranium enrichment cultures. *Geobacter* and unclassified *Veillonellaceae* were shared by all four samples (Figure 3.5). Unclassified *Ruminococcaceae*, unclassified Bacteroidetes, *Sporomusa*, *Desulfosporomusa*, *Clostridium* III were only found in uranyl acetate enriched FW102-3 consortia. Among FW107, FW102-2 and FW102-3 uranium enrichments,

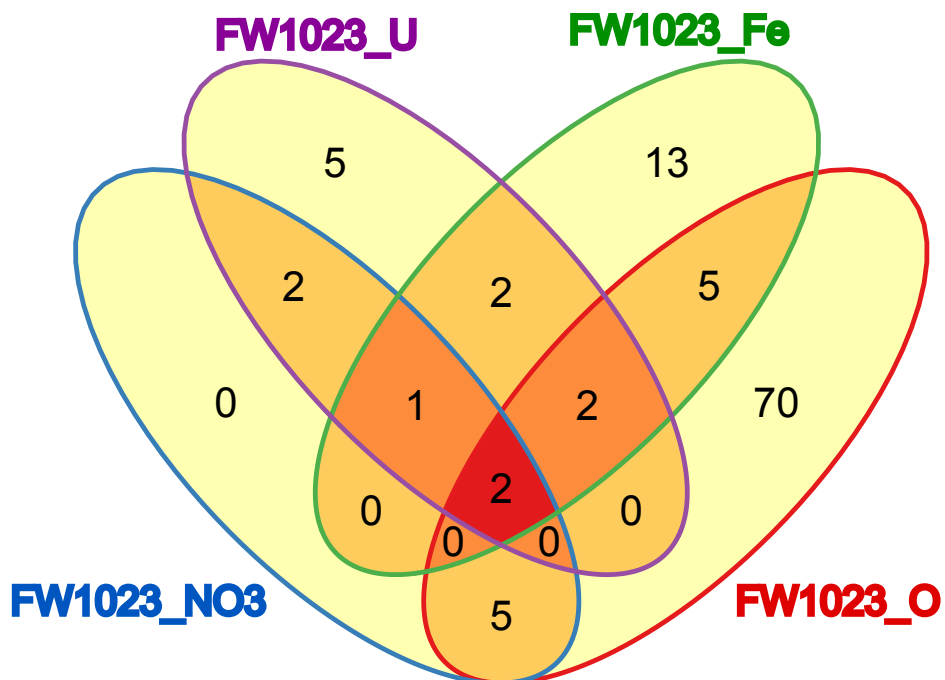


Figure 3.5: The shared genera among FW102-3 samples. The color of sample font is the same as the cognate ellipse.

Sporomusa and *Psychrosinus* were the two numerically dominant taxa based on sequence frequency.

3.4.5 Functional Gene Profiles

GeoChip profiles revealed that there were 1532 functional genes (between different GeoChip platforms) found in different microorganisms. Four uranium enriched samples, FW107_U(2), FW107_U, FW1022_U(2), and FW1023_U(2) appeared to be substantially different from the others (Figure 3.6). These four samples had many fewer abundant functional genes suggesting that uranium selects for a smaller collection of taxa. Three out of four samples were analyzed by GeoChip3. Although both FW107 uranium enrichment duplicates clustered close to each other, uranium enrichment duplicate 2 of FW102-2 and FW102-3 appeared

to be different from duplicate 1 (Figure 3.6). Analysis on GeoChip5.0 enrichment culture replicate 1 alone showed that the overall variation among all samples was small (Figure B.1). Thus, we suspect the different GeoChip platforms contributed substantially to the differences among samples we observed.

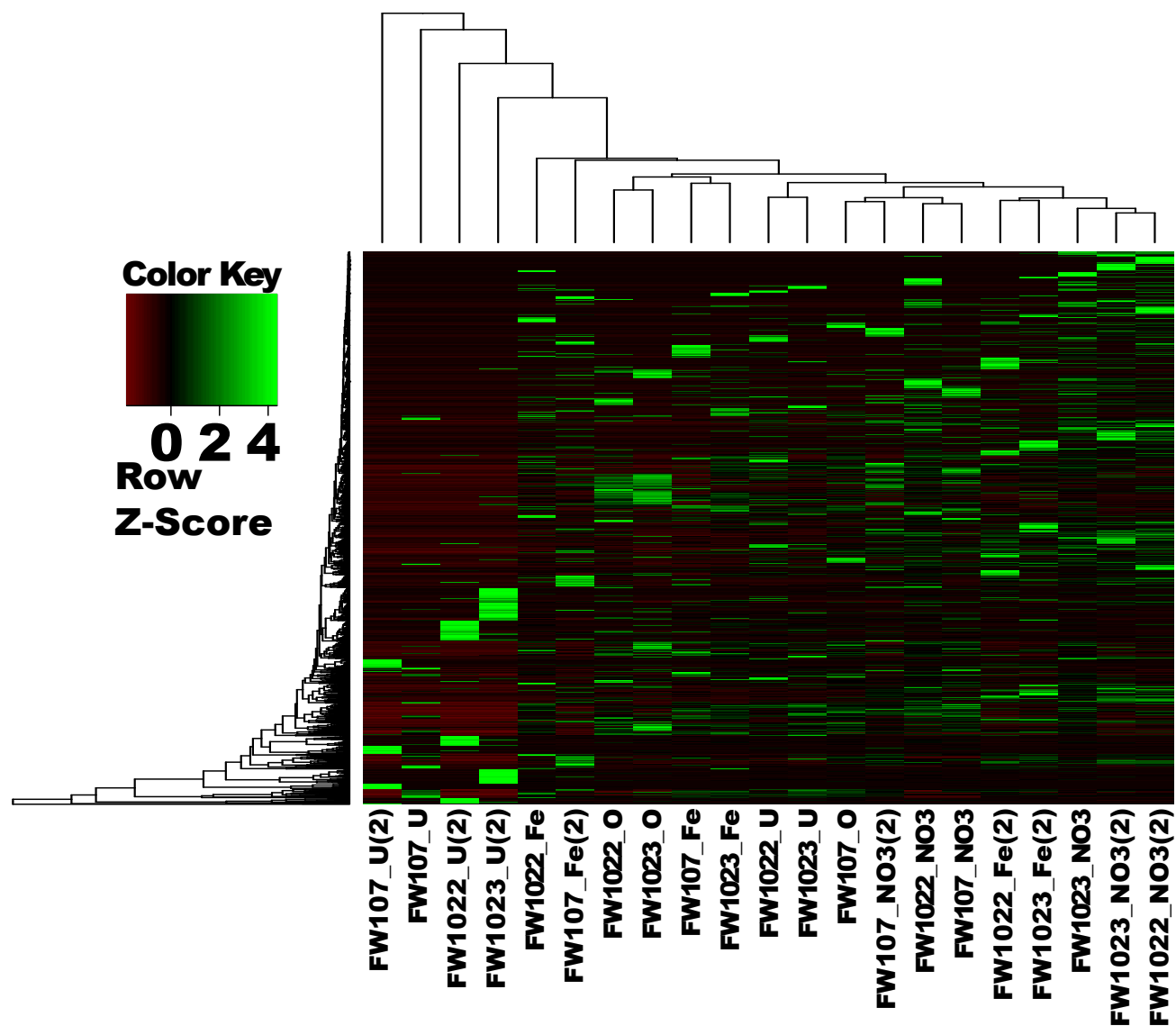


Figure 3.6: The functional gene profiles of the original soil sediment and enrichment samples. The functional gene signals of all samples (columns) were standardized to the same amount. Each functional gene (row) was then scaled among all 21 samples to show the differences in abundance. Green indicates high abundance and red indicates low abundance.

3.4.6 Non-metric multidimensional scaling (NMDS) analysis

Non-metric multidimensional scaling (NMDS) analysis was performed to correlate the β -diversity of enrichment samples and bacterial community or functional gene shifts. The original soil sediment sample community compositions appeared to be substantially different from the enriched communities (Figure 3.7). This difference also influenced the bacterial genera and functional gene correlations substantially (Figure 3.7 and Figure 3.8). Both Figure 3.7 and Figure 3.8 showed that the most significant shifts were observed between original soil sediment samples and the enrichments. Significant decreases in bacterial genera, including many unclassified bacteria were observed in the enriched cultures (Figure 3.7). The functional gene profile revealed that genes involved in the sulfur cycle (e.g., *sox* and *dsrA*) and lincosamide resistance (*linB*) decreased significantly in enriched cultures.

Within the enrichments we also noticed some significant phylogenetic and functional shifts among bacterial communities due to the enriching conditions (Figure 3.9 and Figure 3.10). In the nitrate enriched communities, unclassified bacteria (β -Proteobacteria, Chitinophagaceae, and Comamonadaceae), *Dechloromonas*, and *Simplicispira* were found significantly more abundant than the other enrichments. We observed that unclassified Enterobacteriaceae, *Clostridium* XIVa, and unclassified Clostridiales were significantly more abundant in FW102-2 and FW102-3 Fe and U enrichment cultures. Unclassified Veillonellaceae, *Sulfurospirillum* and *Trichococcus* were significantly more abundant in FW107 Fe and U enrichments. The abundance of *Geobacter* shifted significantly towards FW102-2 and FW102-3 U enrichments (Figure 3.9). The abundance of a large number of functional genes shifted substantially among all enrichments ($P \leq 0.01$, data not shown). We observed

the abundance of three groups changed most significantly ($P \leq 0.001$). Group III includes seven different bacterial functional genes, which appeared to be significantly more abundant in FW107 Fe enrichments. The abundance of chromate transporter encoding gene (*chrA*, specifically found in *Burkholderia xenovorans* LB400) decreased significantly from FW107 enrichments to FW102-2 and FW102-3 enrichments (Figure 3.10).

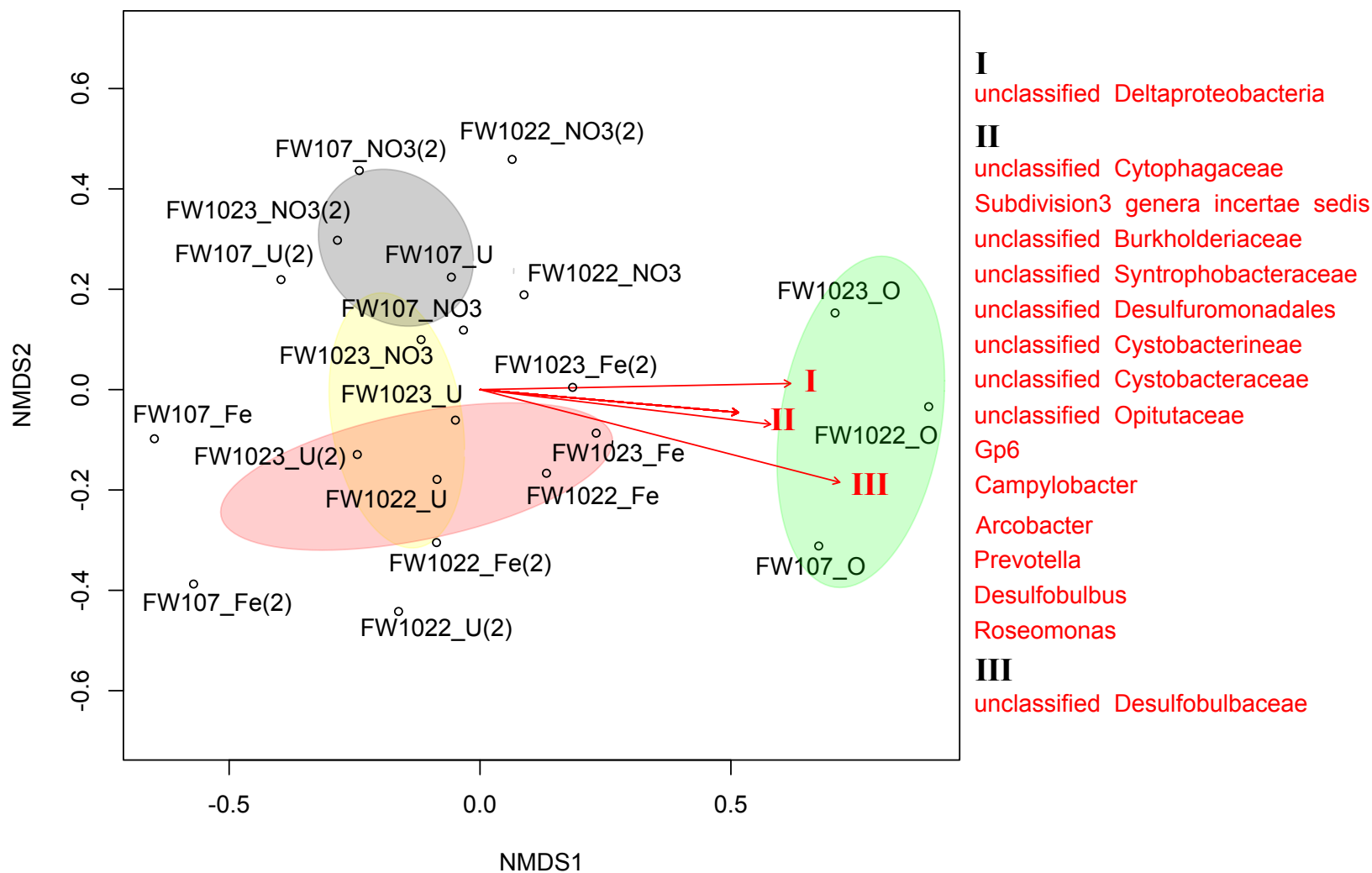


Figure 3.7: NMDS analysis of NO_3^- enrichments (grey), Fe^{3+} enrichments (pink), U^{6+} enrichments (yellow), and original samples (green). Each ellipse was drawn around each group centroid based on a group distance standard error at 95% confidence level. The changes in genera abundances that drive comparative community differences are indicated with red arrows. The arrows point to the areas of high abundance. The red arrows indicate the abundance of genera that changed significantly ($P \leq 0.001$). The specific genera are shown in red according to the group labeling.

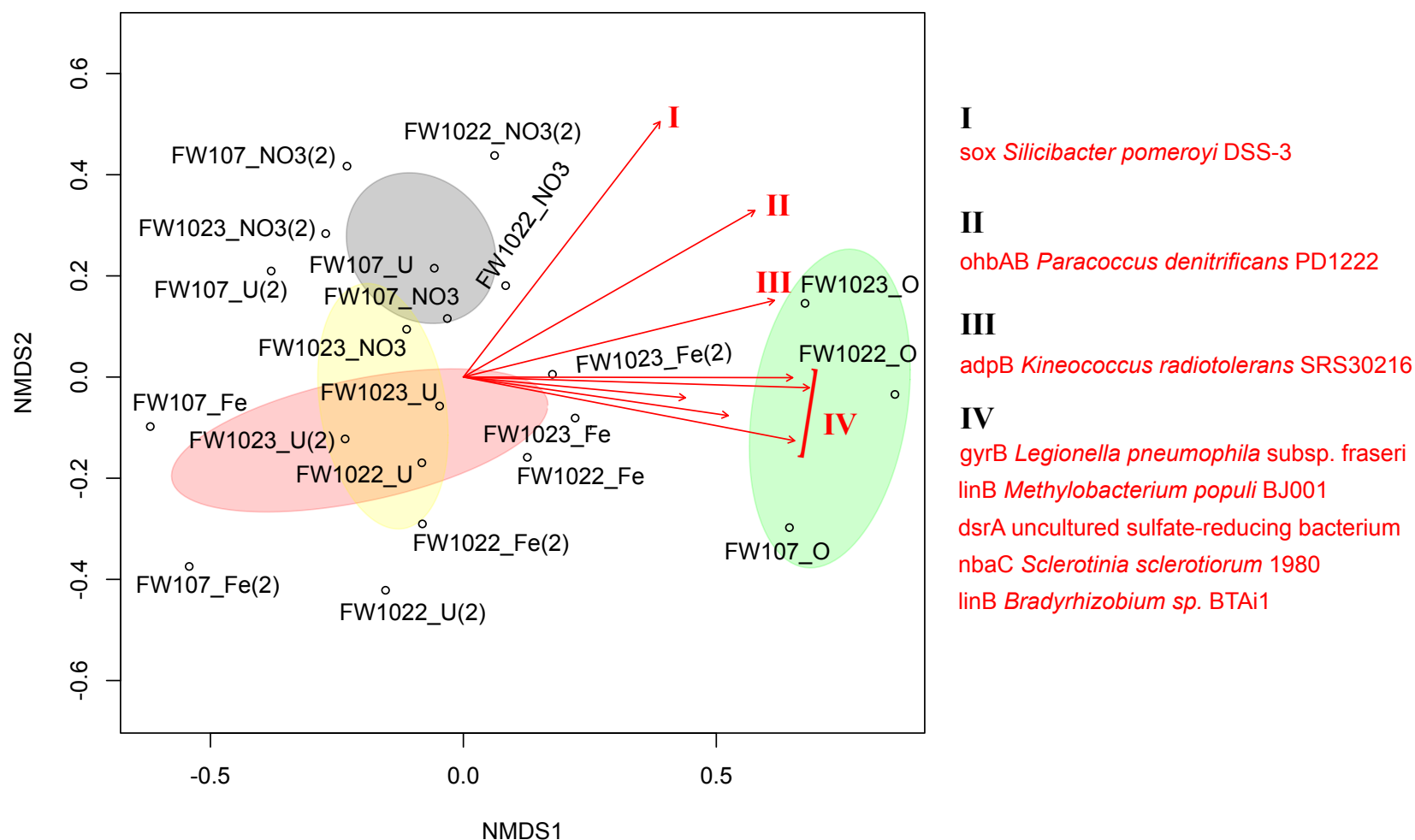


Figure 3.8: NMDS analysis of NO_3^- enrichments (grey), Fe^{3+} enrichments (pink), U^{6+} enrichments (yellow), and original samples (green). Each ellipse was drawn around each group centroid based on group distance standard error at 95% confidence level. The changes in functional gene (with the specific microorganism from which the probes were designed) abundance were correlated to the shifts observed in community structures. The red arrows indicate the abundance of functional genes that changed significantly ($P \leq 0.001$). The specific genera are shown in red according to the group labeling. The arrows point to the areas of high abundance.

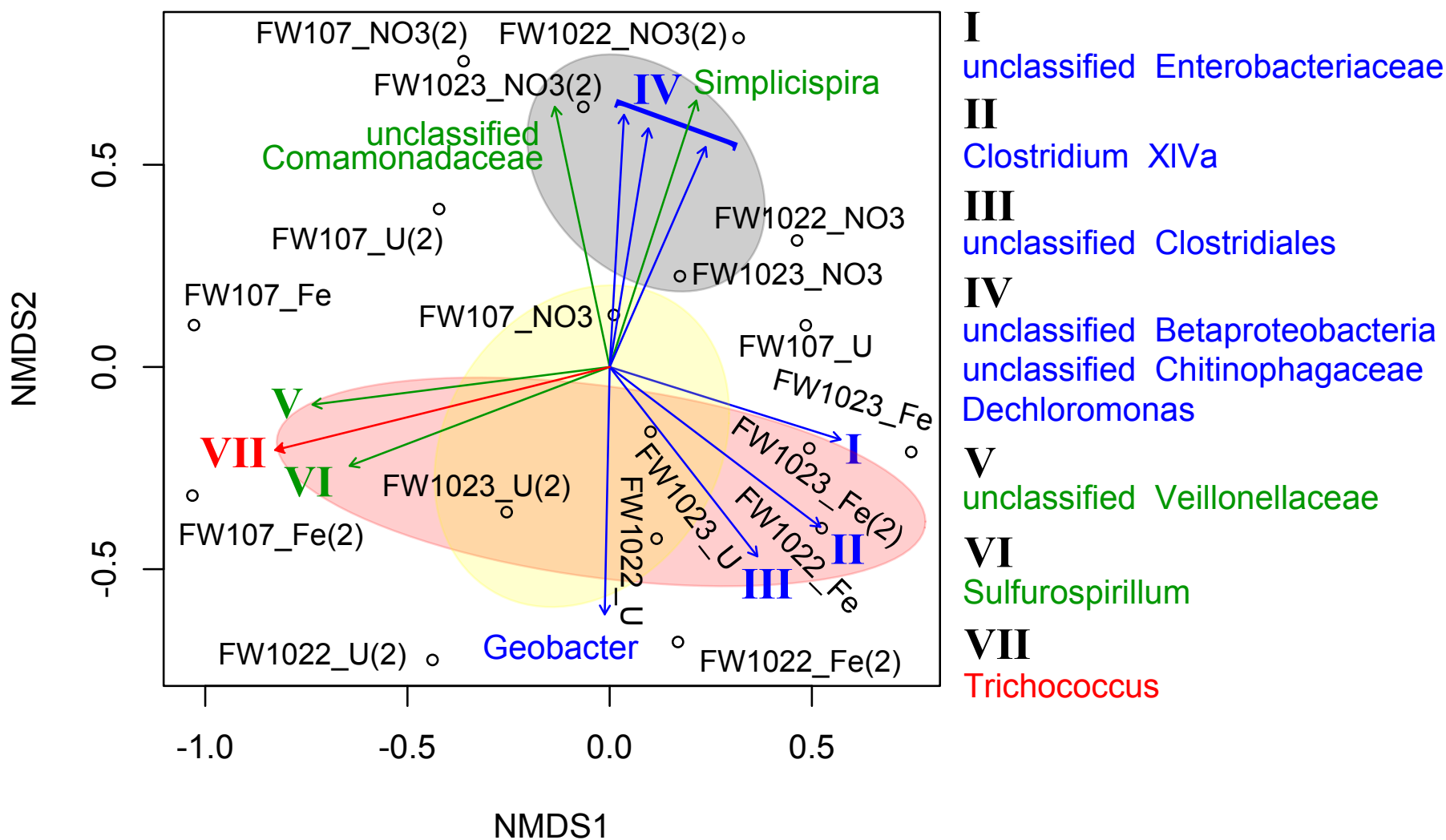


Figure 3.9: NMDS analysis of NO_3^- enrichments (grey), Fe^{3+} enrichments (pink), and U^{6+} enrichments (yellow). Each ellipse was drawn around each group centroid based on group distance standard error at 95% confidence level. The changes in genera abundance were correlated to the shifts observed in community structures. The colored arrows indicate the abundance of genera that changed significantly (red: $P \leq 0.001$, blue: $P \leq 0.05$, and green: $P \leq 0.01$). The genera names are shown in the same color according to the group labeling. The arrows point to the areas of high abundance.

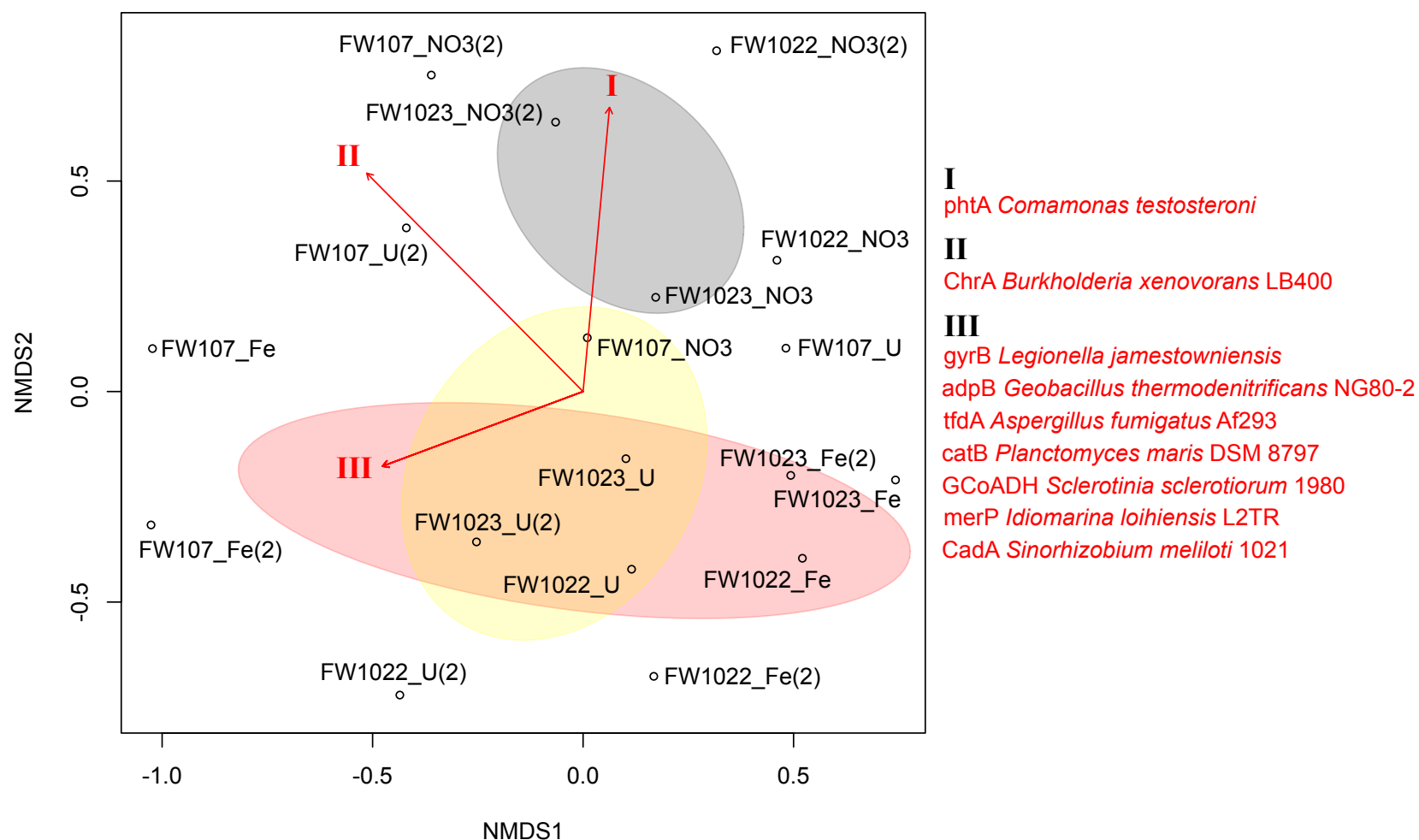


Figure 3.10: NMDS analysis of NO_3^- enrichments (grey), Fe^{3+} enrichments (pink), and U^{6+} enrichments (yellow). Each ellipse was drawn around each group centroid based on group distance standard error at 95% confidence level. The changes in functional gene abundance were correlated to the shifts observed in community structures. The red arrows indicate the abundance of functional genes that changed significantly ($P \leq 0.001$). The functional genes and the specific microorganisms from which the probes were designed are shown in the red according to the group labeling on the side. The arrows point to the areas of high abundance.

3.5 Discussion

The identification of uncultured uranium immobilizers in sub-surface environments is instrumental in the optimization of *in situ* bioremediation. Our assessment of bacterial communities indicated, not surprisingly, that enrichment was an effective method for identifying bacterial populations that might play important roles in sub-surface uranium immobilization. We were able to reduce the bacterial diversity and identify common populations under different stressors (ie. iron, nitrate, and uranium) to evaluate their potentials.

From the ferric citrate enrichment cultures, we observed that FW107 enrichments were not as effective at iron reduction as the FW102-2 and FW102-3 enrichments. Bacterial community analysis revealed that FW107 iron enrichments were predominantly populated by unclassified *Veillonellaceae* (Figure 3.2). Gihring et al. observed that although this group was abundant in their enrichment cultures, *Veillonellaceae* did not contribute to uranium reduction but to initial nutrient degradation in their study [50]. This might explain why FW107 ferric citrate enrichments appeared to be less effective at iron reduction and the accumulation of acetate than FW102-2 and FW102-3 ferric citrate enrichments (Figure 3.1). Thus we suspect that *Veillonellaceae* did not contribute to uranium immobilization directly but was responsible for early nutrient consumption. The other two genera, *Trichococcus* and *Sulfurospirillum*, observed in FW107 iron enrichments were reported to be associated with sulfate and metal reducers [41, 152]. We suspect the iron reduction observed in FW017 ferric citrate enrichments were mainly contributed by members of *Trichococcus* and *Sulfurospirillum*. In contrast to the FW107 iron enrichment culture, FW102-2 and FW102-3 ferric citrate enrichments appeared to be much more diverse. Genus *Geobacter*, well-known for

its metal-reducing and acetate utilizing members [132], was found abundant in both sets of consortia. The genus is likely a major contributor to iron reduction and acetate utilization in FW102-2 and FW102-3 iron enrichments.

The shifts in the bacterial communities revealed that FW102-2 and FW102-3 enrichments became abundant with Proteobacteria while Firmicutes became numerically dominant in FW107 enrichments (Figure 3.2). Venn diagrams revealed that uranium enrichments shared genera with both iron and nitrate enrichments (Figure 3.3, 3.4, and 3.5). Among all of the shared genera, *Psychrosinus* and *Sporomusa*, genera of phylum Firmicutes, were found in all uranium enrichment cultures. A member of genus *Psychrosinus* was previously isolated from near freezing temperature and identified as a lactate fermenting bacterium [137]. No evidence has been shown that members of *Psychrosinus* are sulfate or metal reducers. However, the *Psychrosinus* group was previously identified as *Pelosinus* according to RDP (spring 2012 update). We found the 16S rRNA sequences from our *Psychrosinus* genus were highly similar to *Pelosinus sp.* UFO1, which was reported as a uranium reducer by Ray et al. [129]. Genus *Sporomusa* has been reported to be found in various U⁶⁺-reducing and sulfate-reducing environments [7, 12, 113]. However, no specific members of this group has been identified as a metal reducer.

The top ten most abundant genera in all samples revealed that the FW107 original soil sediment sample was drastically different from FW102-2 and FW102-3 (Figure 3.2). This was expected as well FW107 was in the neutralized zone and was never stimulated [187, 188]. The most significant influence was the enrichment process. The NMDS analyses revealed that the most significant shifts were decreases in genera abundance (Figure 3.7 and functional gene abundance (Figure 3.8) from original soil sediment samples to enrichment cultures. Analysis

of bacterial community shifts induced by the addition of NO_3^- , Fe^{3+} and U^{6+} revealed that bacteria belonging to phylum Firmicutes were significantly more abundant in Fe^{3+} and U^{6+} consortia (Figure 3.9). The shifts in bacterial functional genes are less conclusive. Figure 3.10 suggests that the original soil sediment samples had a substantial impact on the functional profile variations. We suspect this result was also due to different GeoChip platforms. When eliminating GeoChip3.0 samples, we were surprised to observe that despite the drastic shifts revealed by 16S rRNA profiles, little variation was found in their functional gene profile (Figure B.1). This observation suggested that the underlying functional profile of these communities were resilient and highly similar. However, it is also possible that important genes were not included on the GeoChip microarray. Thus, a different and more effective method might be needed to investigate enrichment community function shifts.

3.6 Conclusion

We studied the shifts in bacterial communities, obtained from uranium contaminated soil sediments (i.e., FW107, FW102-2, FW102-3) and bacterial community shifts induced by supplemented resources (i.e., NO_3^- , Fe^{3+} , and U^{6+}). The enriched community structures changed drastically according to bacterial 16S rRNA sequences. We observed that *Geobacter* was abundant in the FW102-2 and FW102-3 U^{6+} enrichment cultures, while *Psychrosinus* was abundant in the FW107 U^{6+} enrichment cultures. *Psychrosinus* was also found common in all enrichment cultures at various levels of abundance. The functional gene profiles of the enrichments and original soil samples appeared to be highly similar despite the large changes we observed in 16S rRNA based community structure analysis. Our observations suggest that

the function potential of these bacterial community requires did not change as much as its corresponding phylogeny structure. According to this study, we hypothesize that Firmicutes play an important role in subsurface uranium immobilization.

CHAPTER 4

THE ROLE OF FIRMICUTES IN URANIUM IMMOBILIZATION

4.1 Abstract

The observation of uranium immobilization by anaerobic bacterial communities is a composite result of bacterial interactions. To understand the bacterial interactions and their impact on uranium immobilization, it is not only important to study the bacterial community structural changes but it is also critical to study individual isolated members of the community. In uranyl acetate supplemented enrichment cultures seeded with microbial communities from uranium contaminated sediments, we observed that the concentration of soluble uranium decreased and the abundance of Firmicutes bacteria increased as a function of time. We hypothesized that members of Firmicutes play an important role in subsurface uranium immobilization. We employed standard cultivation techniques under strictly anaerobic conditions and isolated 51 bacterial strains from the uranium enrichment cultures. Bacterial 16S rRNA gene sequences revealed that these isolates belong to four distinct phylogenetic clades of Firmicutes. However, comparative analysis of growth rates and genome structure using REP-BOX-GTG₅-PCR profiles indicated that these isolates are distinct strains and might react differently in the presence of soluble uranium. We screened ten isolates (based on their 16S rRNA identifications and REP-BOX-GTG₅-PCR profiles) for their abilities to immobilize uranium and six isolates were more proficient at removing soluble uranium than the original enrichment community.

4.2 Introduction

Bacterial phylum Firmicutes are comprised of a group of ancient and metabolically versatile anaerobic bacteria [38, 96, 99]. They were frequently found in various environments and reported in bacterial enrichments. Many members of this group have also been identified as sulfate and metal reducing bacteria using carbon sources as electron donors [3, 32, 45, 58, 60, 118]. Members of Firmicutes, such as Clostridia are also well-known for their ability to produce hydrogen via [FeFe]-hydrogenase (HydA) [10, 103]. In resource scarce subsurface environments, metabolic hydrogen could be readily used as an electron donor to support bacterial growth and dissimulatory reduction (eg. Fe, Mn, and etc.) [79, 151, 194].

We have found large numbers of Firmicutes 16S rRNA gene sequences in iFRC (integrated Field Research Challenge site at Oak Ridge National Laboratory, TN) original soil sediment samples as well as our sequentially enriched microcosms (see Chapter 3). In the previous chapter, we were able to identify potential genera that might play important roles in subsurface uranium immobilization. In this chapter we report on the isolation and characterization of strains capable of immobilizing U^{6+} . We monitored the decrease of soluble U^{6+} , the corresponding changes in the U^{6+} enriched bacterial communities, and isolate potential U^{6+} immobilizers. We hypothesize that members of Firmicutes play a substantial role in U^{6+} removal in iFRC.

4.3 Materials and Methods

4.3.1 Uranium Immobilization by FW107 and FW102-2 Enrichment Cultures

Enrichment cultures with uranyl acetate as the terminal electron acceptor (Chapter 3) were used as a starting culture. To obtain an initial high cell density, they were first enriched anaerobically in 1/2X R2B medium at 15°C for 10 days. The 1/2X R2B enrichments were then centrifuged at 5000 RPM to collect all of the cells. Cell pellets were washed twice in 30 mM anaerobic sodium bicarbonate buffer (pH 7. cells were collected via centrifuging in between) inside of an aerobic chamber (2.5% H₂). Final washed cell pellets were resuspended in anaerobic PIPES buffered artificial ground water media (PBAGW) supplemented with 10 mM sodium pyruvate [69] to a final OD₆₀₀ of 0.01. Microcosms were set up in duplicate and incubated at 15°C. Over a period of 64 days, the concentration of soluble U⁶⁺ was determined by a spectrophotometric U⁶⁺-azide assay [145]. All samples were taken from microcosms anaerobically. Samples for HPLC and U⁶⁺ analysis were passed through 0.22 μm HPLC certified syringe filters (Sun Titan2, Fisher Scientific) under anaerobic condition. Community analysis samples were also taken from one set of the microcosms (replicate 1) on days 0 (1/2X R2B cultures), 10, 20 and 64 of incubation with uranyl acetate.

4.3.2 Quantitative Analyses

A uranyl-azide assay was modified from a previously described method [145]. Briefly, HNO₃ was added to filtered samples to a final concentration of 4.9%. Acidified samples (40 μl) were then added to sodium azide solution (3M, 160 μl) in a clear bottom 96-well microtiter plate (Corning Scientific, Tewksbury, MA). Absorbance measurements were performed at 340 nm.

To correlate the absorbance and U^{6+} concentration, a standard curve was constructed (in duplicate) for each measurement (Figure C.1). This assay was found to be valid for soluble U^{6+} ranging from 5 μ M to 1000 μ M.

4.3.3 DNA Extraction and Sequencing Preparation

Community DNA was extracted by using Powersoil DNA Extraction Kit (Mo Bio Laboratory, Carlsbad, CA). Pyrosequencing chemistries (454 FLX) were used to evaluate the bacterial 16S community structures. Bacterial 16S rRNA gene V4-V5 regions (Forward 5'AYTGGGYDTAAAGNG3' and Reverse 5'TACNVGGGTATCTAATCC3') were amplified as previously described with 454 FLX chemistry [157]. Polymerase Chain Reactions (PCR) were carried out by mixing 1X Taq reaction buffer, 2 mM $MgSO_4$, 0.1 mg/ml BSA, 0.2 mM of each dNTP, 0.33 μ M of each primer, 0.125 U/ μ l of Platinum High Fidelity Taq Polymerase (Invitrogen, Carlsbad, CA), 10 ng DNA template and DNase and RNase free water. The amplification conditions include an initial denaturing step at 95°C for 5 minutes, followed by 30 cycles of 3 temperature steps consisting of denaturing at 95°C for 45 seconds, annealing at 50°C for 45 seconds, and an elongation at 72°C for 90 seconds, and a final extension at 72°C for 5 minutes following the completion of 30 cycles. Amplified 16S rRNA gene PCR products were visualized on 2% Tris-Borate-EDTA (TBE) agarose gel. DNA fragments at ~450 bp were excised and extracted from the gels by using Qiagen Gel Extraction Kit. The extracted products were further purified by using a QiaQuick PCR Product Purification Kit (Qiagen, Valencia, CA). All final purified DNA products were quantitated by using Qubit HS Double-stranded DNA Kit (Invitrogen, Carlsbad, CA) prior to combining at equal mass for a final DNA concentration of 0.5 ng/ μ l. Pyrosequencing was performed at Michigan

State University RTSF by using Roche 454 GSFLX Sequencer.

FeFe-hydrogenase (HydA) genes were amplified as described previously [11] and cloned with Topo Cloning (Invitrogen, Carlsbad, CA) and sequenced at the MSU-RTSF. Briefly, the primers used were FeFe-272F (5'GCHGAYMTBACHATWATGGARGA3') and FeFe-427R (5'GCNGCYTCCATDACDCCDCCNGT3') [11]. Each HydA PCR consists of a mixture of 1X Taq reaction buffer, DNase and RNase free water, 2 mM MgCl₂, 0.1 mg/ml BSA, 0.2 mM of each dNTP, 2 μM of each primer, 0.05 U/μl of Platinum Taq Polymerase (Invitrogen, Carlsbad, CA), and 20 ng DNA template. The amplification conditions include an initial denaturing step at 94°C for 4 minutes, followed by 35 cycles of 3 temperature steps consisting of denaturing at 94°C for 60 seconds, annealing at 56.5°C for 60 seconds, and an elongation at 72°C for 90 seconds, and a final extension at 72°C for 20 minutes following the completion of 35 cycles. All PCR products were stored at -20°C until needed. HydA PCR products (~500 bp) were confirmed via electrophoresis (1% Tris-Acetate-EDTA agarose gel). Clone libraries of FeFe-hydrogenase were constructed by using Invitrogen Topo PCR2.1 Cloning Kit (Invitrogen, Carlsbad, CA) following the vendor's protocol. The cloned fragments were purified and sequenced at RTSF via an ABI 3730 Genetic Analyzer.

4.3.4 Community Analysis

Bacterial 16S rRNA gene sequences obtained from pyrosequencing were processed and analyzed by using Ribosomal Database Project (RDP) Pyrosequencing pipeline [180]. Sequences that were shorter than 250 bp, containing any N's in sequencing region, or with an average quality score less than 20 were discarded. Chimeras were removed from RDP processed sequences by using USEARCH (UCHIME reference mode with Silva gold alignment database

as reference). RDP Multi-classifier was used to identify each sequence to bacterial genus level (threshold 80). RDP SeqMatch was used for further identification of bacterial clusters of interest. To eliminate the clustering artifacts, sequences were also trimmed to the same length (250 bp) based on alignment profiles prior to RDP complete linkage clustering.

[FeFe]-hydrogenase gene sequences were identified by BLAST against NCBI non-redundant amino acid database. The BLAST E-value (expect value) was set at $E < 10^{-5}$. Top 50 best matches were generated for each sequence. The annotated match with the best E-value was then selected to be used to determine bacterial species information.

4.3.5 Isolation of Potential Uranium Immobilizing Bacteria

Potential uranium immobilizers were isolated from FW107 and FW102-3 uranyl acetate enrichments on R2A agar plates in a Coy Lab anaerobic chamber ($(\text{H}_2:\text{CO}_2:\text{N}_2 = 3:10:87)$). A volume of 100 μl enrichment culture from each microcosm was initially spread on R2A plates anaerobically. Individual colonies were then picked and restreaked for isolation. Final isolates were stored in 7.5% DMSO at -80°C .

4.3.6 Growth Curves of Isolates

The growth of each isolate under anaerobic conditions ($\text{H}_2:\text{CO}_2:\text{N}_2 = 3:10:87$) was determined by measuring turbidities at 620 nm wavelength (OD₆₂₀). Isolates were grown in 1/2X R2B broth in 96 well microtiter plates for 63 hours at 25°C . To determine if any isolates can utilize U^{6+} as an electron acceptor at 25°C , isolates were grown for 200 hours in minimal media (30 mM NaHCO_3 , pH 6.8) supplemented with 20 mM sodium pyruvate as a carbon source and electron donor and 500 μM uranyl acetate. Isolates were also grown in minimal

media (30 mM NaHCO₃, pH 6.8) supplemented with 20 mM sodium pyruvate but without addition of an electron acceptor to determine if these strains were capable of fermentation. The turbidity measurements were performed under the same anaerobic conditions by using a Bio-Rad PR 3100 TSC Microplate Reader (Bio-Rad, Hercules, CA)

4.3.7 Isolate Identifications

Final isolates were identified via 16S rRNA sequencing, which was carried out by the MSU RTSF. Isolate cultures were supplied in 96 well microtiter plate and MSU RTSF carried out 16S rRNA gene amplification and sequencing (primer 27F, 5'AGAGTTTGATCCTGGCTCAG3' was employed). REP-BOX-(GTG)₅-PCR was also used to differentiate isolates that are substantially different at genomic level [49]. We used four primers, REP1R-I (5'IIICGICGICATCIGGC3'), REP2-I (5'IIICGNCGNCATCNGGC3'), GTG₅ (5'GTG-GTGGTGGTGGTG3'), and BOXA1R (5'CTACGGCAAGGCGACGCTGACG3') for each reaction and set up PCR reactions as previously described [174]. Briefly, each 15 μ l PCR reaction consisted of 3 μ l 5X Gitschier buffer (Table C.1), 1.5 μ l 10% DMSO, 30 pmol of each primers except BOXA1R (50 pmol), 0.75 μ l of dNTP (25 mM of each), 0.85 mg/ml BSA, 0.24 μ l of 5U/*mul* DNA Taq polymerase, 100 ng DNA template and water. To standardize the REP-BOX-(GTG)₅-PCR profile, *Desulfitobacterium hafniense* DCB-2 was also included in each batch of reactions. Gel electrophoresis was conducted with 2% TAE (tris-acetate-EDTA) agarose gels and a 72 Volt electric potential. Final REP-BOX-(GTG)₅-PCR files were analyzed using Kodak Molecular Imaging Software.

4.3.8 Cell Suspension Assay

To evaluate the uranium immobilization abilities of the isolates, we selected nine strains based on their REP-BOX-(GTG)₅-PCR profiles (presence and absence of DNA fragments). All of these strains were isolated from FW107 uranium enriched culture. Cell suspension assays [27, 88] were performed on these nine isolates along with the FW107 enrichment culture and a false positive control (sterile media without the inoculation of cells). Briefly, individual isolates (-80°C freezer stocks) were inoculated into anaerobic 1/2X R2B broth and grown to late exponential phase (OD₆₀₀ ~ 0.2). Cells were then washed with 30 mM bicarbonate buffer twice (centrifugations at 13,000 g for 15 minutes were carried out at the end of each wash). Final clean cell pellets were suspended in the reaction buffer (30 mM sodium bicarbonate at pH 6.8, 20 mM sodium pyruvate, 1 mM uranyl acetate) to OD₆₀₀ 0.1. Suspended cells were incubated at 25°C for 70 hours in anaerobic chamber (H₂:CO₂:N₂ = 3:10:87)

4.4 Results

4.4.1 Soluble U⁶⁺ Immobilization by FW107 and FW102-2 Enrichments

Over a period of 64 days, we observed that both FW107 and FW102-2 enrichments were able to reduce the soluble U⁶⁺ concentrations from over 250 μM to under 150 μM (Figure 4.1). The U⁶⁺ concentration variations at day 0 were likely due to the inoculation method. An excess amount of uranyl acetate in the needle was injected, which was supposed to be retained. A slight increase in U⁶⁺ concentration was also observed during the early stage of incubation (0-10 days) in both enrichment microcosms and the control culture. This could be

due to interactions between media and uranyl acetate. All four enrichment cultures yielded a similar U^{6+} removal trend (Figure 4.1).

4.4.2 Bacterial Community Compositions of FW107 and FW102-2 Enrichments

Pyrosequencing results showed that genera *Clostridium* and *Pelosinus* were abundant in the FW107 uranium enrichment culture. Together, they constituted over 80% of the community. As time increased, we observed an increasing amount of unclassified *Clostridiales* and a decreasing amount of *Clostridium* (Figure 4.2). Unlike FW107, the FW102-2 uranium enrichment culture was dominated by *Tolomonas*, which was initially found over 90% abundant. The relative abundance of this genus decreased as a function of time. Meanwhile, we observed that *Pelosinus* (currently identified as *Psychrosinus* by RDP) became more abundant (from approximately 0 to almost 15%) as the incubation time increased (Figure 4.3).

The uranium enriched FW102-2 consortia initially (at time 0) contained few copies of [FeFe]-hydrogenase genes initially. With the same amount of DNA template, the *hydA* amplicon fragment was barely visible (data not shown). Fewer *hydA* clones were derived from FW102-2 enrichments than from FW107 enrichments at time 0 (8 clones VS. 66 clones) (Figure 4.4). The difficulty in [FeFe]-hydrogenase gene amplification and cloning could be due to either the lack of a *hydA* containing population or experimental procedure bias. The abundance of *hydA* genes detected increased significantly (to 50) after enriching in uranyl acetate (Figure 4.4 FW102-2 U64days). While the changes in *hydA* clones obtained were not quantitatively proven, it is likely due to the increase of [FeFe]-hydrogenase containing bacteria after incubation.

A large number of *hydA* sequences in the FW102-2 uranium consortia were found in

uncultured bacteria. In contrast, *hydA* genes identified in both FW107 1/2X R2B enrichment and the uranium enriched consortia belonged to two large genera groups, *Clostridium* and *Desulfotomaculum*. We also observed that *hydA* sequences from these two groups became more abundant after the uranium enrichment process (Figure 4.4 FW107).

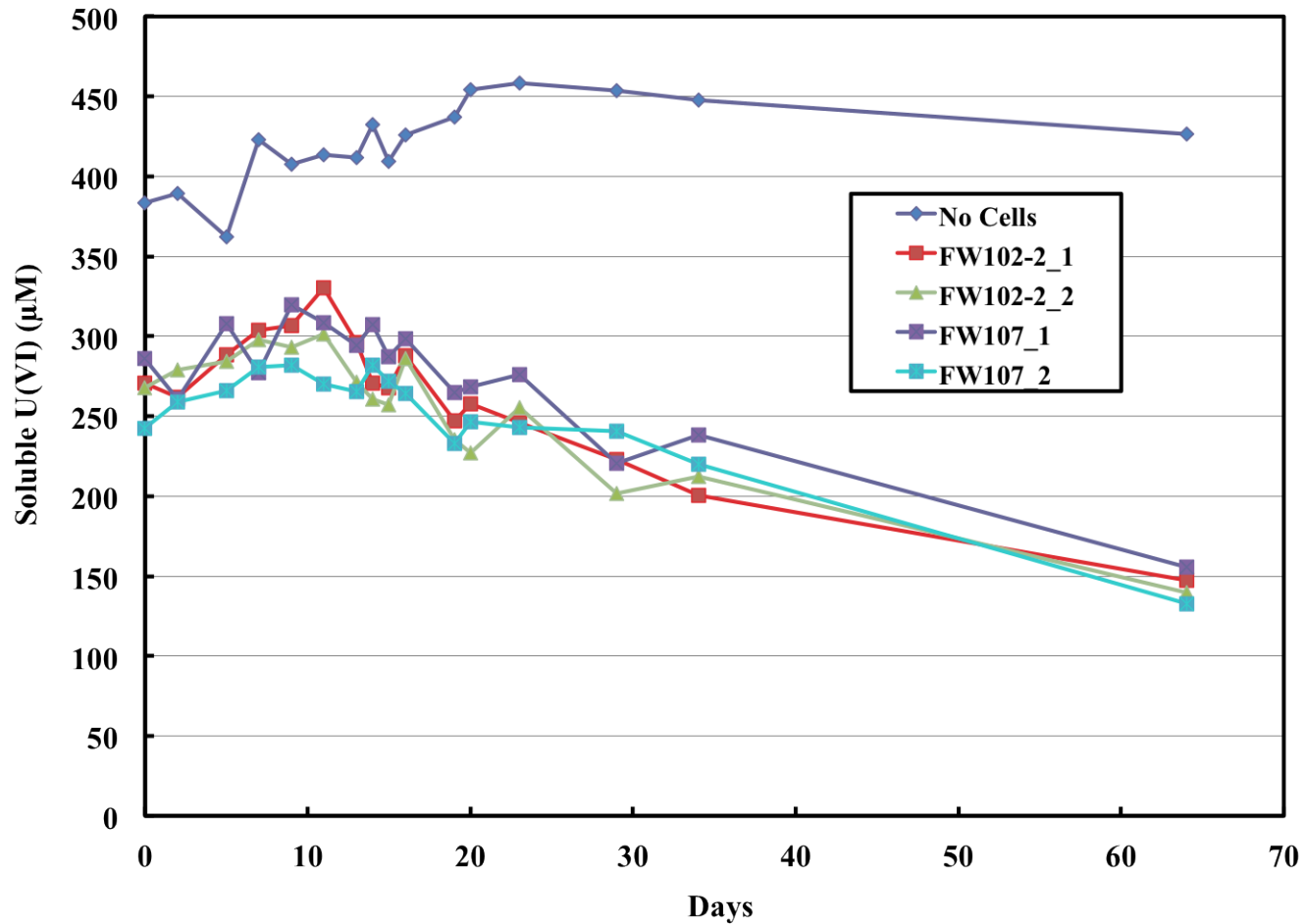


Figure 4.1: The removal of soluble U^{6+} in FW107 and FW102-2 enrichments. The high soluble U(VI) concentration in the control culture (No Cells) was due to the excess amount of uranyl acetate carried over from the syringe needle during inoculation.

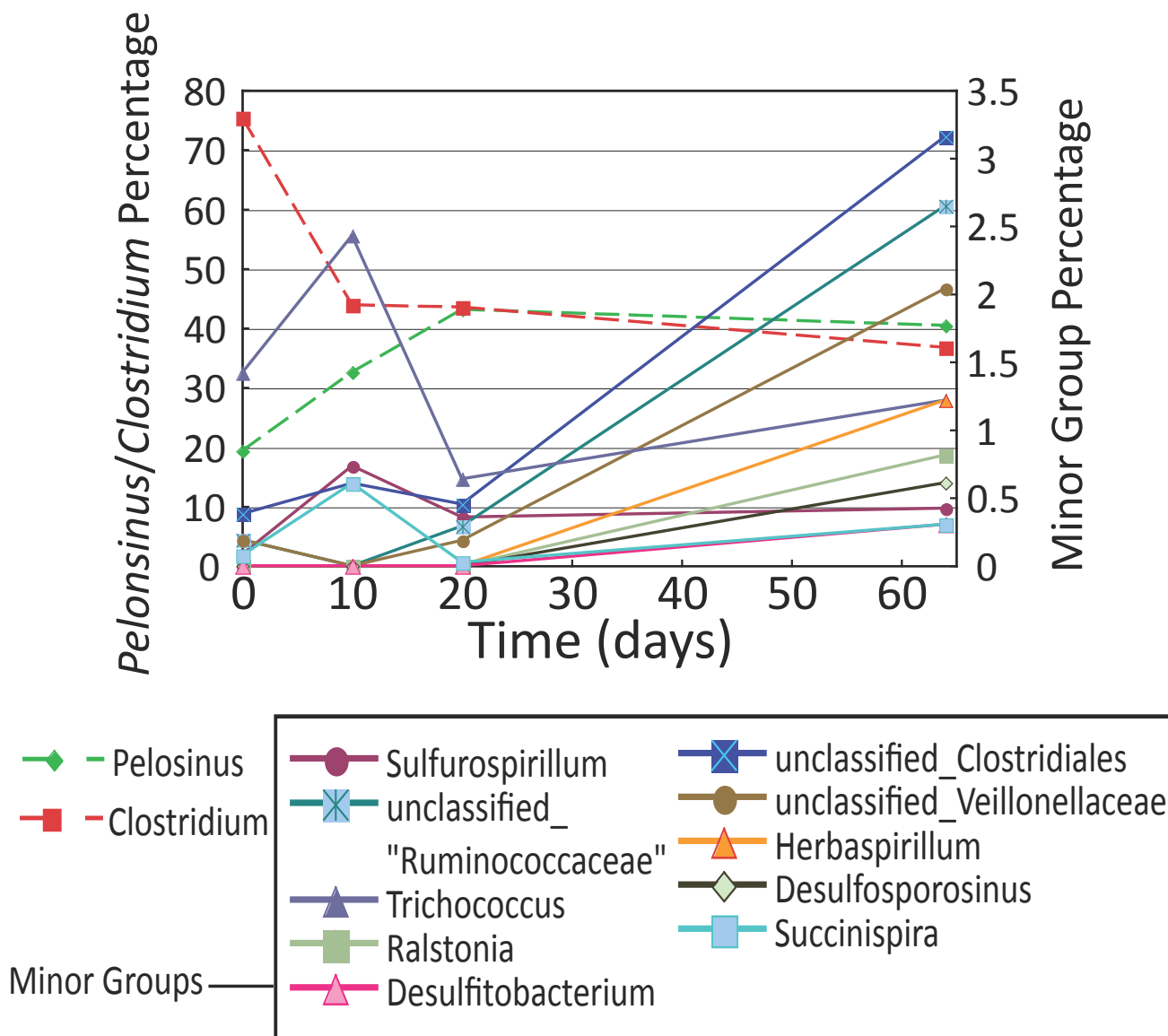


Figure 4.2: Bacterial community shifts with the increasing of incubation time in FW107 U-PBAGW microcosm.

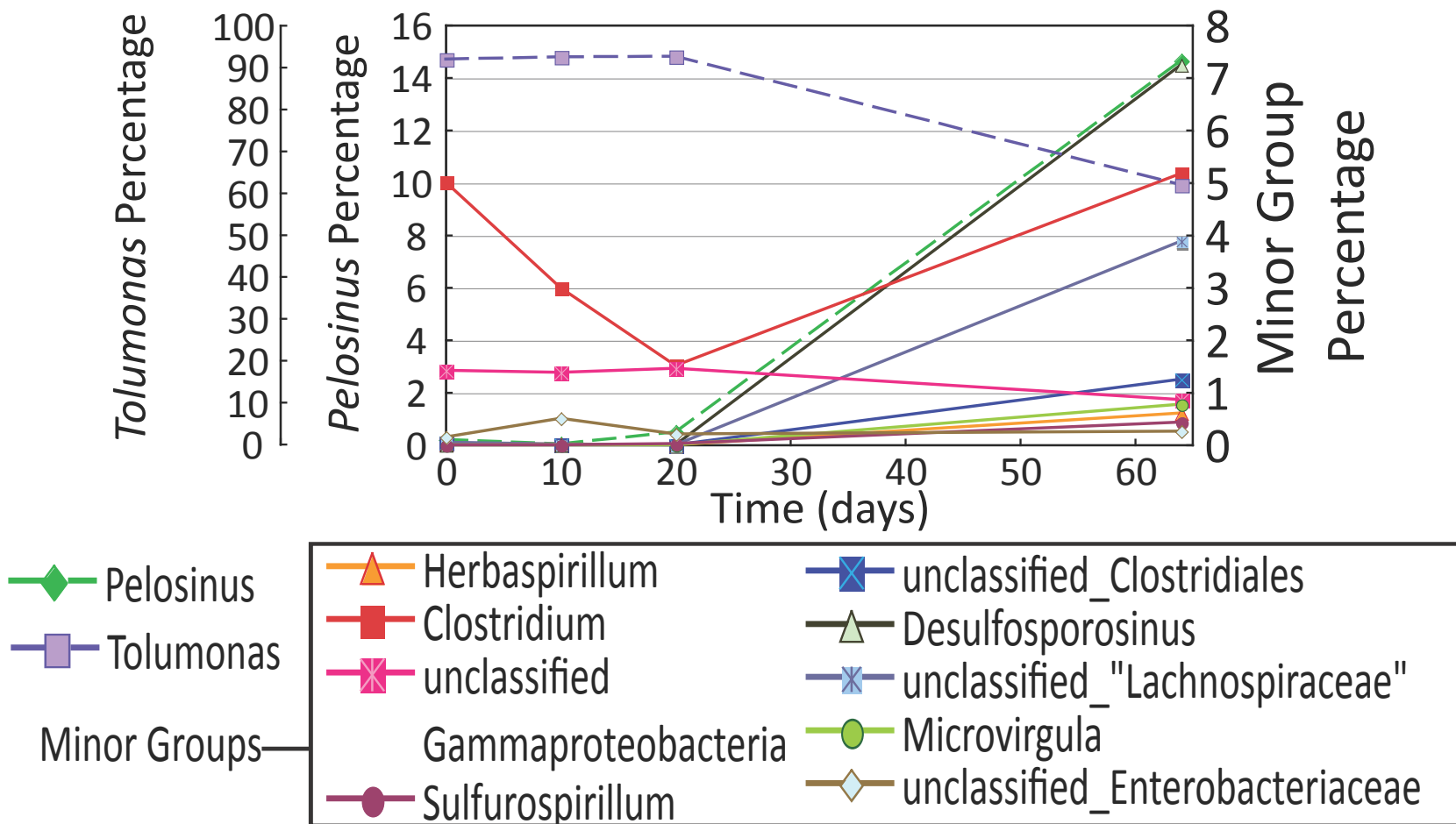


Figure 4.3: Bacterial community shifts with the increase of incubation time in FW102-2 U-PBAGW microcosm.

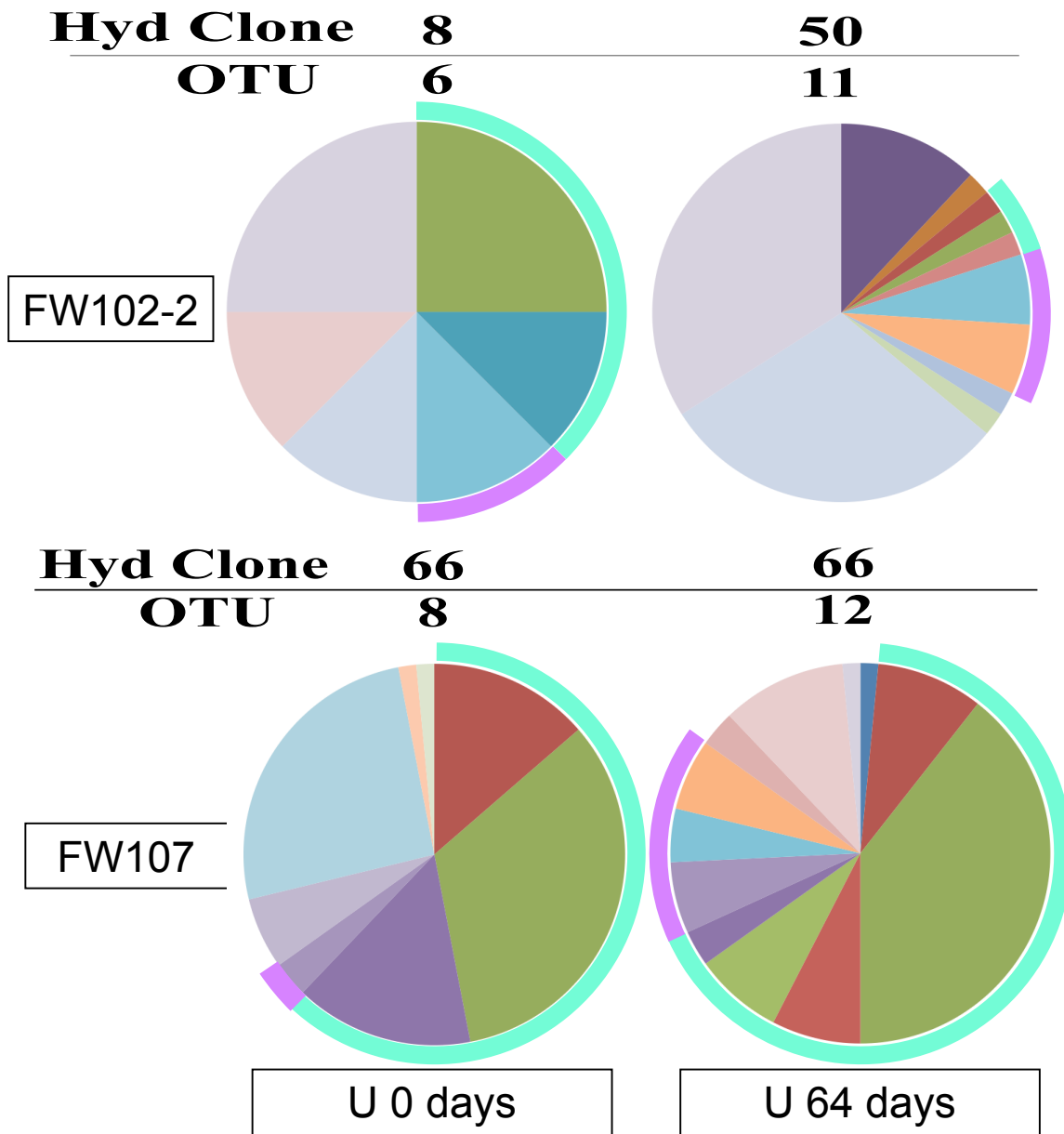


Figure 4.4: Distribution of [FeFe]-hydrogenase containing bacteria in FW107 and FW102-2 grown in 1/2X R2B media (U 0 days) and in uranyl acetate enrichments (U 64 days). The bacterial populations represented by the small fractions of each pie chart are listed on the right hand side with color blocks corresponding to the colors found in each pie chart. The distribution of genera *Clostridium* (cyan color) and *Desulfotomaculum* (purple color) are shown as the outer ring of each pie chart.

Figure 4.4 (cont'd)

- Acetivibrio cellulolyticus CD2
- Aminomonas paucivorans DSM 12260
- Carboxydibrachium pacificum DSM 12653
- Clostridium sticklandii DSM 519
- Ethanoligenens harbinense YUAN-3
- Shewanella decolorationis
- Alkaliphilus metalliredigens QYMF
- Bacteroides sp. D1
- Clostridium hathewayi DSM 13479
- Desulfovibrio fructosovorans JJ
- Ferrimonas balearica DSM 9799
- Clostridium
- Desulfotomaculum

4.4.3 Potential U⁶⁺ Immobilizers

We have isolated 51 anaerobic bacteria from FW107 and FW102-2 uranium enrichments. We were able to identify 48 of them according to their 16S rRNA sequences. All of these isolates belonged to phylum Firmicutes. RDP SeqMatch identified these isolates as *Clostridium* XI, *Clostridium* XIVa, *Clostridium sensu stricto*, and *Pelosinus*. Phylogenetic analysis of the isolates 16S rRNA sequences by Arb agreed with RDP SeqMatch and revealed that 29 isolates clustered closest to *Clostridium sardiniense* (Figure 4.5 Cluster I), 13 isolates clustered closest to uncultured bacteria that are similar to *Clostridium methylopentosum* (Figure 4.5 Cluster II), and 4 isolates clustered closest to *Pelosinus fermentans* (Figure 4.5 Cluster III). Two isolates, A04 and B03 did not belong to any of the clusters but appeared more closely related to Cluster I than the other groups (Figure 4.5). Although the 16S rRNA sequences indicated that majority of the isolates were highly similar, we observed substantial differences in their growth rates at 25°C in anaerobic 1/2X R2B (Figure 4.6). Thus the 16S rRNA sequence alone is not sufficient to differentiate these isolates. We employed REP-BOX-(GTG)₅-PCR and the profiles revealed that isolates identified as the same bacterial species according to their 16S rRNA sequences were substantially different in their genome organization based on REP-BOX-(GTG)₅ profiles. These profiles were clustered and are presented in Figure 4.7.

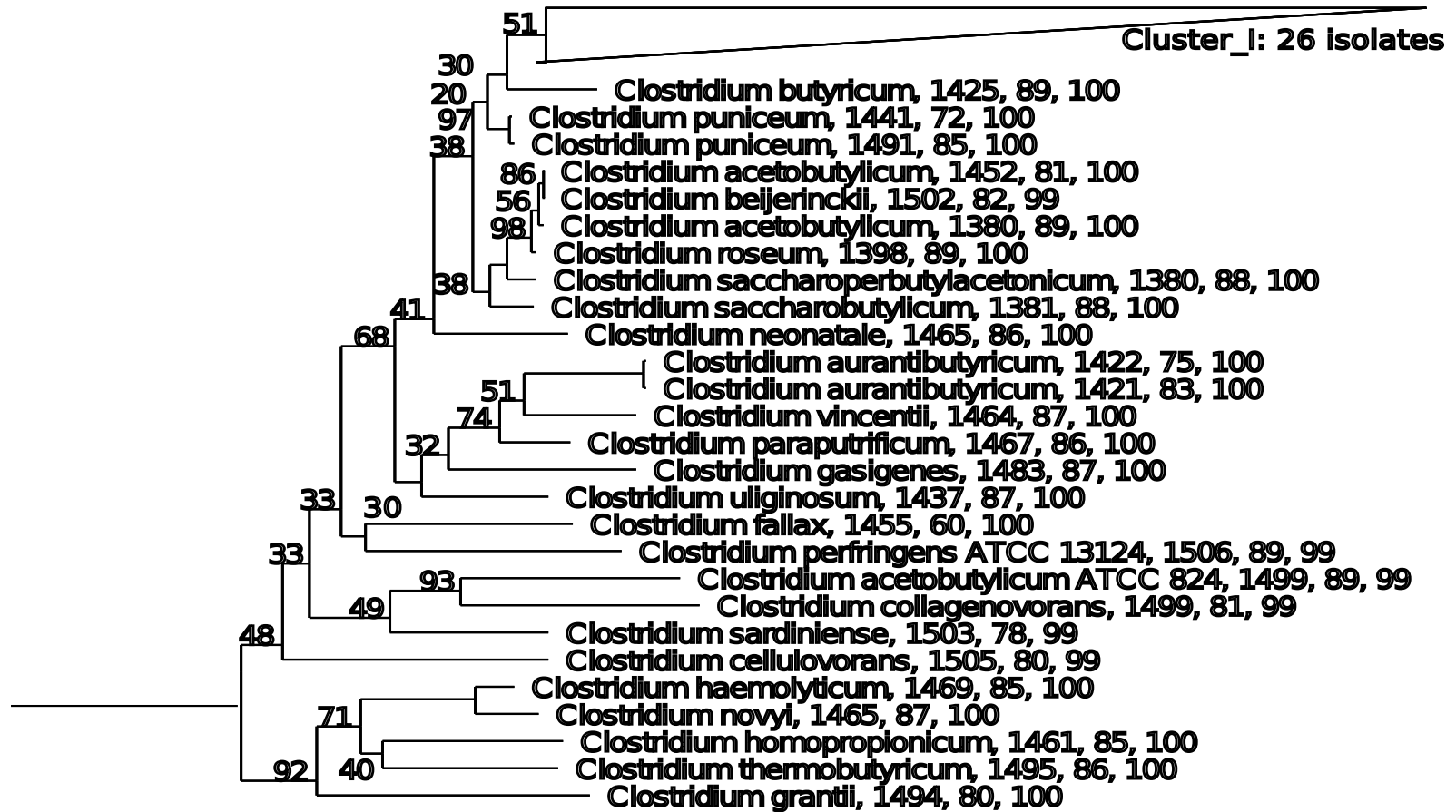
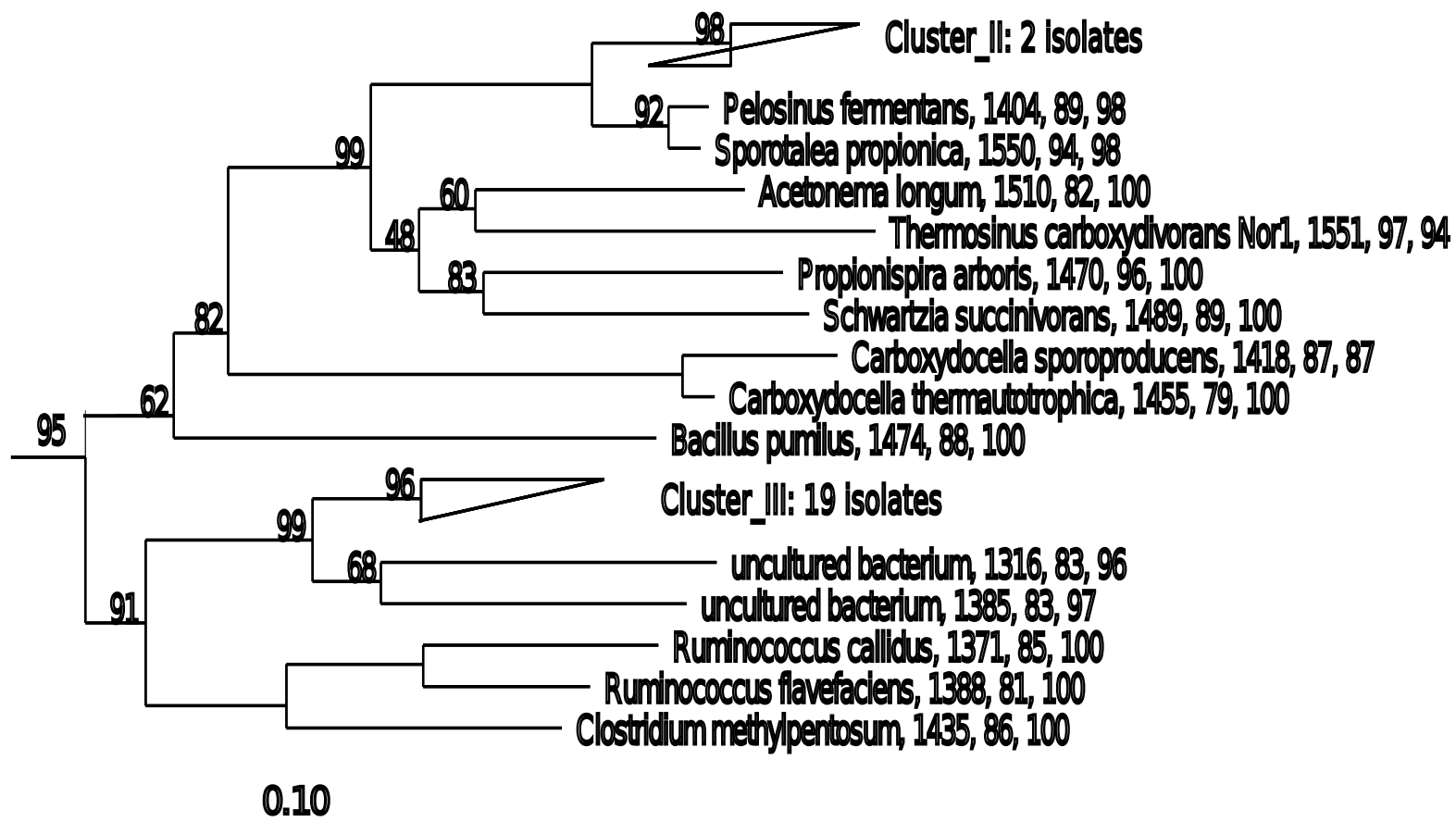


Figure 4.5: The phylogenetic distribution of the anaerobic isolates based on their 16S rRNA gene sequences. The numbers on the branches represent the bootstrap values (1000 permutations).

Figure 4.5 (cont'd)



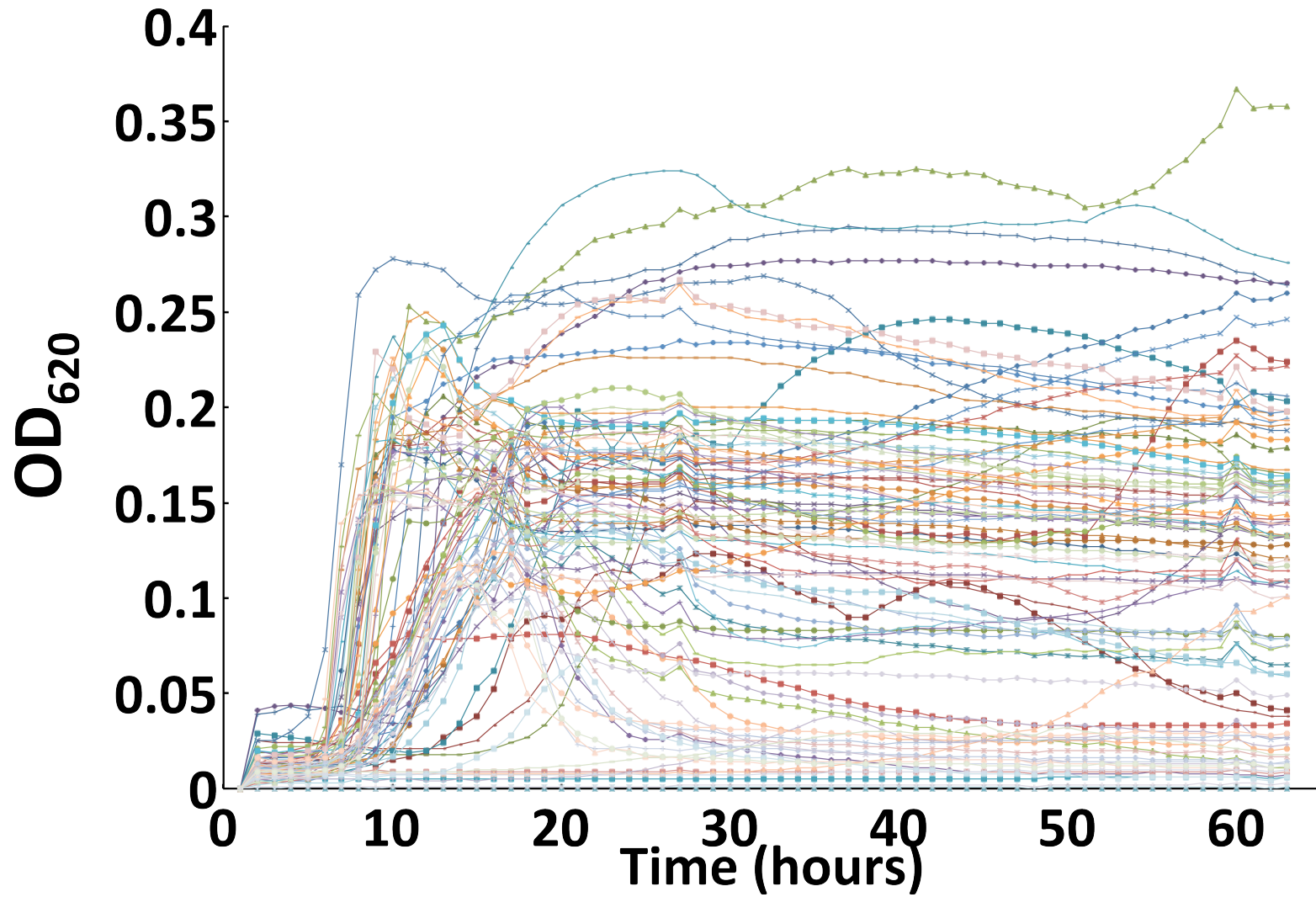
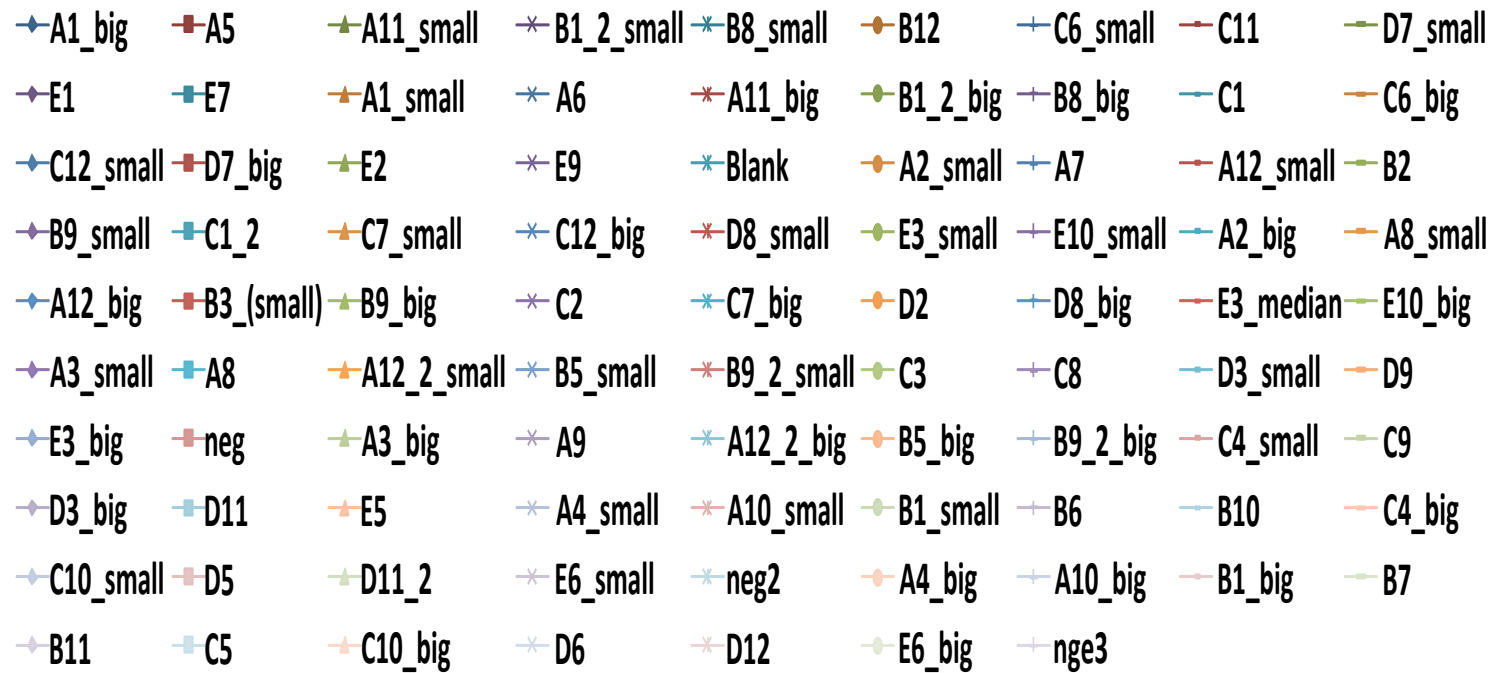


Figure 4.6: The growth curves of FRC isolates in 1/2X R2B under anaerobic condition ($H_2:CO_2:N_2$ 3:10:87). See next page for legends.

Figure 4.6 (cont'd)



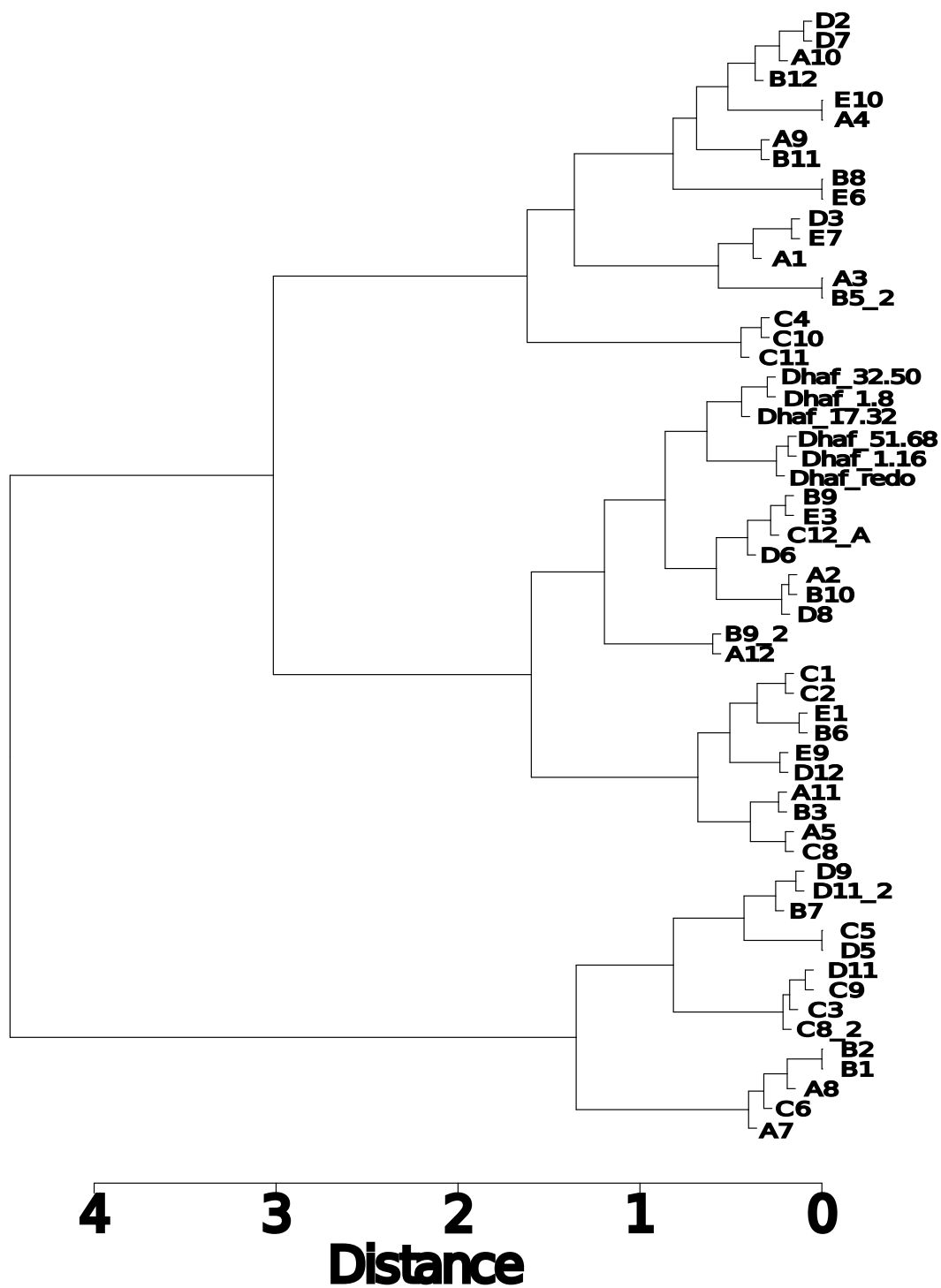


Figure 4.7: REP-BOX-(GTG)₅-PCR profiles of potential uranium immobilizing bacteria. Branches labeled Dhaf represent control samples. The rest represents enrichment isolates.

4.4.4 U⁶⁺ Immobilization By Isolates

We observed that some isolates were able to grow anaerobically in minimal media supplemented with uranyl acetate and sodium pyruvate, while little or no growth was observed in minimal media supplemented with sodium pyruvate alone (Figure C.2 B9 and D5, and Figure C.3 A1, C9 and E2). We also observed isolates grew better in sodium pyruvate media instead of uranyl acetate and sodium pyruvate media (Figure C.2 B10 and C1, and Figure C.3 A10 and C1). However, due to the long incubation time in 96 well plates, we could not obtain reliable results (Figure C.2 and Figure C.3). Therefore we employed REP-BOX-(GTG)₅ profiles and 16S rRNA identifications to dereplicate our isolate collection. Within each bacteria group that was identified by 16S rRNA gene sequences, the isolates were subgrouped based on their REP-BOX-(GTG)₅-PCR profiles. From FW107 consortia, nine strains were selected based on their unique REP-BOX-(GTG)₅-PCR profiles and 16S rRNA sequences combinations to examine their ability of anaerobic uranium immobilization. These nine isolates are shown in Figure 4.8 as A4 (Figure 4.5 A04), A5 (Figure 4.5 Cluster III), A8 (Figure 4.5 Cluster I), A9 (Figure 4.5 Cluster I), A11 (Figure 4.5 Cluster I), A12 (Figure 4.5 Cluster I), B1 (Figure 4.5 Cluster I), B8 (Figure 4.5 Cluster II), and B10 (Figure 4.5 Cluster III). Sample FW107 represent the FW107 uranium enrichment culture. The cell suspension assays were performed on these ten cultures to determine the amount of soluble uranium removed. After 70 hours of incubation, we observed that isolates A11, A12, B1 and B8 removed the largest amount of U⁶⁺, some uranium removal was observed in A8 and A9, A4 and A5 showed a comparable amount of removal to FW107, and little to no uranium removal was observed in B10. (Figure 4.8).

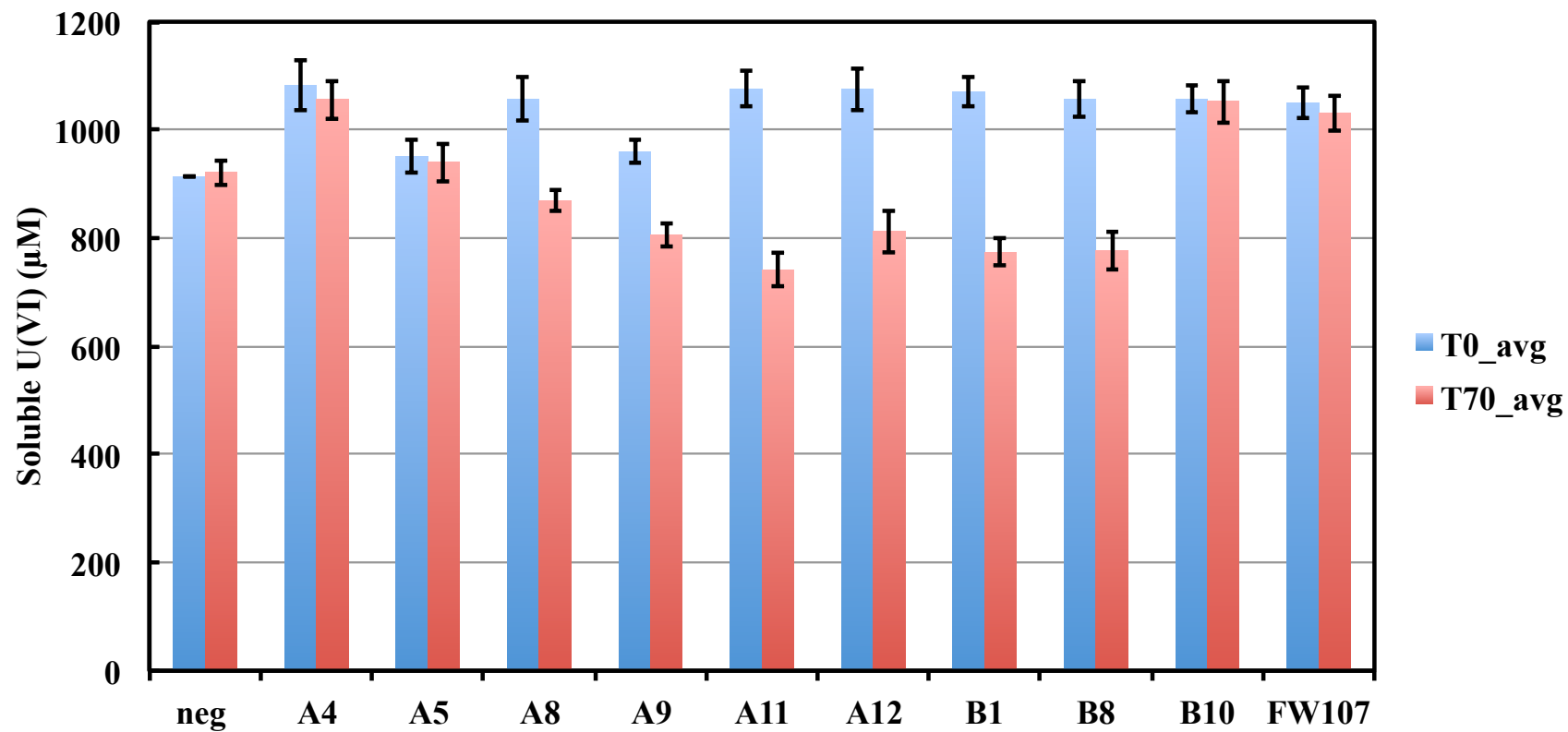


Figure 4.8: Soluble U^{6+} removal by Firmicutes isolates (from FW107) and FW107 uranium enriched community after 70 hours (T70) of incubation at room temperature in an anaerobic chamber ($H_2:CO_2:N_2$ 3:10:87). Sample "neg" represents a control culture without the addition of any bacterial cells. The error bars represent measurements of two replicates.

4.5 Discussion

In this part of our study, we were able to monitor the reduction of soluble U^{6+} in FW107 and FW102-2 uranium enrichments. Consistent with our findings in studies performed in Chapter 3, we observed that the abundance of *Pelosinus* (currently identified as *Psychrosynus* by RDP) increased along with the enrichment time (Figure 4.2 and 4.3). In addition, unclassified *Clostridiales* become more abundant in both enrichments during the same period, while soluble U^{6+} decreased (Figure 4.1). Thus, it is likely that members of *Pelosinus* and unclassified *Clostridiales* contributed to the U^{6+} removal processes.

[FeFe]-hydrogenase distributions in the enrichment cultures suggested that *Clostridium* and *Desulfotomaculum* might be contributing to metabolic hydrogen production. However, some members of these two groups are known uranium reducers [45, 72], their predominant presence in the [FeFe]-hydrogenase gene communities might also be a simple statement of their uranium reduction dependent growth from U^{6+} removal. The combined sequence data from the 16S rRNA genes and [FeFe]-hydrogenases indicates that the Clostridia are numerically important members of the community with possible uranium reduction responsibilities, as well as participants in the hydrogen economy of the bioreactors.

Although RDP SeqMatch and Arb phylogenetic analysis were consistent with each other and showed that the isolates grouped into four major Firmicute categories, RDP SeqMatch showed different species identifications. Among 48 Firmicute bacterial isolates, RDP SeqMatch revealed that the majority of the sequences in *Clostridium* XIVa group were identical to the 16S rRNA gene sequence of *Desulfotomaculum guttoideum*, which is a rarely studied sulfate-reducing bacterium [51]. At 95% to 97% similarity, sequences in *Clostridium sensu*

stricto group were closely related to *Clostridium acetobutylicum*, *Clostridium butyricum*, and *Clostridium puniceum*. While *Clostridium acetobutylicum* was recently reported as a uranium reducing bacterium [32], the other two were mostly studied for their chemical producing ability, such as butanol and 1,3-propanediol [22, 62]. The *Pelosinus* isolates we have identified were closely related to *Pelosinus sp.* strain UFO1, which was recently reported for its role multi-mode uranium immobilization [129]. Out of 48 isolates, only one was identified as *Clostridium venationis* in group *Clostridium XI* and no studies on anaerobic respiration or metal immobilization have been reported on this species.

The above taxonomy information and literature reports suggest that studying Firmicutes has a great potential in understanding bacterial community activities in U^{6+} removal. The growth patterns and REP-BOX-(GTG)₅-PCR profiles suggested that these 48 isolates should not be treated simply as four groups. Instead, it is important to test isolates based on their REP-BOX-(GTG)₅-PCR profiles for their abilities to immobilize U^{6+} . Out of the ten isolates we selected, four removed substantially more soluble uranium than the others, including the FW107 uranium enriched community. It was to our surprise that the *Pelosinus* isolate A5 was not proficient at uranium removal despite its high abundance in the enrichment cultures. It was even more surprising to observe the drastic differences in uranium removal abilities between strains (e.g., Cluster I A9 VS. Cluster I A11 in Figure 4.8). Considering the high variabilities among isolates of the same species, it is very likely that we did not obtain a uranium removal efficient *Pelosinus* strain during the isolation processes.

4.6 Conclusion

We previously described our observations on the prominence of Firmicute bacteria in uranium supplemented enrichment cultures (Chapter 3). In this work, we studied the shifts of bacterial communities during uranium immobilization. We have anaerobically isolated and identified 48 bacterial strains, which belong to phylum Firmicutes. These isolates were categorized into four different species according to their 16S rRNA gene sequences. However, their growth patterns and REP-BOX-(GTG)₅-PCR profiles indicated that they are physiologically and genomely distinct within each species. We evaluated the ability of uranium immobilization of isolate representatives. Our results indicated that many isolates with close phylogenetic affiliation to *Clostridium sardiniense* could immobilize uranium.

CHAPTER 5

PHYLOGENETIC COMPOSITION OF BACTERIA IN ANAEROBIC CO-DIGESTION OF DAIRY MANURE AND CORN STOVER

5.1 Abstract

More than 160 million dry tons of animal waste are produced annually from animal farms in the United States. These wastes pose a great environmental and health risk if not disposed of properly. Anaerobic digestion is an effective method in breaking down animal wastes to reduce the risks and it produces methane as an alternative energy source. Previous studies suggested that optimization of feed composition, HRT, and other operational conditions can greatly improve total solids removal and increase methane productivity. Despite these improvements, the relationships between system performance and the underlying bacterial community shifts are not well understood. Therefore, we constructed anaerobic bioreactors fed with dairy manure (DS) and dairy manure supplemented with corn stover (DM+CS) to compare the bacterial community structures and identify important bacterial populations correlating to total solids removal and methane production. Our results suggested that unique uncultivated strains of Bacteroidetes played a substantial role in cellulose/hemicellulose degradation in the DM+CS bioreactors. *Aminomonas paucivorans* and Clostridia populations utilize secondary metabolites produced during cellulose/hemicellulose degradation to generate hydrogen and acetate. Thus, promoting the growth of unclassified Bacteroidetes, Clostridia, and *A. paucivorans* might optimize the efficiency of co-digestion system and control the variability.

5.2 Introduction

Agriculture is a significant part of the US economy. The Food and Agriculture Organization of the United Nations (FAO) estimated that approximately \$0.2 trillion of production was contributed from agriculture in the US in 2010. The top three commodities based on production values were indigenous cattle meat, dairy products and maize. Maize was the most produced commodity based on quantity (at least three times more than other commodities). This large agricultural output resulted in considerable amounts of waste being produced. Approximately 6.7 million tons of agriculture wastes were produced in 2010 in the US (estimated based on 1993 data) [44]. The wastes were mainly used as fertilizer for crop growth. However, applying agricultural wastes, especially manures, to fields raises significant environmental concerns of greenhouse gas emissions, spread of animal pathogens, and release of excess nutrients to the environment, all of which may pose a great risk to human health and the ecosystem [20, 24, 100, 112]. Hence, a controlled animal waste management strategy that simultaneously treats the wastes and utilizes them for fuel/chemical production would have both environmental and economic benefits.

Anaerobic digestion can effectively degrade farm wastes and concomitantly produce methane, thereby reducing the health and environmental risks while producing energy [59]. Methane is produced via methanogenesis in anaerobic digestion. Methanogenesis is a syntrophic process that takes place under anaerobic conditions when organic matter is in high concentration [140]. It is a highly cooperative process carried out by different groups of bacteria and archaea with distinct responsibilities [13]. Schink [140] schematically showed that methanogenic degradation of organic matter was executed by three groups of microor-

ganisms. During anaerobic methanogenesis, organic substrates are degraded by fermentative bacteria. Fermentation by-product hydrogen is used by hydrogen-oxidizing methanogens to produce methane, while acetate-cleaving methanogens produce methane from acetate. Previous research has shown that the substrate C:N ratio influences the production of methane in anaerobic digestion [46]. Several studies have demonstrated that a mixture of nutrient-rich manures and carbohydrate-rich crop and food wastes are suitable substrates for anaerobic digestion and support methanogenesis [30, 42, 46, 85, 110, 179]. While a large number of studies were focused on optimizing system operational parameters, the microbial communities within the anaerobic digestion have not been not well explored. As pointed out by Schink et al. [140], these microbial communities are the primary force behind methane production and community shifts could effect overall performance. Herein we report on a pilot study describing microbial communities of anaerobic bioreactors fed with dairy manure (DM) and corn stover (CS) using gene targeted metagenomics.

5.3 Materials and Methods

5.3.1 Anaerobic Bioreactors

Feedstock composition and the laboratory-scale anaerobic bioreactors (5 L working volume anaerobic fermenters) were set up and described by Yue et al. [192]. Briefly, six continuously stirred tank reactors (CSTR) were operated at 35°C with hydraulic retention times (HRTs) of 30 days, 40 days, and 50 days. The feed for dairy manure bioreactors was 5% dry matter and 95% water. The feed for manure and corn stover (DM+CS) bioreactors was a mixture of dairy manure and corn stover in a ratio of 4:1 (wt:wt) and diluted to 5% DM using water.

Both feeds were homogenized using a blender prior to feeding. Analytical analyses of biogas, total solids (TS), and fiber composition were reported by Yue et al. [192].

5.3.2 DNA Extraction and Targeted Gene Amplifications

Anaerobic bioreactors were fed with DM or DM+CS at three different HRTs. Samples were taken from each bioreactor once digestion reached the stabilized phase (after two HRTs). The samples were centrifuged at 10,000 RPM for 20 minutes in a Sorvall SS-34 rotor and the pellet was stored at -20°C until extraction of community DNA. DNA was extracted by using Powersoil DNA Extraction Kit (Mo Bio Laboratory, Carlsbad, CA). Polymerase Chain Reactions (PCR) were carried out to amplify bacterial 16S rRNA gene (16S) and FeFe-hydrogenase genes (HydA) with universal primer sets: 357F (5'CCTACGGGAGGCAGCAG3') and 926R (5'CCGTCAATTCMTTTRAGT3') for 16S, and FeFe-272F (5'GCHGAYMTBACHATWATGGARGA3') and FeFe-427R (5'GCNGCYTCCATDACDCCDCCNGT3') for HydA [11].

Bacterial 16S rRNA genes were amplified with sequence-tagged primers developed by the Human Microbiome Project (HMP) targeting the V3-V5 region of 16S rRNA genes. Briefly, 1X Taq reaction buffer, 2 mM MgSO₄, 0.1 mg/ml BSA, 0.2 mM of each dNTP, 0.33 μM of each primer, 0.125 U/μl of Platinum High Fidelity Taq Polymerase (Invitrogen, Carlsbad, CA), and 10 ng DNA template were mixed with DNase and RNase free water for each PCR reaction. The amplification conditions include an initial denaturing step at 95°C for 5 minutes, followed by 30 cycles of 3 temperature steps consisting of denaturing at 95°C for 45 seconds, annealing at 50°C for 45 seconds, and elongation at 72°C for 90 seconds, and a final extension at 72°C for 5 minutes following the completion of 30 cycles. All PCR products were stored at -20°C until sequencing at the MSU Research Technologies Support Facilities

(MSU-RTSF).

FeFe-hydrogenase genes were amplified as described previously [11] and cloned with Topo Cloning (Invitrogen, Carlsbad, CA) and sequenced at the MSU-RTSF. Each HydA PCR consists of a mixture of 1X Taq reaction buffer, DNase and RNase free water, 2 mM MgCl₂, 0.1 mg/ml BSA, 0.2 mM of each dNTP, 2 μ M of each primer, 0.05 U/ μ l of Platinum Taq Polymerase (Invitrogen, Carlsbad, CA), and 20 ng DNA template. The amplification conditions include an initial denaturing step at 94°C for 4 minutes, followed by 35 cycles of 3 temperature steps consisting of denaturing at 94°C for 60 seconds, annealing at 56.5°C for 60 seconds, and elongation at 72°C for 90 seconds, and a final extension at 72°C for 20 minutes following the completion of 35 cycles. All PCR products were stored at -20°C until needed.

5.3.3 Preparation for Pyrosequencing and Construction of Clone Libraries

The 16S rRNA gene PCR products were visualized on 2% Tris-Borate-EDTA (TBE) agarose gel. DNA fragments at \sim 569 bp were excised and extracted from the gels by using Qiagen Gel Extraction Kit and further purified with QiaQuick PCR Product Purification Kit (Qiagen, Valencia, CA). All purified DNA products were quantitated with Qubit HS Double-stranded DNA Kit (Invitrogen, Carlsbad, CA) then composited at equal mass for a final DNA concentration of 0.5 ng/ μ l. Pyrosequencing was performed at Michigan State University RTSF by using a Roche 454 GSFLX Titanium Sequencer.

HydA encoding gene sequence PCR products (\sim 500 bp) were confirmed via electrophoresis (1% Tris-Acetate-EDTA agarose gel). Clone libraries of FeFe-hydrogenase were constructed by using Invitrogen Topo PCR2.1 Cloning Kit (Invitrogen, Carlsbad, CA) following the vendor's protocol. The cloned fragments were purified and sequenced at RTSF via an

ABI 3730 Genetic Analyzer.

5.3.4 Sequence and Community Analyses

Bacterial 16S rRNA gene sequences obtained from pyrosequencing were processed and analyzed by using the Ribosomal Database Project (RDP) Pyrosequencing pipeline [26]. Sequences that were shorter than 250 bp, containing any N's in sequencing region, or with an average quality score less than 20 were discarded. Chimeras were removed from RDP processed sequences by using USEARCH (UCHIME reference mode with Silva gold alignment database as reference). RDP Multi-classifier was used to identify each sequence to bacterial genus level (threshold 80). RDP SeqMatch was used for further identification of bacterial clusters of interest. To eliminate the clustering artifacts, sequences were also trimmed to the same length (250 bp) based on alignment profiles prior to complete linkage clustering at the RDP.

[FeFe]-hydrogenase gene sequences were identified by BLAST against the NCBI non-redundant amino acid database. The top 50 best matches were generated for each sequence. The annotated match with the best expected value ($E < 10^{-5}$) was selected in determining bacterial species information.

OTU- and phylotype-based community analyses were performed by using statistical software R [128]. Ecological indices were estimated for each bioreactor sample based on clustered sequences by using the R package Vegan [117]. Specifically, community richness (chaoI), diversity indices (Shannon H' and Simpson's D) and community evenness (E) were calculated based on equations previously described [94]. The sampling coverage (C) of each sample was calculated based on Good's method, $C=1-n_1/N$, where n_1 represents the number of OTUs

that is a singleton and N is the total number of sequences in the sample [39]. The R package Vegan was also used to perform non-metric multidimensional scaling analysis (NMDS) to correlate the dissimilarities among bioreactor samples and the shifts in phylotype abundance [117]. Shared OTUs among samples were calculated and plotted by using the R package Venerable [159].

5.4 Results

5.4.1 The Influence of HRT and Corn Stover on System Performance

For bioreactors fed with DM, a substantial increase on biogas productivity was observed once the HRT increased from 30 to 40 days (Figure 5.1). The biogas productivity of the DM bioreactors increased from 209 to 399 ml/g TS loading/day. A similar increase was also observed in the DM+CS bioreactors (from 270 to 497 ml/g TS loading/day). Further increases in HRT had no significant ($P > 0.05$) influence on the biogas productivity for either feeds. The TS reduction for both feeds also increased with the increases in HRT (Figure 5.1). The HS reduction increased from 27% (HRT of 30 days) to 50% (HRT of 50 days) in the DM bioreactors. A similar trend was observed in the DM+CS bioreactors (from 35% at a HRT of 30 days to 53% at a HRT of 50 days). In addition, digestion performance demonstrated that under the same HRT, both biogas productivity and TS reduction were significantly ($P < 0.05$) higher in the DM+CS bioreactors than in the DM bioreactors, presumably due to the introduction of fast-hydrolyzing components from corn stover in DM+CS feed [192].

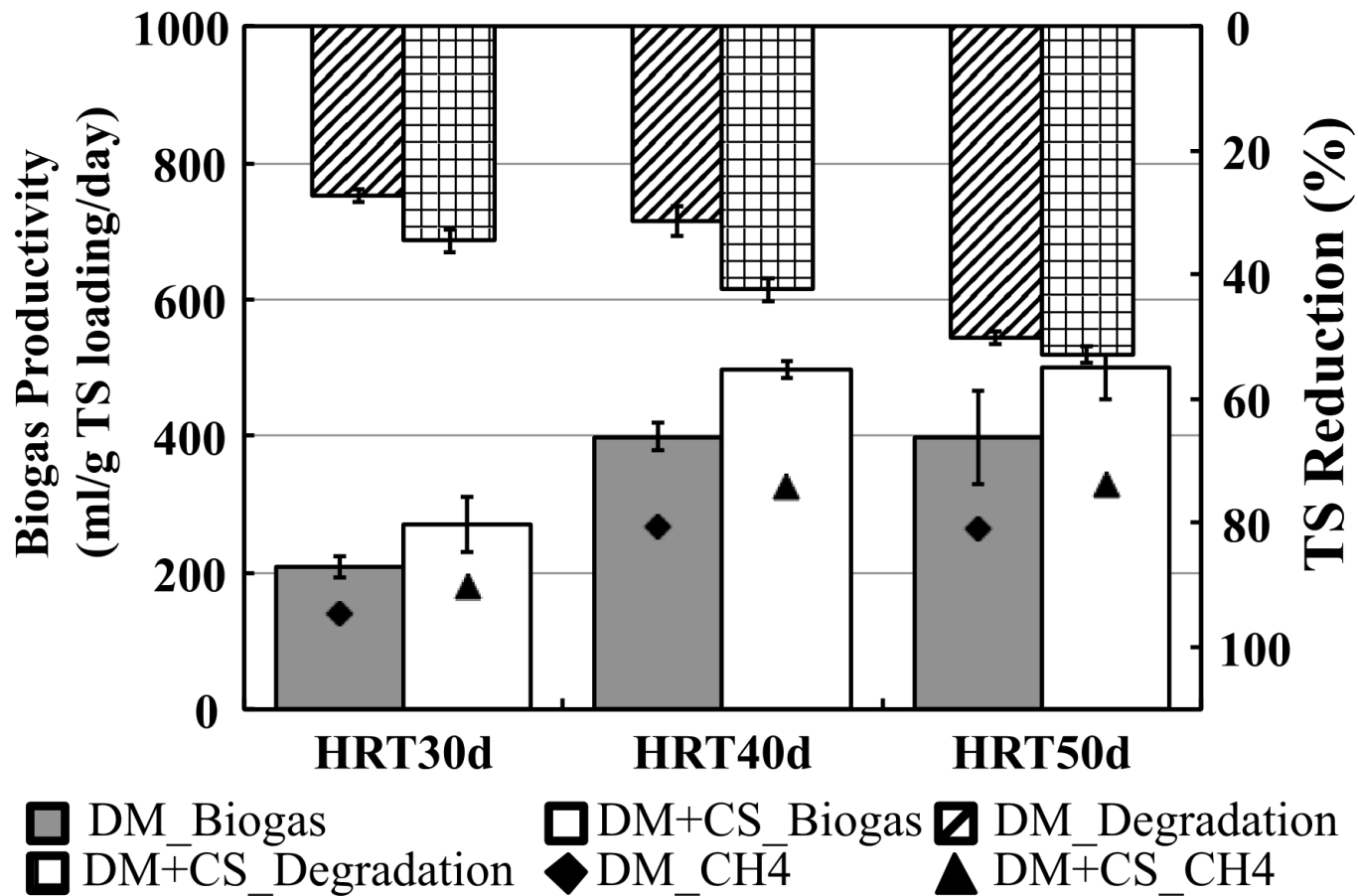


Figure 5.1: The total solids (TS) reduction efficiency (diagonal and grid lined columns) and the production rate of biogas (grey and white columns) in the DM and DM+CS bioreactors at four HRTs: a HRT of 30 days (HRT30d), a HRT of 40 days (HRT40d) and a HRT of 50 days (HRT50d). Solid diamonds and solid triangles represent the amount of methane produced in the DM and DM+CS bioreactors, respectively.

The trend of biogas productivity and TS reduction indicated that bioreactor performance underwent significant ($P < 0.05$) changes from 30 days of HRT to 40 days or longer of HRT. The biogas productivities for both DM and DM+CS bioreactors were maximized at 40 days of HRT. Longer HRTs did not increase the biogas productivity but significantly more TS was removed ($P < 0.05$). In spite of different biogas production rates and TS reduction levels from different bioreactors, the methane content of biogas from all six bioreactors fell within the narrow range from 65.7% to 67.4%, and this was relatively stable throughout the experiment. The pH measurements indicated that all six bioreactors were maintained at near neutral condition (pH 6.58-6.94).

5.4.2 Phylogenetic Comparisons of Anaerobic Bioreactor Bacterial Communities

Bacterial 16S rRNA gene targeted sequencing revealed that we sampled over 98% of each anaerobic bioreactor community (Table D.1 and Figure D.2). The evenness of the bacterial communities were relatively stable (0.68 to 0.78) but bacterial diversity shifted drastically from sample to sample. All diversity indices indicated that the DM+CS bioreactor with a HRT of 40 days had the most diverse bacterial community (Table D.1).

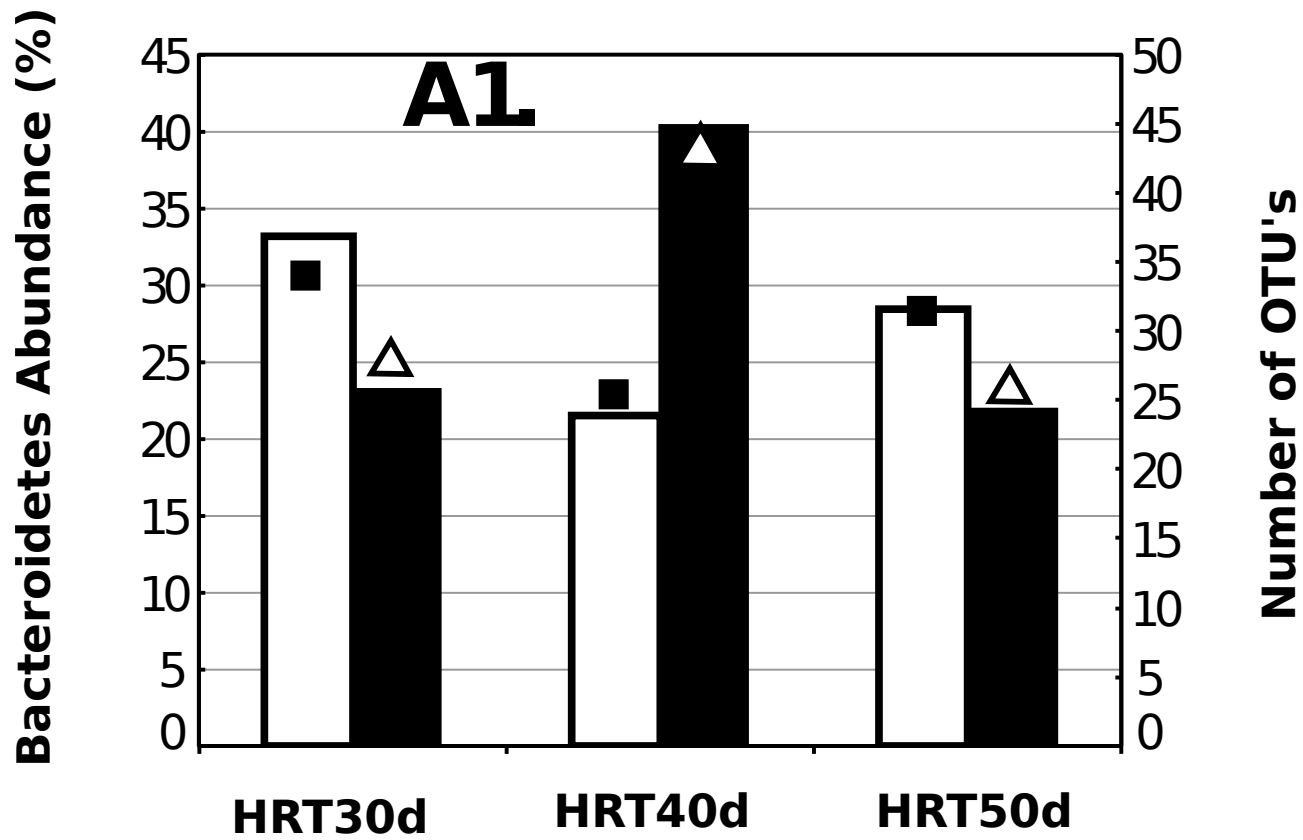


Figure 5.2: The abundance and diversity (OTU at 97% sequence similarity) of phyla Bacteroidetes (panel A1), class Clostridia (panel B1), and *Escherichia / Shigella* (panel C1) in each bioreactor bacterial community. The distribution of OTUs among samples are presented as Venn diagrams in panel A2 (Bacteroidetes), B2 (Clostridia) and C2 (*Escherichia/Shigella*). The colors of the bioreactor/HRT font corresponds to an area bounded by the same color. Labels HRT30d, HRT40d and HRT50d represent bioreactors with a HRT of 30, 40, and 50 days, respectively.

Figure 5.2 (cont'd)

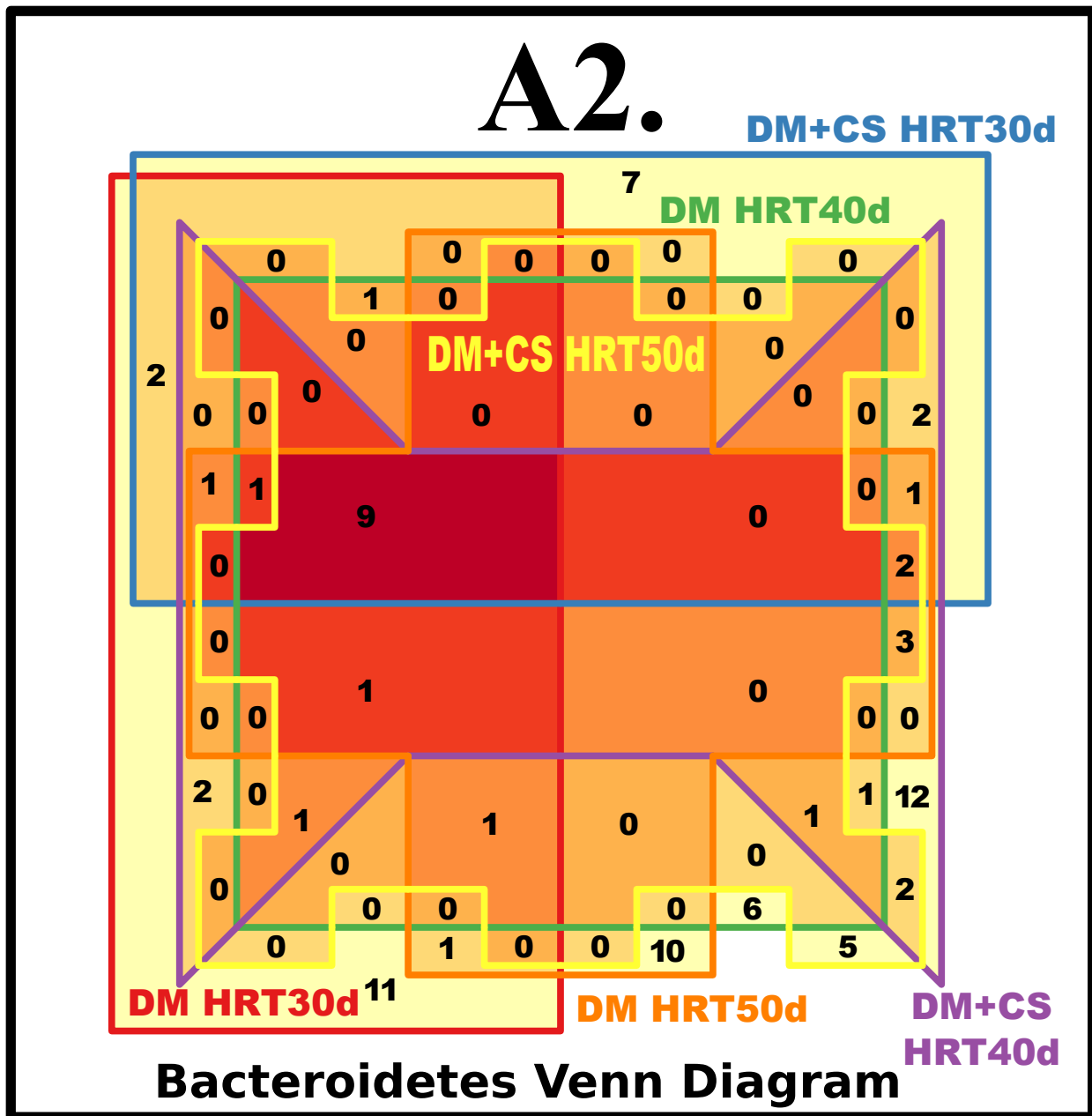


Figure 5.2 (cont'd)

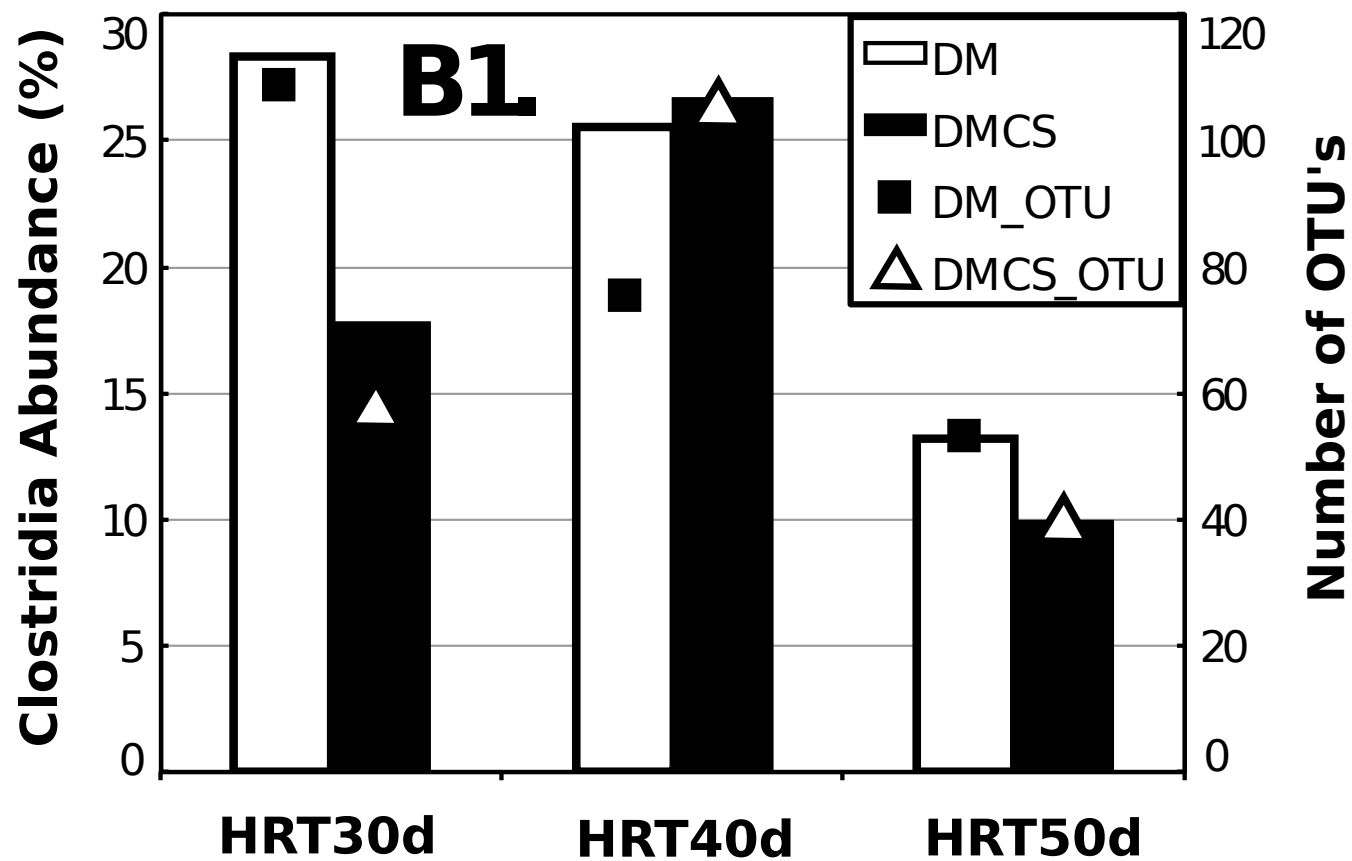


Figure 5.2 (cont'd)

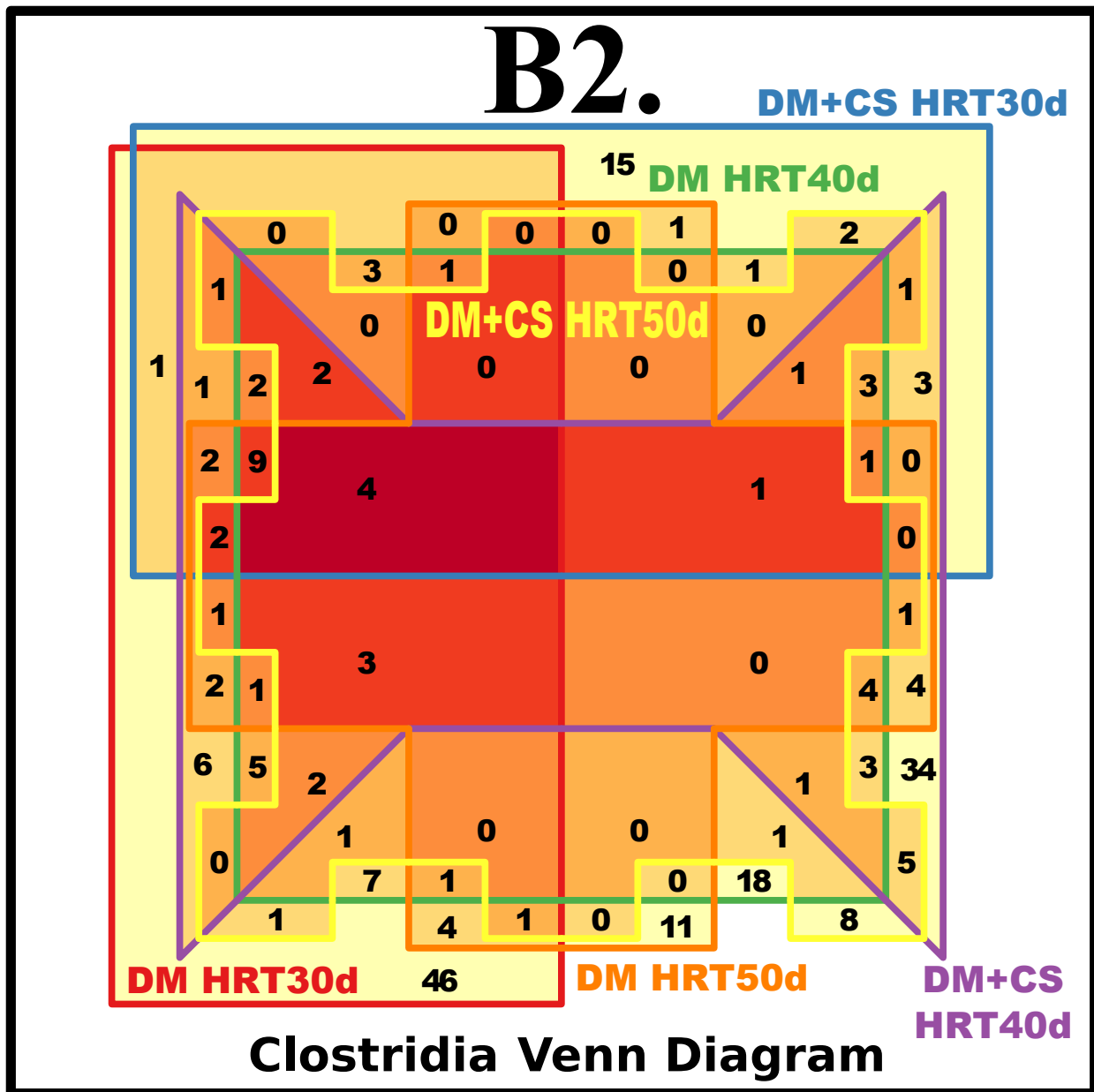


Figure 5.2 (cont'd)

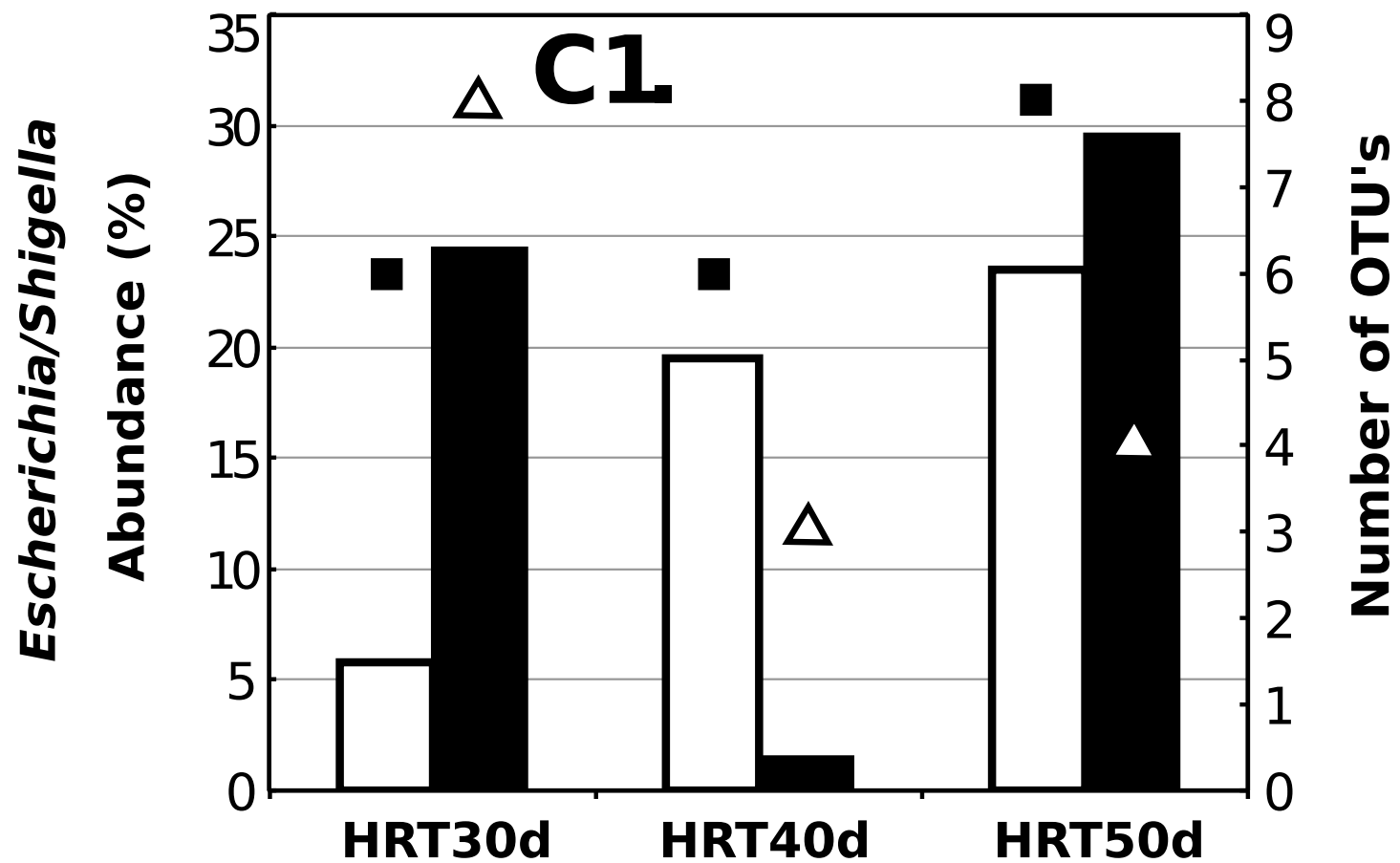
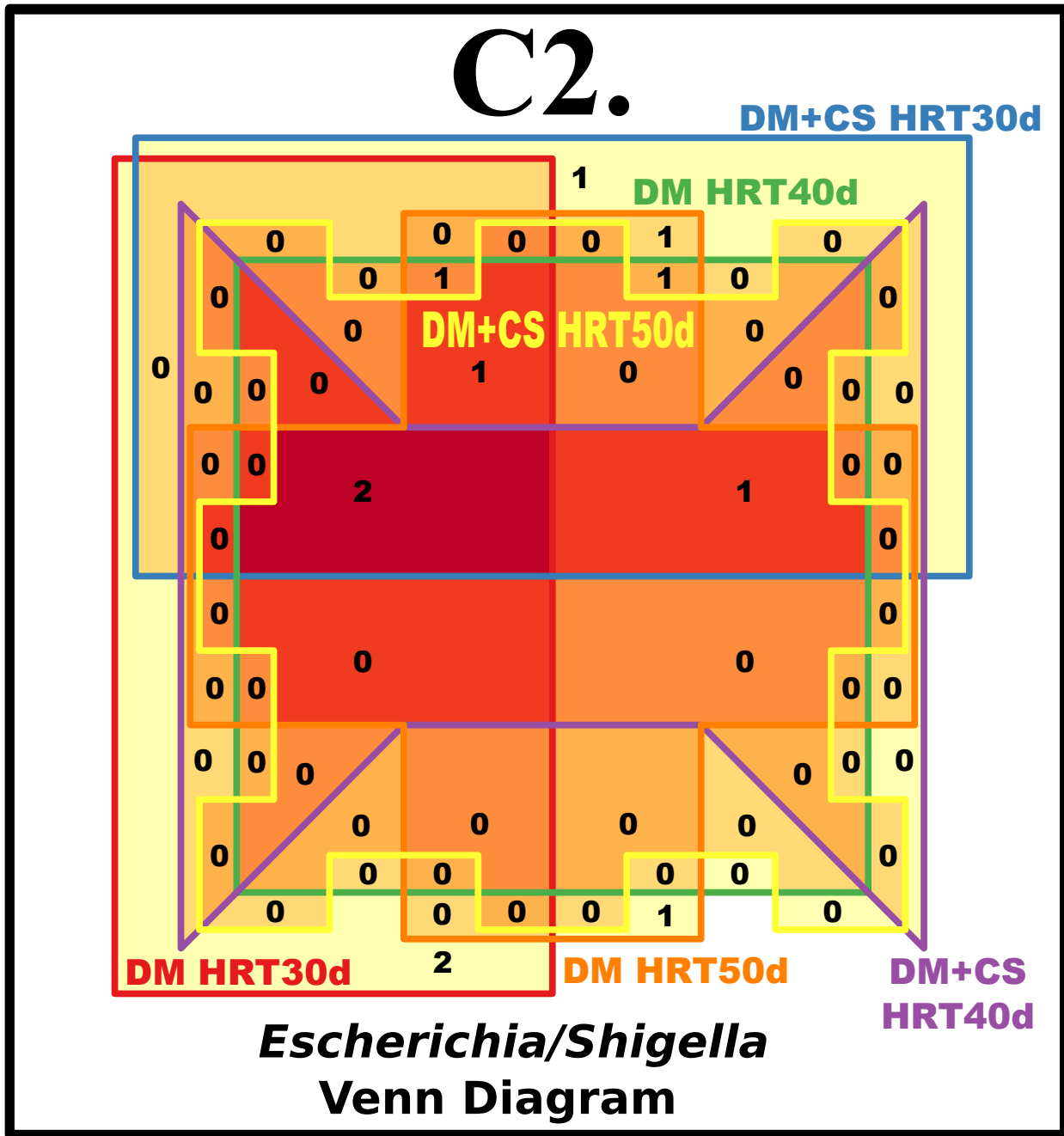


Figure 5.2 (cont'd)



Bacterial taxa were determined based on 16S rRNA genes via RDP Multi-Classifer with a minimal bootstrap value of 80 (assigned as unclassified if score is smaller than 80). A total of 16 bacterial phyla were assigned and approximately 5% of total sequence was categorized

as unclassified bacteria (3-7% unclassified bacteria in each sample). At the genus level, a total of 198 bacterial groups (137 classified and 61 unclassified) were identified. Firmicutes, Bacteroidetes, and Proteobacteria were the most abundant phyla in all six anaerobic bioreactor samples (Figure D.2 wide columns). Within these three phyla, Clostridia, unclassified Bacteroidetes, and *Escherichia/Shigella* were found to be highly abundant (Figure D.2 thin columns). We observed that Clostridia comprised 74-84% of the Firmicutes in the bioreactors. Phylum Bacteroidetes was largely composed of unclassified Bacteroidetes, except in the DM a HRT of 30 days bioreactor that had abundant *Alkaliflexus*, *Petrimonas*, unclassified Porphyromonadaceae and *Flavobacterium*. Although the abundance of phylum Bacteroidetes was similar across the six bioreactors, the abundance of unclassified Bacteroidetes increased as the HRT increased. In the DM+CS bioreactor with a HRT of 40 days, 35.45% of the community populations were identified as unclassified Bacteroidetes, representing 87% of the Bacteroidetes populations. Within phylum Proteobacteria, we observed that genera *Escherichia/Shigella* were consistently abundant and its abundance variation reflected the abundance of Proteobacteria except in the DM+CS bioreactor with a HRT of 40 days. Thus, the population of *Escherichia/Shigella* increased as a function of HRT and on average constituted 17% of the bacterial community except in the DM+CS bioreactor with a HRT of 40 days, where it decreased to 1.53%. Over 50% of the phylum Proteobacteria in the DM+CS bioreactors with a HRT of 30 days, the DM bioreactors with a HRT of 40 days and the DM+CS bioreactors with a HRT of 50 days were identified as *Escherichia/Shigella*, while 37.71% and 21.21% of Proteobacteria were classified as *Escherichia/Shigella* in the DM bioreactor with a HRT of 30 days and DM+CS bioreactor with a HRT of 40 days, respectively (Figure D.2). Besides the changes in abundance, we also observed the diversity shifts within

phylum Bacteroidetes, class Clostridia, and genera *Escherichia/Shigella* (Figure 5.2). When operated at the HRTs of 30 days and 50 days, phylum Bacteroidetes was more abundant in DM bioreactors than in DM+CS bioreactors. Phylum Bacteroidetes also appeared to be less abundant in both DM and DM+CS bioreactors under the HRT of 50 days than when they were operated with a HRT of 30 days. At a HRT of 40 days, the abundance of phylum Bacteroidetes was substantially larger in DM+CS bioreactors than DM bioreactors (40.38% in DM+CS a HRT of 40 days VS. 21.47% in DM a HRT of 40 days). The Bacteroidetes diversity (OTU) pattern followed its abundance trend (Figure 5.2 A1). A larger numbers of OTUs were observed in DM bioreactors than in DM+CS bioreactors at HRTs of 30 and 50 days. The number of OTUs decreased in DM and DM+CS bioreactors slightly as HRT increased from 30 to 50 days. The lowest Bacteroidetes diversity was observed in the DM bioreactor at a HRT of 40 days (25 OTUs). In contrast, the DM+CS bioreactor at a HRT of 40 days revealed the largest Bacteroidetes diversity (43 OTUs). A total nine OTUs were shared by all six samples. The proportion of unique OTUs in each sample ranged from 19% in the DM+CS bioreactor at a HRT of 50 days bioreactor to 32% in DM a HRT of 30 days and DM a HRT of 50 days bioreactors (Figure 5.2 A2). Similar to phylum Bacteroidetes, the abundance of class Clostridia decreased when HRT increased from 30 days to 50 days (Figure 5.2 B1). When operated at HRTs of 30 and 50 days, class Clostridia was more abundant in DM bioreactors than DM+CS bioreactors. The abundances of class Clostridia were similar in the DM (25.5%) and DM+CS (26.6%) bioreactors operated at a HRT of 40 days. The diversity within class Clostridia followed the same trend as observed in the abundance profiles at HRTs of 30 and 50 days. At a HRT of 40 days, class Clostridia was substantially more diverse in the DM+CS bioreactor than in the DM bioreactor. With an

abundance difference of 1.1% at a HRT of 40 days, the DM+CS bioreactor was observed to have 105 OTUs of Clostridia, while only 75 Clostridia OTUs were detected in the DM bioreactor (Figure 5.2 B1). There were four Clostridia OTUs shared by all six samples. A large portion of the OTUs were unique to each sample, ranging from 20% in DM a HRT of 50 days and DM+CS a HRT of 50 days bioreactors to 42% in DM a HRT of 30 days bioreactor (Figure 5.2 B2). Unlike phylum Bacteroidetes and class Clostridia, the abundance of genera *Escherichia/Shigella* increased in the bioreactors as HRT increased from 30 to 50 days (Figure 5.2 C1). It was also observed that the genera *Escherichia/Shigella* was more abundant in the DM+CS bioreactors than in the DM bioreactors when operational HRTs were 30 and 50 days. *Escherichia/Shigella* were the least abundant (1.53%) in the DM+CS bioreactor operated at HRT 40 days. In contrast, the DM bioreactor operated at a HRT of 40 days was substantially more abundant with *Escherichia/Shigella* (19.55%). The diversity profile revealed that when the abundance of *Escherichia/Shigella* increased from 5.82% (the DM bioreactor with a HRT of 30 days) to 19.55% (the DM bioreactor a HRT of 40 days), the number of OTUs stayed the same (6). However, the *Escherichia/Shigella* OTUs decreased from 8 to 3 in DM+CS bioreactors when the *Escherichia/Shigella* abundance decreased substantially at a HRT of 40 days. Finally, the number of *Escherichia/Shigella* OTUs remained the same (from 3 to 4) when their abundance increased from 1.53% (the DM+CS bioreactor with a HRT of 40 days) to 29.56% (the DM+CS bioreactor with a HRT of 50 days) (Figure 5.2 C1). Among these OTUs, two were found in all six samples. Two of six OTUs were unique to the DM bioreactor with a HRT of 30 days, and one of eight was unique to the DM+CS bioreactor with a HRT of 30 days and the DM bioreactor with a HRT of 50 days. No unique *Escherichia/Shigella* OTUs were found in the DM bioreactor with a HRT of 40

days, the DM+CS bioreactor with a HRT of 40 days and the DM+CS bioreactor with a HRT of 50 days (Figure 5.2 C2).

5.4.3 Bacteroidetes

Bacteroidetes was one of the most abundant phyla in the bioreactor samples described above. The genera abundance revealed that unclassified Bacteroidetes was also predominant and highly variable (Appendix C Figure C.2). Sequences identified as members of phylum Bacteroidetes by RDP Classifier were extracted and separated into groups of unclassified Bacteroidetes and classified Bacteroidetes (all taxon groups that could be identified further than phylum Bacteroidetes). The abundance of phylum Bacteroidetes in bacterial communities varied from 21% to approximately 40% (Figure 5.3 vertical striped area). We observed that the composition of phylum Bacteroidetes shifted from classified Bacteroidetes to unclassified Bacteroidetes. Across six bioreactor samples, unclassified Bacteroidetes comprised as much as 88% of the phylum Bacteroidetes (the DM+CS bioreactor a HRT of 40 days). The least amount of unclassified Bacteroidetes was observed in the DM bioreactor with a HRT of 30 days, where only 15% of Bacteroidetes were unable to be identified further than the phylum level. The composition of phylum Bacteroidetes revealed that unclassified Bacteroidetes were more abundant than classified Bacteroidetes in the DM+CS bioreactors regardless of HRT (Figure 5.3). However, in the DM bioreactor samples, classified Bacteroidetes were substantially more abundant than unclassified Bacteroidetes at HRT 30 days (the DM bioreactor at a HRT of 30 days) and became much less abundant in the DM bioreactor with a HRT of 50 days. At the same retention time, unclassified Bacteroidetes were more abundant in the DM+CS bioreactors than in the DM bioreactors and vice versa for classified

Bacteroidetes. It was also observed that unclassified Bacteroidetes increased in abundance as the HRT increased in both the DM and DM+CS bioreactors, while the abundance of classified Bacteroidetes decreased (Figure 5.3).

At 97% similarity, sequences in phylum Bacteroidetes were clustered into different groups. It was observed that phylum Bacteroidetes was abundant (40%) and diverse (over 40 OTU) in the DM+CS bioreactor operated at a HRT of 40 days (Figure 5.2A). In contrast, Bacteroidetes was the least abundant and diverse (approximately 25 OTU) in DM bioreactor operated at a HRT of 40 days. The Bacteroidetes clusters (at 97% similarity) in the DM+CS bioreactor with a HRT of 40 days were compared to the Bacteroidetes clusters in other samples and four distinct clusters (#11, #14, #43, and #69) were identified (Figure 5.4). These four clusters were abundant in the DM+CS bioreactor with a HRT of 40 days where together they comprised of 62% of the Bacteroidetes populations in the DM+CS bioreactor with a HRT of 40 days. These clusters were among the unclassified Bacteroidetes. Cluster #69 appeared unique to the DM+CS bioreactor with a HRT of 40 days as it was not detected in other samples (the DM bioreactor with a HRT of 30 days, the DM bioreactor with a HRT of 40 days, the DM bioreactor with a HRT of 50 days and the DM+CS bioreactor with a HRT of 50 days) or detected with a 0.3% abundance (the DM+CS bioreactor with a HRT of 30 days). Cluster #11 and #14 were observed in the DM+CS bioreactor samples (the DM+CS bioreactor with a HRT of 30 days, the DM+CS bioreactor with a HRT of 40 days and the DM+CS bioreactor with a HRT of 50 days) at high abundance (6-27% and 15-29% of the phylum Bacteroidetes in each sample, respectively). These two clusters were also observed in the DM bioreactor samples (the DM bioreactor with a HRT of 30 days, the DM bioreactor with a HRT of 40 days and the DM bioreactor with a HRT of 50 days) but at a substantially

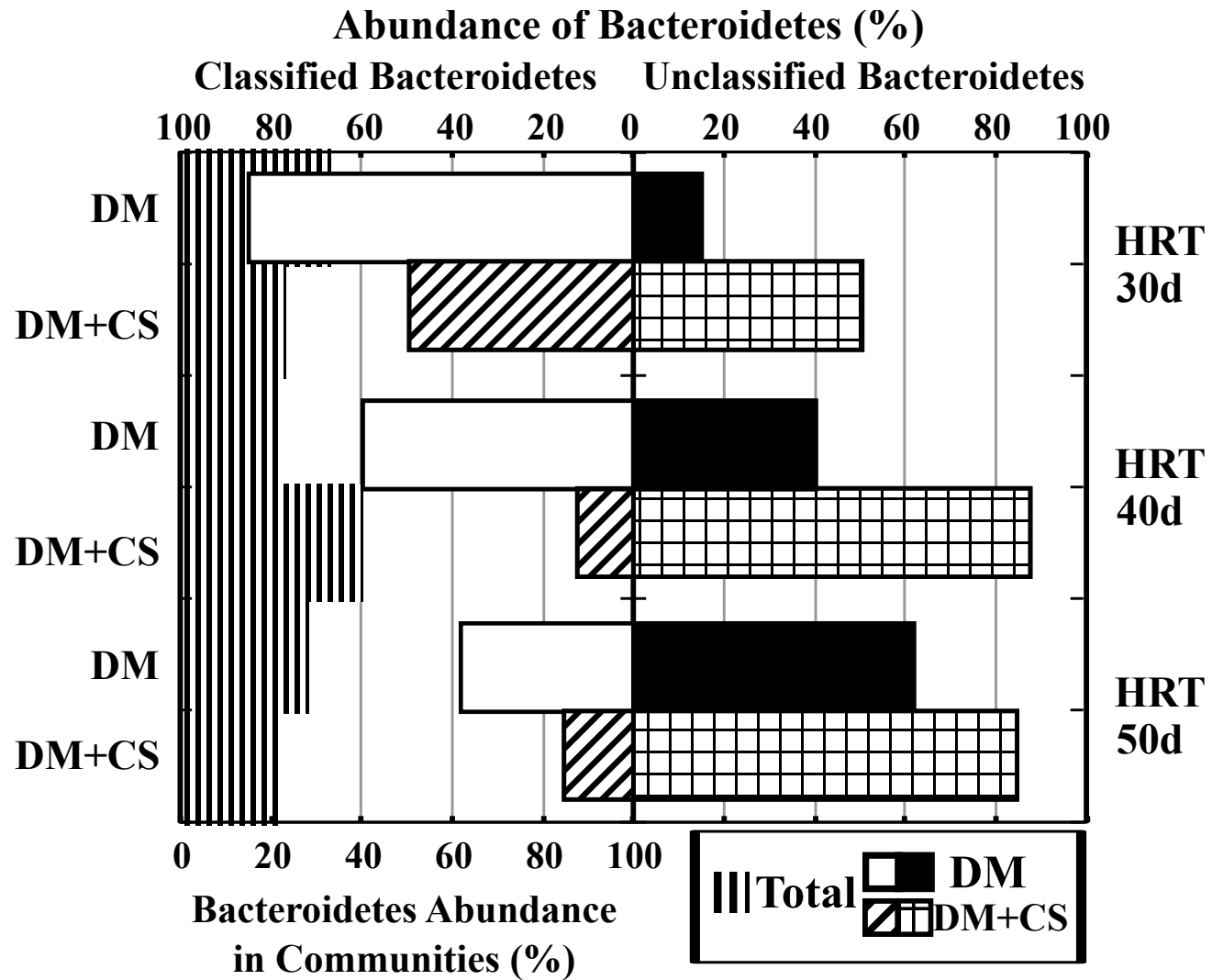


Figure 5.3: The abundance of phyla Bacteroidetes (vertical stripes) in each bioreactor bacterial communities. The distribution of classified and unclassified Bacteroidetes within phylum Bacteroidetes were calculated and displayed in left panel (white and diagonal striped bars) and right panel (black and gridded bars) respectively. Labels HRT30d, HRT40d and HRT50d represent bioreactors with a HRT of 30, 40, and 50 days, respectively.

lower abundance (1-7% and 0.4-2% of the phylum Bacteroidetes in each sample, respectively) but became more abundant as the HRT increased. Thus, the abundance of #11 and #14 could be ranked as the DM bioreactor with a HRT of 30 days < the DM bioreactor with a HRT of 40 days < the DM bioreactor with a HRT of 50 days and the DM+CS bioreactor with a HRT of 30 days < the DM+CS bioreactor with a HRT of 40 days < the DM+CS bioreactor with a HRT of 50 days. Over 11% of the Bacteroidetes abundance was contributed by cluster #43. This cluster was present in the DM+CS bioreactors operated at HRT greater than 40d (the DM+CS bioreactors at HRT of 40 and 50 days). All three populations were highly similar to uncultured Bacteroidetes and no isolates with similar 16S rRNA sequences could be found (RDP Sequence Match).

5.4.4 Hydrogen Producing Population Profiles

We obtained 45 to 76 HydA gene clones (total 352 HydA gene clones). The coverage based on Good's method ranged from 72%-94% with a median of 87%. A total of 49 hydrogenase OTUs were detected of which 28 were affiliated with class Clostridia. Three major taxonomic affiliations (phylum Synergistetes, class Clostridia and phylum Bacteroidetes) were identified that accounted for 64-86% of the detected hydrogenases sequences.

The abundance of *Synergistetes*-like [FeFe]-hydrogenase genes increased from less than 15% to over 30% in the DM bioreactors and remained over 35% in the DM+CS bioreactors as the HRT increased. The largest abundance of *Synergistetes* (42.86%) was observed in the DM+CS bioreactor operated at a HRT of 40 days. The abundance of Clostridia-like [FeFe]-hydrogenase genes decreased in the DM bioreactors (40.68% to 20%) and increased in the DM+CS bioreactors (18.42% to 36.92%) as the operational HRT increased. Phylum

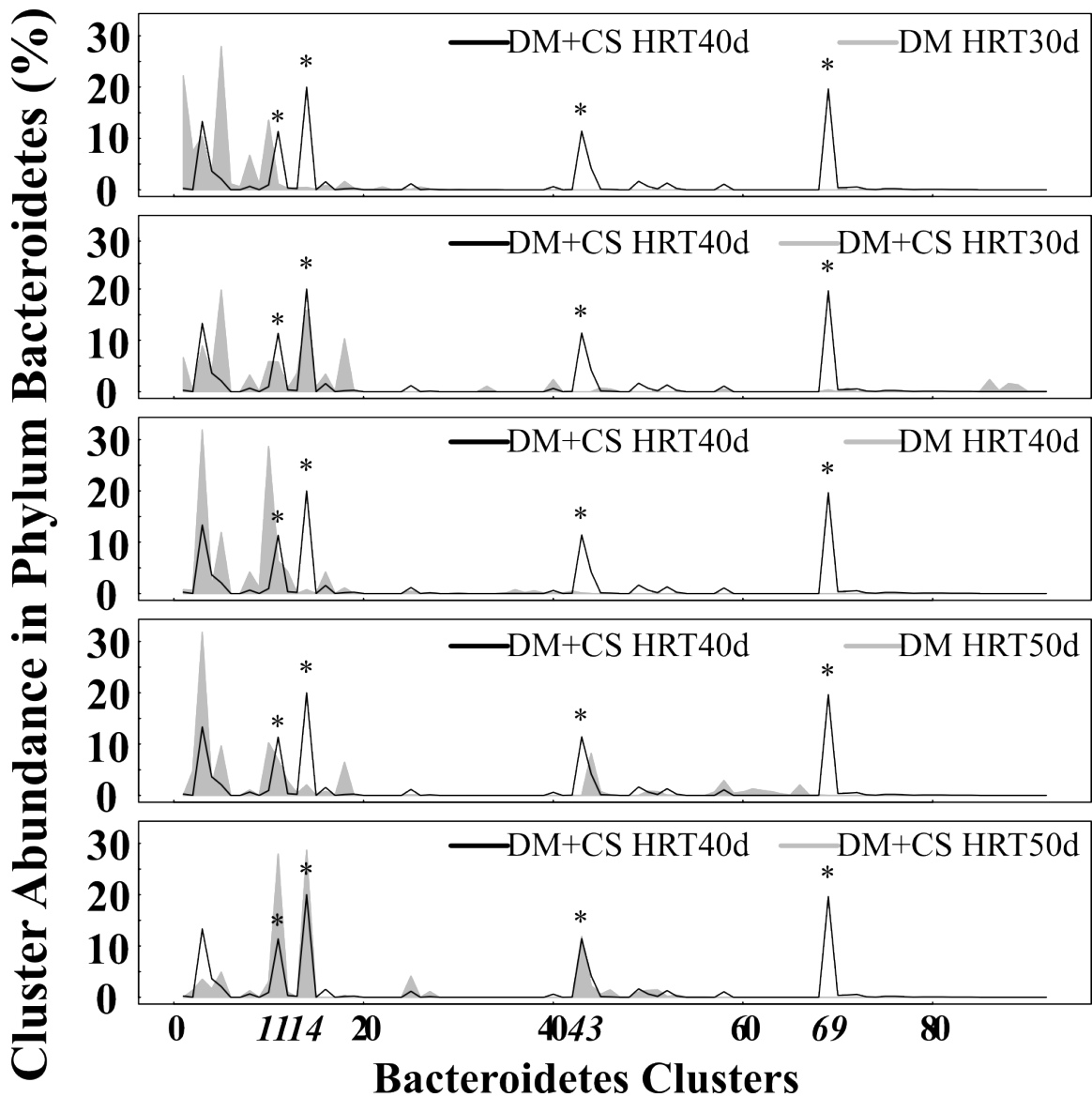


Figure 5.4: The comparisons of Bacteroidetes clusters (97% sequence similarity) between the DM+CS bioreactor with a HRT of 40 days and other bioreactor samples. Labels HRT30d, HRT40d and HRT50d represent bioreactors with a HRT of 30, 40, and 50 days, respectively. Symbol * denote peaks that are clusters of unclassified Bacteroidetes that are highly abundant in all DM+CS bioreactors (#11 and #14), in DM+CS bioreactors at long HRTs (#43), and in the DM+CS bioreactor with a HRT of 40 days (#69).

Bacteroidetes-like [FeFe]-hydrogenase genes appeared to be more abundant in the DM bioreactors than in the DM+CS bioreactors. The overall abundance of Bacteroidetes decreased as the HRT increased (Figure 5.5).

Detailed abundance analysis at the species level revealed that *Aminomonas paucivorans* (main contributors of *Synergistetes*-like [FeFe]-hydrogenase genes) was the most abundant [FeFe]-hydrogenase containing population (Figure 5.6). Hence, *A. paucivorans* shared the same pattern as phylum *Synergistetes* abundance trend. [FeFe]-hydrogenase genes similar to those of *Moorella thermoacetica*, a member of class Clostridia, were also found abundant in the DM+CS bioreactors. *M. thermoacetica* like [FeFe]-hydrogenase genes appeared to be more abundant in the DM+CS bioreactors, except in the DM+CS bioreactor with a HRT of 30 days. It was the most abundant hydrogenase phylotype in the DM+CS bioreactor with a HRT of 40 days (18.37%). We also observed that the abundance patterns of *A. paucivorans*- and *M. thermoacetica*-like hydrogenase genes were similar to the abundance pattern of unclassified Bacteroidetes determined based on 16S rRNA gene sequences (Figure 5.6).

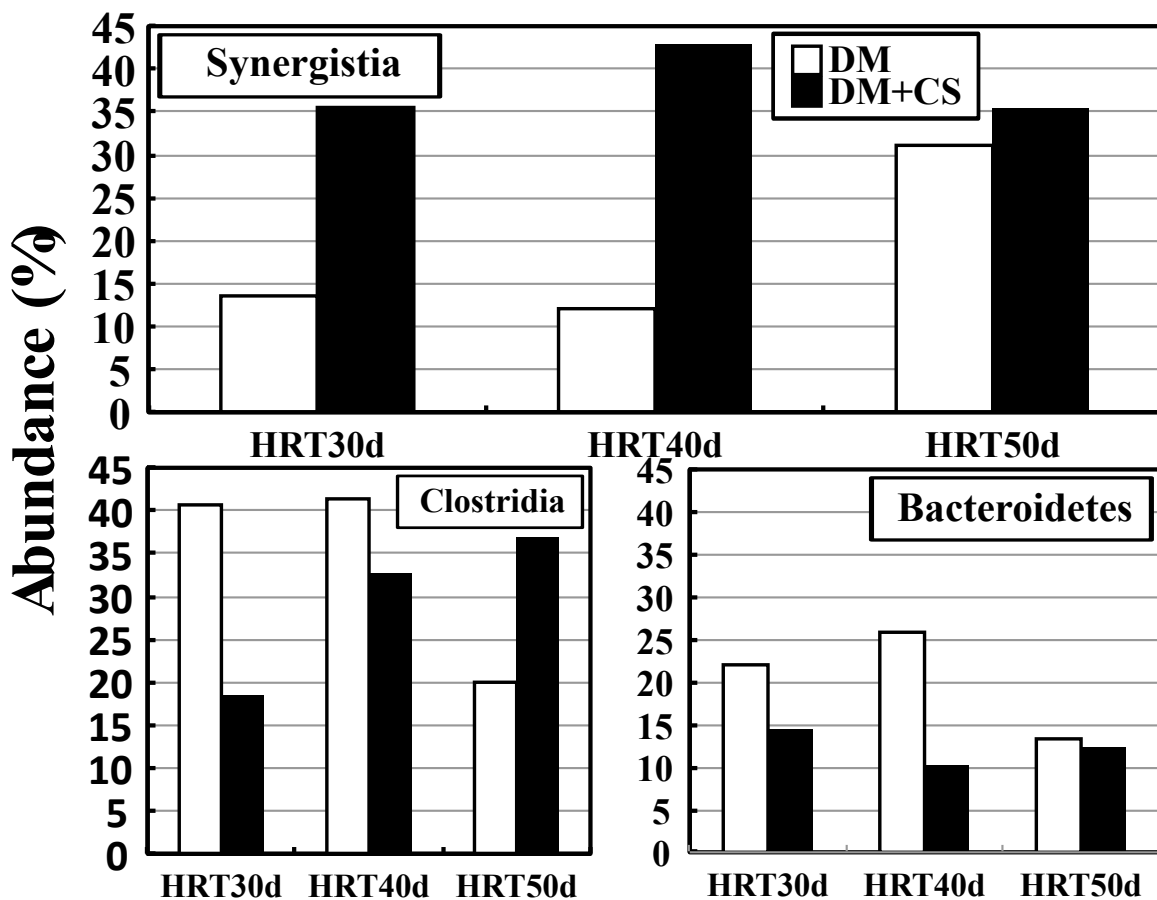


Figure 5.5: The shifts of abundance of the three most abundant [FeFe]-hydrogenases containing bacterial groups in anaerobic bioreactors fed with DM and DM+CS. Labels HRT30d, HRT40d and HRT50d represent bioreactors with a HRT of 30, 40, and 50 days, respectively.

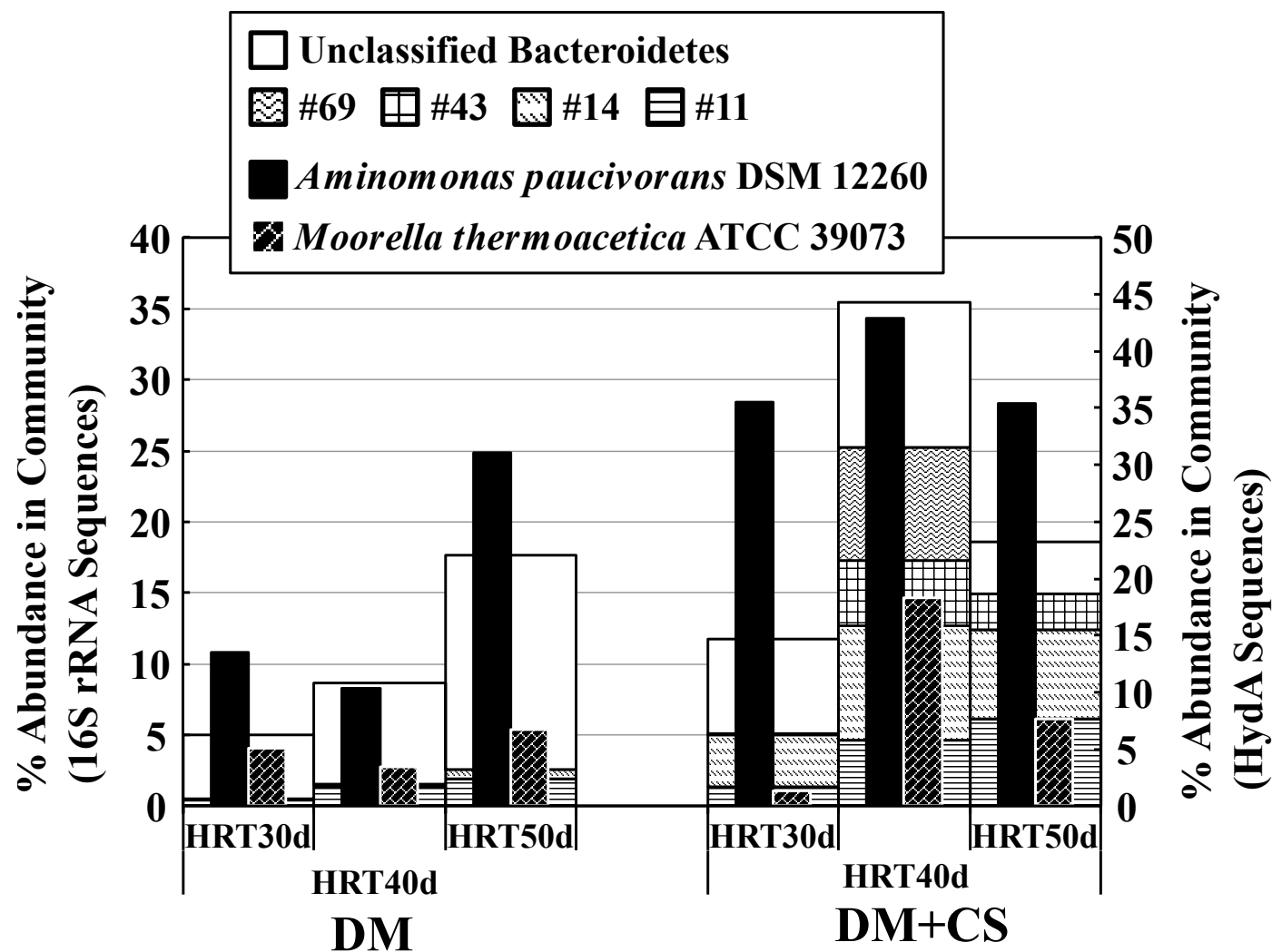


Figure 5.6: The abundance of [FeFe]-hydrogenase containing bacteria in anaerobic bioreactor samples compared to the abundance pattern of unclassified Bacteroidetes (background) determined by 16S rRNA gene sequencing. The distribution of clusters #11, #14, #43 and #69 were also plotted as part of unclassified Bacteroidetes within each sample. Labels HRT30d, HRT40d and HRT50d represent bioreactors with a HRT of 30, 40, and 50 days, respectively.

5.4.5 Non-metric multidimensional scaling (NMDS) analysis

Non-metric multidimensional scaling (NMDS) analysis was performed on the six anaerobic bioreactor samples based on the complete linkage clustering of 16S rRNA gene sequences (Figure 5.7). The DM bioreactor community shifts correlated strongly with changes in HRT while the DM+CS reactors had additional factors that diminished any correlation with HRT. The high rates of biogas production observed in the DM+CS bioreactor with a HRT of 40 days correlates with the unique community composition that we detected in this reactor (Figure 5.7).

Fitting the detected bacterial genera to the bioreactor community distances revealed that the abundance of *Petrimonas* decreased significantly as the HRT increased and corn stover was added. The abundance of several genera, including *Caryophanon*, *Blastopirellula*, *Ke-togulonicigenium*, unclassified *Syntrophaceae* and unclassified Bacteroidetes were also found significantly associated with the DM+CS bioreactor with a HRT of 40 days (Figure 5.7 red and blue arrows). Fitting of the [FeFe]-hydrogenase gene sequence data showed that the abundance of those most closely affiliated with *Clostridium lentocellum* and *Candidatus Cloacamonas acidaminovoransa* were found significantly associated with the DM+CS bioreactor with a HRT of 40 days. The abundance of several [FeFe]-hydrogenase sequences closest to members of Clostridia, such as *Clostridium therocellum*, and Bacteroidetes, such as *Bacteroides sp. 20_3*, shifted significantly along the HRT gradient and upon the addition of corn stover.

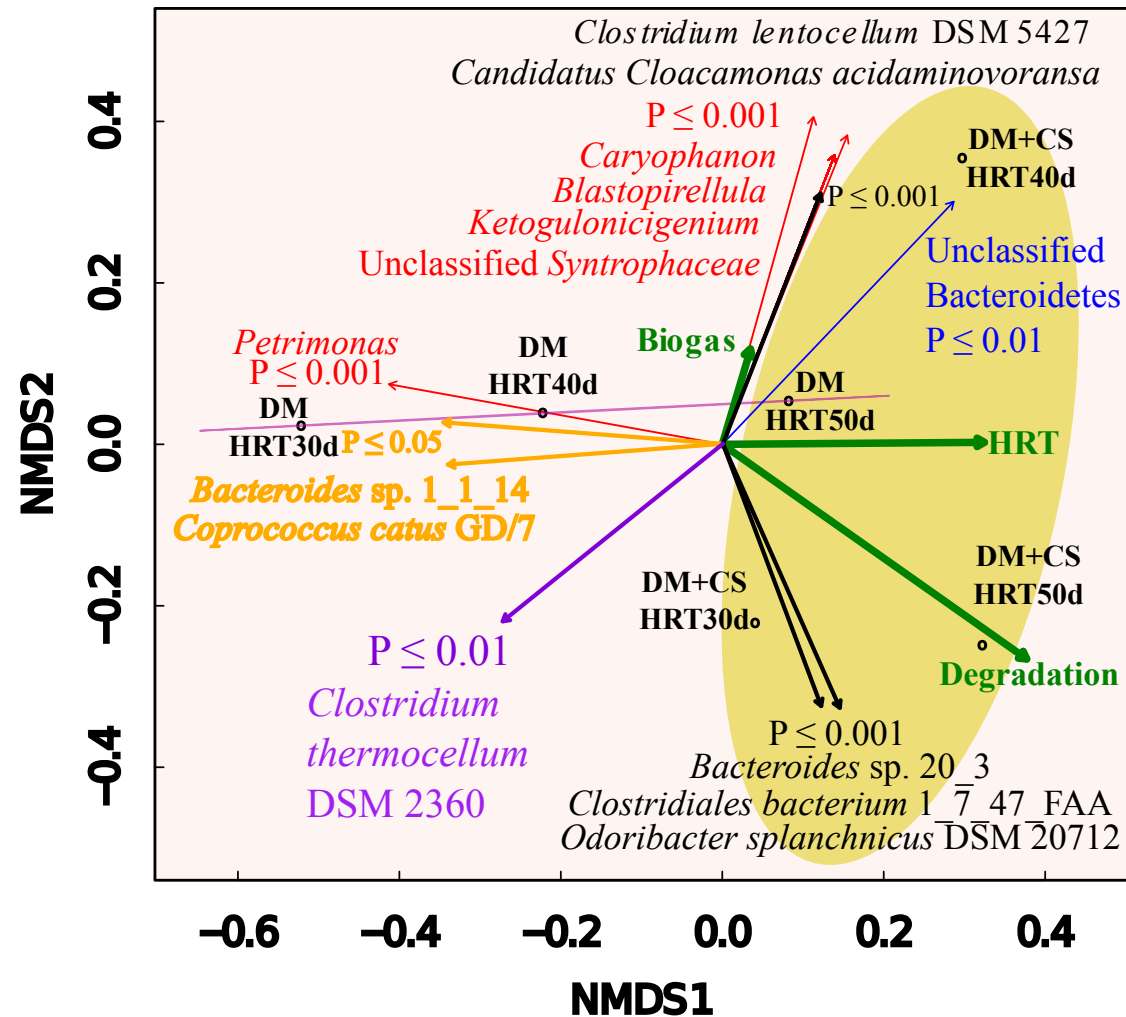


Figure 5.7: NMDS analysis of the bacterial community in anaerobic bioreactors (based on 16S rRNA gene sequences at 97% similarity cutoff). The green arrows indicate the increase of biogas production (Biogas), HRT (HRT) and dairy manure degradation rate (Degradation). The red and blue arrows indicate bacterial genera that shifted significantly, where $P \leq 0.001$ and $P \leq 0.01$, respectively. The black, yellow and purple arrows represent the [FeFe]-hydrogenase phylogenetic affiliations that shifted significantly ($P \leq 0.001$, $P \leq 0.05$, and $P \leq 0.01$, respectively). All arrows point towards the abundant range of the gradients. Labels HRT30d, HRT40d and HRT50d represent bioreactors with a HRT of 30, 40, and 50 days, respectively.

5.5 Discussion

Anaerobic digestion is an effective method of processing farm wastes. Methane produced from digestion can be collected and used as alternative energy source to reduce the system's carbon footprint. Schink et al. [140] emphasized the importance of the microbial community in anaerobic digestion and that undesirable structural shifts the community might result in little or no methane production. Thus it is critical to understand the roles and distributions of fermentative bacteria within anaerobic bioreactors so that both digestion and methane production can be optimized. The inverted relationship observed between dairy manure degradation rate and biogas/methane production rate could be explained by the abundance of fermentative bacteria. Schink et al. [140] previously reported that a co-culture of *Caloramator proteoclasticus* (a glutamate fermenter, which produces acetate and hydrogen) and *Methanobacterium thermoautotrophium* (a hydrogen oxidizing methanogen) would produce methane only when the abundance of *C. proteoclasticus* was low. With a relatively high concentration of *C. proteoclasticus*, the co-culture was effective at degradation but not biogas production [140, 162]. Thus a community shift caused a reduction of methane production.

The addition of corn stover in anaerobic digestion appeared to improve overall system performance (Figure 5.1) in that it maximized biogas production and enhanced total solids reduction. Biogas methane content remained relatively stable across the six bioreactors (66-67%) but overall biogas production increased significantly in the DM+CS bioreactors. The latter is consistent with other reported studies that the addition of crop remnants was beneficial to methane production [30, 42, 46, 85, 110, 179]. The increase in biogas production rate could be related to cellulose and hemicellulose degradation as observed by Yue et al.

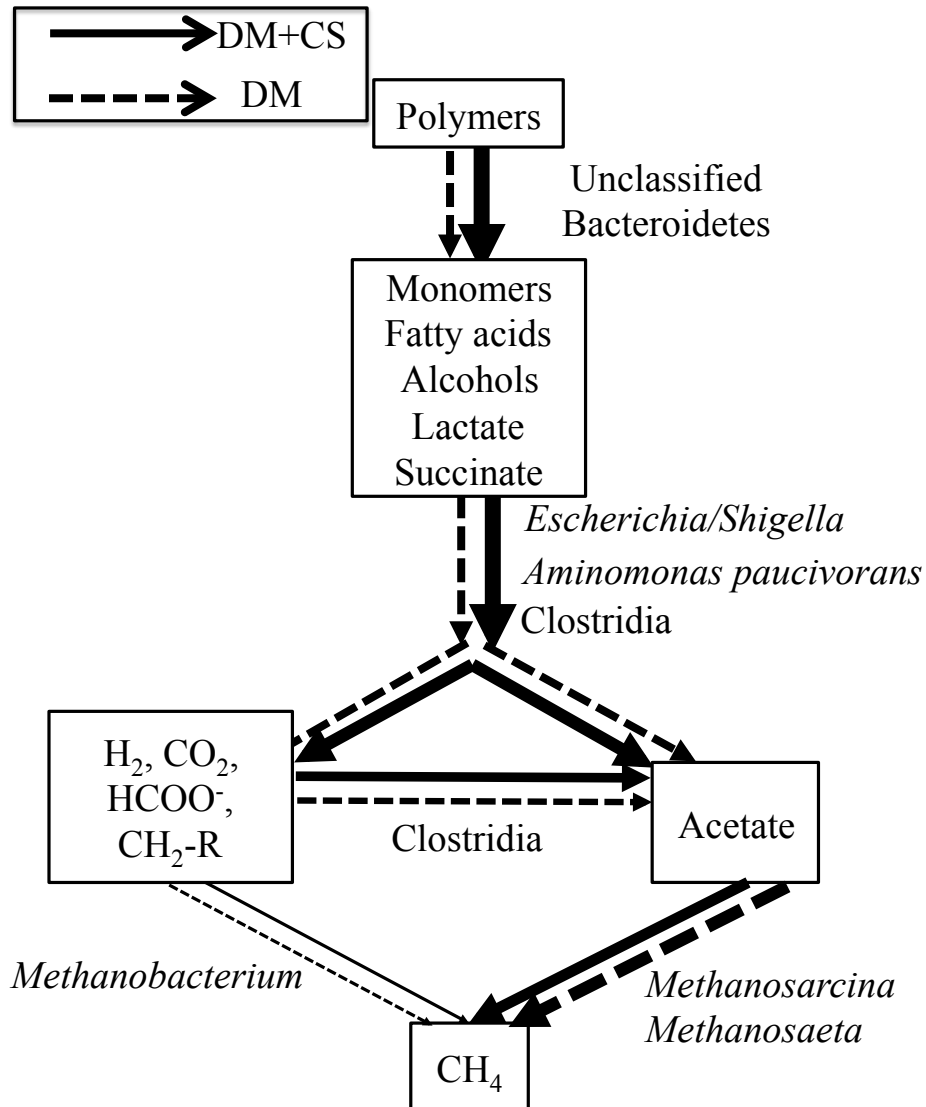


Figure 5.8: Diagram (adapted from Schink et al. [140]) of microbial corporation during methane generation in DM and DM+CS bioreactors operated at HRT 40 days. The thickness of the arrow represent the relative abundance of microbial populations possibly associated with the methanogenesis step.

[192]. Thus it may be that cellulose and hemicellulose degrading bacteria and associates contributed to the generation of hydrogen and acetate which in turn supported the growth of methanogens.

Members of class Clostridia were frequently reported in other anaerobic digestion studies. Class Clostridia describes a diverse group of anaerobic bacteria with versatile metabolic pathways, many members of which have been reported to have high cellulolytic activity and are capable of both hydrogen consumption and acetate production through the reductive acetyl-CoA pathway [185]. For these reasons we expected to see a substantial amount of class Clostridia in our anaerobic bioreactors. A recent metagenomic study on methane producing community reported by Wirth et al. revealed that 36% of the community were Clostridia and 23 out of 40 most frequently found bacterial species in the community were members of class Clostridia [185]. In another similar study, Schlüter et al. showed that class Clostridia was highly abundant (52%) in a production-scale biogas plant fermenter [142]. As expected, we observed a large amount of Clostridia in both the DM and DM+CS bioreactors. However, class Clostridia appeared to be more abundant in the DM bioreactors than in the DM+CS bioreactors, except in the DM+CS bioreactor with a HRT of 40 days (Figure D.2 B). Clustering analysis revealed that the populations within this group varied substantially from condition to condition and only a few populations were common in all six anaerobic bioreactors (Figure 5.2 B2). Hence, populations within class Clostridia were dynamic and different members of the group assumed different responsibilities (Figure 5.2 B2). Our observation of unpredictable shifts within Clostridia revealed by 16S rRNA sequences agreed with the conclusion by Werner et al. that Clostridia populations were relatively unstable compared to other bacterial populations in their methanogenic bioreactor bacterial communities

[182]. Thus, the abundance of Clostridia as a group based on their 16S rRNA sequences could not be used to correlate methane production in the anaerobic bioreactors. In contrast, hydrogen producing populations identified by [FeFe]-hydrogenase gene clone libraries were correlated with anaerobic digestion and methane production. For example, we observed that [FeFe]-hydrogenase genes affiliated with *M. thermoacetica* (a member of Clostridia) were more abundant in the reactors that were supplemented with corn stover (Figure 5.6). However, genus *Moorella* was not detected according to the 16S rRNA gene profile. Moreover, one could infer from the high abundance of Clostridia-like [FeFe]-hydrogenase genes observed in the DM bioreactors at HRT of 30 and 40 days that Clostridia played a crucial role in hydrogen production in the DM bioreactors. Clostridia-like [FeFe]-hydrogenase genes became more abundant in the DM+CS bioreactor as the HRT increased, perhaps indicating that an increased amount of time was required to reduce TS. Class Clostridia could be producing hydrogen from secondary fermentation of cellobiose or glucose generated by other bacteria from primary cellulose/hemicellulose degradation (Figure 5.8).

Phylum Bacteroidetes constituted approximated 21-40% of each anaerobic bioreactor bacterial community in this study. Like class Clostridia, Bacteroidetes populations were also commonly reported in anaerobic digestion but are usually less abundant. Wirth et al. observed approximately 4% of Bacteroidetes in their metagenomic analysis [185]. Schlüter et al. [142] reported that there were 16% of Bacteroidetes in the production-scale biogas plant fermenter. Wang et al. [181] observed a slightly larger amount of phylum Bacteroidetes (up to 23%). Members of Bacteroidetes including *Cytophaga sp.*, *Sporocytophaga myxococcoides*, *Flavobacterium johnsoniae* have been reported as cellulose/hemicellulose degraders [29, 83, 107]. A recent study conducted by Stursová et al. [155] revealed that Bacteroidetes

populations played a substantial role in natural cellulose/hemicellulose degradation in forest soil. We observed that phylum Bacteroidetes showed a similar abundance pattern to class Clostridia, where they were generally more abundant in the DM+CS than in the DM bioreactors (Figure D.2 A). However, unlike Clostridia, a substantial amount of unclassified Bacteroidetes were observed in the DM+CS bioreactors. In the DM+CS bioreactor with a HRT of 40 days, over 80% of the phylum Bacteroidetes could not be classified further than phylum level (Figure 5.3). Clustering of all Bacteroidetes sequences at 97% cut off revealed that three unique unclassified Bacteroidetes populations were associated with the DM+CS bioreactors. These three populations contributed substantially to the shifts from classified to unclassified bacteria within phylum Bacteroidetes observed in this study. RDP SeqMatch results revealed that these three groups of unclassified Bacteroidetes were highly similar to bacterial 16S rRNA gene clones found in methanogenic environments, specifically, domestic wastewater enriched microbial fuel cells (#43, SeqMatch score=0.998), biogas slurry (#11, SeqMatch score=0.966), Kinneret lake sediments (#14, SeqMatch score=0.983), methanogenic zone of a hydrocarbon- and chlorinated-solvent contaminated aquifer (#69, SeqMatch score=0.988) and an anaerobic bioreactor fed with butyrate and sulphate enriched paper mill wastewater (#69, SeqMatch score=0.988, unpublished work) [37, 84, 134, 143]. Thus based on prior observations as well as ours, these three Bacteroidetes clusters can play an important role in some methanogenic environments. Moreover, their high abundance in corn stover supplemented bioreactors suggests that cellulose and hemicellulose may play a role in selecting for their presence. We observed that the dairy manure degradation rate increased along with the increase in HRT and groups #11, #14 and #43 became more abundant in the DM+CS bioreactors operated at long HRTs. Cluster #69 was observed only in the DM+CS

bioreactor with a HRT of 40 days and at considerable abundance, which suggested that this specific group of Bacteroidetes might contribute to the high biogas production rate in the DM+CS bioreactor with a HRT of 40 days. Agreeing with our prediction, NMDS analysis revealed that unclassified Bacteroidetes shifted significantly ($P \leq 0.01$) towards the DM+CS bioreactor with a HRT of 40 days (Figure refnmds). Besides cellulolytic activities, members of phylum Bacteroidetes have also been identified as hydrogen producers. While the 16S rRNA gene based survey suggested that members of Bacteroidetes played an important role in the anaerobic digestion, the [FeFe]-hydrogenase clone library profile revealed that Bacteroidetes-like [FeFe]-hydrogenase genes were not as abundant as would be expected if they were linked to these important Bacteroidetes populations. It was observed that a larger amount of Bacteroidetes-like [FeFe]-hydrogenase genes were detected in bioreactors despite the differences in their operational HRT. In addition, the higher abundance of Bacteroidetes-like hydrogenase genes were observed in the DM bioreactors than in the DM+CS bioreactors under all three HRTs. These trends indicate that classified Bacteroidetes populations directly contributing to the hydrogen economy through [FeFe]-hydrogenases were not responding to the presence of corn stover, as were other unclassified populations of Bacteroidetes. Correlating 16S rRNA gene analysis to the [FeFe]-hydrogenase gene study, we speculate that classified Bacteroidetes contributed to methane production in anaerobic bioreactors by generating hydrogen during dairy manure degradation and unclassified Bacteroidetes participated solely in primary degradation of cellulose and hemicellulose. The degraded products, such as cellobiose and glucose, could be then consumed by secondary fermenters (e.g., Clostridia and *Escherichia/Shigella* for hydrogen generation (Figure 5.8).

While we expected to observe class Clostridia and phylum Bacteroidetes in abundance

in anaerobic bioreactors, it was surprising to observe genera *Escherichia/Shigella* as one of the dominant groups in the DM+CS bioreactor. These genera include species that are commonly found in animal gastrointestinal tracks, including pathogens. They are not well known for cellulose and hemicellulose degradation but frequently excel at metabolism of sugars. Therefore, *Escherichia/Shigella* are not likely contributing to cellulose and hemicellulose degradation despite their high abundance in the DM+CS bioreactors. It is known that *Escherichia/Shigella* are found in feces, studies have shown that anaerobic fermentation is effective at reducing their abundance, especially pathogenic populations [70, 101]. We have observed an increase in both the abundance and the diversity of genera *Escherichia/Shigella* as HRT increased from 30 to 50 days. More surprisingly, the abundance of *Escherichia/Shigella* was generally higher in the DM+CS bioreactors than in the DM bioreactors, except the DM+CS bioreactor with a HRT of 40 days (Figure D.2 C). Such a large abundance of *Escherichia/Shigella* group was not observed in other previously reported anaerobic bioreactor studies. SeqMatch revealed that these *Escherichia/Shigella* sequences are similar to those of *Shigella* and non-pathogenic *E. coli*. The increase in *Escherichia/Shigella* abundance and diversity suggested that facultative fermenters may survive and even actively grow in anaerobic bioreactors, and be further enriched by increasing C:N ratio (the more corn stover in the feed the higher C:N ratios). The smallest populations of *Escherichia/Shigella* were observed in the DM+CS bioreactor with a HRT of 40 days (1.53% of community). The small abundance of *Escherichia/Shigella* was likely offset by the large abundance of class Clostridia and phylum Bacteroidetes.

The high abundance of *Synergistia*-like hydrogenase genes (at least 35%) observed in all of the DM+CS bioreactors suggested that this group of bacteria were highly active in cel-

lulose/hemicellulose rich environments. The increase in *Synergistia* like [FeFe]-hydrogenase genes in the DM bioreactors along with the increase in the HRT suggested that phylum *Synergistia* grew on dairy manure degradation products. At species level, clone libraries revealed that the abundance of *Synergistia* was solely contributed by *Aminomonas paucivorans*, an anaerobic bacterium that was previously identified as an amino-acid-degrader. Baena et al. [5] described an *A. paucivorans* isolate that was able to grow on arginine, histidine and glutamate when cultivated syntrophically with methanogen *Methanobacterium formicicum*. The end products of the co-culture were propionate, acetate, CO₂ and methane [5]. There are no previous studies indicating that *Aminomonas paucivorans* is capable of cellulose degradation. The available information on *Aminomonas paucivorans* indicate that its high abundance in the DM+CS bioreactors was likely a result of growth due to secondary fermentation of degraded dairy manure [5].

NMDS analysis revealed a complex network among bacterial communities in the methane producing anaerobic bioreactors. Correlating 16S rRNA gene with [FeFe]-hydrogenase gene diversities, we observed that the high abundance of unclassified Bacteroidetes was significantly associated with the DM+CS bioreactor with a HRT of 40 days that produced the most methane. Besides unclassified Bacteroidetes, the abundance of *Caryophanon*, *Blastopirellula*, *Ketogulonicigenium* and unclassified *Syntrophaceae* increased significantly in the DM+CS bioreactor with a HRT of 40 days. Little has been discovered regarding the metabolic capabilities of *Caryophanon* and *Blastopirellula*. Members of *Ketogulonicigenium* and *Syntrophaceae* were previously identified as fermenters [53, 93, 156]. Based on these information, we speculate that unclassified Bacteroidetes played a substantial in primary cellulose/hemicellulose degradation. It is likely that genera *Caryophanon*, *Blastopirellula*,

Ketogulonicigenium and unclassified *Syntrophaceae* participated in secondary fermentation. NMDS analysis also showed that different members of Clostridia and Bacteroidetes participated in different activities among all six anaerobic bioreactors. For example, *Bacteroides sp.* 1_1_14 appeared to be affiliated with hydrogen production during dairy manure digestion at a low HRT, while *Bacteroides sp.* 20_3 was found significantly associated with DM+CS digestion at an elevated HRT. Similarly, *C. thermocellum* like [FeFe]-hydrogenase genes were found to be significantly correlated with the low HRT bioreactors and *Clostridiales* bacterium and *Odoribacter splanchnicus* might play a significant role during methane production in DM+CS digestion at elevated HRT.

Although *A. paucivorans*- and *M. thermoacetica*- (a member of class Clostridia) like [FeFe]-hydrogenase genes were highly abundant and varied in anaerobic bioreactors, NMDS analysis indicated that the shifts of their abundance were not significant across all bioreactors. However, we observed that the abundance of these two groups of [FeFe]-hydrogenase genes followed the abundance pattern of unclassified Bacteroidetes determined based on 16S rRNA gene sequences (Figure 5.6). We speculate that hydrogen producing population *A. paucivorans* responds to the growth of unclassified Bacteroidetes. It agrees with our prediction that unclassified Bacteroidetes were responsible for cellulose/hemicellulose degradation but not for hydrogen production. Subsequently, cellulose/hemicellulose degradation products, such as xylose, glucose and cellobiose, were consumed by hydrogen producers (*A. paucivorans* and *M. thermoacetica*).

Yue et al. [192] reported the archaeal community structures resided in these anaerobic bioreactors, where they observed that the communities were dominated by *Methanobacterium*, *Methanosarcina* and *Methanosaeta* populations. Members of *Methanobacterium*

are known for producing methane via hydrogen oxidation. The presence of this group of methanogens could explain the consumption of hydrogen produced by *A. paucivorans*, Clostridia and Bacteroidetes. Accompanied to the production of hydrogen. The literature indicates that many members of [FeFe]-hydrogenase containing bacteria generate acetate as one of the final products [11]. The presence of a large amount of *Methanosarcina* and *Methanosaeta* suggests that acetate was a sole source for methane generation. Yue et al. [192] also concluded that the community shifts from *Methanosarcina* dominant to *Methanosaeta* dominant was due to the decrease in acetate concentration in the bioreactors as HRT increased. This also explains the decreasing trend in *Methanobacterium* abundance in both the DM and DM+CS bioreactors as the HRT increased from 30 to 50 days. These observations are consistent with the observation that the biogas/methane production rate approached plateau when the operational HRT was more than 40 days.

5.6 Conclusion

In conclusion, the DM+CS bioreactor with a HRT of 40 days was unique for its distinct community structure and high methane production rate. We predict that unclassified *Bacteroidetes* populations might act as primary fermenters and play a significant role in cellulose/hemicellulose degradation. *A. paucivorans* and members of Clostridia, such as *M. thermoacetica* are likely participating substantially in hydrogen and acetate production (Figure 5.8). The observations made by Yue et al. [192] suggested that methane production from H₂ and CO₂ decreased as HRT increased. However, we observed [FeFe]-hydrogenase gene containing populations at high abundance in bioreactors operated at large HRTs. The high-

est rate of methane production was detected in the bioreactor fed with both dairy manure and corn stover at a HRT of 40 days. This bioreactor had a unique community with an unclassified population of Bacterioidetes not found in other bioreactors. The population size of *Escherichia/Shigella* was suppressed in this bioreactor while the hydrogen economy was likely driven by Clostridia and *A. paucivorans*, the former through the reductive acetyl-CoA pathway. We speculate that the acetate concentration was somewhat low at this retention time, thus selecting for *Mathanoseta* rather than *Methanosarcina*.

APPENDICES

APPENDIX A

COMPARATIVE GENOMICS OF *RALSTONIA PICKETTII* 12D AND 12J

A.1 Metabolic Pathways of *R. pickettii* 12D and 12J

We observed minor differences in the *R. pickettii* 12D and 12J available KEGG pathway maps. Strain 12J has glucose-1-phosphate thymidyltransferase, mannose-1-phosphate guanylyltransferase / mannose-6-phosphate isomerase, and GDP-mannose 4,6-dehydratase genes, which are missing in 12D (confirmed with JGI-IMG BLAST). On the other hand, *R. pickettii* 12D has N-acylneuraminate-9-phosphate synthase and 4,5-dihydroxyphthalate decarboxylase genes that could not be identified by JGI-IMG BLAST in strain 12J.

MetaCyc showed that *R. pickettii* 12D and 12J contain several detoxification pathways, including arsenate reduction, cytoplasm Hg^{2+} reduction, methylglyoxal detoxification, cyanate degradation and superoxide radical degradation. Among these detoxification pathways, arsenate detoxification was only mentioned in *R. pickettii* 12D by MetaCyc. However, arsenate reductase encoding genes were identified in *R. pickettii* 12J via JGI-IMG BLAST. Besides the detoxification pathways, MetaCyc also revealed that both of *R. pickettii* 12D and 12J are capable of organic acid, aromatic compound and chlorinated compound degradation. They also contain genes that are essential for assimilating inorganic elements like P, N and S from ammonium, nitrate, phosphate and sulfate. We have experimentally confirmed that both 12D and 12J are capable of denitrification under anaerobic minimal growth conditions (unpublished data).

A.2 Clustering of *R. pickettii* 12D and 12J and other 23 Proteobacteria

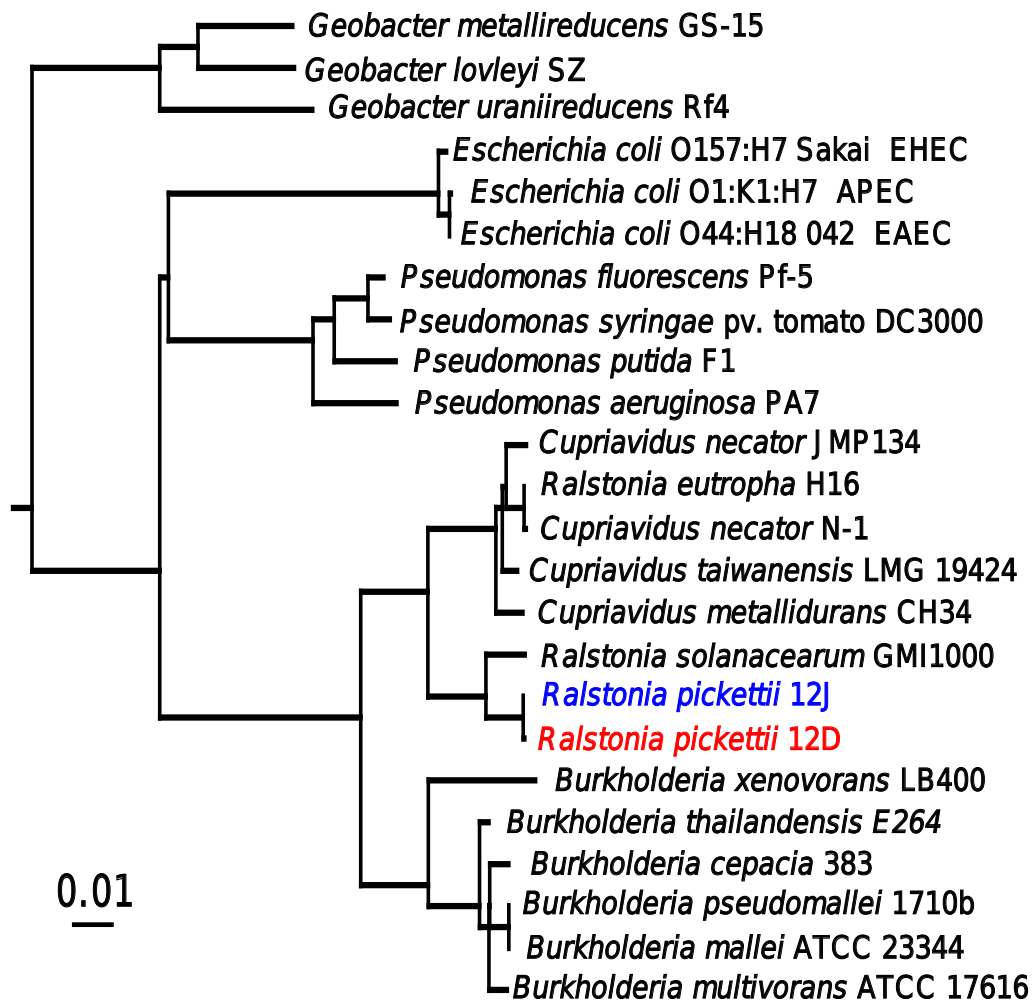


Figure A.1: Distance tree of *R. pickettii* 12D and 12J in relationship to 23 other Proteobacteria based on their 16S rRNA gene sequences. The bar in the bottom left corner represents the distance scale.

A.3 Genetic Elements in *R. pickettii* 12D and 12J

Table A.1: Side-by-side genome comparison of *R. pickettii* 12D and 12J genetic elements by genomic scaffolds.

	C1		P2	C2		P3	P1	P1
	12D	12J	12D	12D	12J	12D	12J	12D
HGT^a	115	118	9	4	3	2	2	157
Transposase	22	28	6	3	3	0	1	2
Filamentous Phage^b	1	3	0	1	1	0	0	0
Unique Genes^c	63	74	1	0	5	0	0	15

^a Number of genes that are identified by IMG as horizontally transferred.

^b Mostly incomplete copies except one in 12J C1.

^c All genes that are absent in the other strain based on IMG annotations.

A.4 Variation of *R. pickettii* 12D and 12J *dif* Sites

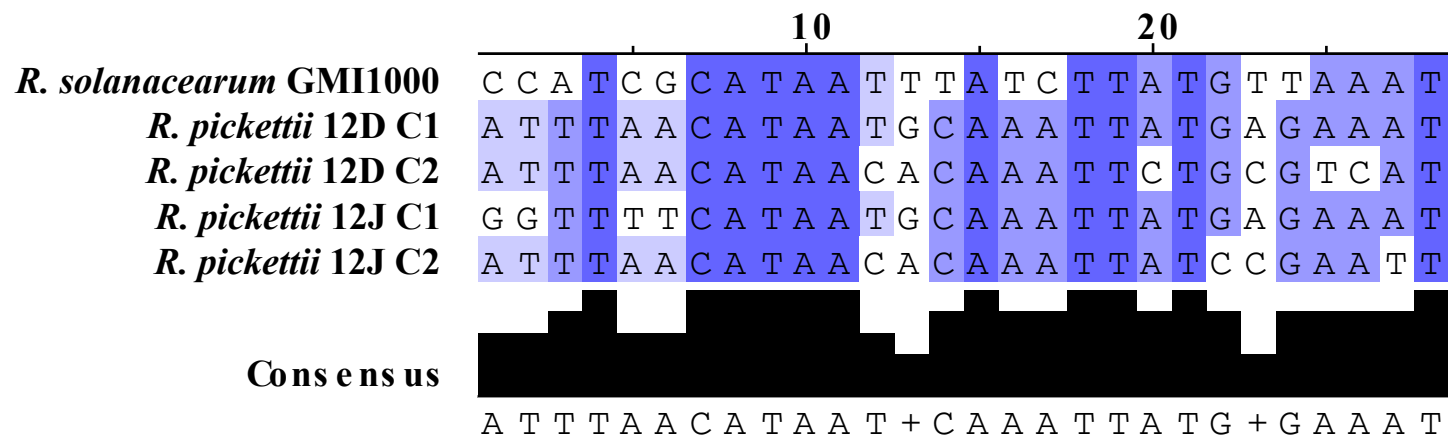


Figure A.2: The sequence variations of *dif* sites of *R. pickettii* 12D and 12J. The consensus reveals the conserved regions.

Four 28 bp *dif* site sequences obtained from *R. pickettii* 12D and 12J chromosomes were compared along with the one from their close relative *R. solanacearum* GMI1000 (Figure A.2). All five sequences are conserved at positions 5, 8-11, 15, 18-19, 21 and 28. *R. pickettii* 12J_C1 *dif* appears to be the most different and is complementary to GMI1000 *dif* at position 1, 2, 16 and 23. *R. pickettii* 12D_C1 *dif* is complementary to 12J_C1 (position 5 and 6). *R. pickettii* 12D_C2 and 12J_C2 *dif* are similar to 12D_C1 and the sequences are complementary at position 25 (12D_C2 to 12D_C1) and position 22 and 27 (12J_C2 to 12D_C1) (Figure A.2).

A.5 Genome Syntenies of *R. pickettii* 12D and 12J

Base-to-base comparisons of *R. pickettii* 12D and 12J scaffolds revealed that the primary chromosomes are in good agreement. The discontinued and gapped line in 12D_C2-12J_C1 frame indicates a DNA fragment was inserted into 12J_C1 (Figure A.3). This inserted portion is highly homologous to 12D_P2 (Figure A.3 12D_P2-12J_C1). The disjointed lines in Figure A.3 12D_C2-12J_C2 frame is an evidence of genome rearrangement, where the origin of replication (*oriC*) appears to be relocated in 12D_C2 in relation to 12J_C2. Figure A.3 also showed that the 12J_P1 sequence largely agrees with 12D_P3 and an approximately 0.03 Mb fragment of 12D_C1 (Figure A.3). *R. pickettii* 12D_P1 shares few syntenies with other scaffolds and appears to be unique to itself (Figure A.3).

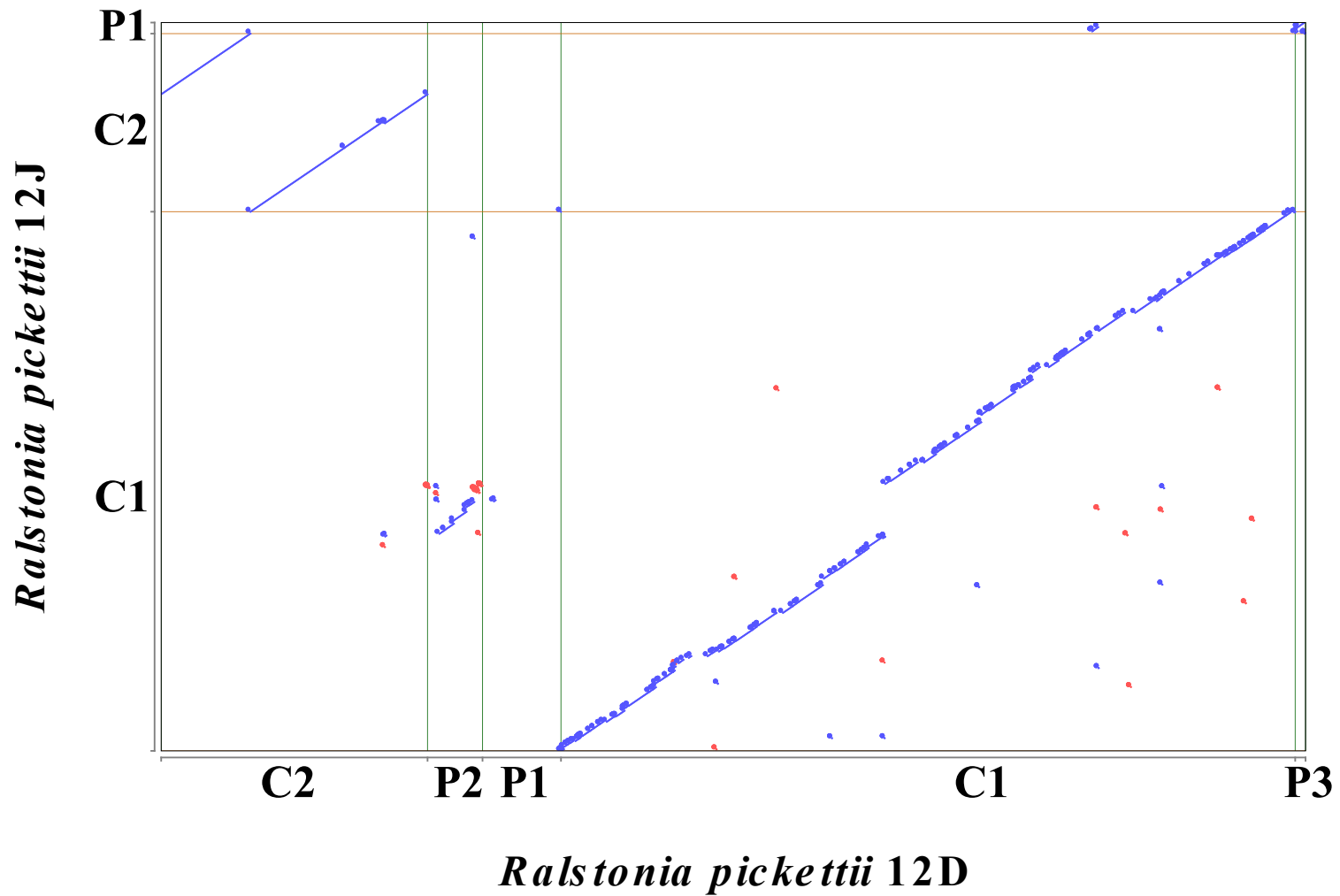


Figure A.3: Genome synteny of *R. pickettii* 12D and 12J revealed by a DNA sequence dotplot. Blue dots represent matching genes on the same direction strands. Red dots represent matching genes on the opposite direction strands. The scaffold nucleotide coordinates are ranked from left to right on the x-axis and bottom to top on the y-axis.

APPENDIX B

ANAEROBIC ENRICHMENTS

B.1 Media Preparation

Table B.1: The composition of the modified FWM.

Ingredients	Concentration
Mineral Mix (100X)	10 ml/L
NaHCO ₃	2.5 g/L
NH ₄ Cl	0.25 g/L
NaH ₂ PO ₄ •H ₂ O	0.6 g/L
KCl	0.1 g/L
Adjust pH to 6.8-7 under N₂:CO₂=80:20.	

Table B.2: The composition of the mineral mix (100X).

Ingredients	g/L
Nitrilo triacetic acid (C ₆ H ₉ NO ₆)	1.5
MgSO ₄ •7H ₂ O	3
MnSO ₄ •2H ₂ O	0.5
NaCl	1
FeSO ₄ •7H ₂ O	0.1
CaCl ₂ •2H ₂ O	0.1
CoCl ₂ •7H ₂ O	0.1
ZnCl ₂	0.13
CuSO ₄ •5H ₂ O	0.01
AlK(SO ₄) ₂ •12H ₂ O	0.01
H ₃ BO ₃	0.01
Na ₂ MoO ₄	0.025
NiCl ₂ •6H ₂ O	0.024
Na ₂ WO ₄ •2H ₂ O	0.025

Table B.3: The composition of the vitamin mix (1000X).

Ingredients	mg/L
Biotin	2
Folic acid	2
Pyridoxine-HCl	10
Thamine-HCl•2H ₂ O	5
Riboflavin	5
Nicothinic acid	5
D-Ca-pantothenate	5
Vitamin B12	0.1
p-Aminobenzoic acid	5
Lipoic acid	5

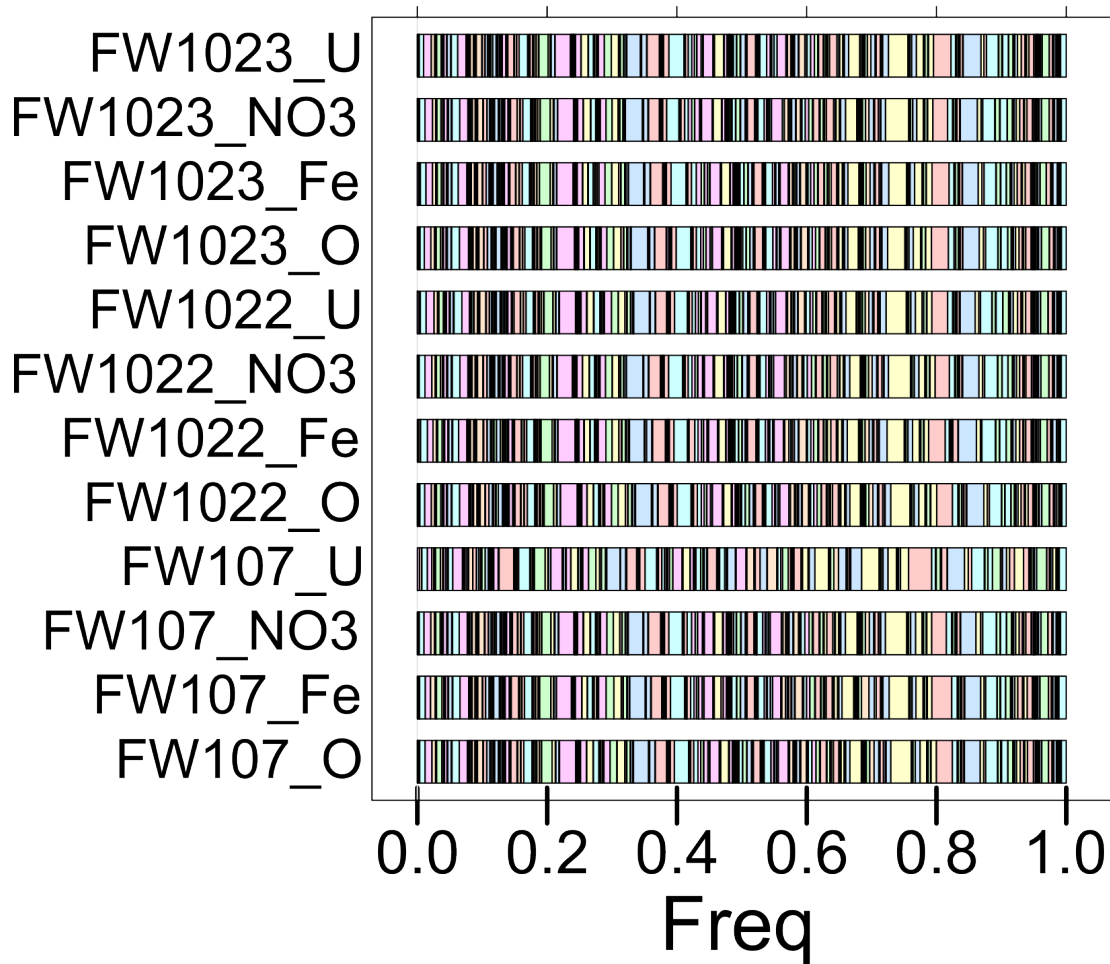


Figure B.1: Functional gene profiles of original soil communities and the enriched communities (replicate 1). Symbol "O" indicates original communities and "Fe", "NO3" and "U" indicate supplemented electron acceptors in enrichments.

B.2 Functional Gene Profiles

GeoChip analysis on the original soil sediment samples and the enrichment replicate 1 revealed a total of 475 different genes. The functional gene profile patterns are highly similar (Figure B.1).

APPENDIX C

URANIUM IMMOBILIZATION BY FIRMICUTES

C.1 Uranium-azide Assay

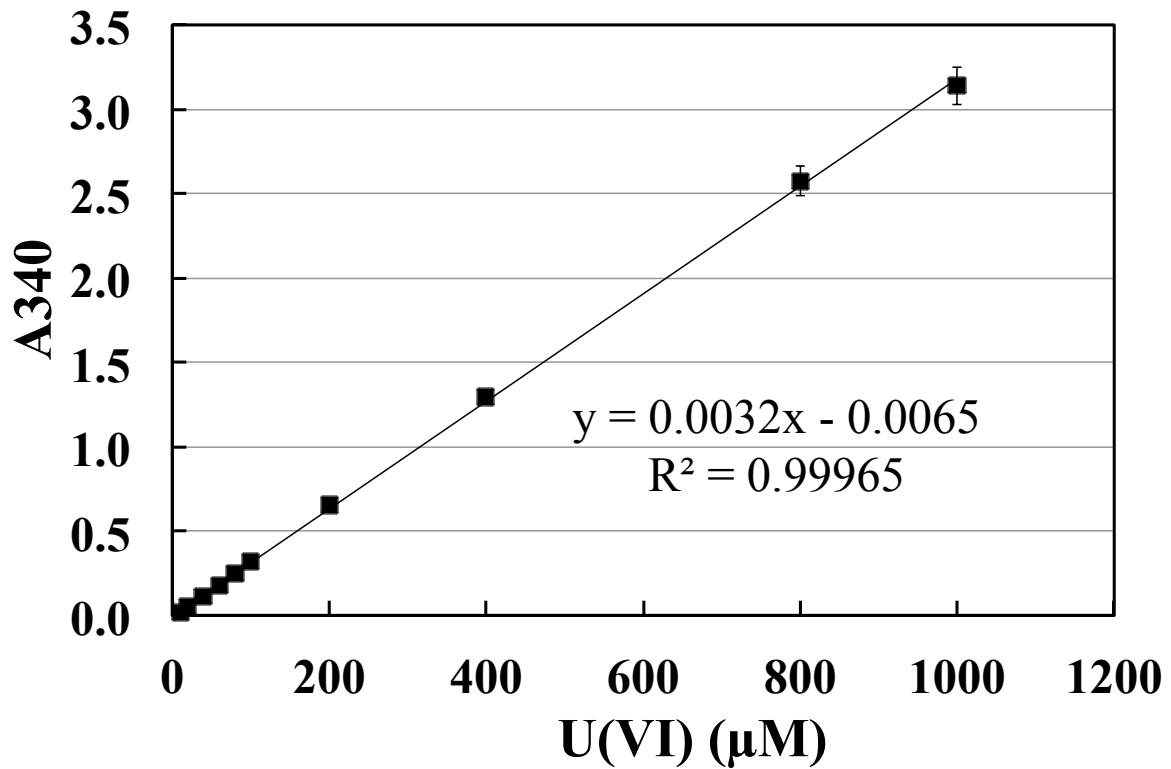


Figure C.1: Standard curve of the uranium-azide assay. The error bars represent data from two replicates.

C.2 5X Gitschier Buffer

Table C.1: Ingredients for 200 ml of 5X Gitschier Buffer.

To prepare 200 ml of 5X Gitschier combine:	Final concentration
16.6 ml of a 1 M $(\text{NH}_4)_2\text{SO}_4$	83 mM $(\text{NH}_4)_2\text{SO}_4$
67 ml of a 1 M Tris-HCl pH 8.8	335 mM Tris-HCl pH 8.8
6.7 ml of a 1 M MgCl_2	33.5 mM MgCl_2
1.3 ml of 1:100 dilution of a 0.5 M EDTA	33.5 μM EDTA
2.08 ml of a 14.4 M commercial stock of β -mercapto-ethanol	150 mM β -mercapto-ethanol

Adjust final volume to 200 ml and autoclave for sterilization.

C.3 Growth Curves of Isolates in Minimal Media

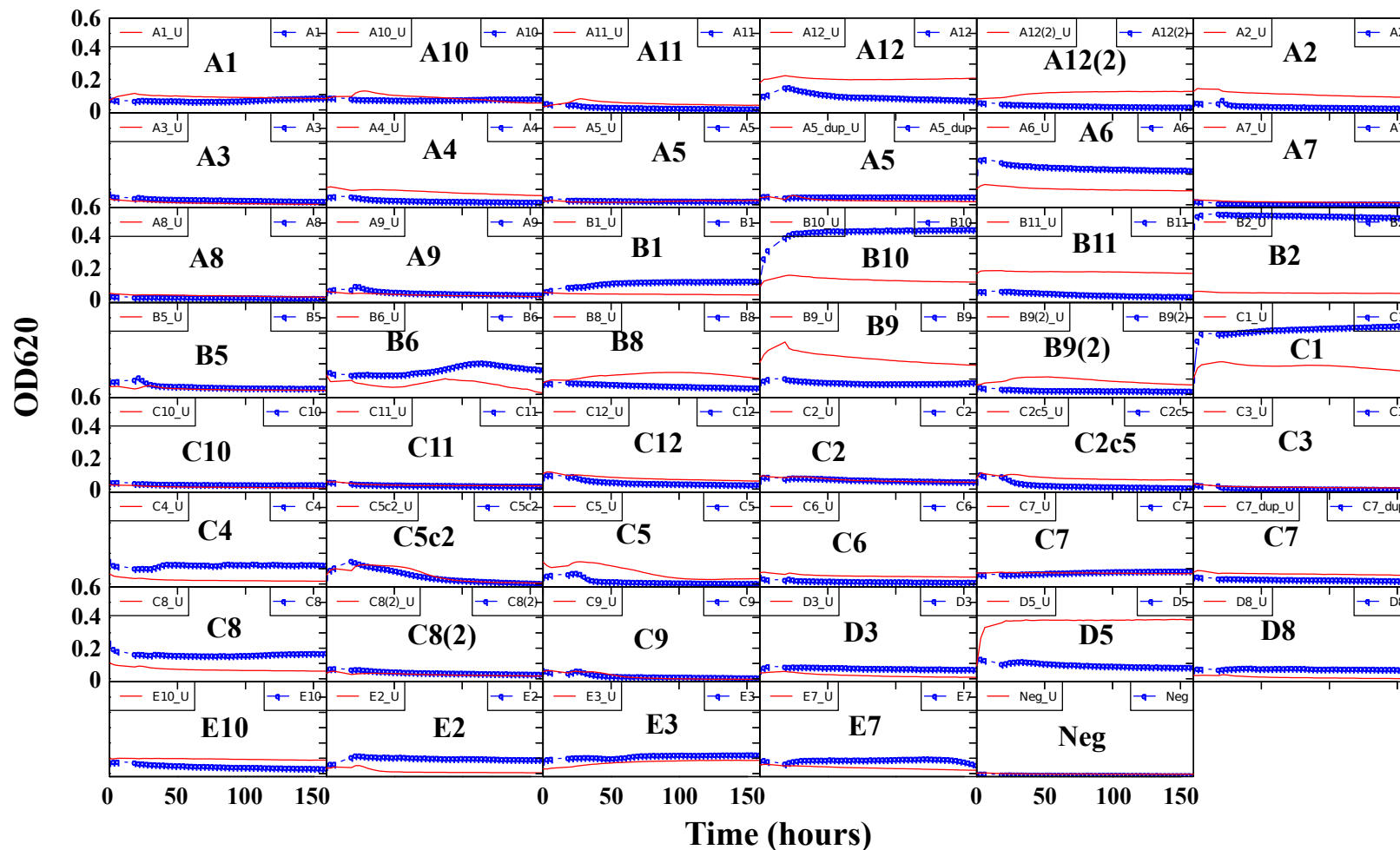


Figure C.2: The growth curves of FRC isolates (first replicate) in minimal media supplemented with sodium pyruvate alone (blue) and minimal media supplemented with sodium pyruvate and uranyl acetate (red) under anaerobic condition.

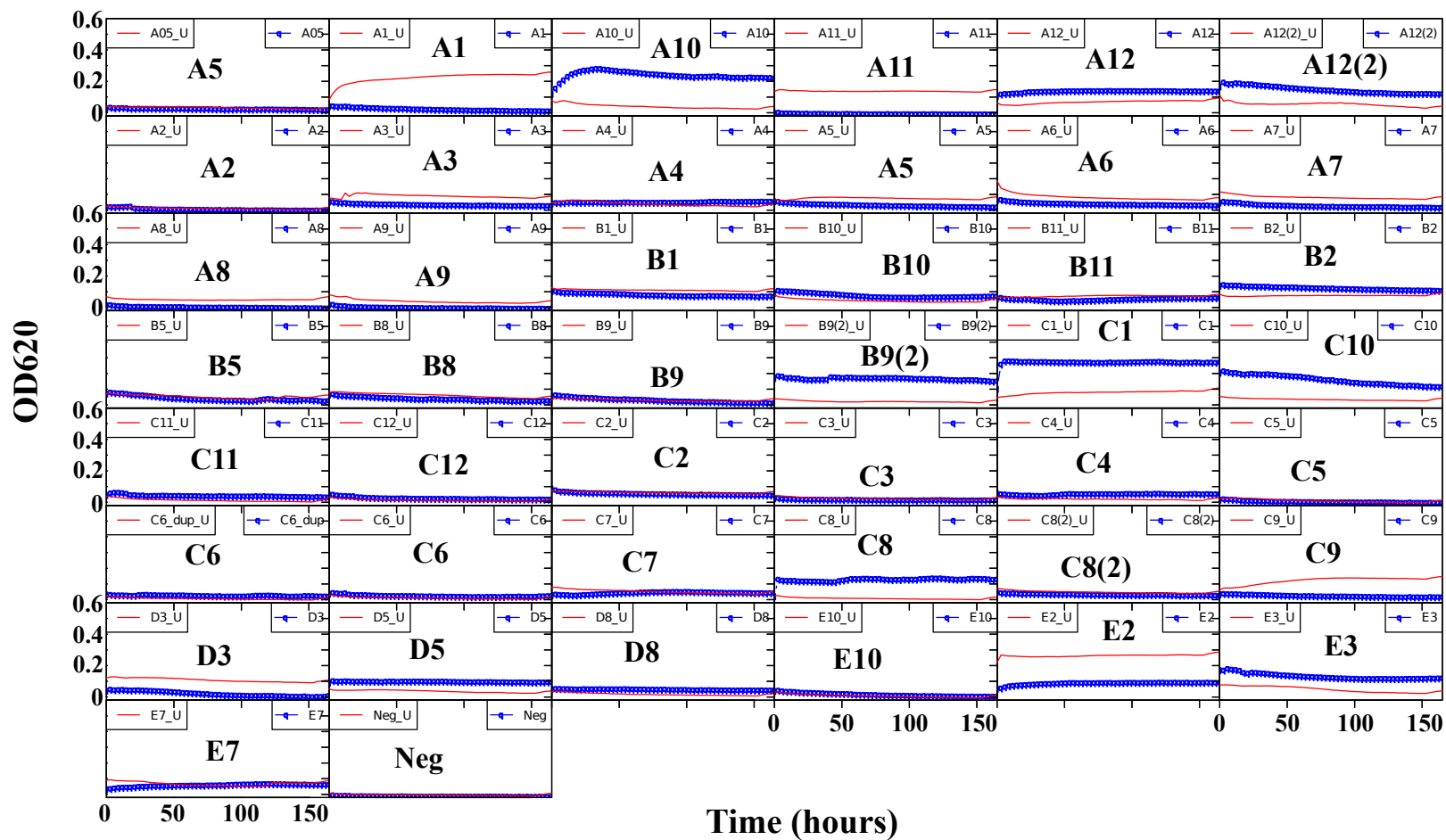


Figure C.3: The growth curves of FRC isolates (second replicate) in minimal media supplemented with sodium pyruvate alone (blue) and minimal media supplemented with sodium pyruvate and uranyl acetate (red) under anaerobic condition.

APPENDIX D

BACTERIAL COMMUNITIES IN ANAEROBIC CO-BIOREACTORS

D.1 Deep Sequencing of Bacterial Communities in Anaerobic Co-bioreactors

Table D.1: Measurements of sampling size and estimation of ecological indices of bacterial community in six anaerobic bioreactors. Calculations were based on the complete linkage clustering of chimera removed and trimmed bacterial 16S rRNA gene sequence alignments at 97% similarity. N represents the total number of non-chimera sequences that passed quality trimming. Shannon index (H') and Simpson's index (D) were expressed in $e^{H'}$ and 1-D, respectively to emphasize the differences. C represents the sampling coverage via gene targeted pyrosequencing.

Influent	100% DM			80% DM + 20% CS		
HRT (days)	30	40	50	30	40	50
N	6729	5003	5328	4939	5684	5323
OTU	230	187	171	163	277	134
ChaoI	240.62	208.94	190.50	193.67	332.80	146.21
$e^{H'}$	70.62	49.30	36.10	40.64	73.62	27.30
E	0.78	0.75	0.70	0.73	0.76	0.68
1-D	0.97	0.94	0.91	0.91	0.97	0.87
C	99.64	99.46	99.49	99.51	98.89	99.64

To determine the phylogenetic structure of the microbial communities in anaerobic co-bioreactors, we collected samples from all six bioreactors. Each anaerobic bioreactor had completed 2 HRT cycles prior to withdrawing the samples. We employed 454-pyrosequencing technology to phylogenetically characterize bacteria in each bioreactor based on bacterial 16S rRNA gene sequences. This level of sampling permitted the detection of bacterial populations that were minorities [16]. At least 4900 sequences per sample met quality prerequisites. Operational Taxonomy Units (OTU) were calculated based on complete linkage clustering

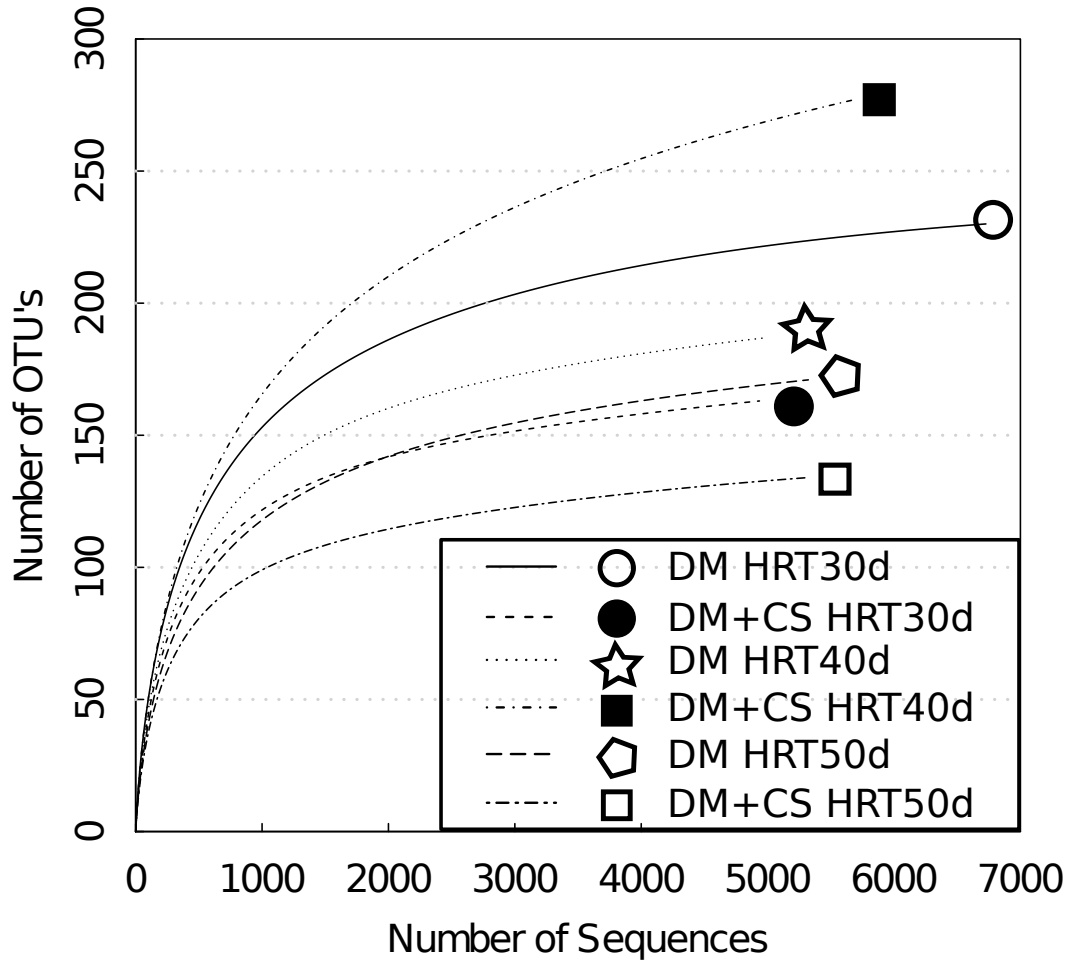


Figure D.1: Estimation of community coverage by rarefaction analysis. Rarefaction curves of anaerobic bioreactor 16S rRNA gene sequences were constructed based on the estimation of OTUs and ChaoI indices at 97% similarity.

of aligned sequences at 97% similarity (Table D.1) (all clustering analyses in this paper refer to clustering done with these parameters). Rarefaction analysis was conducted on each sample by dividing rarefied number of OTU with rarefied ChaoI estimator. At 97% sequence similarity, the rarefaction curves approached plateau (Figure D.1). Good's non-parametric coverage estimator was used to determine the community coverage (Table D.1) [39]. The results indicated that at least 98% of each bacterial community could be described by sequences obtained (Table D.1). Magnified Shannon diversity index ($e^{H'}$) indicated that

the DM bioreactor with a HRT of 30 days and the DM+CS bioreactor with a HRT of 40 days were more diverse than the others, consistent with their Simpson's indices (1-D) and ChaoI estimations. Shannon evenness (E) indices revealed that the communities in all six bioreactors were relatively skewed.

Pyrosequencing appeared to be an effective method in studying anaerobic bioreactor bacterial communities in depth (Figure D.1). Analysis of bacterial 16S rRNA gene sequences revealed that 99% of the populations in each community were described phylogenetically. Interestingly, we observed that the bacterial communities fed with DM appeared to be more diverse than DM+CS bioreactor communities, except the DM+CS bioreactor with a HRT of 40 days, the bioreactor with the highest methane production rate (Table D.1). This suggested that bacterial diversities do not correlate with biogas production and that subtle environmental factors may influence community structure and resulting biogas production levels.

D.2 Anaerobic Co-bioreactor Bacterial Community Compositions at Phylum Level

Phylum Bacteroidetes, Firmicutes and Proteobacteria were highly abundant in all six bioreactor samples. The populations from these three phyla comprised 83% or greater of all six bioreactor communities (Figure D.2). In the DM bioreactor samples, the abundance of Proteobacteria increased and the abundance of Firmicutes decreased as HRT increased. The abundance of phylum Bacteroidetes fluctuated slightly with no correlation to HRT, shifting from 33.21% in the DM bioreactor with a HRT of 30 days to 21.47% in the DM bioreactor with a HRT of 40 days, and 28.40% in the DM bioreactor with a HRT of 50 days. Similar ob-

servations were made in the DM+CS bioreactor samples. Proteobacteria was more abundant in the DM+CS bioreactor with a HRT of 50 days than the DM+CS bioreactor with a HRT of 30 days. The abundance of Firmicutes decreased in the DM+CS bioreactor with a HRT of 50 days when comparing to the DM+CS bioreactor with a HRT of 30 days. The abundance of Bacteroidetes stayed approximately the same (23.20% in the DM+CS bioreactor with a HRT of 30 days and 21.87% in the DM+CS bioreactor with a HRT of 50 days). Phylum Proteobacteria was abundant in the DM+CS bioreactor with a HRT of 30 days (44.60%) and the DM+CS bioreactor with a HRT of 50 days (55.55%). However, unlike the rest of the samples, the DM+CS bioreactor at a HRT of 40 days had a distinctive pattern. Only 7.23% of the populations were assigned to phylum Proteobacteria in the DM+CS bioreactor with a HRT of 40 days and 35.40% and 40.38% of the populations were assigned to Firmicutes and Bacteroidetes, respectively (Figure D.2).

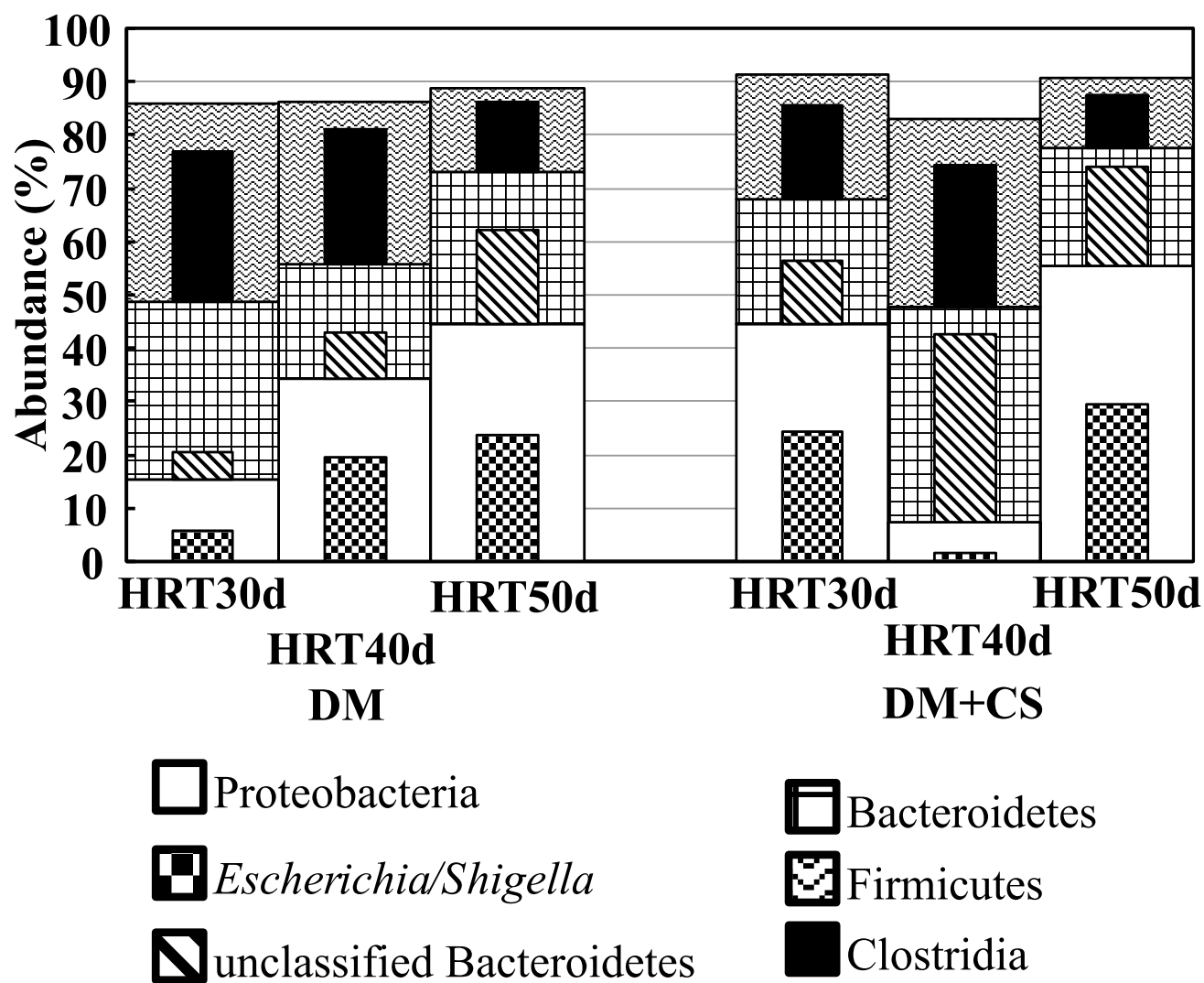


Figure D.2: The distribution of the top three most abundant phyla (wide columns) in bioreactor samples. The narrow columns represent the abundance of genera *Escherichia/Shigella* (checker box), group unclassified Bacteroidetes (diagonal stripes) and class Clostridia (blacks) in each community.

BIBLIOGRAPHY

BIBLIOGRAPHY

- [1] Acinas, S. G., Klepac-Ceraj, V., Hunt, D. E., Pharino, C., Ceraj, I., Distel, D. L., and Polz, M. F. Fine-scale phylogenetic architecture of a complex bacterial community. *Nature* *430*, 6999 (July 2004), 551–4.
- [2] Akob, D. M., Mills, H. J., Gihring, T. M., Kerkhof, L., Stucki, J. W., Anastácio, A. S., Chin, K.-J., Küsel, K., Palumbo, A. V., Watson, D. B., and Kostka, J. E. Functional diversity and electron donor dependence of microbial populations capable of U(VI) reduction in radionuclide-contaminated subsurface sediments. *Applied and Environmental Microbiology* *74*, 10 (May 2008), 3159–70.
- [3] Akob, D. M., Mills, H. J., and Kostka, J. E. Metabolically active microbial communities in uranium-contaminated subsurface sediments. *FEMS Microbiology Ecology* *59*, 1 (Jan. 2007), 95–107.
- [4] Andersson, A. F., Lindberg, M., Jakobsson, H., Bäckhed, F., Nyrén, P. I., and Engstrand, L. Comparative analysis of human gut microbiota by barcoded pyrosequencing. *PLoS One* *3*, 7 (Jan. 2008), e2836.
- [5] Baena, S., Fardeau, M., Ollivier, B., Labat, M., T, P., and De, A. *Aminomonas paucivorans* gen. nov., sp. nov., a mesophilic, anaerobic, amino-acid-utilizing bacterium. *International Journal of Systematic Bacteriology* *49* (1993), 975–982.
- [6] Bastviken, D., Tranvik, L. J., Downing, J. A., Crill, P. M., and Enrich-Prast, A. Freshwater methane emissions offset the continental carbon sink. *Science (New York, N.Y.)* *331*, 6013 (Jan. 2011), 50.
- [7] Blöthe, M., Akob, D. M., Kostka, J. E., Göschel, K., Drake, H. L., and Küsel, K. pH gradient-induced heterogeneity of Fe(III)-reducing microorganisms in coal mining-associated lake sediments. *Applied and Environmental Microbiology* *74*, 4 (Feb. 2008), 1019–29.
- [8] Borch, T., Kretzschmar, R., Kappler, A., Cappellen, P. V., Ginder-Vogel, M., Voegelin, A., and Campbell, K. Biogeochemical redox processes and their impact on contaminant dynamics. *Environmental Science and Technology* *44*, 1 (Jan. 2010), 15–23.
- [9] Boswell, C. D., Dick, R. E., and Macaskie, L. E. The effect of heavy metals and other environmental conditions on the anaerobic phosphate metabolism of *Acinetobacter johnsonii*. *Microbiology (Reading, England)* *145* (July 1999), 1711–20.
- [10] Boyd, E. S., Hamilton, T. L., Spear, J. R., Lavin, M., and Peters, J. W. [FeFe]-hydrogenase in Yellowstone National Park: evidence for dispersal limitation and phylogenetic niche conservatism. *The ISME Journal* *4*, 12 (Dec. 2010), 1485–95.

- [11] Boyd, E. S., Spear, J. R., and Peters, J. W. [FeFe] hydrogenase genetic diversity provides insight into molecular adaptation in a saline microbial mat community. *Applied and Environmental Microbiology* 75, 13 (July 2009), 4620–3.
- [12] Brodie, E. L., Desantis, T. Z., Joyner, D. C., Baek, S. M., Larsen, J. T., Andersen, G. L., Hazen, T. C., Richardson, P. M., Herman, D. J., Tokunaga, T. K., Wan, J. M., and Firestone, M. K. Application of a high-density oligonucleotide microarray approach to study bacterial population dynamics during uranium reduction and reoxidation. *Applied and Environmental Microbiology* 72, 9 (Sept. 2006), 6288–98.
- [13] Bryant, M. P., Wolin, E. a., Wolin, M. J., and Wolfe, R. S. Methanobacillus omelianskii, a symbiotic association of two species of bacteria. *Archiv für Mikrobiologie* 59, 1 (Jan. 1967), 20–31.
- [14] Burgos, W., Mcdonough, J., Senko, J., Zhang, G., Dohnalkova, a., Kelly, S., Gorby, Y., and Kemner, K. Characterization of uraninite nanoparticles produced by Shewanella oneidensis MR-1. *Geochimica et Cosmochimica Acta* 72, 20 (Oct. 2008), 4901–4915.
- [15] Campbell, C. The end of cheap oil. *Scientific American* 278, March (1998).
- [16] Cardenas, E., Wu, W.-M., Leigh, M. B., Carley, J., Carroll, S., Gentry, T., Luo, J., Watson, D., Gu, B., Ginder-Vogel, M., Kitanidis, P. K., Jardine, P. M., Zhou, J., Criddle, C. S., Marsh, T. L., and Tiedje, J. M. Microbial communities in contaminated sediments, associated with bioremediation of uranium to submicromolar levels. *Applied and Environmental Microbiology* 74, 12 (June 2008), 3718–29.
- [17] Cardenas, E., Wu, W.-M., Leigh, M. B., Carley, J., Carroll, S., Gentry, T., Luo, J., Watson, D., Gu, B., Ginder-Vogel, M., Kitanidis, P. K., Jardine, P. M., Zhou, J., Criddle, C. S., Marsh, T. L., and Tiedje, J. M. Significant association between sulfate-reducing bacteria and uranium-reducing microbial communities as revealed by a combined massively parallel sequencing-indicator species approach. *Applied and Environmental Microbiology* 76, 20 (Oct. 2010), 6778–86.
- [18] Carnoy, C., and Roten, C.-A. The dif/Xer recombination systems in proteobacteria. *PLoS One* 4, 9 (Jan. 2009), e6531.
- [19] Caspi, R., Altman, T., Dreher, K., Fulcher, C. a., Subhraveti, P., Keseler, I. M., Kothari, A., Krummenacker, M., Latendresse, M., Mueller, L. a., Ong, Q., Paley, S., Pujar, A., Shearer, A. G., Travers, M., Weerasinghe, D., Zhang, P., and Karp, P. D. The MetaCyc database of metabolic pathways and enzymes and the BioCyc collection of pathway/genome databases. *Nucleic Acids Research* 40, Database issue (Jan. 2012), D742–53.
- [20] Ceylan, A., Ertem, M., Ilcin, E., and Ozekinci, T. A special risk group for hepatitis E infection: Turkish agricultural workers who use untreated waste water for irrigation. *Epidemiology and Infection* 131, 1 (Feb. 2003), 753–756.

- [21] Chan, C. X., Beiko, R. G., and Ragan, M. a. Lateral transfer of genes and gene fragments in *Staphylococcus* extends beyond mobile elements. *Journal of Bacteriology* 193, 15 (Aug. 2011), 3964–77.
- [22] Chatzifragkou, A., Aggelis, G., Gardeli, C., Galiotou-Panayotou, M., Komaitis, M., and Papanikolaou, S. Adaptation dynamics of *Clostridium butyricum* in high 1,3-propanediol content media. *Applied Microbiology and Biotechnology* 95, 6 (Sept. 2012), 1541–52.
- [23] Cheng, X.-Y., Li, Q., and Liu, C.-Z. Coproduction of hydrogen and methane via anaerobic fermentation of cornstalk waste in continuous stirred tank reactor integrated with up-flow anaerobic sludge bed. *Bioresource Technology* 114 (June 2012), 327–33.
- [24] Chern, E. C., Tsai, Y.-L., and Olson, B. H. Occurrence of genes associated with enterotoxigenic and enterohemorrhagic *Escherichia coli* in agricultural waste lagoons. *Applied and Environmental Microbiology* 70, 1 (Jan. 2004), 356–362.
- [25] Clerget, M. Site-specific recombination promoted by a short DNA segment of plasmid-R1 and by a homologous segment in the terminus region of the *Escherichia coli* chromosome. *New Biologist* 3, 8 (Aug. 1991), 780–788.
- [26] Cole, J. R., Wang, Q., Cardenas, E., Fish, J., Chai, B., Farris, R. J., Kulam-Syed-Mohideen, A. S., McGarrell, D. M., Marsh, T., Garrity, G. M., and Tiedje, J. M. The Ribosomal Database Project: improved alignments and new tools for rRNA analysis. *Nucleic Acids Research* 37, Database issue (Jan. 2009), D141–5.
- [27] Cologgi, D. L., Lampa-Pastirk, S., Speers, A. M., Kelly, S. D., and Reguera, G. Extracellular reduction of uranium via *Geobacter* conductive pili as a protective cellular mechanism. *Proceedings of the National Academy of Sciences of the United States of America* 108, 37 (Sept. 2011), 15248–52.
- [28] Cooper, V. S., Vohr, S. H., Wrocklage, S. C., and Hatcher, P. J. Why genes evolve faster on secondary chromosomes in bacteria. *PLoS Computational Biology* 6, 4 (Apr. 2010), e1000732.
- [29] Coughlan, M., and F, M. The cellulose-decomposing bacteria and their enzyme systems. In *Prokaryotes: a handbook on the biology of bacteria*, A. Balows, H. Truper, M. Dworkin, W. Harder, and K. Schleifer, Eds., 2 ed. Springer New York, 1992, pp. 460–516.
- [30] Cuetos, M. J., Fernández, C., Gómez, X., and Morán, A. Anaerobic co-digestion of swine manure with energy crop residues. *Biotechnology and Bioprocess Engineering* 16, 5 (Sept. 2011), 1044–1052.
- [31] Curtis, T. P., Sloan, W. T., and Scannell, J. W. Estimating prokaryotic diversity and its limits. *Proceedings of the National Academy of Sciences of the United States of America* 99, 16 (Aug. 2002), 10494–9.

- [32] Dalla, E., Veeramani, H., Suvorova, E. I., Wigginton, N. S., Bargar, J. R., and Bernierlatmani, R. U(VI) reduction by spores of *Clostridium acetobutylicum*. *Research in Microbiology* 161, 9 (2010), 765–771.
- [33] Darling, A. C. E., Mau, B., Blattner, F. R., and Perna, N. T. Mauve: multiple alignment of conserved genomic sequence with rearrangements. *Genome Research* 14, 7 (July 2004), 1394–403.
- [34] Darling, A. E., Miklós, I., and Ragan, M. A. Dynamics of genome rearrangement in bacterial populations. *PLoS Genetics* 4, 7 (Jan. 2008), e1000128.
- [35] Davis, K. E. R., Joseph, S. J., and Janssen, P. H. Effects of growth medium, inoculum size, and incubation time on culturability and isolation of soil bacteria. *Applied and Environmental Microbiology* 71, 2 (Feb. 2005), 826–34.
- [36] Desvaux, M. Unravelling carbon metabolism in anaerobic cellulolytic bacteria. *Biotechnology Progress* 22, 5 (2006), 1229–38.
- [37] Dojka, M., and Hugenholtz, P. Microbial diversity in a hydrocarbon- and chlorinated-solvent-contaminated aquifer undergoing intrinsic bioremediation. *Applied and Environmental Microbiology* 64, 10 (1998), 3869–3877.
- [38] Drake, H. L., Gössner, A. S., and Daniel, S. L. Old acetogens, new light. *Annals of the New York Academy of Sciences* 1125 (Mar. 2008), 100–28.
- [39] Esty, W. The efficiency of Good ’ s nonparametric coverage estimator. *The Annals of Statistics* 14, 3 (1986), 1257–1260.
- [40] Euzéby, J. List of prokaryotic names with standing in nomenclature, 2012.
- [41] Evans, E. a., Evans, K. M., Ulrich, A., Ellsworth, S., and Khan, W. Anaerobic Processes. *Water Environment Research* 82, 10 (Jan. 2010), 1235–1287.
- [42] Fang, C., Boe, K., and Angelidaki, I. Anaerobic co-digestion of by-products from sugar production with cow manure. *Water Research* 45, 11 (May 2011), 3473–80.
- [43] Fletcher, K. E., Boyanov, M. I., Thomas, S. H., Wu, Q., Kemner, K. M., and Löffler, F. E. U(VI) reduction to mononuclear U(IV) by *Desulfitobacterium* species. *Environmental Science and Technology* 44, 12 (June 2010), 4705–9.
- [44] Food and Agriculture Organization of the United Nations. FAOSTAT, 2012.
- [45] Francis, A. J., Dodge, C. J., Lu, F., Halada, G. P., and Clayton, C. R. XPS and XANES studies of uranium reduction by *Clostridium* sp. *Environmental Science and Technology* 28, 4 (Apr. 1994), 636–9.
- [46] Frear, C., Liao, W., Ewing, T., and Chen, S. Evaluation of co-digestion at a commercial dairy anaerobic digester. *CLEAN - Soil, Air, Water* 39, 7 (July 2011), 697–704.

- [47] Frey, M. Hydrogenases: hydrogen-activating enzymes. *Chembiochem: A European Journal of Chemical Biology* 3, 2-3 (Mar. 2002), 153–60.
- [48] Gao, P., Shi, C., Tian, J., Shi, X., Yuan, K., Lu, X., and Xu, G. Investigation on response of the metabolites in tricarboxylic acid cycle of *Escherichia coli* and *Pseudomonas aeruginosa* to antibiotic perturbation by capillary electrophoresis. *Journal of Pharmaceutical and Biomedical Analysis* 44, 1 (May 2007), 180–7.
- [49] Gevers, D., Huys, G., and Swings, J. Applicability of rep-PCR fingerprinting for identification of *Lactobacillus* species. *FEMS Microbiology Letters* 205 (2001), 31–36.
- [50] Gihring, T. M., Zhang, G., Brandt, C. C., Brooks, S. C., Campbell, J. H., Carroll, S., Criddle, C. S., Green, S. J., Jardine, P., Kostka, J. E., Lowe, K., Mehlhorn, T. L., Overholt, W., Watson, D. B., Yang, Z., Wu, W.-M., and Schadt, C. W. A limited microbial consortium is responsible for extended bioreduction of uranium in a contaminated aquifer. *Applied and Environmental Microbiology* 77, 17 (Sept. 2011), 5955–65.
- [51] Gogotova, G. I., and Vainshtein, M. B. Spre-Forming, sulfate-reducing bacterium *Desulfotomaculum Guttoideum* sp. nov. *Microbiology* 52, 5 (1983), 618–622.
- [52] Gorby, Y. a., Yanina, S., McLean, J. S., Rosso, K. M., Moyles, D., Dohnalkova, A., Beveridge, T. J., Chang, I. S., Kim, B. H., Kim, K. S., Culley, D. E., Reed, S. B., Romine, M. F., Saffarini, D. a., Hill, E. a., Shi, L., Elias, D. a., Kennedy, D. W., Pinchuk, G., Watanabe, K., Ishii, S., Logan, B., Nealson, K. H., and Fredrickson, J. K. Electrically conductive bacterial nanowires produced by *Shewanella oneidensis* strain MR-1 and other microorganisms. *Proceedings of the National Academy of Sciences of the United States of America* 103, 30 (July 2006), 11358–63.
- [53] Graber, J. R., Leadbetter, J. R., and Breznak, J. A. Description of *Treponema azotonutricium* sp. nov. and *Treponema primitia* sp. nov., the first Spirochetes isolated from termite guts. *Applied and Environmental Microbiology* 70, 3 (Mar. 2004), 1315–1320.
- [54] Haferburg, G., and Kothe, E. Microbes and metals: interactions in the environment. *Journal of basic microbiology* 47, 6 (Dec. 2007), 453–67.
- [55] Hartman, H. *Introductory mining engineering*, 2 ed. No. 1980. Wiley, 2002.
- [56] Hayes, F., and Sherratt, D. J. Recombinase binding specificity at the chromosome dimer resolution site *dif* of *Escherichia coli*. *Journal of Molecular Biology* 266, 3 (Mar. 1997), 525–37.
- [57] He, Z., Gentry, T. J., Schadt, C. W., Wu, L., Liebich, J., Chong, S. C., Huang, Z., Wu, W., Gu, B., Jardine, P., Criddle, C., and Zhou, J. GeoChip: a comprehensive microarray for investigating biogeochemical, ecological and environmental processes. *The ISME Journal* 1, 1 (May 2007), 67–77.
- [58] He, Z., Piceno, Y., Deng, Y., Xu, M., Lu, Z., Desantis, T., Andersen, G., Hobbie, S. E., Reich, P. B., and Zhou, J. The phylogenetic composition and structure of soil

- microbial communities shifts in response to elevated carbon dioxide. *The ISME Journal* 6, 2 (Feb. 2012), 259–72.
- [59] Hedegaard, M., and Jaensch, V. Anaerobic co-digestion of urban and rural wastes. *Renewable Energy* 16 (1999).
- [60] Herrera, L. K., and Videla, H. a. Role of iron-reducing bacteria in corrosion and protection of carbon steel. *International Biodeterioration and Biodegradation* 63, 7 (Oct. 2009), 891–895.
- [61] Heukelekian, H. Activated sludge bulking. *Sewage Works Journal* 13, 1 (1941), 39–42.
- [62] Holt, R. A., Cairns, A. J., and Morris, J. G. Production of butanol by *Clostridium puniceum* in batch and continuous culture. *Applied Microbiology and Biotechnology* 27, 4 (Jan. 1988), 319–324.
- [63] Huber, K. E., and Waldor, M. K. Filamentous phage integration requires the host recombinases XerC and XerD. *Nature* 417, 6889 (June 2002), 656–9.
- [64] Hwang, C., Wu, W., Gentry, T. J., Carley, J., Corbin, G. A., Carroll, S. L., Watson, D. B., Jardine, P. M., Zhou, J., Criddle, C. S., and Fields, M. W. Bacterial community succession during in situ uranium bioremediation: spatial similarities along controlled flow paths. *The ISME Journal* 3, 1 (Jan. 2009), 47–64.
- [65] Jahn, M. K., Haderlein, S. B., and Meckenstock, R. U. Reduction of Prussian Blue by the two iron-reducing microorganisms *Geobacter metallireducens* and *Shewanella alga*. *Environmental Microbiology* 8, 2 (Feb. 2006), 362–7.
- [66] Jakobsson, K., Bentley, R., Söderbergh, B., and Aleklett, K. The end of cheap oil: Bottom-up economic and geologic modeling of aggregate oil production curves. *Energy Policy* 41 (Feb. 2012), 860–870.
- [67] Janssen, P. J., Van Houdt, R., Moors, H., Monsieurs, P., Morin, N., Michaux, A., Benotmane, M. a., Leys, N., Vallaey, T., Lapidus, A., Monchy, S., Médigue, C., Taghavi, S., McCorkle, S., Dunn, J., van der Lelie, D., and Mergeay, M. The complete genome sequence of *Cupriavidus metallidurans* strain CH34, a master survivalist in harsh and anthropogenic environments. *PLoS One* 5, 5 (Jan. 2010), e10433.
- [68] Jensen, R. B. Analysis of the terminus region of the *Caulobacter crescentus* chromosome and identification of the dif site. *Journal of Bacteriology* 188, 16 (Aug. 2006), 6016–9.
- [69] Jeon, O.-H., Kelly, S. D., Kemner, K. M., Barnett, M. O., Burgos, W. D., Dempsey, B. a., and Roden, E. E. Microbial reduction of U(VI) at the solid-water interface. *Environmental Science and Technology* 38, 21 (Nov. 2004), 5649–55.
- [70] Joshi, S., Parhad, N., and Rao, N. Elimination of *Salmonella* in stabilization ponds. *Water Research* 7 (1973), 1357–1365.

- [71] Julian, D. J., Kershaw, C. J., Brown, N. L., and Hobman, J. L. Transcriptional activation of MerR family promoters in *Cupriavidus metallidurans* CH34. *Antonie van Leeuwenhoek* 96, 2 (Aug. 2009), 149–59.
- [72] Junier, P., Frutschi, M., Wigginton, N. S., Schofield, E. J., Bargar, J. R., and Bernier-Latmani, R. Metal reduction by spores of *Desulfotomaculum reducens*. *Environmental Microbiology* 11, 12 (Dec. 2009), 3007–17.
- [73] Kanehisa, M., Goto, S., Sato, Y., Furumichi, M., and Tanabe, M. KEGG for integration and interpretation of large-scale molecular data sets. *Nucleic Acids Research* 40, Database issue (Jan. 2012), D109–14.
- [74] Kato, S., Haruta, S., Cui, Z. J., Ishii, M., and Igarashi, Y. Effective cellulose degradation by a mixed-culture system composed of a cellulolytic *Clostridium* and aerobic non-cellulolytic bacteria. *FEMS Microbiology Ecology* 51, 1 (Dec. 2004), 133–42.
- [75] Kato, S., Haruta, S., Cui, Z. J., Ishii, M., and Igarashi, Y. Network relationships of bacteria in a stable mixed culture. *Microbial ecology* 56, 3 (Oct. 2008), 403–11.
- [76] Kato, S., Hashimoto, K., and Watanabe, K. Microbial interspecies electron transfer via electric currents through conductive minerals. *Proceedings of the National Academy of Sciences of the United States of America* (June 2012), 22–23.
- [77] Kelly, S. D., Kemner, K. M., Carley, J., Criddle, C., Jardine, P. M., Marsh, T. L., Phillips, D., Watson, D., and Wu, W.-M. Speciation of uranium in sediments before and after in situ biostimulation. *Environmental Science and Technology* 42, 5 (Mar. 2008), 1558–64.
- [78] Kiely, G., Tayfur, G., and Dolan, C. Physical and mathematical modelling of anaerobic digestion of organic wastes. *Water Research* 31, 3 (1997), 534–540.
- [79] Komlos, J., and Jaffé, P. R. Effect of iron bioavailability on dissolved hydrogen concentrations during microbial iron reduction. *Biodegradation* 15, 5 (Oct. 2004), 315–25.
- [80] Konstantinidis, K. T., Isaacs, N., Fett, J., Simpson, S., Long, D. T., and Marsh, T. L. Microbial diversity and resistance to copper in metal-contaminated lake sediment. *Microbial ecology* 45, 2 (Feb. 2003), 191–202.
- [81] Kotrba, P. *Microbial Biosorption of Metals*, 1 ed. Springer New York, 2011.
- [82] Labrenz, M. Formation of Sphalerite (ZnS) Deposits in Natural Biofilms of Sulfate-Reducing Bacteria. *Science* 290, 5497 (Dec. 2000), 1744–1747.
- [83] Lednicka, D., Mergaert, J., Cnockaert, M., and Swings, J. Isolation and identification of cellulolytic bacteria involved in the degradation of natural cellulosic fibres. *Systematic and Applied Microbiology* 23 (2000), 292–299.
- [84] Lefebvre, O., Nguyen, T. T. H., Al-Mamun, a., Chang, I. S., and Ng, H. Y. T-RFLP reveals high β -Proteobacteria diversity in microbial fuel cells enriched with domestic wastewater. *Journal of applied microbiology* 109, 3 (Sept. 2010), 839–50.

- [85] Lehtomäki, A., Huttunen, S., and Rintala, J. Laboratory investigations on co-digestion of energy crops and crop residues with cow manure for methane production: Effect of crop to manure ratio. *Resources, Conservation and Recycling* 51, 3 (Sept. 2007), 591–609.
- [86] Lovley, D. R., and Phillips, E. J. Organic matter mineralization with reduction of ferric iron in anaerobic sediments. *Applied and Environmental Microbiology* 51, 4 (Apr. 1986), 683–9.
- [87] Lovley, D. R., and Phillips, E. J. Novel mode of microbial energy metabolism: organic carbon oxidation coupled to dissimilatory reduction of iron or manganese. *Applied and Environmental Microbiology* 54, 6 (June 1988), 1472–80.
- [88] Lovley, D. R., and Phillips, E. J. Bioremediation of uranium contamination with enzymatic uranium reduction. *Environmental Science and Technology* 26, 11 (1992), 2228–2234.
- [89] Lovley, D. R., and Phillips, E. J. Reduction of uranium by *Desulfovibrio desulfuricans*. *Applied and Environmental Microbiology* 58, 3 (Mar. 1992), 850–6.
- [90] Lu, W.-B., Shi, J.-J., Wang, C.-H., and Chang, J.-S. Biosorption of lead, copper and cadmium by an indigenous isolate *Enterobacter* sp. J1 possessing high heavy-metal resistance. *Journal of Hazardous Materials* 134, 1-3 (June 2006), 80–6.
- [91] Macaskie, L. E., Empson, R. M., Cheetham, a. K., Grey, C. P., and Skarnulis, a. J. Uranium bioaccumulation by a *Citrobacter* sp. as a result of enzymically mediated growth of polycrystalline HUO_2PO_4 . *Science (New York, N. Y.)* 257, 5071 (Aug. 1992), 782–4.
- [92] Madigan, M. T., Martinko, J. M., Stahl, D., and Clark, D. P. *Brock Biology of Microorganisms*, 13 ed. Benjamin Cummings, 2010.
- [93] Magot, M., Fardeau, M.-L., Arnauld, O., Lanau, C., Ollivier, B., Thomas, P., and Patel, B. *Spirochaeta smaragdinae* sp. nov., a new mesophilic strictly anaerobic spirochete from an oil field. *FEMS Microbiology Letters* 155, 2 (Jan. 1997), 185–191.
- [94] Magurran, A. E. *Measuring Biological Diversity*. Malden, Ma.: Blackwell Pub., 2004.
- [95] Malik, A. Metal bioremediation through growing cells. *Environment International* 30, 2 (Apr. 2004), 261–78.
- [96] Martin, W. F. Hydrogen, metals, bifurcating electrons, and proton gradients: the early evolution of biological energy conservation. *FEBS letters* 586, 5 (Mar. 2012), 485–93.
- [97] Martinez, R. J., Beazley, M. J., Taillefert, M., Arakaki, A. K., Skolnick, J., and Sobecky, P. a. Aerobic uranium (VI) bioprecipitation by metal-resistant bacteria isolated from radionuclide- and metal-contaminated subsurface soils. *Environmental Microbiology* 9, 12 (Dec. 2007), 3122–33.

- [98] Martinez, R. J., Wang, Y., Raimondo, M. A., Coombs, J. M., Barkay, T., and Sobecky, P. A. Horizontal gene transfer of PIB-type ATPases among bacteria isolated from radionuclide- and metal-contaminated subsurface soils. *Applied and environmental microbiology* 72, 5 (May 2006), 3111–8.
- [99] Matson, E. G., Gora, K. G., and Leadbetter, J. R. Anaerobic carbon monoxide dehydrogenase diversity in the homoacetogenic hindgut microbial communities of lower termites and the wood roach. *PLoS One* 6, 4 (Jan. 2011), e19316.
- [100] McDaniels, T. L., Axelrod, L. J., Cavanagh, N. S., and Slovic, P. Perception of ecological risk to water environments. *Risk Analysis : An Official Publication of The Society for Risk Analysis* 17, 3 (June 1997), 341–52.
- [101] Menz, G., Vriesekoop, F., Zarei, M., Zhu, B., and Aldred, P. The growth and survival of food-borne pathogens in sweet and fermenting brewers' wort. *International Journal of Food Microbiology* 140, 1 (May 2010), 19–25.
- [102] Merroun, M. L., Nedelkova, M., Ojeda, J. J., Reitz, T., Fernández, M. L., Arias, J. M., Romero-González, M., and Selenska-Pobell, S. Bio-precipitation of uranium by two bacterial isolates recovered from extreme environments as estimated by potentiometric titration, TEM and X-ray absorption spectroscopic analyses. *Journal of Hazardous Materials* 197 (Dec. 2011), 1–10.
- [103] Meyer, J. [FeFe] hydrogenases and their evolution: a genomic perspective. *Cellular and Molecular Life Sciences* 64, 9 (May 2007), 1063–84.
- [104] Mijndonckx, K., Provoost, A., Monsieurs, P., Leys, N., Mergeay, M., Mahillon, J., and Van Houdt, R. Insertion sequence elements in *Cupriavidus metallidurans* CH34: distribution and role in adaptation. *Plasmid* 65, 3 (May 2011), 193–203.
- [105] Mikolay, A., and Nies, D. H. The ABC-transporter AtmA is involved in nickel and cobalt resistance of *Cupriavidus metallidurans* strain CH34. *Antonie van Leeuwenhoek* 96, 2 (Aug. 2009), 183–91.
- [106] Mulligan, C., Yong, R., and Gibbs, B. Remediation technologies for metal-contaminated soils and groundwater: an evaluation. *Engineering Geology* 60, 1-4 (June 2001), 193–207.
- [107] Mullings, R., and Parish, J. Mesophilic aerobic Gram negative cellulose degrading bacteria from aquatic habitats and soils. *Journal of Applied Microbiology*, 1981 (1984).
- [108] Neidhardt, F. *Escherichia coli and Salmonella: cellular and molecular biology*, 2 ed. ASM Press, Washington, DC, 1996.
- [109] Neilson, L., Blakely, G., and Sherratt, D. Site specific recombination at dif by *Haemophilus influenzae* XerC. *Molecular Microbiology* 31, 3 (2002), 915–926.
- [110] Nges, I. A., Escobar, F., Fu, X., and Björnsson, L. Benefits of supplementing an industrial waste anaerobic digester with energy crops for increased biogas production. *Waste Management (New York, N.Y.)* 32, 1 (Jan. 2012), 53–9.

- [111] Nies, D. H. Heavy metal-resistant bacteria as extremophiles: molecular physiology and biotechnological use of *Ralstonia* sp. CH34. *Extremophiles: Life Under Extreme Conditions* 4, 2 (Apr. 2000), 77–82.
- [112] Nolan, B. T., Ruddy, B. C., Hitt, K. J., and Helsel, D. R. Risk of Nitrate in Groundwaters of the United States - A National Perspective. *Environmental Science and Technology* 31, 8 (Aug. 1997), 2229–2236.
- [113] Nyman, J. L., Wu, H.-I., Gentile, M. E., Kitanidis, P. K., and Criddle, C. S. Inhibition of a U(VI)- and sulfate-reducing consortia by U(VI). *Environmental Science and Technology* 41, 18 (Sept. 2007), 6528–33.
- [114] Ochman, H., Lawrence, J. G., and Groisman, E. a. Lateral gene transfer and the nature of bacterial innovation. *Nature* 405, 6784 (May 2000), 299–304.
- [115] Ogi, T., Tamaoki, K., Saitoh, N., Higashi, A., and Konishi, Y. Recovery of indium from aqueous solutions by the Gram-negative bacterium *Shewanella* algae. *Biochemical Engineering Journal* 63 (Apr. 2012), 129–133.
- [116] Ohmiya, K. Anaerobic Bacterial Degradation for the Effective Utilization of Biomass. *Biotechnology and Bioprocess . . .* (2005).
- [117] Oksanen, J., Blanchet, F. G., Kindt, R., Legendre, P., Minchin, P. R., O’Hara, R. B., Simpson, G. L., Solymos, P., Stevens, M. H. H., and Wagner, H. *Vegan: Community Ecology Package*, 2012.
- [118] Oregaard, G., and Sørensen, S. r. J. High diversity of bacterial mercuric reductase genes from surface and sub-surface floodplain soil (Oak Ridge, USA). *The ISME Journal* 1, 5 (Sept. 2007), 453–67.
- [119] O’Sullivan, C. a., Burrell, P. C., Clarke, W. P., and Blackall, L. L. Structure of a cellulose degrading bacterial community during anaerobic digestion. *Biotechnology and Bioengineering* 92, 7 (Dec. 2005), 871–8.
- [120] Pagés Díaz, J., Pereda Reyes, I., Lundin, M., and Sárvári Horváth, I. Co-digestion of different waste mixtures from agro-industrial activities: Kinetic evaluation and synergistic effects. *Bioresource Technology* 102, 23 (Dec. 2011), 10834–40.
- [121] Pagnanelli, F., Cruz Viggi, C., and Toro, L. Isolation and quantification of cadmium removal mechanisms in batch reactors inoculated by sulphate reducing bacteria: biosorption versus bioprecipitation. *Bioresource Technology* 101, 9 (May 2010), 2981–7.
- [122] Pan, J.-h., Liu, R.-x., and Tang, H.-x. Surface reaction of *Bacillus cereus* biomass and its biosorption for lead and copper ions. *Journal of Environmental Sciences (China)* 19, 4 (Jan. 2007), 403–8.
- [123] Passot, F. M., Calderon, V., Fichant, G., Lane, D., and Pasta, F. Centromere binding and evolution of chromosomal partition systems in the Burkholderiales. *Journal of Bacteriology* 194, 13 (July 2012), 3426–36.

- [124] Peña, A., Teeling, H., Huerta-Cepas, J., Santos, F., Yarza, P., Brito-Echeverría, J., Lucio, M., Schmitt-Kopplin, P., Meseguer, I., Schenowitz, C., Dossat, C., Barbe, V., Dopazo, J., Rosselló-Mora, R., Schüler, M., Glöckner, F. O., Amann, R., Gabaldón, T., and Antón, J. Fine-scale evolution: genomic, phenotypic and ecological differentiation in two coexisting *Salinibacter ruber* strains. *The ISME Journal* 4, 7 (July 2010), 882–95.
- [125] Petit, J., Jouzel, J., Raynaud, D., and Barkov, N. Climate and atmospheric history of the past 420,000 years from the Vostok ice core, Antarctica. *Nature* (1999).
- [126] Pobeheim, H., Munk, B., Müller, H., Berg, G., and Guebitz, G. M. Characterization of an anaerobic population digesting a model substrate for maize in the presence of trace metals. *Chemosphere* 80, 8 (Aug. 2010), 829–36.
- [127] Qin, J., Li, R., Raes, J., Arumugam, M., Burgdorf, K. S., Manichanh, C., Nielsen, T., Pons, N., Levenez, F., Yamada, T., Mende, D. R., Li, J., Xu, J., Li, S., Li, D., Cao, J., Wang, B., Liang, H., Zheng, H., Xie, Y., Tap, J., Lepage, P., Bertalan, M., Batto, J.-M., Hansen, T., Le Paslier, D., Linneberg, A., Nielsen, H. B. r., Pelletier, E., Renault, P., Sicheritz-Ponten, T., Turner, K., Zhu, H., Yu, C., Li, S., Jian, M., Zhou, Y., Li, Y., Zhang, X., Li, S., Qin, N., Yang, H., Wang, J., Brunak, S. r., Doré, J., Guarner, F., Kristiansen, K., Pedersen, O., Parkhill, J., Weissenbach, J., Bork, P., Ehrlich, S. D., and Wang, J. A human gut microbial gene catalogue established by metagenomic sequencing. *Nature* 464, 7285 (Mar. 2010), 59–65.
- [128] R Core Team. *R: A Language and Environment for Statistical Computing*. R Foundation for Statistical Computing, Vienna, Austria, 2012.
- [129] Ray, A. E., Bargar, J. R., Sivaswamy, V., Dohnalkova, A. C., Fujita, Y., Peyton, B. M., and Magnuson, T. S. Evidence for multiple modes of uranium immobilization by an anaerobic bacterium. *Geochimica et Cosmochimica Acta* 75, 10 (May 2011), 2684–2695.
- [130] Renninger, N., McMahon, K. D., Knopp, R., Nitsche, H., Clark, D. S., and Keasling, J. D. Uranyl precipitation by biomass from an enhanced biological phosphorus removal reactor. *Biodegradation* 12, 6 (Jan. 2001), 401–10.
- [131] Reynolds, T. D., and Richards, P. A. *Unit Operations and Processes in Environmental Engineering*, 2nd ed. PWS Publishing Company, Boston, MA, 1996.
- [132] Roden, E. E., and Lovley, D. R. Dissimilatory Fe(III) Reduction by the Marine Microorganism *Desulfuromonas acetoxidans*. *Applied and Environmental Microbiology* 59, 3 (Mar. 1993), 734–42.
- [133] Rodríguez-Tirado, V., Green-Ruiz, C., and Gómez-Gil, B. Cu and Pb biosorption on *Bacillus thioparans* strain U3 in aqueous solution: Kinetic and equilibrium studies. *Chemical Engineering Journal* 181-182 (Feb. 2012), 352–359.

- [134] Roest, K., Heilig, H. G., Smidt, H., de Vos, W. M., Stams, A. J., and Akkermans, A. D. Community analysis of a full-scale anaerobic bioreactor treating paper mill wastewater. *Systematic and Applied Microbiology* 28, 2 (Mar. 2005), 175–185.
- [135] Sandegren, L., and Andersson, D. I. Bacterial gene amplification: implications for the evolution of antibiotic resistance. *Nature Reviews. Microbiology* 7, 8 (Aug. 2009), 578–88.
- [136] Sar, P., Kazy, S. K., and Singh, S. P. Intracellular nickel accumulation by *Pseudomonas aeruginosa* and its chemical nature. *Letters in Applied Microbiology* 32, 4 (Apr. 2001), 257–61.
- [137] Sattley, W. M., Jung, D. O., and Madigan, M. T. *Psychrosinus fermentans* gen. nov., sp. nov., a lactate-fermenting bacterium from near-freezing oxycline waters of a meromictic Antarctic lake. *FEMS Microbiology Letters* 287, 1 (Oct. 2008), 121–7.
- [138] Scherer, J., and Nies, D. H. CzcP is a novel efflux system contributing to transition metal resistance in *Cupriavidus metallidurans* CH34. *Molecular Microbiology* 73, 4 (Aug. 2009), 601–21.
- [139] Schiewer, S., and Volesky, B. Biosorption process for heavy metal removal. In *Environmental Microbe-Metal Interactions*, D. R. Lovley, Ed. ASM Press, Washington, DC,, 14, 2000, p. 329.
- [140] Schink, B., and Stams, A. J. M. Syntrophism among prokaryotes. In *The Prokaryotes*, M. Dworkin, S. Falkow, E. Rosenberg, K.-H. Schleifer, and E. Stackebrandt, Eds. Springer New York, 2006, pp. 309–335.
- [141] Schloter, M., Lebuhn, M., Heulin, T., and Hartmann, a. Ecology and evolution of bacterial microdiversity. *FEMS Microbiology Reviews* 24, 5 (Dec. 2000), 647–60.
- [142] Schlüter, A., Bekel, T., Diaz, N. N., Dondrup, M., Eichenlaub, R., Gartemann, K.-H., Krahn, I., Krause, L., Krömeke, H., Kruse, O., Mussgnug, J. H., Neuweger, H., Niehaus, K., Pühler, A., Runte, K. J., Szczepanowski, R., Tauch, A., Tilker, A., Viehöver, P., and Goesmann, A. The metagenome of a biogas-producing microbial community of a production-scale biogas plant fermenter analysed by the 454-pyrosequencing technology. *Journal of biotechnology* 136, 1-2 (Aug. 2008), 77–90.
- [143] Schwarz, J. I. K., Eckert, W., and Conrad, R. Community structure of Archaea and Bacteria in a profundal lake sediment Lake Kinneret (Israel). *Systematic and Applied Microbiology* 30, 3 (Apr. 2007), 239–54.
- [144] Sciochetti, S. A., Piggot, P. J., and Blakely, G. W. Identification and characterization of the dif Site from *Bacillus subtilis*. *Journal of Bacteriology* 183, 3 (Feb. 2001), 1058–68.
- [145] Sherif, F., and Awad, A. Spectrophotometric determination of uranium (VI) by the azide reaction. *Analytica Chimica Acta* 26 (1962), 235–241.

- [146] Shoeb, E., Badar, U., Akhter, J., Shams, H., Sultana, M., and Ansari, M. a. Horizontal gene transfer of stress resistance genes through plasmid transport. *World Journal of Microbiology and Biotechnology* 28, 3 (Mar. 2012), 1021–5.
- [147] Silver, S., and Phung, L. T. A bacterial view of the periodic table: genes and proteins for toxic inorganic ions. *Journal of Industrial Microbiology and Biotechnology* 32, 11-12 (Dec. 2005), 587–605.
- [148] Sitte, J., Akob, D. M., Kaufmann, C., Finster, K., Banerjee, D., Burkhardt, E.-M., Kostka, J. E., Scheinost, A. C., Büchel, G., and Küsel, K. Microbial links between sulfate reduction and metal retention in uranium- and heavy metal-contaminated soil. *Applied and Environmental Microbiology* 76, 10 (May 2010), 3143–52.
- [149] Slater, S. C., Goldman, B. S., Goodner, B., Setubal, J. a. C., Farrand, S. K., Nester, E. W., Burr, T. J., Banta, L., Dickerman, A. W., Paulsen, I., Otten, L., Suen, G., Welch, R., Almeida, N. F., Arnold, F., Burton, O. T., Du, Z., Ewing, A., Godsy, E., Heisel, S., Houmiel, K. L., Jhaveri, J., Lu, J., Miller, N. M., Norton, S., Chen, Q., Phoolcharoen, W., Ohlin, V., Ondrusek, D., Pride, N., Stricklin, S. L., Sun, J., Wheeler, C., Wilson, L., Zhu, H., and Wood, D. W. Genome sequences of three agrobacterium biovars help elucidate the evolution of multichromosome genomes in bacteria. *Journal of Bacteriology* 191, 8 (Apr. 2009), 2501–11.
- [150] Sommer, M. O. a., Dantas, G., and Church, G. M. Functional characterization of the antibiotic resistance reservoir in the human microflora. *Science (New York, N.Y.)* 325, 5944 (Aug. 2009), 1128–31.
- [151] Stams, A. J. M., de Bok, F. a. M., Plugge, C. M., van Eekert, M. H. a., Dolfing, J., and Schraa, G. Exocellular electron transfer in anaerobic microbial communities. *Environmental Microbiology* 8, 3 (Mar. 2006), 371–82.
- [152] Stams, A. J. M., de Bok, F. a. M., Plugge, C. M., van Eekert, M. H. a., Dolfing, J., Schraa, G., Bok, F. A. M. D., and Eekert, M. H. A. V. Exocellular electron transfer in anaerobic microbial communities. *Environmental Microbiology* 8, 3 (Mar. 2006), 371–82.
- [153] Stern, D., and Kaufmann, R. Annual estimates of global anthropogenic methane emissions: 1860-1994. Trends Online: A Compendium of Data on Global Change. Tech. rep., Carbon Dioxide Information Analysis Center, Oak Ridge National Laboratory, U.S. Department of Energy, Oak Ridge, Tenn., U.S.A., 1998.
- [154] Stookey, L. L. Ferrozine—a new spectrophotometric reagent for iron. *Analytical Chemistry* 42, 7 (June 1970), 779–781.
- [155] Stursová, M., Zifčáková, L., Leigh, M. B., Burgess, R., and Baldrian, P. Cellulose utilization in forest litter and soil: identification of bacterial and fungal decomposers. *FEMS Microbiology Ecology* 80, 3 (June 2012), 735–46.

- [156] Sugisawa, T., Miyazaki, T., and Hoshino, T. Microbial Production of L-ascorbic acid from D-sorbitol, L-sorbose, L-gulose, and L-sorbose by *Ketogulonigenium vulgare* DSM 4025. *Bioscience, Biotechnology, and Biochemistry* 69, 3 (2005), 659–662.
- [157] Sul, W. J., Cole, J. R., Jesus, E. D. C., Wang, Q., Farris, R. J., Fish, J. a., and Tiedje, J. M. Bacterial community comparisons by taxonomy-supervised analysis independent of sequence alignment and clustering. *Proceedings of the National Academy of Sciences of the United States of America* 108, 35 (Aug. 2011), 14637–42.
- [158] Sundararaj, S., Guo, A., Habibi-Nazhad, B., Rouani, M., Stothard, P., Ellison, M., and Wishart, D. S. The CyberCell Database (CCDB): a comprehensive, self-updating, relational database to coordinate and facilitate in silico modeling of *Escherichia coli*. *Nucleic Acids Research* 32, Database issue (Jan. 2004), D293–5.
- [159] Swinton, J. *Vennerable: Venn and Euler area-proportional diagrams*.
- [160] Taghavi, S., Lesaulnier, C., Monchy, S., Wattiez, R., Mergeay, M., and van der Lelie, D. Lead(II) resistance in *Cupriavidus metallidurans* CH34: interplay between plasmid and chromosomally-located functions. *Antonie van Leeuwenhoek* 96, 2 (Aug. 2009), 171–82.
- [161] Tamura, K., Peterson, D., Peterson, N., Stecher, G., Nei, M., and Kumar, S. MEGA5: molecular evolutionary genetics analysis using maximum likelihood, evolutionary distance, and maximum parsimony methods. *Molecular Biology and Evolution* 28, 10 (Oct. 2011), 2731–9.
- [162] Tarlera, S., Muxí, L., Soubes, M., and Stams, a. J. *Caloramator proteoclasticus* sp. nov., a new moderately thermophilic anaerobic proteolytic bacterium. *International Journal of Systematic Bacteriology* 47, 3 (July 1997), 651–6.
- [163] Truex, M. J., Peyton, B. M., Valentine, N. B., and Gorby, Y. a. Kinetics of U(VI) reduction by a dissimilatory Fe(III)-reducing bacterium under non-growth conditions. *Biotechnology and Bioengineering* 55, 3 (Aug. 1997), 490–6.
- [164] Tsuruta, T. Microbes and microbial technology. In *Microbes and Microbial Technology*, I. Ahmad, F. Ahmad, and J. Pichtel, Eds. Springer New York, New York, NY, 2011, pp. 267–281.
- [165] Tunali, S., Çabuk, A., and Akar, T. Removal of lead and copper ions from aqueous solutions by bacterial strain isolated from soil. *Chemical Engineering Journal* 115, 3 (Jan. 2006), 203–211.
- [166] U.S. Environmental Protection Agency. Agriculture, 2012.
- [167] U.S. Environmental Protection Agency. NPL Mining Sites, 2012.
- [168] U.S. Environmental Protection Agency. NPL Site Status Information, 2012.
- [169] U.S. Environmental Protection Agency. Torch Lake, 2012.

- [170] Val, M.-E., Kennedy, S. P., El Karoui, M., Bonné, L., Chevalier, F., and Barre, F.-X. FtsK-dependent dimer resolution on multiple chromosomes in the pathogen *Vibrio cholerae*. *PLoS Genetics* 4, 9 (Jan. 2008), e1000201.
- [171] Van Houdt, R., Monsieurs, P., Mijndonckx, K., Provoost, A., Janssen, A., Mergeay, M., and Leys, N. Variation in genomic islands contribute to genome plasticity in *Cupriavidus metallidurans*. *BMC Genomics* 13, 1 (Jan. 2012), 111.
- [172] Van Nostrand, J. D., Wu, W.-M., Wu, L., Deng, Y., Carley, J., Carroll, S., He, Z., Gu, B., Luo, J., Criddle, C. S., Watson, D. B., Jardine, P. M., Marsh, T. L., Tiedje, J. M., Hazen, T. C., and Zhou, J. GeoChip-based analysis of functional microbial communities during the reoxidation of a bioreduced uranium-contaminated aquifer. *Environmental Microbiology* 11, 10 (Oct. 2009), 2611–26.
- [173] Verberkmoes, N. C., Russell, A. L., Shah, M., Godzik, A., Rosenquist, M., Halfvarson, J., Lefsrud, M. G., Apajalahti, J., Tysk, C., Hettich, R. L., and Jansson, J. K. Shotgun metaproteomics of the human distal gut microbiota. *The ISME Journal* 3, 2 (Feb. 2009), 179–89.
- [174] Versalovic, J., Schneider, M., De Bruijn, F. J., and Lupski, J. R. Genomic fingerprinting of bacteria using repetitive sequence-based polymerase chain reaction. *Methods in Molecular and Cellular Biology* 5, 1 (1994), 25–40.
- [175] Verstraete, W., Wittebolle, L., Heylen, K., Vanparys, B., de Vos, P., van de Wiele, T., and Boon, N. Microbial resource management: the road to go for environmental biotechnology. *Engineering in Life Sciences* 7, 2 (Apr. 2007), 117–126.
- [176] Vignais, P., Billoud, B., and Meyer, J. Classification and phylogeny of hydrogenases. *FEMS Microbiology Reviews* 25 (2001).
- [177] Volesky, B. Detoxification of metal-bearing effluents: biosorption for the next century. *Hydrometallurgy* 59, 2-3 (Feb. 2001), 203–216.
- [178] Volesky, B., and Holan, Z. R. Biosorption of heavy metals. *Biotechnology Progress* 11, 3 (1995), 235–50.
- [179] Wang, H., Lehtomäki, A., Tolvanen, K., Puhakka, J., and Rintala, J. Impact of crop species on bacterial community structure during anaerobic co-digestion of crops and cow manure. *Bioresource Technology* 100, 7 (Apr. 2009), 2311–5.
- [180] Wang, H., Tolvanen, K., Lehtomäki, A., Puhakka, J., and Rintala, J. Microbial community structure in anaerobic co-digestion of grass silage and cow manure in a laboratory continuously stirred tank reactor. *Biodegradation* 21, 1 (Feb. 2010), 135–46.
- [181] Wang, H., Vuorela, M., Keränen, A.-L., Lehtinen, T. M., Lensu, A., Lehtomäki, A., and Rintala, J. Development of microbial populations in the anaerobic hydrolysis of grass silage for methane production. *FEMS Microbiology Ecology* 72, 3 (June 2010), 496–506.

- [182] Werner, J. J., Knights, D., Garcia, M. L., Scalfone, N. B., Smith, S., Yarasheski, K., Cummings, T. a., Beers, A. R., Knight, R., and Angenent, L. T. Bacterial community structures are unique and resilient in full-scale bioenergy systems. *Proceedings of the National Academy of Sciences of the United States of America* 108, 10 (Mar. 2011), 4158–63.
- [183] White, C., Sharman, A. K., and Gadd, G. M. An integrated microbial process for the bioremediation of soil contaminated with toxic metals. *Nature Biotechnology* 16, 6 (June 1998), 572–5.
- [184] Whitman, W. B., Coleman, D. C., and Wiebe, W. J. Perspective prokaryotes : the unseen majority. *Proceedings of the National Academy of Sciences* 95, June (1998), 6578–6583.
- [185] Wirth, R., Kovács, E., Maróti, G., Bagi, Z., Rákhely, G., and Kovács, K. L. Characterization of a biogas-producing microbial community by short-read next generation DNA sequencing. *Biotechnology for Biofuels* 5, 1 (June 2012), 41.
- [186] Wu, Q., Sanford, R., and Löffler, F. Uranium (VI) reduction by *Anaeromyxobacter dehalogenans* strain 2CP-C. *Applied and Environmental Microbiology* 72, 5 (2006), 3608–3614.
- [187] Wu, W.-M., Carley, J., Fienen, M., Mehlhorn, T., Lowe, K., Nyman, J., Luo, J., Gentile, M. E., Rajan, R., Wagner, D., Hickey, R. F., Gu, B., Watson, D., Cirpka, O. a., Kitanidis, P. K., Jardine, P. M., and Criddle, C. S. Pilot-scale in situ bioremediation of uranium in a highly contaminated aquifer. 1. Conditioning of a treatment zone. *Environmental Science and Technology* 40, 12 (June 2006), 3978–85.
- [188] Wu, W.-M., Carley, J., Gentry, T., Ginder-Vogel, M. a., Fienen, M., Mehlhorn, T., Yan, H., Carroll, S., Pace, M. N., Nyman, J., Luo, J., Gentile, M. E., Fields, M. W., Hickey, R. F., Gu, B., Watson, D., Cirpka, O. a., Zhou, J., Fendorf, S., Kitanidis, P. K., Jardine, P. M., and Criddle, C. S. Pilot-scale in situ bioremediation of uranium in a highly contaminated aquifer. 2. Reduction of u(VI) and geochemical control of u(VI) bioavailability. *Environmental Science and Technology* 40, 12 (June 2006), 3986–95.
- [189] Xing, D., Ren, N., and Rittmann, B. E. Genetic diversity of hydrogen-producing bacteria in an acidophilic ethanol-H₂-coproducing system, analyzed using the [Fe]-hydrogenase gene. *Applied and Environmental Microbiology* 74, 4 (Feb. 2008), 1232–9.
- [190] Xu, M., Wu, W.-M., Wu, L., He, Z., Van Nostrand, J. D., Deng, Y., Luo, J., Carley, J., Ginder-Vogel, M., Gentry, T. J., Gu, B., Watson, D., Jardine, P. M., Marsh, T. L., Tiedje, J. M., Hazen, T., Criddle, C. S., and Zhou, J. Responses of microbial community functional structures to pilot-scale uranium in situ bioremediation. *The ISME Journal* 4, 8 (Aug. 2010), 1060–70.
- [191] Yang, F., Pecina, D. a., Kelly, S. D., Kim, S.-H., Kemner, K. M., Long, D. T., and Marsh, T. L. Biosequestration via cooperative binding of copper by *Ralstonia pickettii*. *Environmental Technology* 31, 8-9 (2010), 1045–60.

- [192] Yue, Z., Chen, R., Yang, F., MacLellan, J., Marsh, T., Liu, Y., and Liao, W. Effects of dairy manure and corn stover co-digestion on anaerobic microbes and corresponding digestion performance. *Bioresource Technology* 128 (Nov. 2012), 65–71.
- [193] Zengler, K. Central role of the cell in microbial ecology. *Microbiology and Molecular Biology Reviews* 73, 4 (Dec. 2009), 712–29.
- [194] Zhang, W., Culley, D. E., Scholten, J. C. M., Hogan, M., Vitiritti, L., and Brockman, F. J. Global transcriptomic analysis of *Desulfovibrio vulgaris* on different electron donors. *Antonie van Leeuwenhoek* 89, 2 (Feb. 2006), 221–37.
- [195] Zoropogui, A., Gambarelli, S., and Covès, J. CzcE from *Cupriavidus metallidurans* CH34 is a copper-binding protein. *Biochemical and Biophysical Research Communications* 365, 4 (Jan. 2008), 735–9.